



THE UNIVERSITY OF QUEENSLAND  
AUSTRALIA

**The Skin Microbiopsy**

Li Lin

Bachelor of Science

*A thesis submitted for the degree of Doctor of Philosophy at*

*The University of Queensland in 2015*

School of Medicine

## **Abstract**

Skin cancer is reported to incur the highest treatment costs of all cancers. The treatment cost of non-melanoma skin cancer (NMSC) was purported to be around AUD\$264 million, and AUD\$30 million for melanoma in 2001. Conventional skin biopsy techniques are performed to identify histopathological signs of malignancy. Suspicious lesions are often present on cosmetically sensitive areas and may be present in large numbers, making biopsies unfeasible. As a result, many atypical lesions are left untreated (leaving patients with early cancerous lesions) or needlessly removed (unnecessary scars). Prognostic biomarkers are useful for assessing borderline cases to facilitate early detection of skin cancer. The development of a novel microbiopsy device (**Figure 1.1**) from this Thesis enables quick, simple, minimally invasive and suture-free sampling of tiny skin samples sufficient for molecular assays.

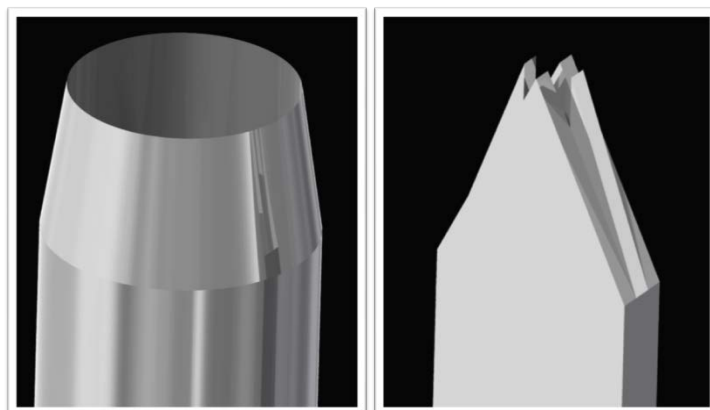


**Figure 1.1:** Diagrams of a conventional punch biopsy and three-dimensional Microbiopsy cutting tip.

Laser cutting technologies have enabled rapid prototyping of microbiopsy devices made from medical-grade stainless steel. Through optimisation of the laser parameters, a two-dimensional microbiopsy that assembles to form a three-dimensional cutting tip with a hollow chamber was successfully constructed. A quick and safe method to facilitate repeated collection over time in human patients is now possible with the microbiopsy-based approach.

Characterisation studies revealed approximately 1000 to 3000 cells from each velocity-aided microbiopsy with an average DNA and RNA yield of  $5.9 \pm 3.4$  ng and  $9.0 \pm 10.1$  ng, respectively. Human volunteer studies have shown that the microbiopsy application

velocity, channel width, edge surface roughness and geometries were important aspects to achieve reproducible tissue sampling.

Genomic profiling of an individual can now be done using microbiopsy sampling approach instead of conventional blood or saliva samples. The limitation of small sample size can be overcome by using high-fidelity amplification technologies for amplifying nucleic acids. The defects left by microbiopsy application observed in histopathological sections were similar to artefacts arising from routine tissue processing. This opens up opportunities for the possibility of *in vivo* sampling and enables molecular diagnosis without the risk of damaging the lesion - which will help to improve patient care by reducing unnecessary excision. Proof-of-concept studies have established the potential of the guided skin microbiopsy device to study *in vivo* molecular changes within a targeted area over time, which was impossible in the past.

Other than clinical applications, the microbiopsy device also offers a novel approach for live cell assays. Current approaches, in particular those related to the cosmeceutical arena are limited to restrictive regulations on animal testing, and the fact it is often not deemed ethical or practical to use conventional biopsy techniques to assess the effect of cosmetics. One debatable topic in this arena is the likelihood of nanoparticles to infiltrate the viable epidermis and cause cell toxicity. Human volunteers treated with common nanoparticle UV-filters showed that no metabolic changes occurred in the viable cells even when the skin barrier was disrupted.

In the final exploratory studies of this Thesis, various downstream omics technologies were used to analyse the microbiopsy samples. The key take-home message from these studies was the technical variations observed for small sample input. Moving forward, it is of priority to address how this issue can be overcome to validate the accuracy of biological information the microbiopsy sample represents.

## **Declaration by author**

This thesis is composed of my original work, and contains no material previously published or written by another person except where due reference has been made in the text. I have clearly stated the contribution by others to jointly-authored works that I have included in my thesis.

I have clearly stated the contribution of others to my thesis as a whole, including statistical assistance, survey design, data analysis, significant technical procedures, professional editorial advice, and any other original research work used or reported in my thesis. The content of my thesis is the result of work I have carried out since the commencement of my research higher degree candidature and does not include a substantial part of work that has been submitted to qualify for the award of any other degree or diploma in any university or other tertiary institution. I have clearly stated which parts of my thesis, if any, have been submitted to qualify for another award.

I acknowledge that an electronic copy of my thesis must be lodged with the University Library and, subject to the policy and procedures of The University of Queensland, the thesis be made available for research and study in accordance with the Copyright Act 1968 unless a period of embargo has been approved by the Dean of the Graduate School.

I acknowledge that copyright of all material contained in my thesis resides with the copyright holder(s) of that material. Where appropriate I have obtained copyright permission from the copyright holder to reproduce material in this thesis.

## Publications during candidature

### Peer-reviewed papers

#### *Published*

1. **Lin LL**, Grice JE, Butler MK, Zvyagin AV, Becker W, Robertson TA, Soyer HP, Roberts MS, Prow TW. Time-correlated single photon counting for simultaneous monitoring of zinc oxide nanoparticles and NAD(P)H in intact and barrier disrupted volunteer skin. *Pharmaceutical Research*. 2011 Nov;28(11):2920-30.
2. Butler MK, Prow TW, Guo YN, **Lin LL**, Webb RI, Martin DJ. High pressure freezing/freeze substitution and TEM for the characterization of metal oxide nanoparticles within sunscreens. *Nanomedicine (Lond)*. 2012 Apr;7(4):541-51.
3. Wurm EM\*, **Lin LL\***, Ferguson B, Lambie D, Prow TW, Walker GJ, Soyer HP. A blueprint for staging of murine melanocytic lesions based on the Cdk4R24C/R24C :: Tyr-NRASQ61K model. *Experimental Dermatology*. 2012 Sep 21(9):676-81. \*Equal contributor.
4. Wheller L, Sinnya S, **Lin LL**, Chai E, Soyer HP, Prow TW. Noninvasive methods for the assessment of photoageing. *The Australasian Journal of Dermatology*. 2013 Nov;54(4):290-5.
5. **Lin LL**, Prow TW, Raphael AP, Harrold III RL, Primiero CA., Ansaldo AB, Soyer HP. Microbiopsy engineered for minimally invasive and suture-free sub-millimetre skin sampling. *F1000Research*. 2013 May 2 [revised 2013 Jul 31];2:120.
6. Banan P, **Lin LL**, Lambie D, Soyer HP, Prow TW. *Ex vivo* skin microbiopsy effects on histopathological diagnosis in melanocytic skin lesions. *JAMA Dermatology*. 2013 Sep 1;149(9):1107-9.
7. Soyer HP, **Lin LL**, Prow TW. A plea for bio-banking of all equivocal melanocytic proliferations. *JAMA Dermatology*. 2013 Sep 1;149(9):1023-4.
8. Prow TW, **Lin LL**, Soyer HP. The opportunity for microbiopsies for skin cancer. *Future Oncology*. 2013 Sep;9(9):1241-3.

9. Mohammed YH, Yamada M, **Lin LL**, Grice JE, Roberts MS, Raphael AP, Benson HAE, Prow TP. Microneedle enhanced delivery of cosmeceutically relevant peptides in human skin. PLOS ONE. 2014 Jul 17;9(7):e101956.
10. Raphael AP, Primiero CA, **Lin LL**, Soyer HP and Prow TW. High aspect ratio elongated microparticles for enhanced topical drug delivery in volunteers. Adv Healthc Mater. 2014 Jun;3(6):860-6.
11. McClenahan P, **Lin LL**, Tan JM, Flewell-Smith, Schaidler H, Jagirdar K, Atkinson V, Lambie D, Prow TW, Sturm RA, Soyer HP. BRAFV600E Mutation Status of Involuting and Stable Nevi in Dabrafenib Therapy With or Without Trametinib. JAMA Dermatol. 2014. doi: 10.1001/jamadermatol.2014.436.
12. Tan JM\*, **Lin LL\***, Lambie D, Flewell-Smith R, Jagirfdar K, Schaidler H, Sturm RA, Prow TW, Soyer HP. BRAF wildtype melanoma in situ arising in a BRAFV600E 1 mutant dysplastic nevus. JAMA Dermatol. 2015. Apr;151(4):417-21. doi: 10.1001/jamadermatol.2014.3775. \*Equal contributor.

### ***Patents***

1. Prow TW and Soyer HP. A microbiopsy device. IP Australia Appl. Num, 2012901490.

### ***Book chapters***

1. Yamada M, Lin LL, Prow TW. (2014) Multiphoton Microscopy Applications in Biology. Fluorescence Microscopy: Super-Resolution and Other Novel Techniques. Anda Cornea and P. Michael Conn (ed.). London, UK. Academic Press, Elsevier. Chapter 13: 185-197.

### **Conference abstracts**

1. Lin LL et al., *Characterization of a micro-biopsy device for detection of skin diseases' biomarkers*. Translational Research Institute Student Retreat. Brisbane, Australia, April 2012. Poster
2. Lin LL et al., *A blueprint for staging of murine melanocytic lesions in genetically modified mice*. 3<sup>rd</sup> World Congress of Dermoscopy. Brisbane, Australia, May 2012. Talk.
3. Lin L.L et al., *Skin microbiopsy for molecular diagnosis of skin cancer*. Princess Alexandra Hospital Health Symposium. Brisbane, Australia, August 2012. Poster.
4. Lin L.L et al., *Characterization of a micro-biopsy device for detection of skin diseases' biomarkers*. Asian Society for Pigment Cell Research (ASPCR) and the Australasian Society for Dermatology Research (ASDR) Conference. Sydney, Australia, May 2013. Talk.
5. Lin LL et al., *Characterisation of a micro-biopsy device for detection of skin diseases' biomarkers*. Translational Research Institute Poster Symposium. Brisbane, Australia, July 2013. Poster.
6. Lin L.L et al., *Characterisation of a micro-biopsy device for detection of skin diseases' biomarkers*. Global Controversies and Advances in Skin Cancer. Brisbane, Australia, November 2013. Talk.
7. Lin LL et al., *Characterization of a micro-biopsy device for detection of skin diseases' biomarkers*. ASPCR-ASDR 2013. Sydney, Australia, May 2013. Talk.
8. Lin LL et al. *Characterization of a micro-biopsy device for detection of skin diseases' biomarkers*. Skin Cancer Conference 2014. Noosa, Australia, August 2014. Talk.
9. Hang LYT, Lin LL et al. *Microbiopsy skin sampling in volunteers reveals no oxidative stress detected after topically applying sunscreen with zinc-oxide nanoparticles*. American Academic of Dermatology 73<sup>rd</sup> Annual Meeting. San Francisco, USA, March 2015. E-Poster.

### ***Publications included in this thesis***

1. Lin LL, Prow TW, Raphael AP et al. *Microbiopsy engineered for minimally invasive and suture-free sub-millimetre skin sampling*. F1000Research. 2013 May 2 [revised 2013 Jul 31];2:120. – partially incorporated as Chapter 4.
2. Banan P, **Lin LL**, Lambie D, Soyer HP, Prow TW. *Ex vivo skin microbiopsy effects on histopathological diagnosis in melanocytic skin lesions*. JAMA Dermatology. 2013 Sep 1;149(9):1107-9 – partially incorporated as Chapter 5.
3. McClenahan P, **Lin LL**, Tan JM, Flewell-Smith, Schaidler H, Jagirdar K, Atkinson V, Lambie D, Prow TW, Sturm RA, Soyer HP. BRAFV600E Mutation Status of Involuting and Stable Nevi in Dabrafenib Therapy With or Without Trametinib. JAMA Dermatol. 2014. doi: 10.1001/jamadermatol.2014.436. – partially incorporated as Chapter 5
4. Tan JM\*, **Lin LL\***, Lambie D, Flewell-Smith R, Jagirdar K, Schaidler H, Sturm RA, Prow TW, Soyer HP. BRAF wildtype melanoma in situ arising in a BRAFV600E 1 mutant dysplastic nevus. Submitted to JAMA Dermatol. in July 2014. – partially incorporated as Chapter 5
5. Soyer HP, **Lin LL**, Prow TW. A plea for bio-banking of all equivocal melanocytic proliferations. JAMA Dermatology. 2013 Sep 1;149(9):1023-4. – partially incorporated as Chapter 8
6. Prow TW, **Lin LL**, Soyer HP. The opportunity for microbiopsies for skin cancer. Future Oncology. 2013 Sep;9(9):1241-3. – partially incorporated as Chapter 8



Publication citation: Lin LL et al., *Microbiopsy engineered for minimally invasive and suture-free sub-millimetre skin sampling*. F1000Research. 2013 May 2 [revised 2013 Jul 31];2:120. – partially incorporated as Chapter 4.

Contributor	Statement of contribution
Author Lin LL (Candidate)	Designed the experiments (60%) Conducted the experiments (100%) Wrote the paper (100%)
Author Prow TW	Designed the experiments (30%) Edited paper (70%)
Author Raphael AP	Designed the experiments (10%) Edited the paper (20%) Contributed Figure 3.4c in the publication
Author Harrold II RL	Contributed Figure 3.4d in the publication
Author Primiero CA	Assisted in the volunteer study of the research
Author Ansaldo AB	Determined the values of application velocities and roughness amplitudes in the study.
Author Soyer HP	Supervision of the project (10%) Edited the paper (10%)

Publication citation: Banan P et al., *Ex vivo skin microbiopsy effects on histopathological diagnosis in melanocytic skin lesions*. JAMA Dermatology. 2013 Sep 1;149(9):1107-9 – partially incorporated as Chapter 5.

Contributor	Statement of contribution
Author Banan P	Recruited the patients  Analysed and interpreted the data (30%)  Wrote the paper (20%)
Author Lin LL (Candidate)	Conducted the experiments (50%)  Analysed and interpreted the data (30%)  Wrote the paper (80%)
Author Lambie D	Designed the experiments (20%)  Conducted the experiments (50%)  Analysed and interpreted the data (40%)
Author Prow TW	Designed the experiments (40%)  Edit the paper (60%)
Author Soyer HP	Designed the experiments (40%)  Supervision of the project  Edit the paper (40%)

Publication citation: McClenahan P et al., BRAFV600E Mutation Status of Involuting and Stable Nevi in Dabrafenib Therapy With or Without Trametinib. JAMA Dermatol. 2014. 150(10):1079-82. – partially incorporated as Chapter 5.

Contributor	Statement of contribution
Author McClenahan P	Conducted the experiments (50%) Wrote the paper (70%)
Author Lin LL (Candidate)	Conducted the experiments (50%) Wrote the paper (30%) Analysed and interpreted the data (20%)
Author Tan JM	Recruited patient
Author Flewell-Smith R	Fabricated microbiopsy devices
Author Schaider H	Designed experiments (30%) Analysed and interpreted the data (20%) Edited the paper (10%)
Author Jagirdar K	Assisted in sequencing experiments.
Author Atkinson V	Edited the paper (10%)
Author Lambie D	Contributed histopathology images
Author Sturm RA	Designed experiments (30%) Analysed and interpreted the data (20%) Edited the paper (25%)
Author Prow TW	Supervision of the project Edited the paper (10%)
Author Soyer HP	Supervision of the project Analysed and interpreted the data (20%) Edited the paper (45%)

Publication citation: Tan JM et al., BRAF wildtype melanoma in situ arising in a BRAFV600E 1 mutant dysplastic nevus. JAMA Dermatol. 2014. doi: 10.1001/jamadermatol.2014.3775. – partially incorporated as Chapter 5

Contributor	Statement of contribution
Author Tan JM	Designed the experiments (30%) Recruited patient Conducted the experiment (20%) Wrote the paper (70%) Analysed and interpreted the data (10%)
Author Lin LL (Candidate)	Designed the experiments (30%) Conducted the experiment (60%) Analysed and interpreted the data (10%) Edited the paper (20%)
Author Lambie D	Contributed histopathology images Analysed and interpreted the data (10%)
Author Flewell-Smith R	Fabricated microbiopsy devices and targeting device
Author Jagirdar K	Conducted the experiment (20%) Analysed and interpreted the data (10%)
Author Schaider H	Analysed and interpreted the data (15%) Edited the paper (30%)
Author Sturm RA	Edited the paper (20%) Analysed and interpreted the data (15%)
Author Prow TW	Analysed and interpreted the data (15%) Edited the paper (10%)

Author Soyer HP	Supervision of the project Designed the experiments (40%) Analysed and interpreted the data (15%) Edited the paper (20%)
-----------------	---

Publication citation: Soyer HP, Lin LL, Prow TW, A plea for bio-banking of all equivocal melanocytic proliferations. JAMA Dermatology. 2013 Sep 1;149(9):1023-4. – partially incorporated as Chapter 8

Contributor	Statement of contribution
Author Soyer	Wrote the paper (50%)
Author Lin LL (Candidate)	Wrote the paper (20%)
Author Prow TW	Wrote the paper (30%)

Publication citation: Prow TW, **Lin LL**, Soyer HP. The opportunity for microbiopsies for skin cancer. Future Oncology. 2013 Sep;9(9):1241-3. – partially incorporated as Chapter 8

Contributor	Statement of contribution
Author Prow TW	Wrote the paper (40%)
Author Lin LL (Candidate)	Wrote the paper (30%)
Author Soyer	Wrote the paper (30%)

### **Contributions by others to the thesis**

**Dr. Tarl W. Prow** – Provided critical input on design and idea of the whole project, analysis and interpretation of data, and was involved in the conception of the thesis.

**Prof. H. Peter Soyer** – Provided input on design, analysis and interpretation of the clinical components of the project, and drafted the thesis.

**Dr. Rick A. Sturm** – Provided input on the design, analysis and interpretation of the genotyping components of the project, and drafted the thesis.

**Dr. Anthony P. Raphael** – Provided input on the design, analysis and interpretation of the mechanical and imaging component of the project, and drafted the thesis.

**Dr. Duncan Lambie** – Processed and analysed histopathological sections described in Chapter 5.

**Prof. Michael Roberts** – Provided excised human skin that was used to generate data in Chapter 4.

**Mr. Alex Ansaldo** – Provided input on the design of the microbiopsy cutting die and applicator.

**Ms. Kasturee Jagirdar** – Performed MC1R and OCA2 genotyping described in Chapter 5.

**Mr. Ross Flewell-Smith** – Provided input and data analysis on the geometry design and surface texturing of the microbiopsy cutting die described in Chapter 4.

**Mr. Xiu Cheng Quek** – Performed RNA sequencing data analysis and provided data that was described in Chapter 5.

### **Statement of parts of the thesis submitted to qualify for the award of another degree**

None.

## **Acknowledgements**

I would like to start off by first expressing my deepest gratitude to my principal supervisor, A/ Prof. Tarl Prow, for giving me the opportunity to embark on this exciting project. You have been a very supportive and inspiring mentor who have always motivated me during trying times, and celebrated my successes and achievements when they are due. I am aware that not many PhD students can say this, but you have not only been a great supervisor, but also a great friend. You have forged the career I have today - Thank you.

I also owe my gratitude to my co-supervisors. Prof. Peter H. Soyer and A/Prof. Richard Sturm, I thank you for all your kindness, guidance, and the opportunities you have given me. Dr. Anthony Raphael, thank you for your guidance and constructive criticisms – which I always find very helpful. It's been a real pleasure being your student and friend, and I wish the best for your future endeavours.

I am grateful to Prof. Roy Hall for his advice, support and generosity as the chairperson of my yearly review committee. I would also like to extend my appreciation to all the members of Dermatology Research Centre – thank you for all your encouragement and help that you have given.

Most importantly, my greatest appreciation goes to my loving husband, Dr. Setoh (Science runs in our family) who has always been my pillar of support. You have been very encouraging and supportive throughout my PhD. You pick me up every time I felt like I cannot do it anymore. You have patiently guided me through things I do not understand, and I know it must be hard for you to explain things over and over again. Thank you for being such an amazing husband and a “funtastic” dad to Zachary. Love you always.

To my parents and extended family, thank you for all the love and support, especially mommy Tang. Thank you for taking such good care of Zac and taking the “night shifts” while I work late – I love you all very much. Sincere thanks to friends in Brisbane, especially Mek and Priscilla, who have been there for me and lending a listening ear whenever I feel down, and for organising “girlfriend trips” at the times when I needed it most. Not forgetting friends and extended family in Singapore, especially Serene, Coreen and Vivien, your emotional support has been incredible. I know I have missed out a lot but

thanks for always making time for me whenever I get a chance to visit home and making me feel like the good old days. Love you girls!

I would like to acknowledge The University of Queensland for the award of a Postgraduate Research Scholarship that provided the necessary financial support. Finally, I would like to acknowledge the Australian Research Council and Epiderm for funding this research.



## **Keywords**

Micro-devices, minimally invasive, diagnostics, non-melanoma skin cancer, melanoma, biomarkers

## **Australian and New Zealand Standard Research Classifications (ANZSRC)**

ANZSRC code: 090304 Medical Devices, 50%

ANZSRC code: 060405 Gene Expression, 40%

ANZSRC code: 110304 Dermatology, 10%

## **Fields of Research (FoR) Classification**

FoR code: 0903 Biomedical Engineering, 50%

FoR code: 0601 Biochemistry and Cell Biology, 40%

FoR code: 1103 Clinical Sciences, 10%

## **Table of Contents**

Abstract.....	i
List of Figures .....	xxiii
List of Tables .....	xxvii
List of Abbreviations .....	xxviii
<b>Chapter 1 Introduction and Literature Review .....</b>	<b>1</b>
1.1 Introduction .....	1
1.2 Conventional skin sampling for diagnostics in dermatology .....	2
1.2.1 Snip biopsy.....	3
1.2.2 Punch biopsy.....	3
1.2.3 Shave biopsy.....	3
1.2.4 Saucerisation (deep scoop shave) .....	4
1.2.5 Curettage biopsy .....	4
1.2.6 Excisional biopsy.....	4
1.3 Emerging skin sampling techniques for biomolecular diagnostics.....	5
1.4 Non-invasive tools and techniques for skin diagnostics .....	7
1.4.1 Dermoscopy .....	8
1.4.2 Total body photography.....	9
1.4.3 Reflectance confocal microscopy.....	11
1.4.4 Optical coherence tomography.....	13
1.5 Novel minimally invasive tools for micro-sampling .....	15
1.6 Fabrication of micro devices.....	16
1.6.1 Solid-based RP processes .....	17
1.6.2 Liquid-based RP processes.....	23
1.6.3 Powder-based RP processes .....	28
1.6.4 Water-Jet cutting – a subtractive manufacturing process .....	30
1.6.5 Rapid prototyping applications in medicine and biomedical fields .....	31

1.7 Literature review summary and Scope of thesis.....	34
<b>Chapter 2 General Materials &amp; Methods .....</b>	<b>35</b>
2.1 Microbiopsy device fabrication .....	35
2.1.1 Fabrication of in-house standard microbiopsy cutting die .....	35
2.1.2 Mass fabrication of standard microbiopsy cutting die .....	36
2.1.3 Fabrication of loader cap .....	36
2.1.4 Assembling of single-use microbiopsy device .....	36
2.1.5 Preparation of excised human skin.....	37
2.1.6 Microbiopsy tissue collection from volunteers.....	37
2.1.7 Microbiopsy tissue collection from excised skin.....	38
2.2 DNA Processing.....	38
2.2.1 DNA extraction from microbiopsy sample.....	38
2.2.2 DNA extraction from lesional sample.....	39
2.2.3 DNA quantification .....	39
2.2.4 DNA whole genomic amplification .....	39
2.2.5 DNA quality control .....	40
2.3 RNA Processing.....	40
2.3.1 RNA extraction from microbiopsy samples .....	40
2.3.2 RNA extraction from lesional sample.....	40
2.3.3 RNA quantification .....	41
2.3.4 RNA quality control .....	41
2.4 Image data collection .....	41
2.4.1 Optical and clinical photography.....	41
2.4.2 Reflectance confocal microscopy .....	42
<b>Chapter 3 Fabrication of the Microbiopsy device .....</b>	<b>43</b>
3.1 Introduction .....	43

3.2	Materials and Methods.....	50
3.2.1	Laser cutting system optimisation.....	50
3.2.2	Surface area calculation .....	51
3.2.3	First generation microbiopsy cutting die functionality test.....	51
3.2.4	Statistical analysis .....	52
3.3	Results and Discussion.....	53
3.3.1	Laser setting optimisation with lines .....	53
3.3.2	Laser setting optimisation with single needle microbiopsy.....	63
3.3.3	Device integrity assessment .....	68
3.4	Conclusions.....	71
<b>Chapter 4 Microbiopsy optimisation and characterisation .....</b>		<b>73</b>
4.1	Introduction .....	73
4.2	Materials and Methods.....	77
4.2.1	Fabrication of cutting tips with varying widths, geometries and micro-texturing.....	77
4.2.2	Punch biopsy and microbiopsy characterisation .....	78
4.2.3	Total cell count.....	79
4.2.4	Histology of microbiopsy skin defect.....	79
4.2.5	DNA isolation comparison .....	79
4.2.6	Channel width pilot study.....	80
4.2.7	Surface roughness ( $R_A$ ) pilot study .....	80
4.2.8	High resolution device imaging.....	81
4.2.9	Quasi-static and velocity-aided biopsy application.....	81
4.2.10	Pre-load and application velocity pilot study .....	81
4.2.11	Wound healing kinetics.....	83
4.2.12	Measurement of pain score .....	83
4.2.13	Human volunteer study.....	84

4.2.14	Channel width, application velocity and surface roughness study .....	84
4.2.15	Micro-texturing and geometry study.....	85
4.2.16	RNA isolation, quantification and quality control .....	85
4.2.17	Molecular characterisation of lesional and microbiopsy samples.....	87
4.3	Results and Discussion .....	88
4.3.1	Characterisation of microbiopsy content and site of application .....	88
4.3.2	Quantification of cellular material.....	90
4.3.3	Wound healing kinetics .....	92
4.3.4	Influence of channel width on tissue extraction .....	94
4.3.5	Influence of pre-loading on tissue extraction .....	96
4.3.6	Influence of application velocity on tissue extraction .....	97
4.3.7	Influence of surface roughness on tissue extraction.....	101
4.3.8	Influence of geometry and surface texturing on tissue extraction .....	103
4.3.9	Microbiopsy RNA isolation optimisation.....	105
4.4	Conclusions.....	107
<b>Chapter 5 Genotyping and mutation profiling applications .....</b>		<b>109</b>
5.1	Introduction .....	109
5.2	Materials and Methods.....	112
5.2.1	Melanocortin 1 receptor (MC1R) and Oculocutaneous albinism II (OCA2) genotyping.....	112
5.2.2	Small clinical study on pigmented skin lesions .....	112
5.2.3	Case Study 1 – BRAF mutation status in regressing and stable naevi .....	115
5.2.4	Case Study 2 – Targeted microbiopsy sampling.....	116
5.2.5	Somatic mutation profiling .....	116
5.3	Results and Discussion .....	118
5.3.1	MC1R and OCA2 genotyping of single and pooled microbiopsy samples ..	118
5.3.2	Effects of microbiopsy application on histopathological diagnosis.....	119

5.3.3	Detection of BRAF Exon 15 and NRAS Exon 2 mutations .....	122
5.3.4	BRAF <sup>V600E</sup> Mutation status in regressed and stable naevi .....	124
5.3.5	Unguided and guided tissue sampling .....	128
5.3.6	Targeted sampling from regions of interest within lesion .....	129
5.3.7	Somatic mutation status in non-pigmented skin lesions .....	134
5.4	Conclusions.....	138
<b>Chapter 6 Microbiopsy – a new approach for live cell assay.....</b>		<b>139</b>
6.1	Introduction.....	139
6.2	Materials and Methods .....	143
6.2.1	Study volunteers.....	143
6.2.2	Tape-stripping and Trans-epidermal water loss (TEWL) .....	143
6.2.3	Zinc-oxide nanoparticle (ZnO-NP) preparation and application.....	143
6.2.4	Microbiopsy sample collection.....	144
6.2.5	Reactive Oxygen and Nitrogen species and Mitochondrial Superoxide assessment .....	144
6.2.6	Confocal Microscopy .....	145
6.2.7	Image analysis and statistical analysis .....	145
6.3	Results and Discussion .....	147
6.4	Conclusions .....	153
<b>Chapter 7 The feasibility of advanced analytical platforms for molecular analysis</b>		<b>154</b>
7.1	Introduction .....	154
7.2	Materials and Methods.....	159
7.2.1	Protein extraction from microbiopsy sample .....	159
7.2.2	Protein extraction from COS cells.....	159
7.2.3	Protein quantification .....	160
7.2.4	Protein separation using polyacrylamide gel electrophoresis (SDS-PAGE)	160

7.2.5	Quantitative reverse-transcriptase PCR (qRT-PCR).....	160
7.2.6	Gene expression analysis via nCounter® assay .....	161
7.2.7	cDNA library preparation for Illumina® sequencing platforms .....	162
7.3	Results and Discussion.....	164
7.3.1	Targeted mass spectrometry approach for peptide identification .....	164
7.3.2	High sensitivity total RNA quantification via qRT-PCR .....	167
7.3.3	Detection limits of NanoString® technologies using microbiopsy samples .	170
7.3.4	Generation of indexed cDNA library .....	172
7.4	Conclusions.....	174
<b>Chapter 8 General Discussion, Conclusions and Future Directions.....</b>		<b>175</b>
8.1	Comparisons of current sampling approaches.....	177
8.2	Fabrication of the microbiopsy device .....	178
8.3	Microbiopsy characterisation and optimisation.....	179
8.4	Microbiopsy applications in dermato-oncology.....	180
8.5	Microbiopsy applications in the research arena .....	181
8.6	Smart-integration of microbiopsy.....	182
8.7	Conclusions.....	183
References .....		185
Appendices.....		196
Appendix 1 – p53/Rb Pathway Mutation PCR Array Genotype Call (n=4).....		196
Appendix 2 – Real-time PCR results summary.....		220
Appendix 3 – Ethics Approval and Publications.....		222

## **List of Figures**

- Figure 1.1** Skin biopsy techniques.
- Figure 1.2** Cross-polarised light dermoscopy in melanoma diagnosis.
- Figure 1.3** Total body photography system from Dermagraphix™ imaging software.
- Figure 1.4** Set-up of reflectance confocal microscopy.
- Figure 1.5** Capacity of OCT images to histology to detect structural changes.
- Figure 1.6** Illustrations of fused deposition modelling process.
- Figure 1.7** Illustrations of laminated object manufacturing process.
- Figure 1.8** Schematics of step-by-step stereolithography process.
- Figure 1.9** Diagrams of the Objet's PolyJet™ technology process.
- Figure 1.10** Illustrations of selective laser sintering operations.
- Figure 1.11** Illustrations of electron beam melting process.
- Figure 1.12** Schematics showing the formation of high velocity in water-jet cutting head.
- Figure 2.1** Folding of two-dimensional micro biopsy cutting die.
- Figure 2.2** Assembly of micro biopsy cutting die.
- Figure 3.1** Laser cut set-up schematics.
- Figure 3.2** Correlation of laser power and cutting speed.
- Figure 3.3** Extended cutting element of micro biopsy cutting die.
- Figure 3.4** Laser power optimisation.
- Figure 3.5** Laser frequency optimisation.
- Figure 3.6** Laser power and speed optimisation.



- Figure 3.7** Repeat of laser frequency optimisation.
- Figure 3.8** Laser speed optimisation.
- Figure 3.9** Laser power optimisation.
- Figure 3.10** Laser speed optimisation using single needle micro biopsy.
- Figure 3.11** Laser frequency optimisation using single needle micro biopsy.
- Figure 3.12** Width and length measurements of array micro biopsies.
- Figure 3.13** Channel width measurements of single micro biopsies.
- Figure 3.14** Functionality test of micro biopsy cutting die.
- Figure 3.15** Functionality test of tapered tip cutting die.
- Figure 3.16** Functionality test of cutting die with 0.01 mm thick outer plates.
- Figure 4.1** Size comparison of needle biopsy devices and biopsy comparisons.
- Figure 4.2** In-house micro biopsy applicator.
- Figure 4.3** Conventional punch biopsy and micro biopsy sites and biopsy materials.
- Figure 4.4** Site of micro biopsy and micro biopsy content.
- Figure 4.5** Visualisation and quantification of tissue biopsy from micro biopsy device.
- Figure 4.6** DNA isolation kits comparison.
- Figure 4.7** Preliminary channel width experiment.
- Figure 4.8** Preliminary surface roughness experiment.
- Figure 4.9** Preliminary application velocity experiment.
- Figure 4.10** Wound healing kinetics of micro biopsy site.
- Figure 4.11** Micro biopsy channel width optimisation.

- Figure 4.12** Application velocity optimisation.
- Figure 4.13** Roughness amplitude optimisation.
- Figure 4.14** Geometry and surface texturing optimisation.
- Figure 4.15** Molecular characterisation of conventional shave biopsies and microbiopsies.
- Figure 5.1** Microbiopsy sample collection and site documentation.
- Figure 5.2** Clinical and histomicrograph of a compound dysplastic naevus.
- Figure 5.3** Clinical and histomicrograph of a junctional lentiginous naevus.
- Figure 5.4** BRAF<sup>V600E</sup> negative case study.
- Figure 5.5** BRAF<sup>V600E</sup> positive case study.
- Figure 5.6** Surveillance of naevi in male patient on clinical trial with BRAF inhibitor and/or MEK inhibitor drugs.
- Figure 5.7** BRAF<sup>V600E</sup> mutation status in regressed and stable naevi.
- Figure 5.8** The targeted skin microbiopsy.
- Figure 5.9** Case study demonstrating precision microbiopsy sampling.
- Figure 5.10** BRAF mutations from microbiopsy samples.
- Figure 5.11** Quantitating BRAF<sup>V600E</sup> mutations from microbiopsy samples.
- Figure 6.1** Schematic and clinical photographs showing ZnO-NP administration to volunteers followed by microbiopsy enabled oxidative stress analysis.
- Figure 6.2** Confocal microscopy images of microbiopsies.
- Figure 6.3** Confocal microscopy images of microbiopsies.
- Figure 6.4** Analysis of oxidative stress in volunteers of cells exposed to topical application of ZnO-NPs.

- Figure 7.1** Comparison of conventional and targeted MS.
- Figure 7.2** Schematic of digital mRNA profiling technology.
- Figure 7.3** Schematics of protein handling and analysis.
- Figure 7.4** Detection and quantification of RPLP0 in microbiopsies.
- Figure 7.5** Detection and quantification of RPLP0 and tyrosinase genes in microbiopsies.
- Figure 7.6** Multiplex gene expression count using NanoString® technology.
- Figure 7.7** Comparison of microbiopsy and sample input in varying concentrations across different levels of gene expression.
- Figure 7.8** cDNA library synthesis validation.
- Figure 8.1** Developmental process of the microbiopsy device.

## **List of Tables**

- Table 1** Sampling techniques to collect tissue or constituents.
- Table 2** Advantages, disadvantages of different rapid prototyping processes.
- Table 3** Advantages and disadvantages of current microneedle fabrication methods.
- Table 4** Comparison of the benefits and limitations of different cutting techniques.
- Table 5** Laser parameters used for micro-texturing of cutting die.
- Table 6** Genotype outcome comparing microbiopsy and saliva samples.
- Table 7** Summary of positive mutation calls in p53/Rb pathway PCR array.
- Table 8** Average gene coverage and read depth of ATM, CDKN2A, RB1 and TP53 genes
- Table 9** List of proteins detected in pooled microbiopsy sample.
- Table 10** Relative quantification of identified peptides.

## **List of Abbreviations**

AK	Actinic keratoses
ANOVA	Analysis of variance
ARMS	Amplification refractory mutation system
ATM	Serine/threonine protein kinase
AWJ	Abrasive water-jet cutting
BCC	Basal cell carcinoma
BRAF	B-Raf proto-oncogene
CAD	Computer-aided design
CAM	Computer-aided manufacturing
CCT	Caprylic capric triglycerides
CDKN2A	Cyclin-dependent kinase inhibitor 2A
CNC	Computer numerical control
DPI	Dots per inch
EBM	Electron beam melting
EGIR™	Epidermal genetic information retrieval
ELISA	Enzyme-linked immunosorbent assay
FDM	Fused deposition modelling
FLIM	Fluorescence lifetime imaging microscopy
HAZ	Heat affected zone
HFU	High frequency ultrasound

IHC	Immunohistochemistry
IEC	Intraepidermal carcinoma
LASOX	Laser-assisted oxygen cutting
LC-MS/MS	Liquid chromatography-tandem mass spectrometry
LOM	Laminated object manufacturing
MAQC	MicroArray Quality Control
MALDI-TOF	Matrix-assisted laser desorption ionization time-of-flight
MEMS	Micro-electromechanical system
MN	Microneedles
MC1R	Melanocortin 1 receptor
mRNA	Messenger ribonucleic acid
MS/MS	Tandem mass spectrometry
NAD(P)H	Nicotinamide adenine dinucleotide phosphate
NMSC	Non-melanoma skin cancer
NRAS	Neuroblastoma RAS viral (v-ras) oncogene homolog
OCA2	Oculocutaneous albinism II
OCT	Optical coherence tomography
OTR	Organ transplant recipients
PBS	Phosphate buffered saline
PCR	Polymerase chain reaction
PWJ	Plain water-jet cutting

qRT-PCR	Quantitative reverse-transcriptase polymerase chain reaction
QqQ	Triple quadrupole mass spectrometer
R <sub>A</sub>	Surface roughness
RCM	Reflectance confocal microscopy
RNA-Seq	RNA sequencing
RP	Rapid prototyping
SCC	Squamous cell carcinoma
SDS-PAGE	Polyacrylamide gel electrophoresis
SEM	Scanning electron microscopy
SGC	Solid ground curing
SLA	Stereolithography apparatus
SLS	Selective laser sintering
SNP	Single nucleotide polymorphism
<i>t</i> BHP	<i>Tert</i> -Butyl hydroperoxide
TP53	Tumor protein p53
TEWL	Trans-epidermal water loss
TBP	Total body photography
UV	Ultraviolet
ZnO-NP	Zinc oxide nanoparticles
2D	Two-dimensional
3D	Three-dimensional

# Chapter 1

## *Introduction and Literature Review*

### 1.1 Introduction

Australia has the highest skin cancer burden compared to the rest of the western world. The total cost for treating non-melanoma skin cancer (NMSC) and melanoma in 2001 was \$264 million and 30 million (Goss J. and Mann N., 2005), ranking skin cancer the most expensive treatment among all cancers (Fransen et al., 2012). Conventional biopsy techniques can provide accurate prognosis of the disease occurrence and progression but they are painful, often require suture, and render the area unsuitably damaged for further scientific study. Patients may be present with many questionable lesions and removing that many lesions is impractical. The development of a minimally invasive biopsy device could prove to be useful in detecting skin cancer earlier and resolving some difficult differential diagnoses. Furthermore, molecular fingerprinting of skin disease has the potential to dramatically improve diagnostic sensitivity and open the door for personalised medicine.

Animal testing of cosmeceutical ingredients have been banned in many countries including the European Union, Norway, Israel and India. Association of Southeast Asian Nations, United States (USA) and South Korea are also moving forward to introduce this legal prohibition. The closest alternative to animal testing for toxicity screening is done *in vitro*. Toxicology and efficacy studies of drug candidates and chemicals can be performed in live cells acquired by the Microbiopsy devices. Accordingly, it provides a more relevant system to execute these assessments. The Microbiopsy is developed for skin tissue sampling in human adults for molecular analysis and toxicology assessment, but its application can also be extended into paediatrics and animal studies. This Thesis discusses the development and validation processes of the first minimally invasive micro sampling tool for the skin.



## 1.2 Conventional skin sampling for diagnostics in dermatology

Skin biopsy is one of the most essential techniques that results in accurate diagnosis of melanoma and NMSC through histopathological assessment. This technique is performed under local anaesthetic by trained personnel, normally a dermatologist, to remove a small skin sample (2 - 4 mm) that is then sent to a pathologist for histopathological examination. Pathological examination using skin biopsy often complements and/or confirms the diagnosis of common neoplastic skin diseases where clinical appearance of lesions is insufficient to obtain an accurate diagnosis (Sina et al., 2009). Incisional (**Figure 1.1a and 1.1b**) and excisional biopsies are the two main types of skin biopsies. Incisional biopsy involves partial removal of a lesion, and is preferred when a wider or deeper portion of the skin is needed. An excisional biopsy is performed when the entire tumour is needed for histopathological examination, or when melanoma is suspected (Pickett, 2011b). There are six key biopsy techniques to perform biopsy of the skin. The selection to the type of

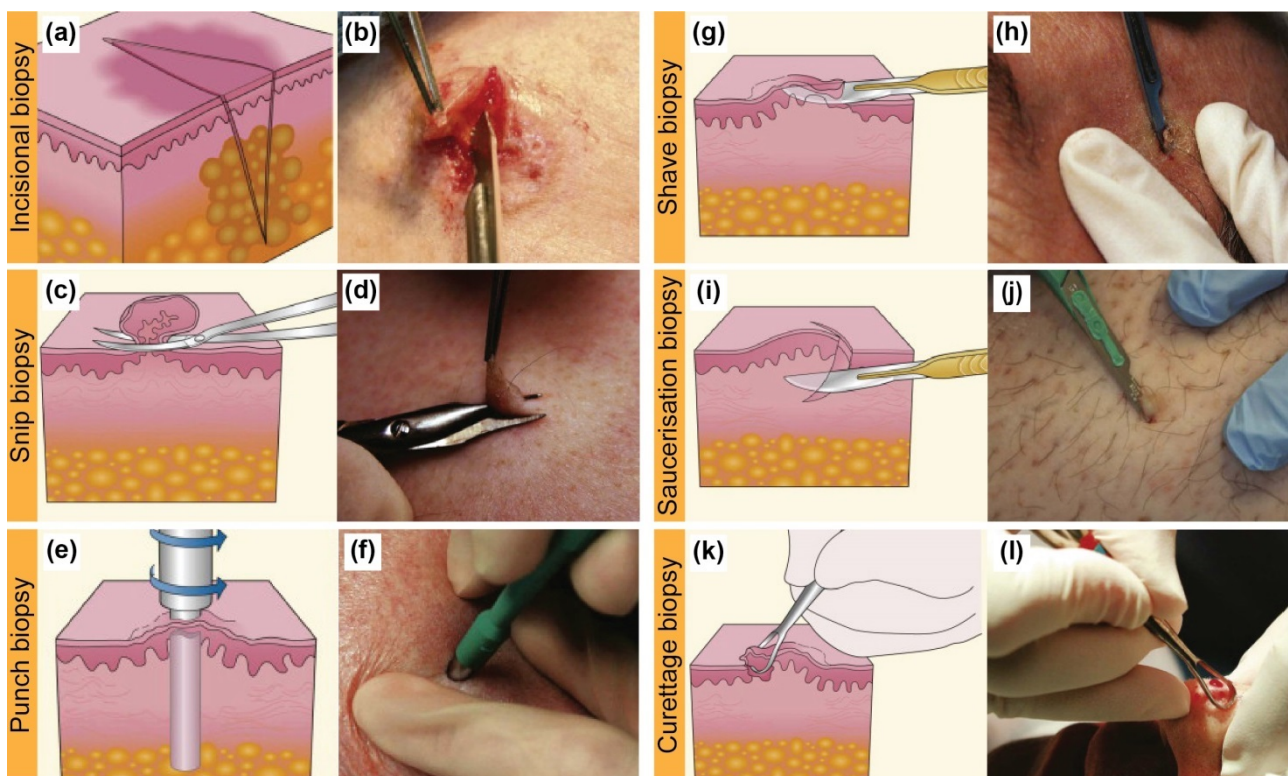


**Figure 1.1: Skin biopsy techniques.**

Diagrams and clinical photographs of different skin biopsy procedures including incisional biopsy (a – b), snip biopsy (c – d), punch biopsy (e – f), shave biopsy (g – h), saucerisation biopsy (i – j), and curettage biopsy (k – l). Figure modified with permission from (Bolognia et al., 2012) Copyright © 2012, Elsevier.

technique employed depends on the type and size of lesion (Bologna et al., 2003).

### **1.2.1 Snip biopsy**

Snip or scissors biopsy are used to remove extruding elongated (i.e. pedunculated) lesions (**Figure 1.1c and 1.1d**). Lesions with very narrow neck can be quickly biopsied without the need for local anaesthetic. The tissue is held by a toothed forceps and the lesion is detached from the base of the skin using a pair of fine iris or sharp gradle scissors. This method of biopsy produces small and often hypo-pigmented macule that may be hard to identify (Bologna et al., 2003).

### **1.2.2 Punch biopsy**

Punch biopsy is the primary procedure physicians use to obtain full-thickness skin samples of inflammatory skin lesions (**Figure 1.1e and 1.1f**). The size of punch biopsy available ranges from as small as 0.35 mm and up to 12 mm. The standard of care is to take a biopsy for conventional histopathological examination but a 0.35 mm punch biopsy is too small for such analysis. Typically, a cylindrical piece of tissue is obtained by rotating and pressing the circular blade into the skin's topmost subcutaneous fat. The skin specimen must be carefully removed using a fine needle to avoid artefacts. Punch biopsy is potentially useful for diagnosis of inflammatory lesions and is also often used for neoplastic skin conditions. This simple technique can be taught easily and gives similar cosmetic outcome for 1 to 4 mm biopsies. On the down side, this procedure may not provide sufficiently wide skin specimen depending on the lesion, given the narrow and deep nature of biopsy. This might affect prognosis and tumour staging but the error can be minimized by taking multiple biopsies. Depending on the size of the skin lesion, the most common sizes of punch biopsy that are routinely used in the clinics are 2-4 mm. Other limitations include the need for local anaesthetic, bleeding, need for suture, and possible damage to arteries, veins or nerves on thin skin areas (e.g. face or dorsum of hand) (Australian Cancer Network Melanoma Guidelines Revision Working Party, 2008, Pickett, 2011b, Sina et al., 2009, Zuber, 2002).

### **1.2.3 Shave biopsy**

Shave biopsies are shallow removal of lesions confined to the depth of the dermis (**Figure 1.1g and 1.1h**). The technique is performed using a scalpel, dermablade, a razor blade, or scissors. Shave biopsies are most commonly performed because it is a low cost

procedure, easy to perform, and have simple post-biopsy wound care. Shave biopsies are commonly used for lesions that are mainly epidermal, such as warts, papillomas, skin tags, superficial basal cell carcinoma (BCC) or squamous cell carcinoma (SCC), and seborrheic or actinic keratoses (AK) and not melanomas (Pickett, 2011b, Swanson et al., 2002).

#### **1.2.4 Saucerisation (deep scoop shave)**

A saucerisation or deep scoop shave, as the name implies, is a biopsy that involves excision through viable dermis and into the reticular dermis or even sub-cutis (**Figure 1.1i and 1.1j**). The procedure is quick and easy to perform, and leaves an oval scar. This technique provides adequate tissue for histopathological examination. The disadvantage of saucerisation is the occurrence of scoop scars that reform over many years that may include residual melanocytic lesions left over by an incomplete excision. These recurring naevi resemble the appearance of a melanoma that is hard to distinguish, and may result in a second excision causing distress to the patient (Swanson et al., 2002).

#### **1.2.5 Curettage biopsy**

Curettage biopsy (**Figure 1.1k and 1.1l**), also known as the broad superficial shave biopsy, provides a larger area of epidermis for histology. However, this technique usually does not remove sufficient dermis for full assessment of invasion. Hence, curettage biopsy is limited to lesions that are likely to be confined to the epidermis. This biopsy method involves applying pressure under or through the lesion using a curette that is 3 – 5 mm in diameter. The benefit of curettage biopsies is that the patient will heal with little or no scarring, with resulting good cosmesis (i.e. biopsies can be performed on sensitive areas such as the face) (Australian Cancer Network Melanoma Guidelines Revision Working Party, 2008, Bologna et al., 2003).

#### **1.2.6 Excisional biopsy**

This technique is commonly performed by dermatologists as well as family physicians for removal of full-thickness lesions. Excisional biopsy has been previously referred to as an elliptical biopsy because of the biconcave appearance of the wound. The incision area should have a three to one length-to-width ratio which will give an angle of less than 30 degrees at the ends of the wound. Typically, doctors who are experienced in skin surgery can often perform the procedure unsupervised after two to five guided sessions. It is a technique that offers cosmetic and diagnostic advantages in certain clinical situations. The

excisional technique is recommended for obtaining biopsy samples of any pigmented lesions that is suspected as melanoma (Zuber, 2003).

### 1.3 Emerging skin sampling techniques for biomolecular diagnostics

Histopathological assessment is the reference standard for many inflammatory and neoplastic skin diseases but it is limited by the qualitative nature and analytical variability (Taylor, 2000). The changes in skin biochemistry have been widely observed in various skin diseases. These biomolecular changes can provide opportunities for disease diagnosis and to assess therapeutic responses. Conventional skin biopsy is one of the common methods to sample the skin's biomolecular information as it allows collection of partial to full thickness of skin. This method, however, is unsuitable as a routine approach due to its invasive nature (SchroInberger et al., 2001), and the biomolecular extraction approaches from these samples are usually multi-step and technically involved.

Less invasive techniques are necessary as alternative diagnosis if monitoring of the lesions over time is required. Techniques such as tape-stripping, iontophoresis, ultrasound, suction-blister, microneedle, electroporation are some of the less invasive or minimally invasive methods to sample skin tissue or constituents. The pros and cons of these techniques are summarised in **Table 1**. Most of these techniques are developed to sample small molecules including drugs, protein and peptides (Rao et al., 1995, Benfeldt et al., 1999, Schmelz et al., 1997, Kost et al., 2000, Mukerjee et al., 2004, Escobar-Chavez et al., 2008, Paliwal et al., 2010, Nair et al., 2014) to study pharmacokinetics and monitoring of therapeutic drugs etc. Conventional skin biopsy and tape-stripping are the only two methods that enable collection of skin cells for extraction of molecular materials (Morhenn et al., 1999, SchroInberger et al., 2001).

Starting in the late 1990s, tape-stripping has been employed as a non-invasive approach to sample messenger RNA (mRNA) to study cytokine expression profiles to differentiate irritant from immunological reactions (Morhenn et al., 1999). Wachsmann et al. have recently also demonstrated the non-invasive method of tape-stripping, together with a gene classifier, as an alternative method to detect genomic biomarkers for melanoma (Wachsmann et al., 2011). The group utilised a patented non-invasive method, epidermal genetic information retrieval (EGIR™), to sample RNA from stratum corneum using four pieces of custom adhesive tapes that successfully identified 312 differentially expressed

genes related to melanoma. With the use of a data mining algorithm, they subsequently developed a 17-gene classifier from the microarray dataset based on 39 melanomas and 89 naevi that provides 100% sensitivity and 88% specificity in melanoma detection.

**Table 1: Sampling techniques to collect skin tissue or constituents. Modified from (Paliwal et al., 2013), Copyright © 2013, Elsevier B.V.**

<b>Sampling methods</b>	<b>Advantages</b>	<b>Disadvantages</b>
Skin biopsy	Morphology, gold standard for skin diagnostics.	Most invasiveness, potential recovery problems, need of liquefying to assess native chemistry.
Tape-stripping	Rapid, convenient, minimally invasive.	Lack of standardised protocol and heterogeneous sampling.
Iontophoresis	Minimally invasive, administration for skin vessel reactivity.	Local irritation.
Ultrasound	Minimally invasive and bioreactive protein harvesting method with detergent mixture.	Potential denaturation of biomarkers, complex device.
Microdialysis	Minimally invasive and continuous method without contamination.	Time-consuming, long recovery time, not for large molecules and proteins, detection sensitivity.
Suction-blister	Simple and possible proteomic analysis.	Topical anaesthesia, time-consuming.
Electroporation	Minimally invasive.	Complex device, limited clinical data.
Microneedles	Minimally invasive and simple to use.	Possible irritation, limited data on extraction.
Submillimetre biopsy	Rapid, simple to use, minimally invasive, may not require local anaesthetic.	Insufficient sample for histopathological analysis.

Concurring with Wachsman et al., a minimally invasive sampling approach to discriminate benign from neoplastic lesions may provide more objective diagnosis than clinical assessment or optical diagnostics. It also improves patient care by subjecting reduced discomfort and possible risk of complications. These are the driving force behind the minimally invasive microbiopsy device that was described in this Thesis (Lin et al., 2013). Unlike the tape-stripping technique where non-nucleated cells (stratum corneum) are collected, the conventional skin biopsy device samples into the dermis. Thus, samples from this device can be processed for both DNA and RNA to analyse not only gene expression but also mutational profiling, DNA profiling and copy number variations. In addition, the noise-to-signal ratio in gene expression profiles of mRNA samples from tape-stripping will be higher than microbiopsy due to high content of corneocytes/keratinocytes within the samples. Therefore, skin biopsy samples can provide more robust detection. Other than the use of molecular analyses for facilitating diagnosis of suspicious lesions, the majority of current medical procedures to provide diagnosis and prognosis are performed using non-invasive tools and techniques. Other than clinical examinations, diagnostic imaging is the other non-invasive technology that is commonly carried out by physicians to assess states of health and disease.

#### **1.4 Non-invasive tools and techniques for skin diagnostics**

Conventional biopsy for histopathology assessment may be the gold standard for skin lesion diagnosis. However, it can be time-consuming, painful, and can be disfiguring in cosmetically sensitive areas. Given when 26.6% of assumed premalignant and malignant lesions were benign (Hallock and Lutz, 1998), this may lead to non-compliance in patients. Non-invasive imaging modalities were developed to provide examination and visualisation of the skin and its organisational structure without the need of conventional skin biopsy. These modalities have shown to increase diagnostic accuracy by improving the clinical examination and reducing variability between physicians (Goodson and Grossman, 2009), particularly in the pigmented lesions. The utility of these imaging modalities were established mostly in screening and diagnosis of melanoma (Ferrari et al., 2014, Salerni et al., 2014, de Giorgi et al., 2005). Dermoscopy and reflectance confocal microscopy (RCM) are one of the few imaging modalities which have shown promising results for accurate diagnosis of non-melanoma skin cancer (Longo et al., 2014a, Ulrich et al., 2008, Rishpon et al., 2009, Peppelman et al., 2014).

### 1.4.1 Dermoscopy

Along with training and experience, the use of dermoscopy can significantly increase clinical diagnosis of non-invasive clinical diagnosis of pigmented (melanocytic and non-melanocytic) and non-pigmented lesions. The dermatoscope (**Figure 1.2a**) is a magnifier that enables improved visualisation of colour and structures of skin that cannot be perceived by the naked eye (Soyer et al., 2011). The use of liquid interface conventional (non-polarised) or cross-polarised light dermoscopy phases out light reflection, increases the transparency of the stratum corneum and facilitates visualisation of the skin structure in deeper layers. In polarised dermoscopy, cross-polarisation of light as achieved with two filters (**Figure 1.2b**). Part of polarised light penetrates the skin and the rest is reflected at the stratum corneum. The penetrated light is backscattered and loses its polarisation after numerous scatterings. The superficially reflected light at the stratum corneum is selectively blocked by the second filter that is placed between the skin and the detector, while capturing the backscattered light from deeper layer of the skin to reach the eyes (Anderson, 1991).

The capabilities of conventional and polarised dermoscopy were different but comparable in patterns, colours and structures to varying extents (Benvenuto-Andrade et al., 2007). An example in the capability differences of conventional and polarised light dermoscopy is shown in **Figure 1.2c-d**. Better visualisation of the red areas such as the vessels was seen with the polarised dermoscopy. In addition, melanin that is seen as dots and streaks appeared darker and the blue naevi had more shades of blue. Other features like milia-like cysts, peppering, comedo-like openings, blue-white areas and lighter colours were enhanced with conventional dermoscopy (Benvenuto-Andrade et al., 2007).

Dermoscopy has been integrated with different non-invasive platforms including digital imaging system, computer-based analysis and laser-based technologies. The use of dermoscopy in combination with total body photography was proven beneficial in early diagnoses of skin cancer (Salerni et al., 2014).

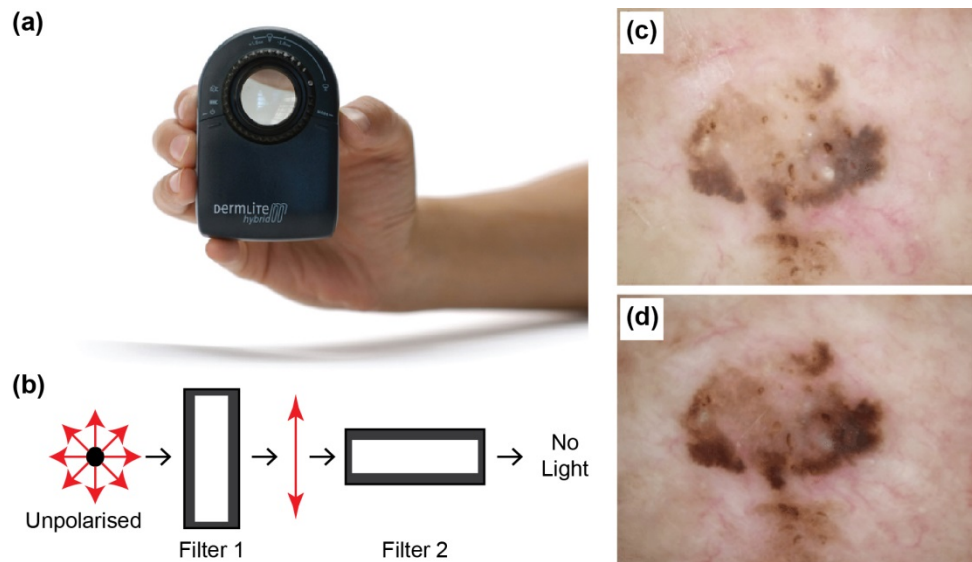


**Figure 1.2: Cross-polarised light dermoscopy in melanoma diagnosis.**

Panel (a) shows a commercially available hand-held polarised dermoscopy. Polarised light is formed when part of the non-polarising light passes through the first filter and emerged. Cross-polarised light is achieved when polarised light beam is blocked when passing through a second filter that is perpendicular to the first filter (b). Example of a seborrheic keratosis documented with a non-polarised dermoscopy and a polarised dermoscopy are shown in Panels (c) and (d) respectively. Figure modified with permission from (3Gen, 2014), Copyright © 2015, 3Gen and (Wang et al., 2008), Copyright © 2008, Blackwell Publishing Ltd.

### 1.4.2 Total body photography

Total body photography (TBP) (**Figure 1.3**) uses a series of high resolution digital photographs taken from different body sectors to screen for melanoma in high-risk patients. It was shown that patients with high total body naevi counts of more than 100 compared to those who had less than 10 naevi had increased risk of melanoma by 12 times (Grulich et al., 1996). A surveillance study over the course of 13 - 120 months was conducted to evaluate the value of two-step digital follow-up procedures (total body photography followed by dermoscopy) for early diagnosis of melanoma with 618 high risk patients (Salerni et al., 2012). A total of 11,396 lesions were monitored, and of which 1152 were excised and assessed for histopathology. Of the patients, 556 had moderate to severe atypical mole syndrome, where 57.6% had more than 100 naevi. Approximately 44.8% had personal history of melanoma and 28.8% had a familial history of melanoma. In total, 53 melanoma in-situ (0.05%) and 45 invasive melanomas (0.04%) with less than 1



mm Breslow index were diagnosed from the 1152 excised lesions. Salerni et al. (2012) concluded that the dual modality allowed detection of early stage melanoma that had few dermatoscopic features or were new or had arisen from monitored existing naevi.

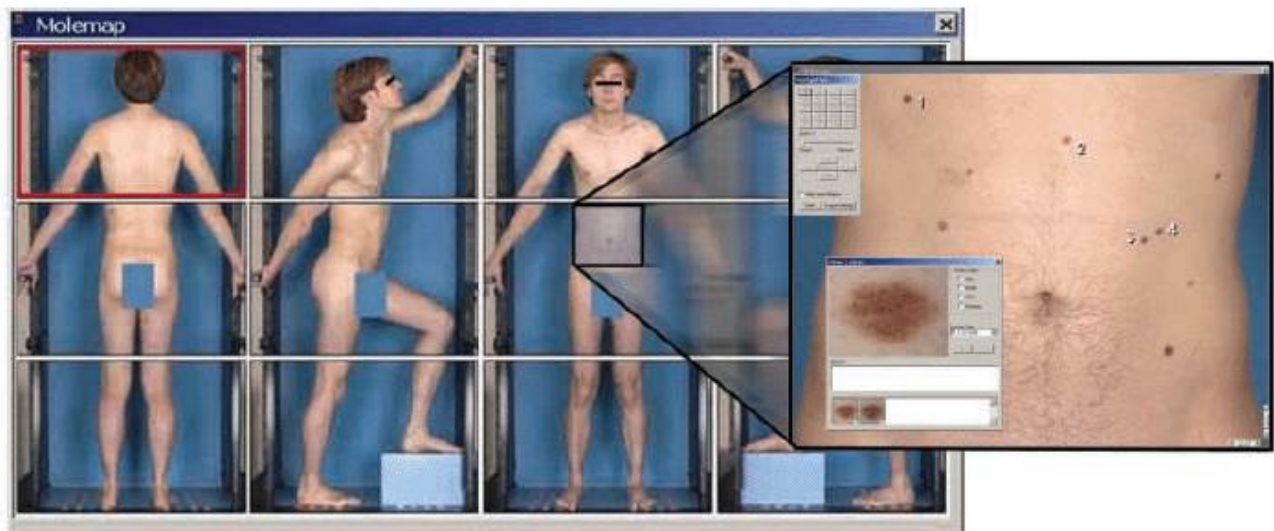


**Figure 1.3: Total body photography system from Dermagraphix™ imaging software.**

A series of body sectors in standard poses are documented from an individual to accurately map and track lesions, especially in pigmented lesions. Dermoscopy and close-up photographs are linked to individually marked lesions. Figure reproduced with permission from (Feit et al., 2004), Copyright © 2004, John Wiley & Sons, Inc.

Majority of the pigmented lesions are stable and do not undergo significant changes, while some regressed and new ones can appear over a course of time. This technique facilitates sequential comparison of lesions, enabling physicians to identify new and/or changing lesions (Feit et al., 2004). Out of the 93 biopsied melanocytic lesions, 43 of them (56%) were excised due to changes in color or size from baseline photographs. Twenty of these 43 (47%) melanocytic lesions were histologically diagnosed as malignant melanoma. A total of 18 lesions (23%) were newly identified lesions from baseline and of which, five (28%) were diagnosed as malignant melanoma. Feit et al. have concluded from their study that TBP has facilitated detection of melanoma by monitoring subtly changing lesions and identifying newly appeared ones. They concluded that TBP provided valuable information to prevent unnecessary biopsy of suspicious but stable melanocytic lesions (Feit et al., 2004).

Risser et al. compared the number of biopsies in 128 patients who received either total body examination alone to those who were assessed in combination with TBP to determine the impact of this technique on the rate of biopsy (Risser et al., 2007). The average number of biopsy was similar for patients who only had total body examination and those who received TBP (0.82 vs. 0.8, respectively). They did not observe an effect of TBP on the number of biopsies and on the number of dysplastic naevi based on the chart review analysis. Unlike Feit et al., they had a control patient group to determine whether TBP has any impact of the biopsy rate. The limitation of their study was the lack of information on the reason for biopsy due to the study design and the number of patients reviewed were also smaller. However, they did support that TBP allowed detection of changes in melanocytic lesions and this has changed the physicians' behavior in biopsy decision-making (Risser et al., 2007). The downside of this technology is the variable cost involved as it is dependent on the sophistication of the equipment used.

#### **1.4.3 Reflectance confocal microscopy**

Reflectance confocal microscopy (RCM) or confocal scanning laser microscopy (CSLM) enables real-time *in vivo* examination of the skin using the visible or near-infrared range low power laser. The first rapid RCM prototype that had the capacity to provide high-resolution and good correlation compared to conventional histology was built by Rajadhyaksha and his colleagues in 1995 (Rajadhyaksha et al., 1995). RCM is the only technique that has the necessary resolution for histological analysis. The low power laser creates a small beam spot that is focused at the skin. Light that is reflected from the focal point towards the objective lens that is then focused through a pinhole spatial filter and detected by the photodetector at the back (**Figure 1.4a**). The cellular organisation and structure details that can be seen within the dermoscopy image (**Figure 1.4b** and **d**) are translated into a two to 5  $\mu\text{m}$  thick optical section (**Figure 1.4c** and **e**).

Different epithelial tissues such as skin and oral mucosa in their healthy and diseased states have been characterised with RCM (Contaldo et al., 2013, Gonzalez et al., 1999, Wurm et al., 2012, Rishpon et al., 2009). This imaging platform has been proven as a useful diagnosis tool to detect melanoma and non-melanoma skin lesions, particularly BCC (Nori et al., 2004, Pellacani et al., 2014, Rishpon et al., 2009, Ulrich et al., 2008).

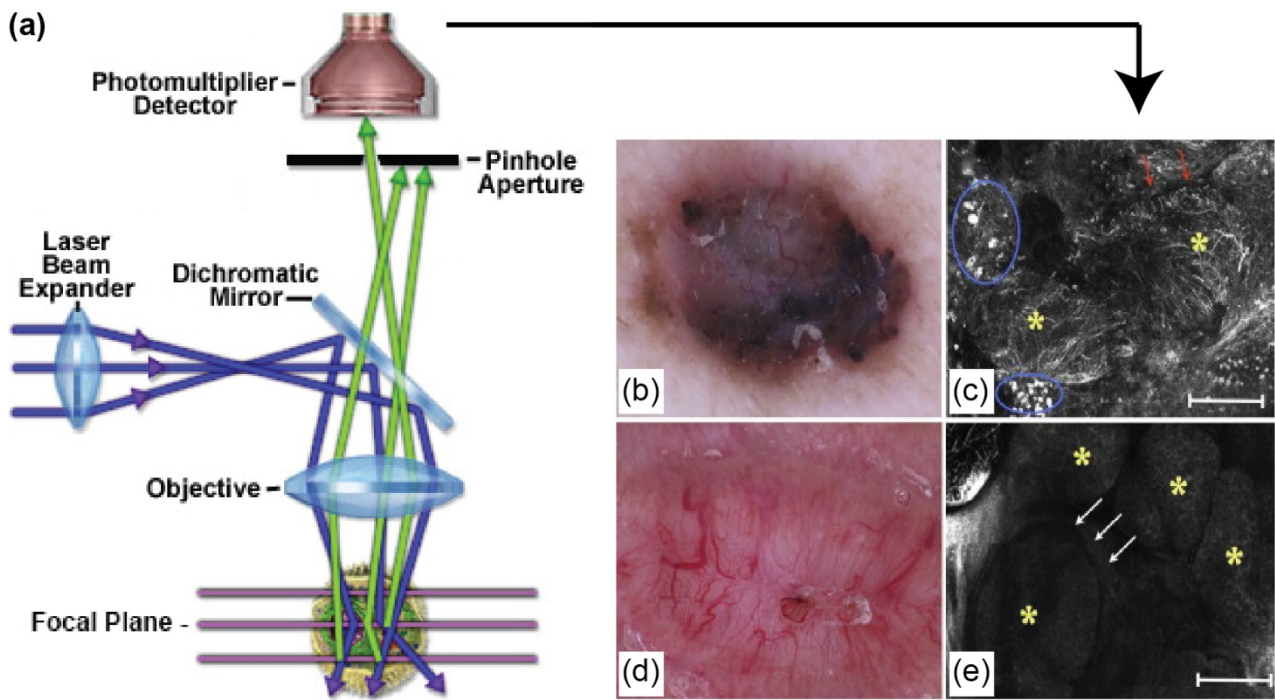


**Figure 1.4: Set-up of reflectance confocal microscopy.**

Panel (a) illustrates the optical set-up of the reflectance confocal microscopy. Figure modified with permission from (Piston et al., 2013) Copyright © 2013 Nikon and (Longo et al., 2014b) Copyright © 2014 Elsevier B.V.

Nori et al. completed a multicenter, retrospective study where they aimed to determine the sensitivity and specificity of RCM images for BCC diagnosis (Nori et al., 2004). Additionally, they combined photography-based clinical assessment and RCM to determine if this approach will provide more accurate diagnosis of BCC. Out of the 152 skin lesions, 83 BCCs were clinically detected and confirmed by histopathology. Blinded retrospective analysis based on 5 selected diagnosis criteria that were previously identified (Gonzalez and Tannous, 2002) was performed to assess the correlation of these characteristics in BCC lesions. The sensitivity and specificity for presence of  $\geq 2$  criteria was 100% and 53.6%, respectively. Increasing the number of criteria to  $4 \geq$  decreased the sensitivity to 82.9% but increased the specificity for BCC to 95.7%. Two dermatologists categorised the likelihood of BCC diagnosis based on high quality clinical images alone and when used in combination with RCM analyses. The addition of RCM analyses increased the diagnosis from 58.72% to 90.74% in the high probability category while the accuracy was increased to 90.00% from 47.06% in the low probability category. The study concluded that diagnosis of BCC using presence of 4 or more RCM criteria provided the

most ideal compromise, enabling accurate detection with high sensitivity and specificity (Nori et al., 2004).

Pellacani and his colleagues also found that the use of RCM provided a second-level examination that improved diagnostic accuracy in equivocal lesions and can prevent unnecessary excisions (Pellacani et al., 2014). This conclusion has also been established in other studies (Pellacani et al., 2007, Guitera et al., 2009, Segura et al., 2009, Gerger et al., 2008). They have shown that RCM had recommended excision for 23 melanomas and 19 BCCs, 121 Clark naevi eight Spitz naevi and 12 benign non-melanocytic lesions. Eighty-three percent of 23 melanomas and 95% of 19 BCCs of same diagnosis that was confirmed with histopathology was made using RCM. RCM was proven to provide 76.3% diagnostic accuracy for melanomas and 89.4% for BCCs. The number of benign lesions that was excised for every melanoma (NNE) reduced from 14.6 to 6.8 with RCM examination (Pellacani et al., 2014). The ability of RCM to distinguish precancerous from malignant lesions is also true for an SCC model. RCM features such as presence of architectural disarray in the viable epidermis and nest-like structures in the dermis resulted in significant odd ratios for SCC (11.0 to 24.0). The presence of architectural disarray in stratum granulosum alone in combination of all three features provided diagnosis accuracy between 84.6% to 88.5% (Peppelman et al., 2014).

One of the limitations RCM faces is the penetration depth of the technology. The maximum imaging depth is between 150 to 200  $\mu\text{m}$  and images past this become unclear. This limits the usefulness of RCM to only non-thickened skin area. Another limitation is pathology diagnosis as the images are presented in black and white, depending on the reflective index of the cellular structures, while conventional histopathology has colour and immunohistochemistry information. This requires training and experience in order to competently make a diagnosis.

#### **1.4.4 Optical coherence tomography**

Optical coherence tomography (OCT) is based on low coherence interferometry to generate two- or three-dimensional cross-sectional images by detecting the intensity of backscattered light and echo delays. This technique is similar to that of high frequency ultrasound (HFU) imaging only that the latter measures acoustic waves instead. Maximum imaging depth is achieved by targeting the window of transmission where the absorption

and scattering in the specimen is minimised. In the case of tissue imaging, this window of transmission is attained with a wavelength between 700 and 1300 nm (Gambichler et al., 2011).

OCT has been widely used in the field of ophthalmology to measure retinal thickness (Massin et al., 2001, Lim et al., 2005, Alamouti and Funk, 2003). This technology was then introduced in dermatology in the late 1990s. The OCT has an optical resolution of 3-15  $\mu$ m and can image up to 1 mm in depth (Kardynal and Olszewska, 2014). Hinz et al. have shown that OCT has a stronger correlation with histopathology than HFU (Spearman correlation,  $r = 0.734$ ) (Hinz et al., 2011). They compared the tumor thickness of 26 melanocytic lesions measured from histopathology to OCT and HFU. The median tumor thickness on histopathology was 0.25 mm while OCT and HFU were 0.31 mm and 0.44 mm, respectively. They concluded that OCT provides more accurate tumour depth than HFU that is frequently used for surgical planning for cutaneous melanocytic lesions (Hinz et al., 2011). OCT may have a lower resolution compared to RCM but it can provide real-time imaging to detect gross alteration in skin structure that can be easily correlated to conventional histopathology (**Figure 1.5**). Others have also demonstrated that OCT has potential to discriminate benign from malignant skin lesions (Gambichler et al., 2007, Boone et al., 2015). This may be one explanation for the rapid gain of popularity of this technology for clinical diagnostics. Despite the advances made in optical imaging for clinical diagnosis, all these technologies are limited either by the imaging penetrance depth, optical resolution and/or the need of training/experience. The lack of objective diagnosis also applies to optical diagnoses. Therefore, there is a need of a suitable sampling tool that can be used routinely for molecular diagnosis. This drives the invention of minimally invasive micro-devices in many medical fields.

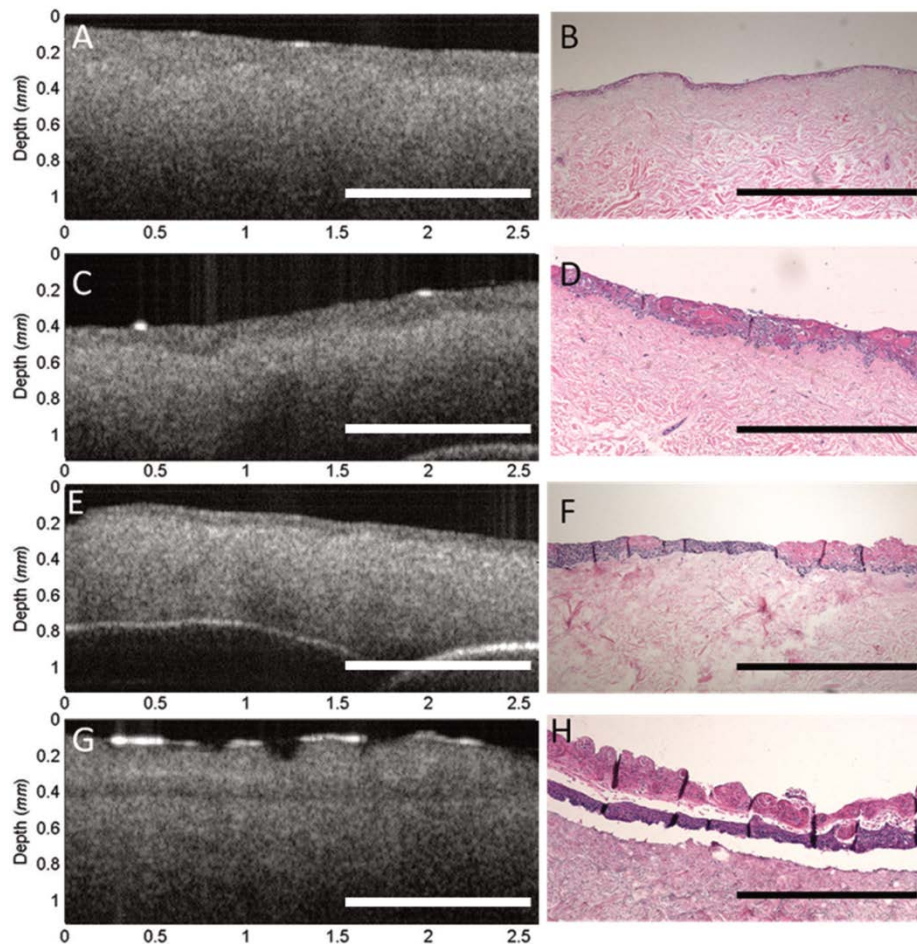


**Figure 1.5: Capacity of OCT images compared to histopathology to detect structural changes.**

Examples of OCT images compared to corresponding histopathology sections in various tissue engineered skin models: oral mucosa (a and b), D20 model of invasive carcinoma (c and d), severely dysplastic skin (e and f) and Cal27 model of invasive carcinoma. Reproduced with permission from (Smith et al., 2011), Copyright © 2011, SPIE.

## 1.5 Novel minimally invasive tools for micro-sampling

There is an emergence of micro devices for minimally invasive tissue biopsy since mid-1990s. Experimental diagnostic devices are evolving towards miniaturised version of their predecessors. This miniaturisation trend is supported by improved micro-manufacturing. The results of these efforts are usually first published as patents and patent applications. One of the earliest micro-devices developed to obtain biopsy was patented by Krulevitch et al. (Krulevitch et al., 1999). Their invention involves microbiopsy/precision cutting devices

fabricated by conventional machining, silicon micromachining, precision machining and injection moulding.

Pflueger and Capistrano filed a patent in 2004 for claims of a novel micro-invasive breast biopsy device. The device contains a handpiece coupled with motorised tissue removal mechanism. Part of the tissue removal mechanism includes a cannula with a rotatable element to allow extension of an open distal tip with an outer diameter of  $> 5\text{mm}$ . The extension of the distal tip past the rotating element will facilitate tissue biopsy samples to prolapse with each turn of the helical threading (Pflueger, 2002).

Another research group from Korea in 2005 published findings of their micro-scale biopsy tool prepared using crystal silicon. The tool is a single planar micro-spike with a dimension of 3 mm (length) by 0.250 mm (width) by 0.100 mm (thickness). Their findings concluded that the micro-scale biopsy tool requires protruding barbs to facilitate successful tissue biopsy as those features help to tear off and retain tissue samples. The team effectively obtained biopsy samples from small intestine of the anaesthetised rabbit and pig (Byun S., 2005). Seven years after publishing their first data on the device, they filed a patent to introduce the device as a micro-electromechanical system-based (MEMS) micro-biopsy catheter that includes a disposable micro-biopsy tool (Cho D., 2011).

Over the years since this patent, there have been many similar patents that report a variety of devices. These micro-scale biopsy devices were all developed to biopsy non-stratified epithelium tissue, and none for stratified epithelium tissue such as the human epidermis. The advances in rapid prototyping technologies over the last two decades have enabled significant development of micro- and nano-size devices using laser-based rapid prototyping methods (Gittard and Narayan, 2010, Lu and Chen, 2004). These small scale devices are mostly used in drug delivery and regenerative medicine. However, these rapid prototyping technologies can also be used to fabricate small medical devices for other biological applications (Henry et al., 2009, Martinez et al., 2008, Lin et al., 2013, Gomaa et al., 2012).

## **1.6 Fabrication of micro devices**

Rapid prototyping (RP), also known as solid freeform fabrication, is the physical creation or assembly of a three-dimensional (3D) object using computer-aided design (CAD),

computer-aided manufacturing (CAM) or computer numerical control (CNC) technologies. It was first developed in the 1980s to enable the fabrication of a model or prototype parts without the need of conventional manufacturing tools and processes. In this present time, the advances from RP technologies can create not only prototypes in plastic materials but also good quality finished products.

There are three fundamental rapid prototyping processes: additive, subtractive and formative. Most RP processes are based on additive manufacturing or fabrication. Additive RP involves depositing of sequential layers until the desired object is formed. Examples of these processes include stereolithography apparatus (SLA) and solid ground curing (SGC). On contrary, the subtractive prototyping process starts off with a block of material and material is cut out until the desired form is achieved. They are mostly in the form of automated machining processes by CNC such as milling, laser cutting and water-jet cutting etc. The formative prototyping process requires application of mechanical or restrictive force to the portions of the material to create the desired form. These processes include bending, forging and injection moulding. Most of the current RP processes are based on additive operations. There are several means of classifying RP technologies and one common type of classification is by the form of the starting material: 1) solid-based, 2) liquid-based and 3) powder-based (Chua et al., 2010, Gene, 2007).

### **1.6.1 Solid-based RP processes**

#### 1.6.1.1 Fused deposition modelling

Fused deposition modelling (FDM) is a type of extrusion-based additive fabrication process (**Figure 1.6**) (Gene, 2007). The dimensions of the part is translated into x, y and z coordinates that is controlled by a computer system to direct the nozzle and build platform. It uses a thin filament of polymer that is fed through an extrusion nozzle. The polymers used in this process are known as thermoplastics that are mouldable when heated to a specific temperature and solidifies when cooled. The nozzle melts the filament of polymer, extrudes and deposits thin beads of molten materials onto the build platform. The nozzle moves in the XY axes and prints the cross-sectional layer, which has a typical thickness of 0.25 mm, of the part using the melted polymer (Wong and Hernandez, 2012). Each layer goes through a cooling period where the polymer hardens and binds to the layer beneath it.



**Table 2: Advantages and disadvantages of different rapid prototyping technologies.**

Rapid prototyping technologies	Advantages	Disadvantages
Fused deposition modelling	<p>No post processing required.</p> <p>No curing of build parts.</p> <p>Materials are stable and do not change with time or environmental exposures.</p> <p>Materials are non-toxic.</p>	<p>Low z-axis resolution of 0.25 mm.</p> <p>Rough surface finish.</p> <p>Relatively slow fabrication process.</p>
Laminated object manufacturing	<p>Build is self-supported.</p> <p>Build parts do not warp, deform or shrink.</p>	<p>Not suitable for making parts with complex internal cavities.</p> <p>Requires installation of a chimney or filtration system to remove fumes.</p>
Stereolithography apparatus	<p>Ability to build parts with multiple materials.</p> <p>Mass manufacturing is quick and inexpensive.</p> <p>Fully automated process.</p> <p>Good dimensional accuracy (<math>\pm 0.1</math> mm).</p> <p>High z-axis resolution of <math>&lt; 0.01</math> mm available with microstereolithography.</p> <p>Good surface finish.</p>	<p>Warping of thin areas.</p> <p>Incomplete curing in most areas of build parts.</p> <p>Labour intensive.</p> <p>High maintenance cost for optical sensors.</p> <p>Liquid may be trapped in parts with enclosed and hollow structures if cleaning or draining is not feasible.</p>

	<p>Ability to produce parts of any geometry.</p> <p>High quality end product comparable to CAD data.</p>	
Solid ground curing	<p>High-throughput process enabled by concurrent printing of multiple parts.</p> <p>Build parts do not warp, deform or shrink.</p> <p>Ability to reverse wrong operation.</p>	<p>Complicated fabrication process.</p> <p>High operation cost due to set-up and the need to monitor fabrication process.</p>
PolyJet™	<p>High-throughput process enabled by concurrent printing of multiple parts.</p> <p>No post processing required.</p> <p>Ability to build wide range of materials.</p> <p>Simple operation process.</p> <p>Materials are non-toxic.</p> <p>High quality end product comparable to CAD data.</p> <p>Good surface finish.</p> <p>Relatively good dimensional accuracy (<math>\leq 0.6</math> mm).</p>	<p>Unsuitable for an office environment due to need of water access for post processing.</p> <p>Thin or delicate parts may be damaged during cleaning.</p> <p>Wastage of support material as they are non-reusable.</p>

<p>Selective laser sintering</p>	<p>Ability to build wide range of materials.</p> <p>Relatively fast fabrication process.</p> <p>No curing of build parts.</p> <p>Good surface finish.</p>	<p>Build parts can shrink by 3-4%.</p> <p>Post processing required.</p> <p>Collection of excess powder on parts' surface.</p> <p>Potential porosity of build parts.</p> <p>Density of build parts may be variable.</p> <p>Requires the access of nitrogen gas.</p>
<p>Electron beam melting</p>	<p>Does not require support structures.</p> <p>Ability to prototype complex shapes.</p> <p>Relatively low maintenance and installation costs.</p> <p>Finishing is improved with vacuum environment.</p>	<p>Potential porosity of build parts.</p>
<p>Water jet cutting</p>	<p>Ability to cut any materials and particularly suitable for processing materials that are difficult to cut.</p> <p>Does not have any thermal effect on workpiece.</p> <p>Inflicts minimal stresses to workpiece.</p> <p>Water usage is very low and can be reused</p>	<p>Slower processing time than plasma cutting technology.</p> <p>Abrasive material is relatively expensive.</p>

	<p>using a closed looped system.</p> <p>Flexible and versatile with wide usage applications.</p> <p>Comparatively low installation and maintenance costs.</p>	
--	---	--

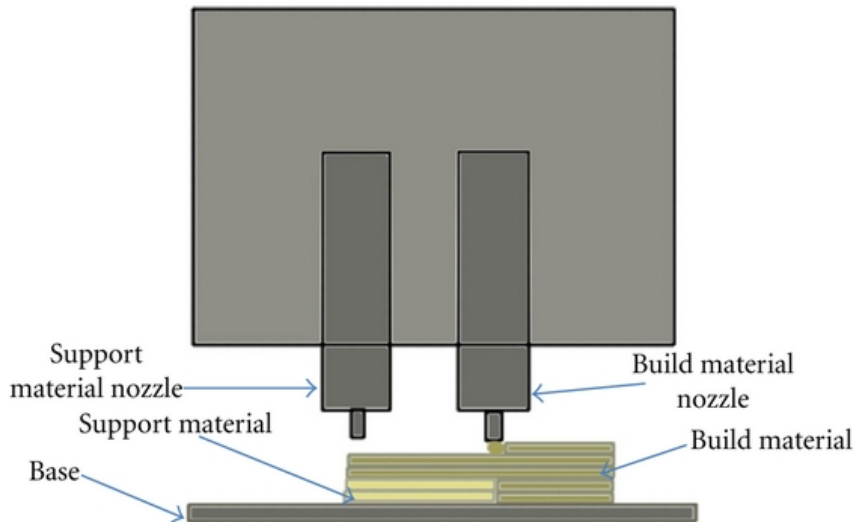
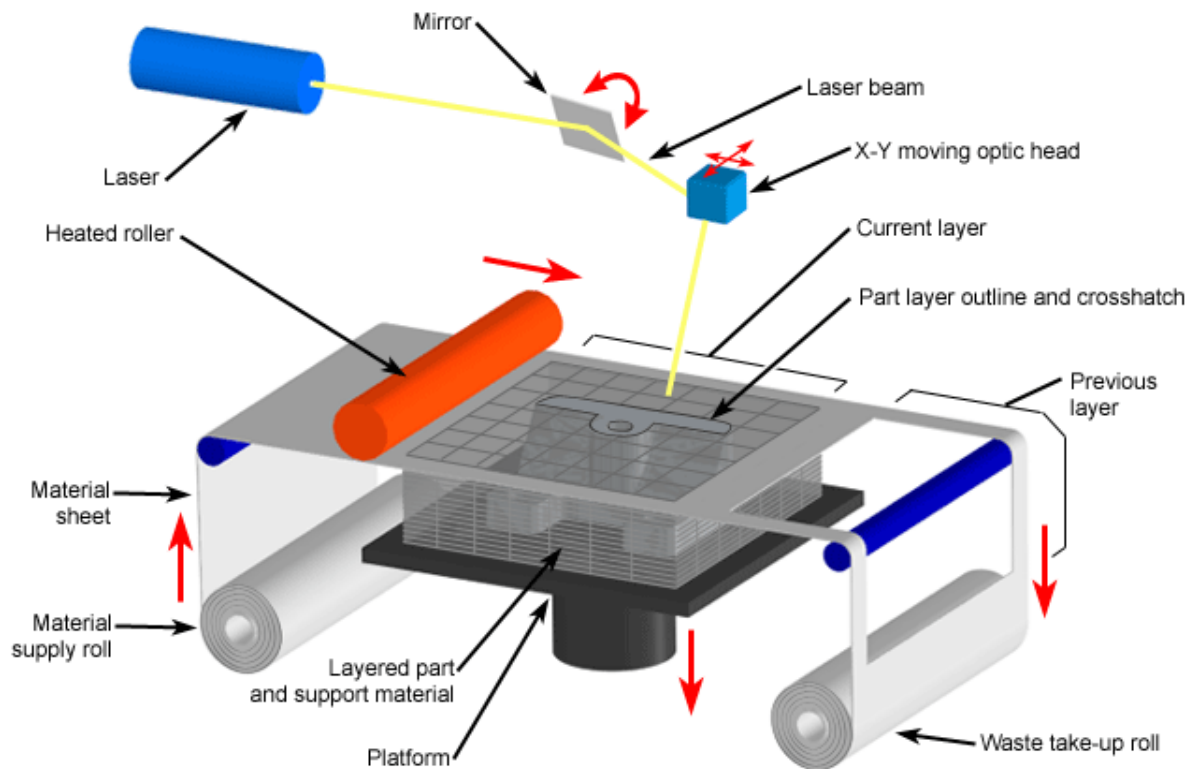


**Figure 1.6: Illustrations of fused deposition modelling process. Reproduced from (Wong and Hernandez, 2012).**

The advantages of this process as summarized in **Table 2** include no post processing, no curing process, stable material properties that do not change with time or environmental exposures such as moisture and no exposure to toxic materials thus it can be set-up in an office environment. Low z-axis resolution (0.25 mm), rougher surface finish that may require manual sanding to smooth surface, and slower fabrication process compared to stereolithography (SLA) and selective laser sintering (SLS) are some of the disadvantages of this RP process (Grimm, 2003, Wong and Hernandez, 2012).

#### 1.6.1.2 Laminated object manufacturing

This is a form of contour-cutting process that combines both additive and subtractive manufacturing techniques for RP. Laminated object manufacturing (LOM) construct parts by layering sheets of thermoplastics such as paper, plastics or composites to form the object. The z-axis resolution is dependent on the material used that can range between 0.025 to 0.13 mm. The set-up of this process is based on feed mechanism system where the material (in sheet) is positioned on the building platform and pressure is applied by a heated roller to bind the top and bottom layers. The profile of the part is cut out by a CO<sub>2</sub> laser reflected by the XY moving optic head. The laser settings are adjusted such that only a single layer of material is cut at a time. Crosshatch pattern surrounding the profile of the part is laser cut to facilitate its removal when the build is complete (**Figure 1.7**) (Wong and Hernandez, 2012, CustomPartNet, 2008, Gene, 2007).



Copyright © 2008 CustomPartNet

**Figure 1.7: Illustrations of laminated object manufacturing process. Reproduced with permission from (CustomPartNet, 2008), Copyright © 2009 CustomPartNet. All rights reserved.**

One of the advantages of this process is that the build is self-supported by the excess material surrounding the part profile. As the complete parts are constructed by applied heat and pressure to bond the stacks of materials, they do not warp, deform or shrink. The disadvantage is given that build is form by subtracting the excess materials around it, hence making this technique not feasible to fabricate complex internal cavities. The process also generates considerable amount of fumes, thus it requires a chimney or a filtration system (Wong and Hernandez, 2012, Gene, 2007).

### 1.6.2 Liquid-based RP processes

Majority of the liquid-based RP processes involve a heat source such as UV light or laser to cure or harden a photosensitive liquid resin. The general advantages are evenness of liquid surface in a steady state and quality surface finish. However, this process can be limited by the type of materials that can be cured.

### 1.6.2.1 Stereolithography apparatus

Stereolithography is the first technique developed for RP and is the benchmark for later technologies. The principle of stereolithography apparatus (SLA) is based on the solidification of photosensitive polymer classified as an epoxy, vinyl ether or acrylate with the use of the UV laser light. A 3D object is built layer-by-layer based on a CAD data that is converted into thin cross-sections or layers during the SLA process. Each layer is constructed by the laser beam that traces a single layer or cross-section on the surface of the photosensitive resin (**Figure 1.8a-b**). The liquid monomer or polymer hardens precisely at the point where the UV laser (the catalyst) selectively hits the surface (**Figure 1.8b**) and is converted into a solidified polymer. This process is known as photopolymerisation. Another layer of the resin is recoated on the platform by a sweeper and the tracing of the UV laser is repeated until the object is completed (**Figure 1.8c-d**). Small structures known as the support materials (**Figure 1.8e**) are constructed in some

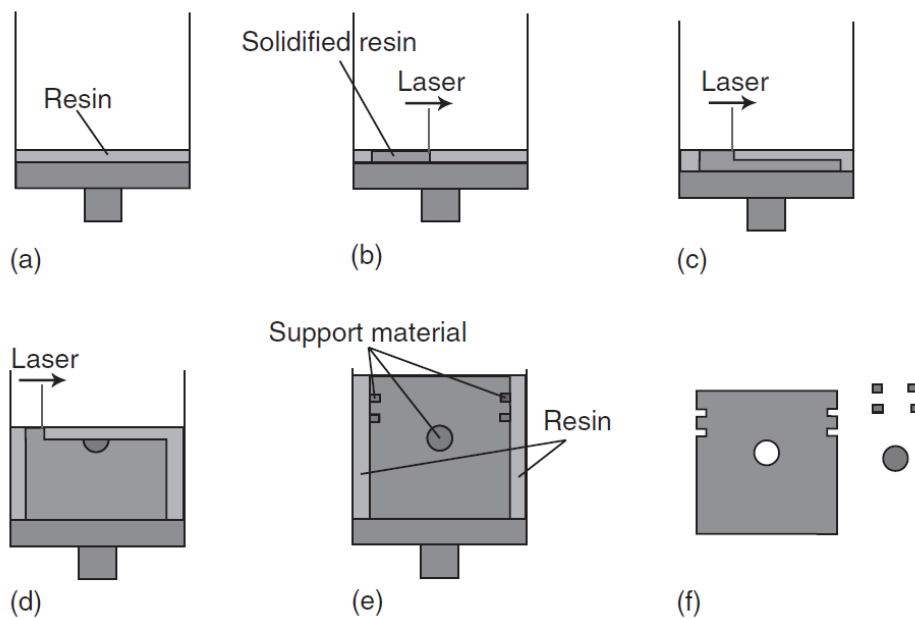


**Figure 1.8: Schematics of step-by-step stereolithography process.**

The process starts off by single layer of photosensitive resin on the platform (a) and the UV laser selectively hits on the surface of the resin to harden the material (b). The tracing of the UV laser is performed on the second layer (c) and repeated to construct the remaining layers of the build (d). Support materials for 'bridging' purpose are built into the object (e) and can be removed after the final part is completed (f). Reproduced with permission from (Gene, 2007) Copyright © (2007), CRC Press.

cases where a 'bridge' is needed to raise the part off the platform. Excess liquid resin is drained off and supports are removed after the build is complete (**Figure 1.8f**) (Gene, 2007). Excess liquid resin that is drained off can be reused for the next build.

An improved version of stereolithography process that can achieve a higher resolution of less than 0.01 mm layer thick, known as microstereolithography, has been developed using photopolymerizable suspensions (Halloran et al., 2011). It is possible to build parts with multiple materials using stereolithography. This process requires a software scheduling system and the use of low viscosity resins where a change in material between layers can be done without the need to sweep post recoating (Kim et al., 2010). This technology is a fully automated process that enables round-the-clock and unattended operations. The process of mass fabrication is also quick and inexpensive, and has the ability to produce parts of any geometry. The resolution of the end product compared to the CAD data is relatively close, with dimensional accuracy within  $\pm 0.1$  mm. The problems of this technology are the high maintenance cost for optical sensors and the need for post processing and curing of the build parts. Build parts with enclosed and hollow structures can trap liquid if cleaning and draining is not feasible and most areas may have incomplete curing due to the cone shape energy properties of the UV laser. Lastly, the thinner areas of the parts may warp over time due to water absorption. The pros and cons of SLA are summarised in **Table 2**.

#### 1.6.2.2 Solid ground curing

A form of mask-based process is the solid ground curing (SGC) technology. This technology works on a similar principle as the SLA process wherein build parts are fabricated based on solidification of photosensitive resin by an UV source. In contrast to SLA, there is no need to construct support materials within the build part as wax is used as a secondary material to support the build (Chua et al., 2010, Liou, 2007). This technology also uses an electron gun to print a charged, cross-sectional image pattern on the glass (mask). A black electrostatic toner is applied and adhered to the charged pattern on the glass. The glass mask is placed over the layer of resin and moved to an exposure cell consisting of a UV source. UV light is exposed to resin that is not covered by the glass mask to cure part of the material. Uncured resin is removed and discarded and a thin layer of wax is applied on top of the solidified resin and fills in the space that formerly held the uncured resin. The layer of wax goes through a cooling process and hardens. The harden



wax provides support for the part. The surface of the build is evened out by a milling cutter to the precise thickness. Additional curing by a longitudinal UV source is repeated after the milling step to ensure complete curing of the build. Hence, no post-curing step is required after the build is completed. The layering and curing process is repeated. Similar to SLA, a post processing step is required for SGC to dissolve the wax (Chua et al., 2010).

The advantage of this technology is the high-throughput process where many different parts can be constructed at once without compromising the vertical accuracy due to the large volume capacity of the system and the addition of milling step. The fabrication process of this system allows construction of parts that do not warp or curl and the inclusion of the milling step enables the reversal of incorrect operations. The downside of this technology is the relative high operating cost as it is a complicated process, which requires monitoring by a skilled worker (Chua et al., 2010, Gene, 2007).

### 1.6.2.3 PolyJet™

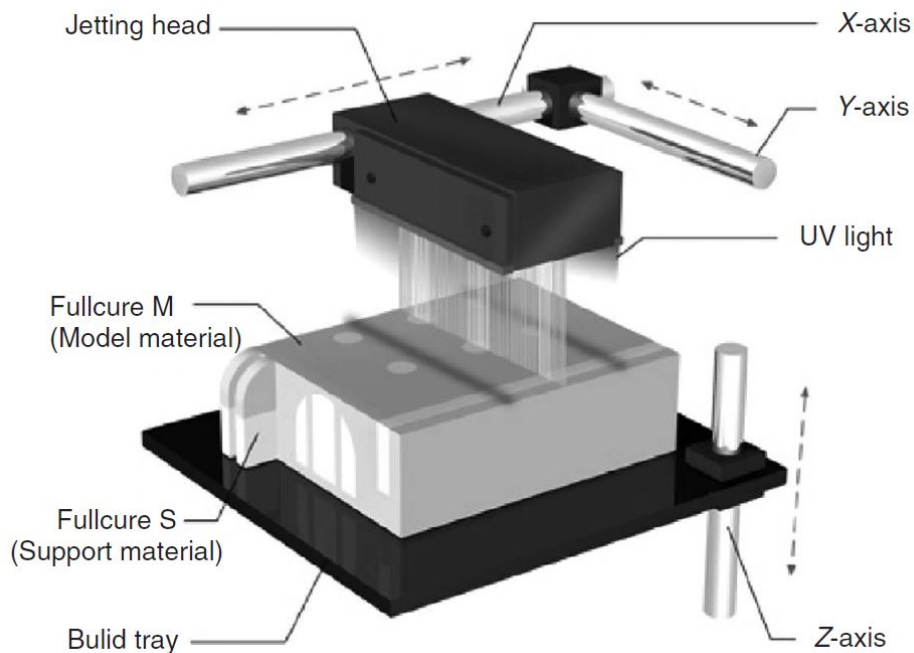


**Figure 1.9: Diagrams of the Objet's PolyJet™ technology process. Reproduced with permission from (Gene, 2007), Copyright © 2007, CRC Press.**

PolyJet™ technology patented by Objet Geometries Ltd. is a type of inject-based technology that can produce high resolution 3D modelling in an office environment. This technology works on the same principle as a normal inkjet printing method and is capable

of producing end-product with good surface finish similar to those from SLA processes (**Figure 1.9**) (Liou, 2007). The resolution of the PolyJet™ technology, depending on the type of models, can range between 42 to 84 µm for both X and Y axes and 16 to 30 µm for Z axis and a printing accuracy of 0.1 to 0.3 mm (Chua et al., 2010, Gaynor et al., 2014). Current systems in the market allow printing of single or multi-materials within each print job. This technology is the only additive fabrication process that has the capacity to use stiff and flexible materials within a single build. Thus, enabling fabrication of complex and multi-material parts (Gaynor et al., 2014). The jetting heads print both the part and gel-like support materials at the same time in each layer by moving along the xy-axes. The layer is then cured by the UV light with multiple passes once the material is deposited on the build tray. The build tray moves down by 16 µm in the z-axis upon the completion of each cross-sectional layer in preparation for the next layer. The printing and curing processes are repeated until the build is finished. The removal of the support materials is then completed either by hand or with a water jet.

Similar to any other rapid prototyping technologies, PolyJet™ also has several advantages and disadvantages (**Table 2**). The process is simple as it uses cartridge systems and replacement of material cartridges is easy without the risk of material contact. The technology is suitable for wide choices of material ranging from durable acrylic-based polymer to rubber-like Tango materials. Multiple models can be concurrently printed, enabling fast production time. This technology can achieve relatively good dimensional accuracy of less than or equal to 0.6 mm depending on the type of materials and the geometry of the build part. High quality end product with reduced stair effect and smooth surfaces can be achieved without the need of post processing. It is possible to set this process in an office environment as users are not exposed to photosensitive resin during modelling process and the support material is non-toxic but may be limited by the lack of water access that is required for post processing. Other weaknesses of PolyJet™ include possible damage to thin or delicate parts during water jet cleaning and wastage of material as support material cannot be recycled.

### 1.6.3 Powder-based RP processes

#### 1.6.3.1 Selective laser sintering

Selective laser sintering (SLS) employs a similar operation principle as SLA but instead of using photosensitive resin, this process involved fine powder material that can be fused when heat is applied. There are a wide range of materials suitable for SLS including polymer, ceramics and numerous composites. Powders with low fusion properties can add a sacrificial binder material to enable the sintering effect (Kruth et al., 2003). Three-dimensional built is created by fusing the layers of thermoplastic powder together. The sequence of the operation is illustrated in **Figure 1.10**. The set-up of SLS is made up of a powder supply system, a fabrication powder bed, a build cylinder and a moving piston that are contained within a sealed chamber. This chamber is maintained at a constant temperature just below the melting point of the material and filled with nitrogen to prevent potential explosion from handling of large powder quantities (Gene, 2007).

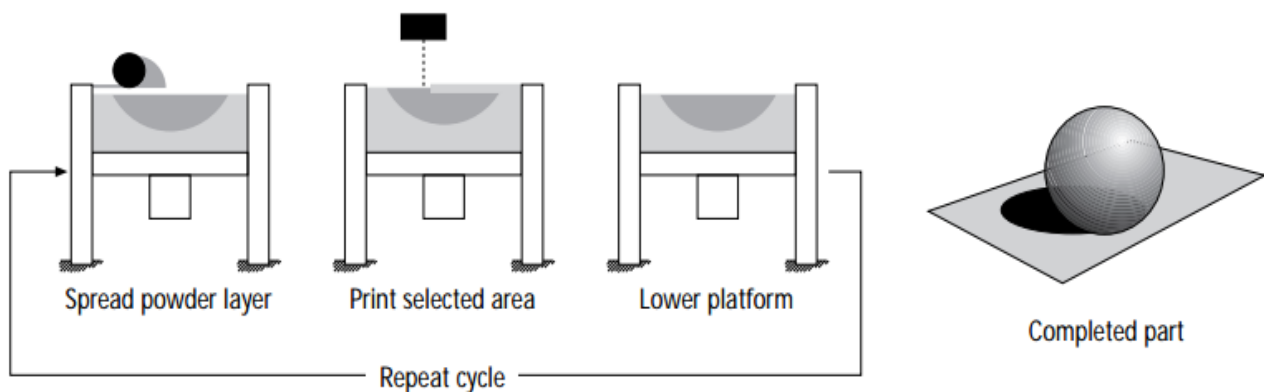


**Figure 1.10: Illustrations of selective laser sintering operations.**

The cycle is started by spreading a thin layer of powder that is coated on the roller. The laser selectively etched the shape of the part to melt and fuse the powder with the layer below. The platform lowers to allow coating of next layer. These cycles repeat until the part is completed. Reproduced with permission from (Lee et al., 1995), Copyright © 1995, Emerald Group Publishing Limited.

Given that the chamber is completely sealed, very little heat from the laser is required for fusion effect to take place, thus the processing time is greatly reduced. There is no need for final curing like in FDM and SGC processes and post processing as part is supported by the fabrication powder bed. The downside of SLS technology is that the part can shrink

by three to four percent (Kruth et al., 2003) unlike SGC technology. Other disadvantages include collection of excess powder on part surface, potential porosity of parts, variable part density and the need of cleaning before changing materials (**Table 2**) (Gene, 2007).

### 1.6.3.2 Electron Beam Melting

The process of electron beam melting (EBM) (**Figure 1.11**) is similar to that of SLS except that the heating source is a scanned 4 kW electron beam. Electron beam is required for a more energy efficient approach to melt conductive metal powder and produced fully dense part. The kinetic energy of the electrons that are projected at half the speed of light melts the powder surface. Pre-heating is first applied to the layer of powder to reduce the level of residual stress that can cause distortion of the part. The filament within the electron beam gun is then heated over 2500°C to accelerate the electrons through the anode to half the

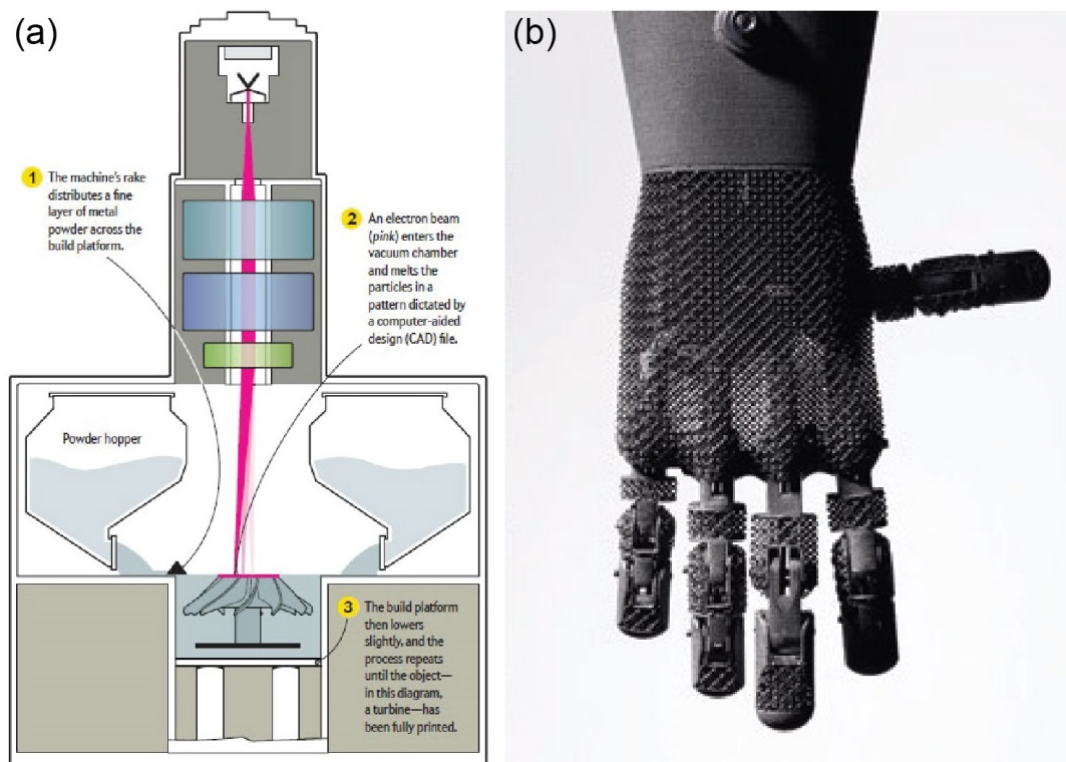


**Figure 1.11: Illustrations of electron beam melting process.**

A fine layer of metal powder that is distributed across the building platform, and the layer of material is selectively melted by an electron beam controlled by a CAD file. The building platform lowers and the process repeats until the part is complete (a). Panel b is a prosthetic hand that is built using EBM. Figure modified with permission from (Greenemeier, 2013), Copyright © 2013, Nature Publishing Group.

speed of light. The beam is focus by a magnetic lens while another is used to deflect the direction. The kinetic energy from the emitted electrons is transferred to heat when they hit the surface of the metal powder, which then melts the material. Selective melting of the layer is controlled by increasing beam power or decreasing the speed.

This additive process is completed within a vacuum environment to provide a clean environment that will improve the metal finishing characteristics. Unfused powder acts as material support for the parts hence support structures are not required in this operation. The dimensional accuracy for EBM is  $\pm 0.4$  mm and the thickness of each layer is between 0.05 to 0.2 mm. The advantage of this technology is the ability to prototype complex shapes with overhangs and undercuts. This technology produces higher energy efficiency that results in lower power consumption, thus lowering maintenance and installation costs. On the other hand, the limitation of EBM is the potential porosity of part due to the nature of sintering process (**Table 2**) (Gene, 2007).

#### **1.6.4 Water-Jet cutting – a subtractive manufacturing process**

Water-jet cutting is a form of subtractive machining process as materials are eroded from a single block of workpiece by high-pressure water jets to create 2D or 3D objects. This method can be classified as abrasive (AWJ) or plain water-jet cutting (PWJ), depending if fine abrasive particles are used during the process. It can essentially cut any kind of material if the device has an ultrahigh-pressure pump and the flexibility in positional movement. Abrasive particles like aluminium oxide are entrained and accelerated to high speed (200 to 800 m/s) when high-pressure water-jet (up to 6200 bar) is forced through a small orifice of 0.1 to 0.3 mm. This technology was first explored in the 1950s to look for a new approach for slicing trees to lumber. PWJ is used for cutting soft and light materials such as plastics, paper and food while AWJ has the capacity to cut glass, metallic sheets and composites (Kulekci, 2002). The development of PWJ in commercial systems was slower than AWJ due to its relatively limited applications. The formation of the high speed AWJ is illustrated in **Figure 1.12**.

AWJ does not cause machine chattering hence it's less sensitive to material properties. It also has no thermal effects (minimum heat generation) and inflicts minimal stresses to workpieces (Azmir and Ahsan, 2009). Water-jet machining is a highly flexible and versatile technology and hence has wide applications including cutting, controlled depth milling,

coat removal, surface polishing, and micromachining etc. (Kong, 2014). It is a key enabling machinery to process materials that are difficult to cut (Wang, 2003, Axinte et al., 2009, Kong et al., 2011).

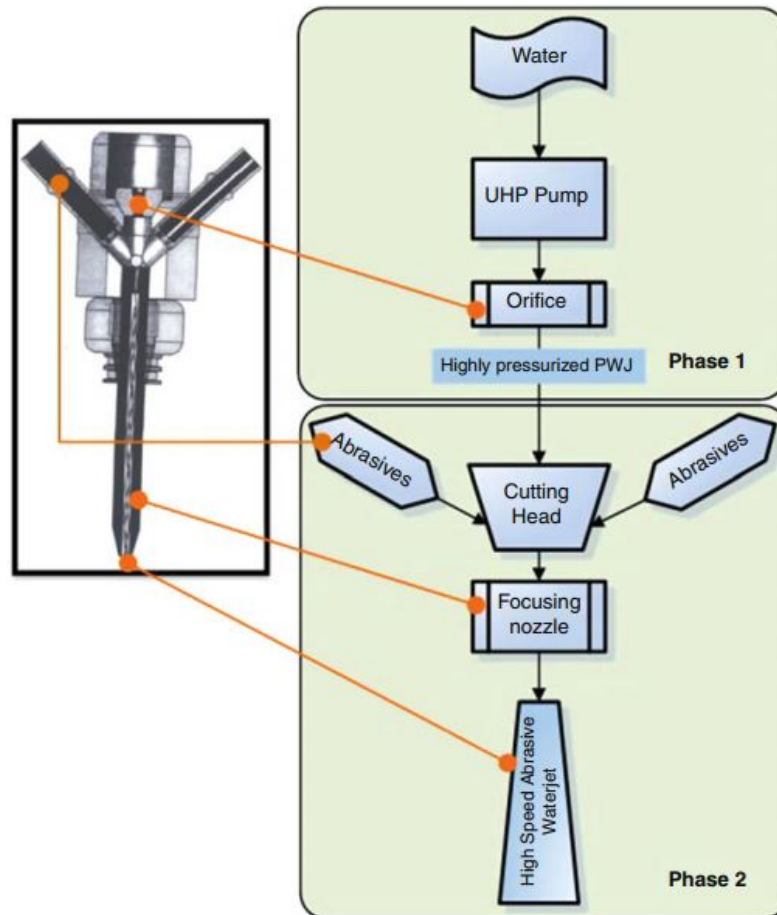


**Figure 1.12: Schematics showing the formation of high velocity in water-jet cutting head.**

The water passes through the ultrahigh-pressure pump into the tiny orifice to form PWJ in the first phase. The highly pressurised PWJ then travel through the jet body, consisting of the cutting head and focusing nozzle, and this process creates a partial vacuum to draw in the abrasive

### **1.6.5 Rapid prototyping applications in medicine and biomedical fields**

The application of RP in the field of medicine was first practise in the 1990s by Mankovich et al. to produce a 3D cranial bone anatomy model using a computed tomography image data (Mankovich et al., 1990). Bone models and implants were fabricated exclusively for various medical specialities in the initial years of medical RP (Minns et al., 2003, Winder and Bibb, 2005, Sailer et al., 1998, D'Urso et al., 1999a). The medical models constructed using medical imaging modalities and RP technologies provided a new approach for

planning and pre-operative simulation of complex surgery (Anderl et al., 1994). The advancement of RP technologies over the years have also facilitated fabrication of anatomical models of the brain (D'Urso et al., 1999b), heart (Kim et al., 2008) and vascular systems (Schuller-Ravoo et al., 2014). These prototyping technologies were not only useful for producing anatomical models but also widely applied in many biomedical science fields, including the fabrication of microneedles (Robison and Finkelstein, 2014, Rasooly et al., 2013, Weibel et al., 2007, Walzik et al., 2015, Gittard et al., 2010).

Two-photon polymerisation is an emerging laser-based microfabrication method that is compatible with numerous photosensitive resins. The compatibility of the materials depends on 1) the ability to polymerise by two-photon absorption in its original form or with the help of a photoinitiator, and 2) the wavelength of the laser is within the window of transparency. The advantage of two-photon polymerisation (near-infrared light) is that it enables three-dimensional processing of the resins unlike in traditional stereolithography processes, the polymerisation occurs at the surface of the material due to the source of laser (UV light).

The choice of fabrication techniques depends on a few factors including whether there is requirement of a cleanroom facilities, the need of hazardous waste services for toxic chemical handling, the dimensional accuracy of the technique and the cost of microneedle precursors and equipment etc. Gittard et al. have provided a review covering different methods for microneedle fabrication, the advantages and disadvantages of each method as shown in **Table 3** (Gittard et al., 2010). The choice of material and technique selected for the production of the microbiopsy device will be discussed in Chapter 3 of this Thesis.

**Table 3: Advantages and disadvantages of current microneedle fabrication methods.**

<b>Production technique</b>	<b>Advantages</b>	<b>Disadvantages</b>
Reactive Ion Etching	High resolution	High operation cost, the need of a clean room, low throughput manufacturing, only compatible with silicon, restrictions on geometry
Photolithography	High resolution	High operation cost, the need of a clean room, geometry restrictions
Cutting and bending	Low operation cost, cleanroom not required, strong materials	Limited to two dimensions control, limited to solid microneedles
Two-photon Polymerisation	Cleanroom not required, good geometry control, resolution is scalable,	Limited to photosensitive materials
Electroplating	Low operation cost, high throughput manufacturing	Geometry is dependent on master structure, biocompatibility issues, thin walls of parts resulting in poor mechanical properties
Casting	Low operation cost, high throughput, compatible with numerous materials	Geometry is dependent on master structure



## **1.7 Literature review summary and Scope of thesis**

The invasive nature of the conventional biopsy and the diagnostic variability from histopathology supported the need for new tools for skin research and a different approach to provide more accurate diagnosis of skin diseases. Optical imaging can provide alternate and non-invasive means of detecting malignancy in skin lesions but like histopathology, this method does not provide objective diagnoses. Molecular changes observed in progressive lesions advocated an opening for alternative analysis. This led to the development of many microbiopsy tools for the detection of tissue abnormality in the breast, intestine, brain and other non-stratified epithelial tissue. Yet, none have been developed for the skin. The concept and establishment of rapid prototyping has revolutionised the manufacturing industry. These technologies are facilitating microfabrication in the field of medicine and biomedical sciences. The goal of this Thesis is to describe the development of a minimally invasive skin sampling technology and explore its analytical potential. The following aims outline the Thesis structure.

**Aim 1:** Establish rapid microneedle prototyping.

**Aim 2:** Microbiopsy geometry and application refinement.

**Aim 3:** Genetic analysis of melanocytic and non-melanocytic skin lesions.

**Aim 4:** Develop live cell assay for microbiopsy.

**Aim 5:** Explore the high-throughput technologies for microbiopsy samples.

## Chapter 2

### General Materials & Methods

#### 2.1 Microbiopsy device fabrication

##### 2.1.1 Fabrication of in-house standard microbiopsy cutting die

In-house standard microbiopsy cutting die were fabricated using the LaserPro S290-20 laser system (GCC World, Taiwan). The laser parameters were set at 100% power, 0.016 m/s speed and 300 kHz frequency. Two-dimensional microbiopsy cutting die were laser cut on 0.05 mm medical grade 304L stainless steel sheet (Mastercut Technologies, Australia). CorelDRAW Graphics Suite X5 (Corel, Canada) was used to draft the microbiopsy designs. A Dremel® rotary tool (Model 225, Mount Prospect, USA) attached with a 428 carbon steel polishing brush was used to polish the microbiopsy cutting die to remove oxidised metal and excess slag. The cutting die were polished while they were still affixed within the stainless steel sheet. Sterilisation was performed with either the Steri Inotech 350 glass bead sterilizer (Inotech Biosystems International Inc., Switzerland) or with 70% ethanol and air-dried prior to folding (**Figure 2.1**). Alignment of the three cutting element plate was checked under stereo microscopy (Stemi 2000, Carl Zeiss Microscopy GmbH, Germany). Microbiopsy cutting die that were not aligned or flush after assembly were discarded.

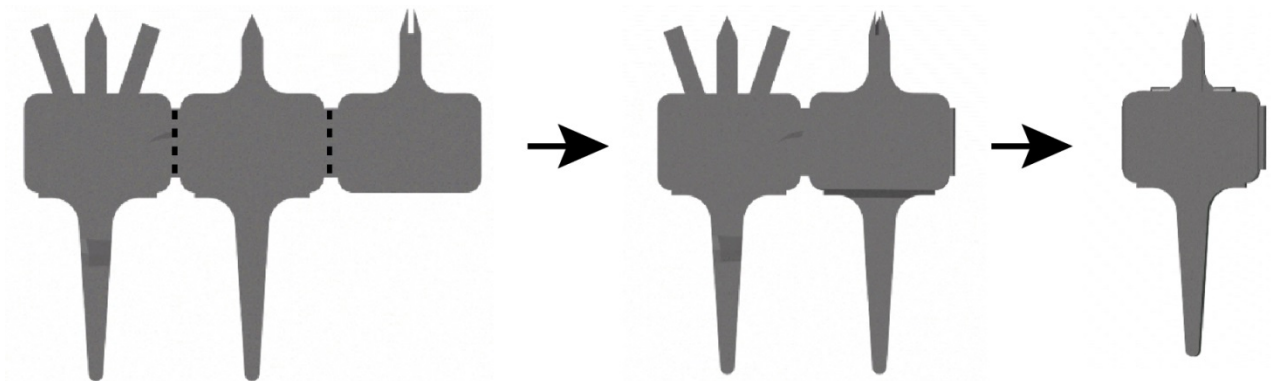


**Figure 2.1: Folding of two-dimensional microbiopsy cutting die.**

Two-dimensional laser cut microbiopsy cutting die was removed from stainless steel sheet and folded along the engraved lines (dotted lines) to assemble into a three-dimensional sampling device.

### **2.1.2 Mass fabrication of standard microbiopsy cutting die**

Mass fabrication of the standard microbiopsy cutting die was done by Mastercut Technologies with a fibre laser system. Five by 20 microbiopsy cutting die were cut on 210 mm x 297 mm x 0.05 mm 304L stainless steel shim. The laser has a standard tolerance of  $\pm 0.5$  mm and precision can be as low as 0.01 mm. Fabrication optimisation was conducted by the company according to defined specifications. Tabs on the side of the base and tip were created to ensure that the cutting die remains attached to the sheet during shipment. The tab was broken by gentle twisting of the cutting die. Sterilisation and folding of the cutting die was done according to protocol described in Section 2.1.1.

### **2.1.3 Fabrication of loader cap**

The loader cap was designed and drafted using Autodesk Inventor Professional software (Autodesk, USA) by Ross Flewell-Smith. The cap was fabricated using either the V-flash FTI 230 3D printer (3D Systems, Australia) or the MakerBot Replicator (MakerBot, USA). Caps that were 3D-printed by the V-flash FTI 230 were cured and rinsed according to supplied instructions before use.

### **2.1.4 Assembling of single-use microbiopsy device**

Commercialised single-use blood sampling device, Unistik® 2 (Owen Mumford, UK, # 08470-0702-01) was modified for use as the microbiopsy applicator. The original 2.4 mm, 21-gauge blood sampling needle was removed from the device plunger and replaced with the microbiopsy cutting die (**Figure 2.2a**). A polymer loader-cap was capped over the opening of the applicator to hold the microbiopsy in position (**Figure 2.2b**). Each assembled microbiopsy device was packed individually in Stericlin® Tyvex® pouch (Medcon, Australia, #801976) and sealed using a heat impulse sealer. Individually packaged microbiopsy devices were sent to a sterilisation and decontamination contractor (Steritech, Australia) for gamma radiation sterilisation at 25,000 Grays. An International Organization of Standardization protocol (AS/NZS ISO 11137:2006) was followed for sterilising the microbiopsy devices by gamma radiation. Single-use microbiopsy devices were only used on volunteer studies described in Chapters 5, 6 and 7.

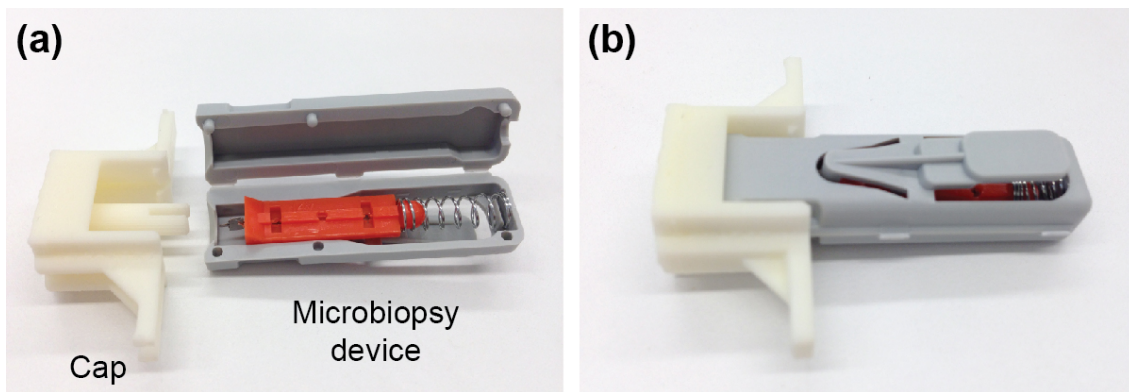


**Figure 2.2: Assembly of microbiopsy cutting die.**

Folded microbiopsy cutting die was fitted onto a modified Unistik® 2 plunger (a) and an in-house loader cap fabricated by a 3D printer attached to the assembled device.

### **2.1.5 Preparation of excised human skin**

Excised human skin was collected from patients who had undergone abdominoplasty surgery. All patients were consented with written consent approved by the Metro South Human Research Ethics Committee in Princess Alexandra Hospital (HREC/12/QPAH/217) and The University of Queensland Human Research Ethics Committee (Approval no. 2012001094/2008001342). The subcutaneous fat was removed and skin tissue containing the epidermis and dermis was kept. Any residual layer of fat tissue was carefully scrap using a scalpel blade to avoid damage to the skin. The tissue was then rinsed with saline or distilled water to remove residual blood. The tissue was packed into a clean ziplock bag and stored at -30°C.

### **2.1.6 Microbiopsy tissue collection from volunteers**

The volunteer's skin was disinfected using an alcohol swab prior to microbiopsy device application. The microbiopsy device was removed from the individual package and loaded by pushing in the loader cap. The device was applied after removing the loader-cap by pressing the spring-loaded applicator onto the skin and releasing the button. No local anaesthetic was required prior to microbiopsy application. Volunteers' skin was cleaned with a new piece of alcohol swab post microbiopsy application and volunteers were advised to keep the biopsied area clean for the next 24 hours to eliminate any potential risk of infection. Simple dressing was made available for the volunteers if required.

Microbiopsy device containing tissue sample was kept in an empty 1.5 ml DNase-/RNase-free microfuge tube and/or immersed in 80 µl of RNeasy® RNA Stabilization Solution (Life Technologies, USA, #AM7024) on ice. Samples kept in RNeasy® solution were stored at 4°C for up to 7 days and transferred to a -80°C freezer if they were not processed immediately. All volunteer studies carried out in this Thesis were conducted under the approval of the Metro South Human Research Ethics Committee in Princess Alexandra Hospital (HREC/12/QPAH/082 & HREC/13/QPAH/551) and The University of Queensland Human Research Ethics Committee (Approval no. 2012000648 & 2013001551).

### **2.1.7 Microbiopsy tissue collection from excised skin**

Excised skin was placed on top of gauze soaked with saline and foam tape. Clinical and/or dermoscopic photography were documented before microbiopsy application. The microbiopsy device was placed on top of the region of interest and applied by releasing the button on the modified applicator. The microbiopsy tissue sample was kept in an empty 1.5 ml DNase-/RNase-free microfuge tube and/or immersed in 80 µl of RNeasy® solution on ice. Samples kept in RNeasy® solution were stored at 4°C for up to 7 days and transferred to a -80°C freezer if they were not processed immediately.

## **2.2 DNA Processing**

### **2.2.1 DNA extraction from microbiopsy sample**

QIAamp DNA Micro Kit (QIAGEN GmbH, Germany, #56304) was used to carry out DNA extraction from microbiopsy samples. Microbiopsy devices containing the tissue samples were opened up and immersed in 180 µl of Buffer ATL and 20 µl of proteinase K. Samples were lysed overnight at 56°C in a thermomixer (Eppendorf, Germany) while mixed constantly at 800 rpm. Tissue lysis was completed by adding and mixing 200 µl of Buffer AL into the solution after overnight incubation. DNA in lysed sample solution was concentrated using 200 µl of 96-100% ethanol. The tube containing the device was briefly centrifuged for ten seconds to remove the solution adhering to the cap of the tube before transferring the lysate into a QIAamp MinElute column. The tube containing the device was centrifuged again at 6000 x g for 30 seconds to remove any lysate adhering to the device. The lysates were combined and the remaining procedure followed the manufacturer's supplied instructions. Twenty to 25 µl of Buffer AE or nuclease-free water

was added to the middle of the membrane and incubated at room temperature for up to five minutes before elution to increase the yield of DNA.

### **2.2.2 DNA extraction from lesional sample**

Excised lesion was weighed to ensure that the tissue was not more than 25 mg in weight. Tissue that weighed more than 25 mg was cut into appropriate sizes and extracted in separate reactions. The tissue was cut up into finer pieces using a single-use surgical blade prior to DNA extraction. Finely cut up tissue was immersed in 180 µl of Buffer ATL and 20 µl of proteinase K from QIAamp DNA Mini Kit (QIAGEN GmbH, Germany, #51304). Tissue lysis involved overnight incubation at 56°C in a thermomixer (Eppendorf, Germany) while mixed constantly at 800 rpm and was completed with an additional ten minutes incubation of 200 µl of Buffer AL at 70°C. If visible tissue was present after overnight incubation, the sample was incubated for a longer period until no visible tissue could be seen prior to addition of Buffer AL. The entire lysate was transferred to QIAamp Mini spin column and the remaining procedure followed the manufacturer's supplied instructions. Buffer AE or nuclease-free water was incubated at room temperature for up to five minutes before elution to increase the yield of DNA.

### **2.2.3 DNA quantification**

The Qubit® dsDNA HS assay (Life Technologies, USA, #Q32854) and dsDNA BR assay kits (Life Technologies, USA, #Q32853), a quantitative fluorometer-based assay were used to determine the concentration of DNA from the microbiopsy samples and excised lesions, respectively, with the instructions provided by the manufacturer. Depending on the selection of the downstream application and the type of sample (microbiopsy or lesion), a typical sample volume of 2-20 µl was used to quantify the concentration of the sample. For amplified DNA samples, a 10- to 15-fold dilution was performed using 1-2 µl of the samples prior to quantification.

### **2.2.4 DNA whole genomic amplification**

DNA from the microbiopsy samples was concentrated using Thermo Scientific™ DNA SPD111V SpeedVac Concentrator (Thermo Fisher Scientific Inc., Australia) for 1.5 hours at 55°C. If the DNA samples dried up during the concentration process, three microliters of nuclease-free water was added to resuspend DNA at the bottom of the tube. Whole

genomic amplification procedure was then carried according to the manufacturer's instructions (REPLI-g Single Cell Kit, QIAGEN, Australia, #150345).

### **2.2.5 DNA quality control**

Agilent DNA 12000 DNA kit (Agilent Technologies, USA, #5067-1508) was used to determine the integrity and quality of DNA after whole genomic amplification of isolated DNA from microbiopsy samples. Alternatively, the quality and integrity of amplified DNA was verified using a 2% agarose gel electrophoresis with the 1 Kb Plus DNA Ladder (Life Technologies, USA, #10787-018) when the 2100 Bioanalyzer instrument (Agilent Technologies, USA) was not available. Samples were diluted to the level within the quantitative range prior to quality analysis.

## **2.3 RNA Processing**

### **2.3.1 RNA extraction from microbiopsy samples**

The microbiopsy device was opened up and checked under stereo microscopy for presence of tissue prior to RNA extraction. The microbiopsy device containing the tissue sample was then transferred to a clean tube containing 100 µl Extraction Buffer. The tube was briefly vortex and centrifuged before incubating at 42°C for 30 minutes. Subsequent RNA extraction procedures were performed according to the instructions from Arcturus® PicoPure® RNA Isolation kit (Life Technologies, USA, #KIT0204) as provided by the manufacturer, with modification to Step b wherein 100 µl of 70% ethanol was added. DNase treatment was included in the extraction process using the RNase-DNase Set (QIAGEN GmbH, Germany, #79254) according to the instructions provided by the manufacturer. Minimum volume of 11 µl Elution Buffer was added to the column and incubated for 2-5 minutes before RNA was eluted from the column.

### **2.3.2 RNA extraction from lesional sample**

Excised lesion was weighed to ensure that the tissue was not more than 30 mg in weight. Tissue that weighed more than 30 mg was cut into appropriate sizes and extracted in a separate reaction. The tissue was cut up into finer pieces using a single-use surgical blade prior to RNA extraction and transferred to a 2 ml screw cap plastic vial half filled with 1.4 mm ceramic spheres or a pre-packed Lysing Matrix D tube (MP Biomedicals, Australia, #116913050), containing 350 µl of Buffer RTL Plus lysis buffer from RNeasy Plus Mini kit

(QIAGEN GmbH, Germany). The tissue sample was disrupted using the FastPrep® FP 120 instrument (Q-biogene,) at a speed of 6.5 for 45 seconds per cycle. Four to six cycles of disruption to the tissue was performed, and the sample was cooled on ice for 1 minute and briefly centrifuged between each cycle. Subsequent RNA extraction steps were performed according to the instructions provided by manufacturer. An additional centrifugation step was performed to eliminate any possible carryover of Buffer RPE by adding nuclease-free water and incubating at room temperature for 2-5 minutes before eluting the RNA.

### **2.3.3 RNA quantification**

The Qubit® RNA HS assay (Life Technologies, USA, #Q32855) and RNA BR assay kits (Life Technologies, USA, #Q10211), were used to determine the concentration of RNA from the microbiopsy samples and excised lesions, respectively, with the instructions provided by the manufacturer. Depending on the selection of the downstream application and the type of sample, a typical volume of 2-20 µl was used to quantify the concentration of the sample.

### **2.3.4 RNA quality control**

Agilent RNA 6000 Pico kit (Agilent Technologies, USA, #5067-1513) was used according to the manufacturer's instructions to determine the integrity and quality (RIN number) of RNA. Samples with concentration outside kit's range were diluted prior to quality analysis.

## **2.4 Image data collection**

### **2.4.1 Optical and clinical photography**

Stemi 2000C stereo microscope (Carl Zeiss Microscopy GmbH, Germany) with an external five megapixel camera (ZEISS AxioCam ERc 5s, Carl Zeiss Microscopy GmbH, Germany) was used to acquire optical photographs. The magnifications of this microscope range between 6.5x to 50x. Photographs are acquired by AxioVision LE64 imaging software (Carl Zeiss Microscopy GmbH, Germany) that has basic image processing and measurement functions. Clinical photographs were acquired using a 14.7 megapixel Canon Power Shot G10 digital camera (Canon, USA) using automatic shooting mode.



### **2.4.2 Reflectance confocal microscopy**

Non-invasive real-time visualisation of the microbiopsy site in volunteers (HREC/12/QPAH/082) or in excised skin (UQ Human Ethics approval no.: 2008001342) was carried out with a Vivascope 1500 Multilaser (Lucid, Inc., USA). The multilaser is a reflectance confocal microscope (RCM) coupled with fluorescent confocal laser scanning microscopy. The fluorescence imaging can be carried out in three different excitation wavelengths: 488 nm, 658 nm and 785 nm. This imaging system has an integrated dermoscopic imaging modality. The horizontal and vertical optical resolution of the system within the tissue is  $< 1.25 \mu\text{m}$  and  $< 5.00 \mu\text{m}$  at the center of field of view. Optimum reflectance confocal images were collected through the microscope head, integrated with a water immersion objective, at a near-infrared wavelength of 785 nm. Block and/or single stack images were acquired at the microbiopsy sampling site. Block images were made up of 0.5 mm by 0.5 mm single frame images that were stitched together.

## Chapter 3

### *Fabrication of the Microbiopsy device*

#### 3.1 Introduction

The focus of this Chapter was the development of protocols to enable rapid fabrication of microbiopsy prototypes. The aims of this Chapter were to:

- Optimise fibre laser parameters (power, frequency and speed) using straight lines
- Reproducibly cut single needle microbiopsy using optimised parameters
- Assess the mechanical integrity of the prototype during application

Stainless steel is an essential component in medical devices and has a wide application in the medical device industry. There are many types of metal machining processes and one of the most common industrial cutting systems is laser cutting. This is because there are numerous benefits that an industrial laser cutting system has over other material machining technologies (**Table 4**), especially in the context of micromedical device prototyping. In the context of mass manufacturing, the ability to automate the process and manufacture at high volumes are vital. Laser cutting was ideal for manufacturing of stainless steel based micromedical device as small kerf width and narrow heat affected zone (HAZ) can be achieved. The kerf width of the laser cut line was defined as the width of the groove measured from one edge of the cut to the other edge. It is fortuitous that laser cutting technology is also preferred in the laboratory context, where the safety of equipment and the flexibility of system to design changes are required. This allows for the direct translation of research activities into scale-up operations without the need for laborious system optimisation steps in between.

The main components for laser cutting are the laser itself, focusing optics, and a moving beam or workpiece on the XY positioning table (**Figure 3.1a**). The beam is directed into the centre of the cutting head by the alignment mirrors. A focusing optic within the cutting head focuses the laser beam to produce an intense microscopic laser spot. The focusing optics can be transmissive or reflective optics depending on the type of laser (i.e. gas, solid-state, dye, or free-electron). The concentrated beam subsequently passes through a

nozzle within the cutting head at which an intersecting gas jet flows. The gas jet is used to assist the cutting process by removing molten material (**Figure 3.1b**) and also to protect the optics from spatter. Fibre laser cutting occurs as a result of either reactive-fusion or fusion depending on whether the gas jet is reactive (e.g. oxygen) or inert (e.g. nitrogen or argon).

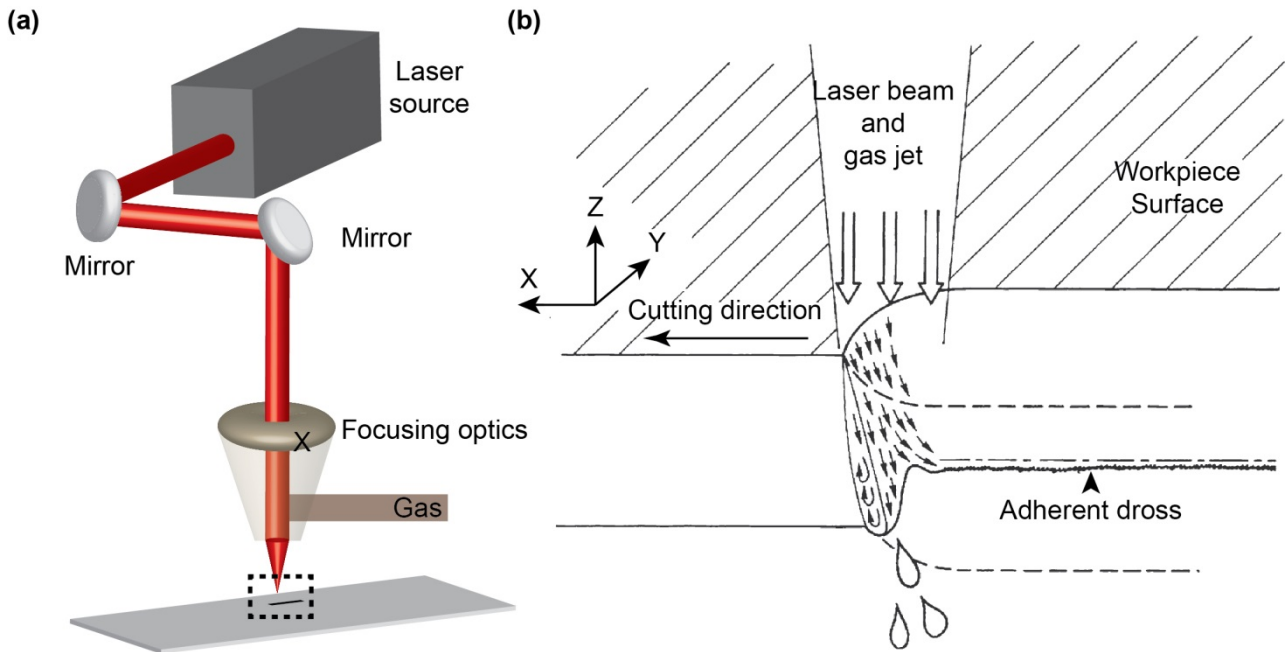


**Figure 3.1: Laser cut set-up schematics.**

Illustrations of a laser cutting system (a) and an enlarged image of the dotted box showing the process of laser cutting with a coaxial gas jet removing the molten material. Molten materials that adhere to the edge of the cut are known as dross, slag or burr. Figure modified with permission from (Powell, 1998) Copyright © 1998, Springer London.

Laser cutting involves using large amount of energy to induce state and phase transformation of the material. Laser cutting can be achieved by vaporisation cutting, fusion cutting (melt and/or blow), reactive fusion cutting, controlled fracture (thermal stress cracking), scribing, cold cutting, and laser-assisted oxygen cutting (LASOX) (Steen and Mazumder, 2010). The choice of laser cutting method depends on the type of lasers to be used, thermo-physical properties as well as the thickness of the material.

**Table 4: Comparison of the benefits and limitations of different cutting techniques (Steen and Mazumder, 2010, Vilumsone-Nemes, 2012).**

<b>Cutting techniques</b>	<b>Benefits</b>	<b>Limitations</b>
Laser	<p>Ability to cut all metals, all plastics, glass, and wood can be cut (depending on the source of energy).</p> <p>Ability to automate process.</p> <p>Fast cutting speed enabling high production volume.</p> <p>Produces small kerf width (0.15 mm).</p> <p>Produces narrowest HAZ.</p> <p>Low machine clean up.</p>	<p>Relatively high equipment cost.</p> <p>Causes thermal stress to materials.</p> <p>Different parameters required for cutting different materials.</p> <p>Efficient for thickness between 0.1 to 10 mm.</p> <p>Difficulties for reflective metals.</p>
Punch	<p>Ability to automate process.</p> <p>Fast cutting speed enabling high production volume.</p> <p>Produces small kerf width.</p> <p>Produces narrow HAZ.</p>	<p>Do not have the ability to cut both metal and non-metal material.</p>
Plasma	<p>Ability to cut all metals including reflective metals.</p> <p>Ability to automate process.</p> <p>Fast cutting speed enabling high production volume.</p>	<p>Do not have the ability to cut non-metal material.</p> <p>Causes thermal stress to materials.</p> <p>Produces relatively large kerf width.</p> <p>Produces relatively large HAZ.</p>

		<p>Medium machine clean up required.</p> <p>Different parameters required for cutting different materials.</p>
Abrasive Water Jet	<p>Ability to cut both metal and non-metal material.</p> <p>Ability to automate process.</p> <p>Settings to cut are the same for all materials.</p> <p>Produces relatively small kerf width (0.05 mm).</p> <p>No thermal stress on materials.</p>	<p>Relatively slow cutting speed.</p> <p>Relatively high equipment cost.</p> <p>High machine clean up.</p> <p>Efficient for thickness between 10 to 50 mm.</p> <p>Personal safety equipment required.</p>
Wire electric discharge machining	<p>Produces small kerf width.</p> <p>Produces narrow HAZ.</p>	<p>Restricted to conductive materials.</p> <p>Process cannot be automated.</p> <p>Relatively slow cutting speed.</p> <p>Different parameters required for cutting different materials.</p>
Sawing	<p>Low equipment and operation costs.</p>	<p>Produces large kerf width.</p>
Ultrasonic	<p>Ability to cut both metal and non-metal material.</p> <p>Excellent accuracy and clean edges finishes.</p>	<p>Low production volume due to relatively slow cutting speed.</p> <p>Requires special surface fixation on vacuum table.</p>

Vaporisation or evaporation laser cutting occurs through direct vaporisation of material after it has reached its evaporation point by laser energy. It is suitable for processing materials with low conductivity and low heat of vaporisation. In fusion cutting, the high intensity laser melts the material and molten material is then expelled by inert gas jet. This method is suited for materials that are high in conductivity. Examples of such material are nonferrous materials like aluminium and titanium. Reactive fusion cutting and LASOX are variations to fusion cutting method. The method requires the introduction of reactive gas or oxidising gas mixture to trigger an exothermic reaction that acts as an additional energy source to cut the material. This approach is suitable for high conductivity and reactive materials including mild steel and stainless steel. Controlled fracture is suited for brittle materials as it uses mechanical stresses created along the path of the laser beam to separate the material (Dahotre and Harimkar, 2008, Steen and Mazumder, 2010).

The key advantages of laser cutting over alternative machining techniques include non-contact process, rapid processing speed, flexible process, ease of automation, precise and better quality of cut (Dahotre and Harimkar, 2008, Steen and Mazumder, 2010). Unlike conventional machining, there is no need to clamp or centre the workpiece on fixtures and precise position can be achieved with a XY table. Laser cutting is highly flexible as changes to the process can be easily programmed. Narrow kerf width with minimum heat affected zone (HAZ) and thermal stresses can be achieved with optimised laser cutting.

Laser cutting is a dynamic process and the quality of laser cuts can be affected by multiple cutting parameters. Some of the most important parameters include laser power, cutting speed, beam properties (size, diameter, focal position) and material thickness. There are limited studies investigating parameter optimisation using fibre lasers. However, the relationship between cutting parameters using CO<sub>2</sub> lasers and cut quality has been well-established (Yilbaş, 1996, Keles and Oner, 2012, Russo Spina et al., 2014, Wang, 2000) and these parameters are directly relevant for other laser systems.

Cutting parameters including thickness of workpiece, assisting gas pressure, cutting speed and laser power were described by Yilbas in 1996 (Yilbaş, 1996). One of the key observations noted in the study was the presence of irregular cut width and holes of variable diameters when mild steel was processed at very low cutting speeds (2 cm/s). This effect, known as self-burning, was reduced when the cutting speed was increased to

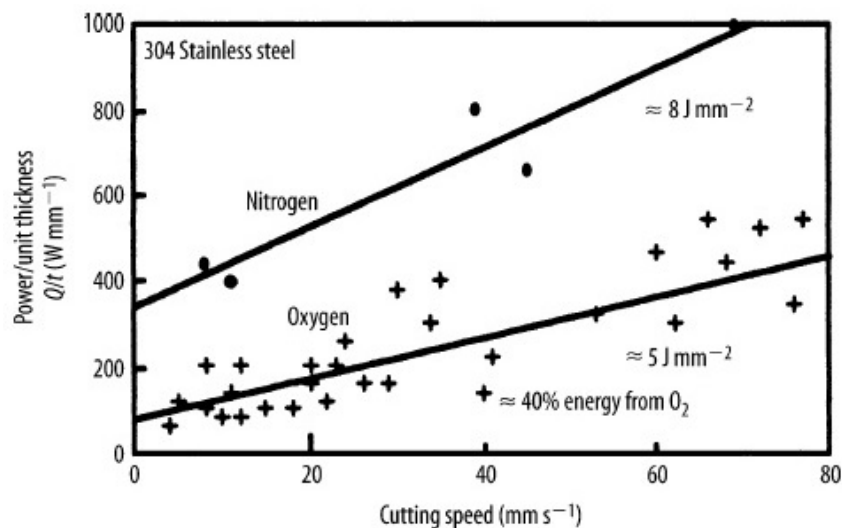


**Figure 3.2: Correlation of laser power and cutting speed.**

Overall effects of increasing power ( $Q$ ) on cutting speed and thickness of cut ( $t$ ) on 304 stainless steel  
 Reproduced with permission from (Steen and Mazumder, 2010).

4 cm/s. Yilbas and others all agreed (Yilbaş, 1996, Steen and Mazumder, 2010, Wang, 2000) that increasing laser power allows laser cutting at faster speeds. This relationship of the laser power and cutting speed is illustrated in **Figure 3.2**.

Spena et al. (2014) assessed the quality of cut on twinning-induced plasticity steel sheet using  $\text{CO}_2$  laser. They examined laser power, cutting speed, pressure of oxygen, and laser frequency in the assessment. The kerf width, kerf deviation, surface roughness and dross attachment was analysed to determine the quality of the cut (Russo Spena et al., 2014). They found that the laser power and cutting speed primarily influenced dross attachment. Based on the analysis of variance (ANOVA) analysis, all the cutting parameters included in the study had significant impact on the kerf width of the cut. The primary contributor was the laser power followed by its interaction with frequency. The possible downside of increasing laser power was that the kerf width increases (impacting precision), and the associated burning damage to the material that affects quality of the finishing (e.g. sharp corners appear rounded).

In the context of the microbiopsy, the goal was to rapidly and accurately prototype a multitude of designs. However, a general feature is that the microbiopsy needed to consist of sharp defined edges capable of piercing and cutting the skin (**Figure 3.3**). Therefore, the following parameters were identified as critical for this purpose: power, speed and

frequency. These parameters were assessed and optimised based on kerf width, heat affected zone (HAZ), dross attachment and cut completeness, which were sufficient for rapid prototyping. A further round of optimisation will be necessary for mass manufacture utilizing an expanded range of assessment parameters, but this is outside the scope of this thesis. The optimised laser parameters were employed to cut single needle microbiopsies to determine the reproducibility of the fabrication process. The possibility of using different material thickness for the microbiopsy device was also explored in this Chapter. Lastly, integrity assessment was performed during microbiopsy prototype application. The focus of the next Chapter was to characterise the content of microbiopsy samples and optimise the physical and mechanical properties of the device to achieve maximum tissue collection.

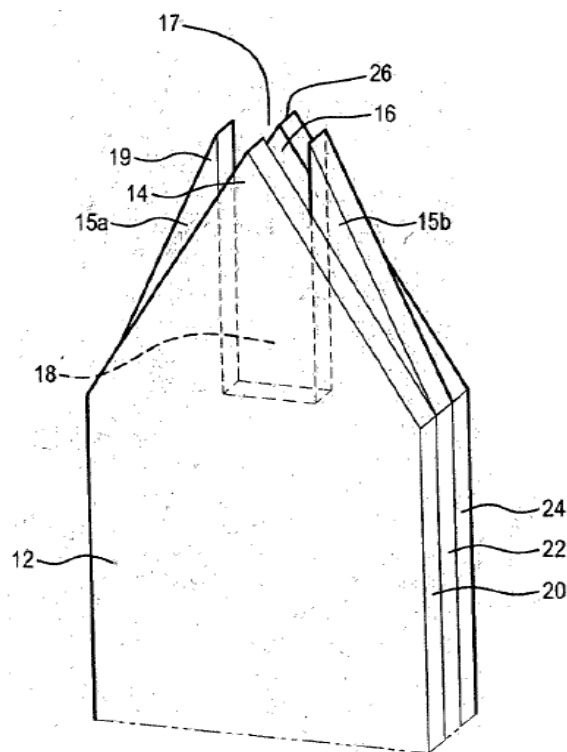


**Figure 3.3: Extended cutting element of microbiopsy cutting die.**

A perspective view of the extended cutting elements with a hollow chamber of an assembled microbiopsy cutting die (PROW, 2013)



## 3.2 Materials and Methods

### 3.2.1 Laser cutting system optimisation

Laser power, speed and frequency were adjusted for the LaserPro S290-20 laser etching system (GCC, Taiwan) to determine the optimal settings for cutting 0.05 mm thick 304L medical grade stainless steel sheet (Mastercut Technologies, Australia). The system has an integrated 20W fibre laser to cut at a resolution ranging from 125 to 1000 dots per inch (DPI). The system consisted of an air compressor to prevent moisture from damaging the laser optics and remove particles generated during the laser cutting process. Assisted gas at ultimate pressure of 8 KPa was used during the laser cutting process. This system is compatible with a variety of graphic design software including AutoCAD, Illustrator, CorelDRAW and Photoshop. CorelDRAW Graphics Suite X5 (Corel, Canada) was the main software used for microbiopsy prototyping.

Optimisation of the laser system was carried out in a two-step process. The first step consisted of cutting a minimum of 10 single lines 3.2 mm in length and 1.6 mm apart. The laser power was varied between 0% and 100%, the speed 0.002 m/s and 0.060 m/s and the frequency 0 kHz and 1000 kHz. After initial optimisation, the second step consisted of cutting at least three microbiopsies per sheet with either a single needle or array design. For both steps, the cuts were characterised via stereo microscopy (Stemi 2000C with AxioCam ERc 5s camera, Carl Zeiss Microscopy GmbH, Germany) using the integrated image analysis software (AxioVision LE64, Carl Zeiss Microscopy GmbH, Germany). The main variables assessed were kerf width, amount of dross and line straightness/uniformity. The microbiopsy designs were further assessed for quality of corners and curved lines. The kerf width of the laser cut line was defined as the width of the groove measured from one edge of the cut to the other edge. The completeness of the cut ranged from complete to partial to no cut.

Post laser cut polishing of the microbiopsy (**Figure 3.3**) was also investigated to improve the overall finish. The cutting die were polished using a Dremel® rotary tool (Model 225, Mount Prospect, USA) attached with a 428 carbon steel polishing brush while they were still affixed within the stainless steel sheet. The finished microbiopsies were analysed as above.

### **3.2.2 Surface area calculation**

Low and high resolution images (6.5x and 20x magnification, respectively) were imported into ImageJ (NIH, USA) for high throughput image analysis of the kerf properties and surface area of removed metal. The image of each line was cropped to remove excess stainless steel area to minimise background noise related to reflectance. The image was converted to 8-bit and automatic greyscale threshold was set by clicking the [Auto] button. Dark background was chosen and the area of materials removed from the line was represented by black signal in the binary image. The image scale was set to 0.304 pixels/ $\mu\text{m}$  using a scale bar exported from Axiovision LE64 software. The total surface area of the materials was calculated using the “Analyze Particles” function in the software. The size of particles was set at zero to infinity. Circularity of particles was defined as 0.00 – 1.00. The results of the analysis were presented as “Outlines” and artefacts that were created due to background were not included in the calculation.

### **3.2.3 First generation microbiopsy cutting die functionality test**

Optimised settings defined in the laser optimisation experiments were used to laser cut 0.05 mm thick sheet to fabricate the first generation microbiopsy cutting die. The microbiopsy cutting die were assembled by stacking three plates of cutting elements together. Assembled microbiopsy cutting die was fitted and held together on a brass applicator with plastic spacers. The microbiopsy alignment was verified using stereo microscopy to ensure that all three plates were flush. It was then applied to excised human skin obtained from abdominoplasty patients. Informed consent approved by The University of Queensland Human Research Ethics Committee (Approval no. 2008001342) was signed by all patients. For preparation procedure of excised human skin, refer to Section 2.2.1. The site of application was assessed by reflectance confocal microscopy (RCM) (Vivascope 1500 Multilaser, Lucid Inc., USA). Confocal image stacks with a field of view of 0.5 x 0.5 mm were taken at 5  $\mu\text{m}$  increments from the surface of the skin. Automatic intensity control was selected during the imaging process.

In the second experiment, the outer plates of the microbiopsy cutting die were filed with sandpaper to create a thin tapered end. The microbiopsy cutting die was examined before and after application. The site of application was assessed by RCM and stacks taken with previous settings.

In the third experiment, the outer cutting plates were replaced with the tapered end cutting element fabricated from 0.01 mm stainless steel. Optimised laser speed and frequency at 0.016 m/s and 300 kHz were set to laser cut 0.01 mm thick 304L stainless steel sheet. The power was reduced to 50% given that the thickness is only one-fifth of the usual stainless steel sheet. Application assessment described in the previous experiment was followed.

### **3.2.4 Statistical analysis**

One-way ANOVA analysis was performed to analyse if there was any significant impact of the cutting parameters on the kerf width. Tukey's multiple comparisons test were used in conjunction with ANOVA to determine whether there was any significant difference between the means of the kerf width. All statistical analysis was done using GraphPad Prism 6.0 (GraphPad Software Inc., USA).

### 3.3 Results and Discussion

#### 3.3.1 Laser setting optimisation with lines

It was hypothesised that reproducible fabrication of microbiopsies from stainless steel sheet was achievable when the laser cutting system was optimised. The important laser parameters that were optimised include power, speed and frequency. In this series of experiment, the optimal settings resulting in a complete cut with the smallest kerf size was defined. Based on previous studies the main performance parameters for quality of cut include kerf width, HAZ and dross attachment (Keles and Oner, 2012, Russo Spena et al., 2014, Uslan, 2005, Wang, 2000, Yilbas et al., 2012).

A recent study conducted by Spena et al. (2014) on 1.5 mm twinning-induced plasticity steel sheets concluded that laser power was the main contributor to kerf width. Laser power itself is a major contributing effect of 36.5% on top kerf width (Russo Spena et al., 2014). Therefore, the optimisation experiments started off with evaluation of the effect of laser power on 0.05 mm stainless steel sheet. Lines (n=3) were cut on the 0.05 mm stainless steel sheet at varying power from 0% to 100%. There was no cut in the first two sets of line across all power settings. Partial cuts with laser power starting from 80% to 100% for the third set of lines were observed. The outcome of the cuts was not similar even though the settings were identical for all three lines (**Figure 3.4a**). Measuring kerf width at similar locations across all three lines was limited given the amount of dross produced. Therefore, the measurements of the kerf width at five random locations that were clear of dross were taken. There was an increase in the width of the cut produced when power increased from 80% to 100% ( $54.8 \pm 7.66 \mu\text{m}$  to  $70.4 \pm 7.65 \mu\text{m}$ ) (**Figure 3.4b**). Tukey's multiple comparisons revealed that the kerf width differences between 80% to 90% and 100% were significant ( $p < 0.05$ ). These results agreed with the data reported in Uslan's study (Uslan, 2005).

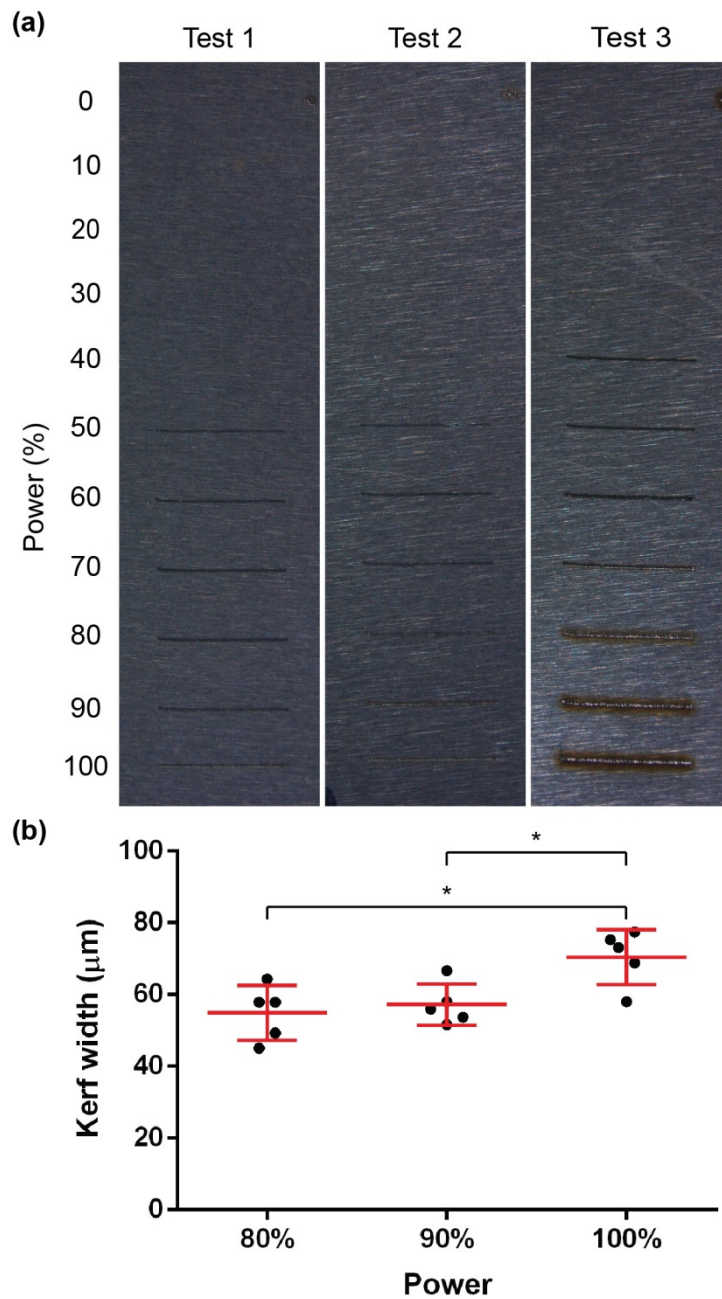


**Figure 3.4: Laser power optimisation.**

The impact of increasing laser power from 0% to 100% was determined with lines ( $n=3$ ), when set at a speed of 0.02 m/s and at a frequency of 0 kHz (a). The average kerf width ( $n=5$ ) of the lines was wider with higher speeds (b). Standard deviation (SD) is represented by the red bar for each data group.

The next parameter that was evaluated was laser frequency. A frequency test with the same speed and at a laser power of 100% was performed to standardise and be able to compare results between experiments. Partial cuts were observed at 0 kHz and frequencies between 700 kHz to 1000 kHz when maximum power was used. However, no cut was seen for frequencies between 100 – 600 kHz (**Figure 3.5**). Further testing revealed that there was a software/hardware issue leading to inaccurate communications between the laser cutting system and CorelDRAW software. The issue was outsourced to the supplier and corrected by the technical team.

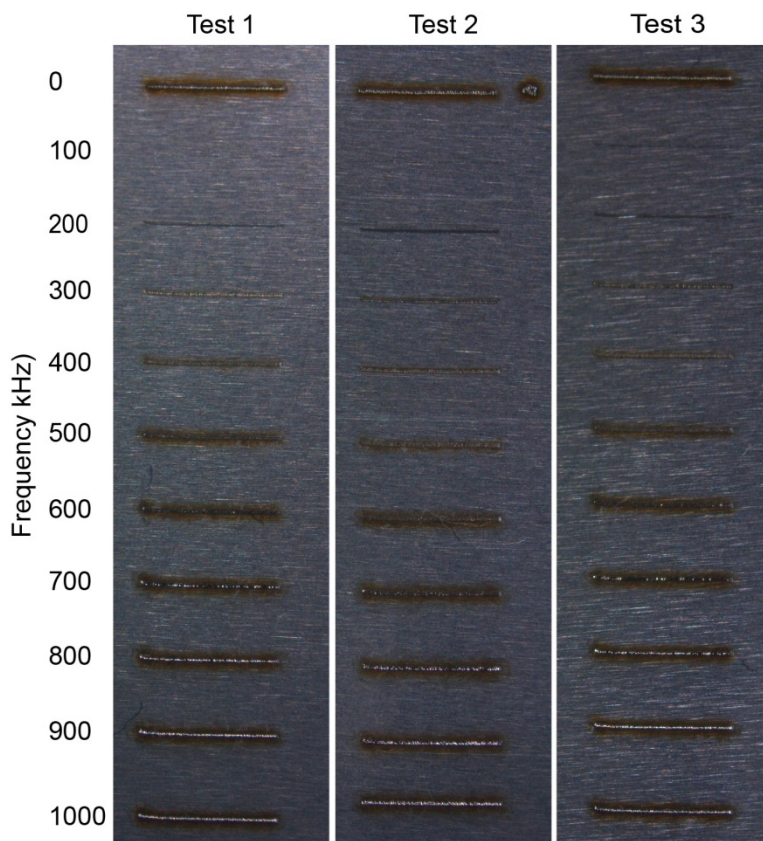


**Figure 3.5: Laser frequency optimisation.**

Three sets of lines (n=3) were laser cut at varying frequency from 0 to 1000 kHz to determine the optimal laser frequency when laser was set at 100% power and 0.02 m/s speed.

A speed and power test was carried out to make sure that the problem of inconsistency caused by the software and laser system was resolved. The lines were laser cut in triplicates using mid (50%) and high (100%) power, at varying speeds from 0.002 to 0.02 m/s and a frequency of 300 kHz (**Figure 3.6a**). The cuts were similar when compared across each setting. None of the lines were cut when power was set at 50% (**Figure 3.6a**,

**left panel**). On the other hand, all 30 lines were cut when power was set to the maximum (**Figure 3.6a, right panel**). This indicated that the minimum threshold to produce a cut was more than 50% power for this laser cutting system.

A reduction of heat affected zone (HAZ) was observed speed was increased for both sets (**Figure 3.6a, left and right panels**). Low cutting speeds resulted in thermal damage to the material. This finding was also reported by Wang when cutting speed was increased from 0.045 m/s to 4 m/s (Wang, 2000). The decreasing trend of HAZ was true regardless of the power. He also reported an increase in HAZ with increased power. Observations in

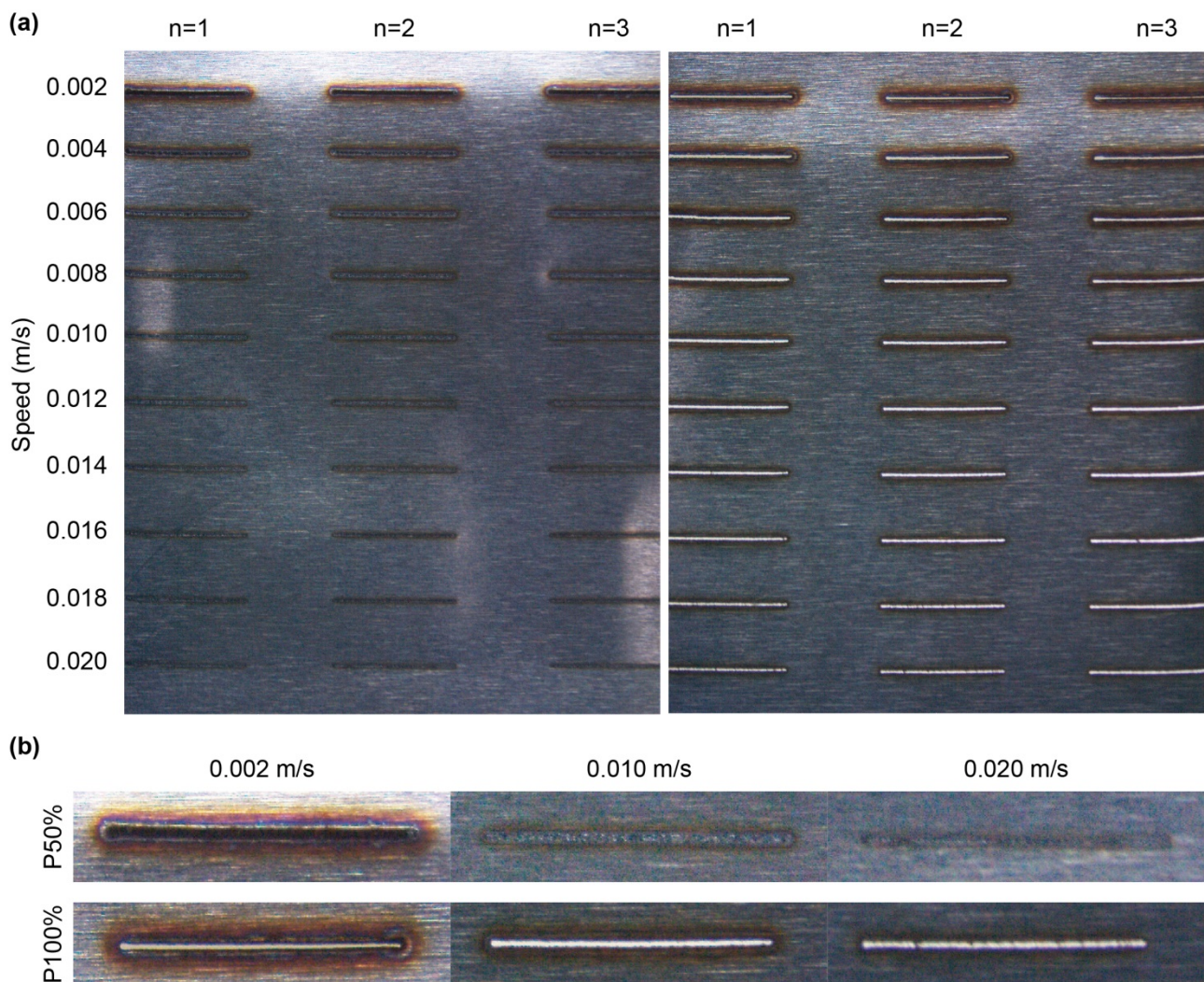


**Figure 3.6 Laser power and speed optimisation.**

Two sets of lines ( $n=3$ ) were laser cut at varying speed from 0.002 to 0.020 m/s at 50% and 100% power. The frequency was set at 300 kHz and kept constant for both sets of lines.

this study also revealed similar a finding with more pronounced heat affected HAZ at 100%

power (**Figure 3.6b**). Presence of dross was observed when laser cutting at higher speeds and at 100% power (**Figure 3.6b, bottom row**).

Based on the previous power and speed test, a complete cut with minimum dross was achieved at 100% power and speeds between 0.002 m/s and 0.020 m/s. In the next study the maximum power and speed of 0.006 m/s was kept constant, while varying the frequency to investigate its influence on the kerf quality. Complete to partial cuts were achieved when the frequency was equal to or less than 700 kHz (**Figure 3.7a, left panel**). The enlarged images on the right panel of **Figure 3.7a** showed that the cuts were wider at higher frequencies (300 kHz to 700 kHz) than lower frequencies (100 kHz to 200 kHz). Only lines cut at 300, 400 and 600 kHz had a complete cut. Minimum dross within the cut was observed at 300 kHz (**Figure 3.7a, right panel**). Five measurements were taken randomly across the entire line and data presented as individual measurements with SD (**Figure 3.7b**). There was an observational trend in decreased kerf widths when frequency shifted from high to low (1000 kHz to 100 kHz). The results agreed with what Keles and Oner reported in their study. They described smaller kerf widths were achieved at higher frequencies between 1000 kHz to 1500 kHz. However, they did not see a clear trend of decreased kerf width with increasing frequency in different workpiece thickness (Keles and Oner, 2012). The cut at 300 kHz had a smaller kerf width ( $44.10 \pm 3.25 \mu\text{m}$ ) than 400 kHz ( $56.52 \pm 3.59 \mu\text{m}$ ). A decreasing trend of HAZ when frequency was reduced was also observed (**Figure 3.7a**). In summary, the optimal frequency was determined to be 300 kHz given that the cut was complete with the smallest kerf width.



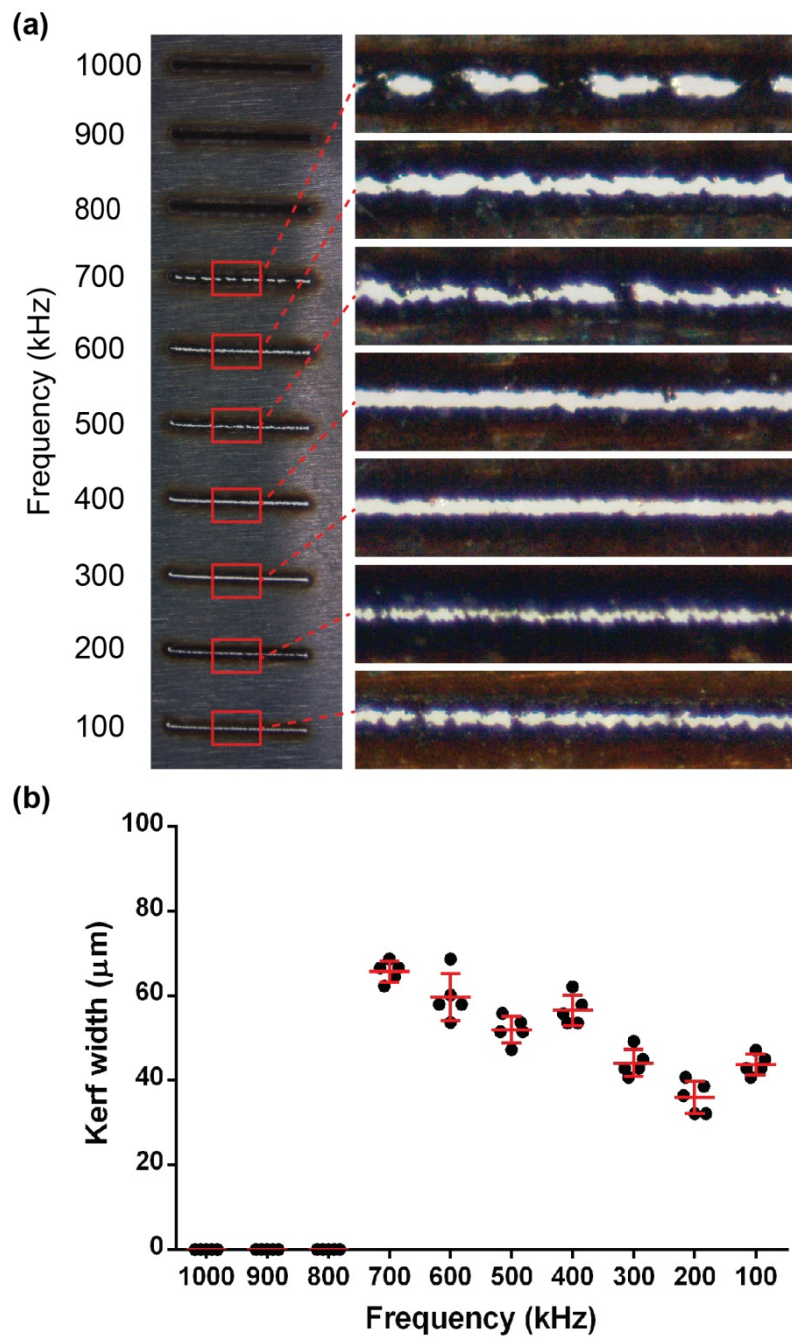


**Figure 3.7: Repeat of laser frequency optimisation.**

Single set of lines were laser cut at varying frequency from 0 kHz to 1000 kHz to determine the optimal laser frequency when laser was set at 100% power and 0.006 m/s speed (a). Five kerf width measurements were taken randomly within each line. Standard deviations of the measurements were indicated as the red bar in the graph (b).

The relationship between laser parameters is complex. Therefore, a wider speed range with 300 kHz and 100% power was performed to re-assess the optimal speed. Complete and partial cuts were observed when speed ranging from 0.002 m/s to 0.060 m/s was tested (**Figure 3.8a**). The cuts were observed to be complete with minimum dross at low speeds (0.002 to 0.018 m/s, left panel). More dross within the cut was observed with increasing speed (0.020 to 0.060 m/s, middle and right panels).

To enable more accurate identification of the optimal speed, lines that had complete cut and the least amount of dross were first selected. Kerf width of the laser cut lines processed at 0.002 m/s to 0.040 m/s were measured. The average kerf width was found to be wider when speed was more than 0.004 m/s (**Figure 3.8b**). The measurements did not indicate any trend of wider kerf width with increasing cutting speed. The lines were re-imaged at higher magnification (20x) for kerf width measurement as the image resolution of **Figure 3.8a** was not sufficient. There were limitations to obtaining kerf width measurements as the edge of the kerfs was not defined. This was caused by varying amount of light passing through the lines due to the positioning of the flexible light guide. The angle at which the light guide was positioned changed the amount of light passing through the lines even though the light intensity was kept the same. The size of the kerf widths was variable within the line when processed at cutting speeds greater than 0.026 m/s. Therefore, the average kerf width of the cut might not be the most accurate representation on how the cutting speed affected the end quality.

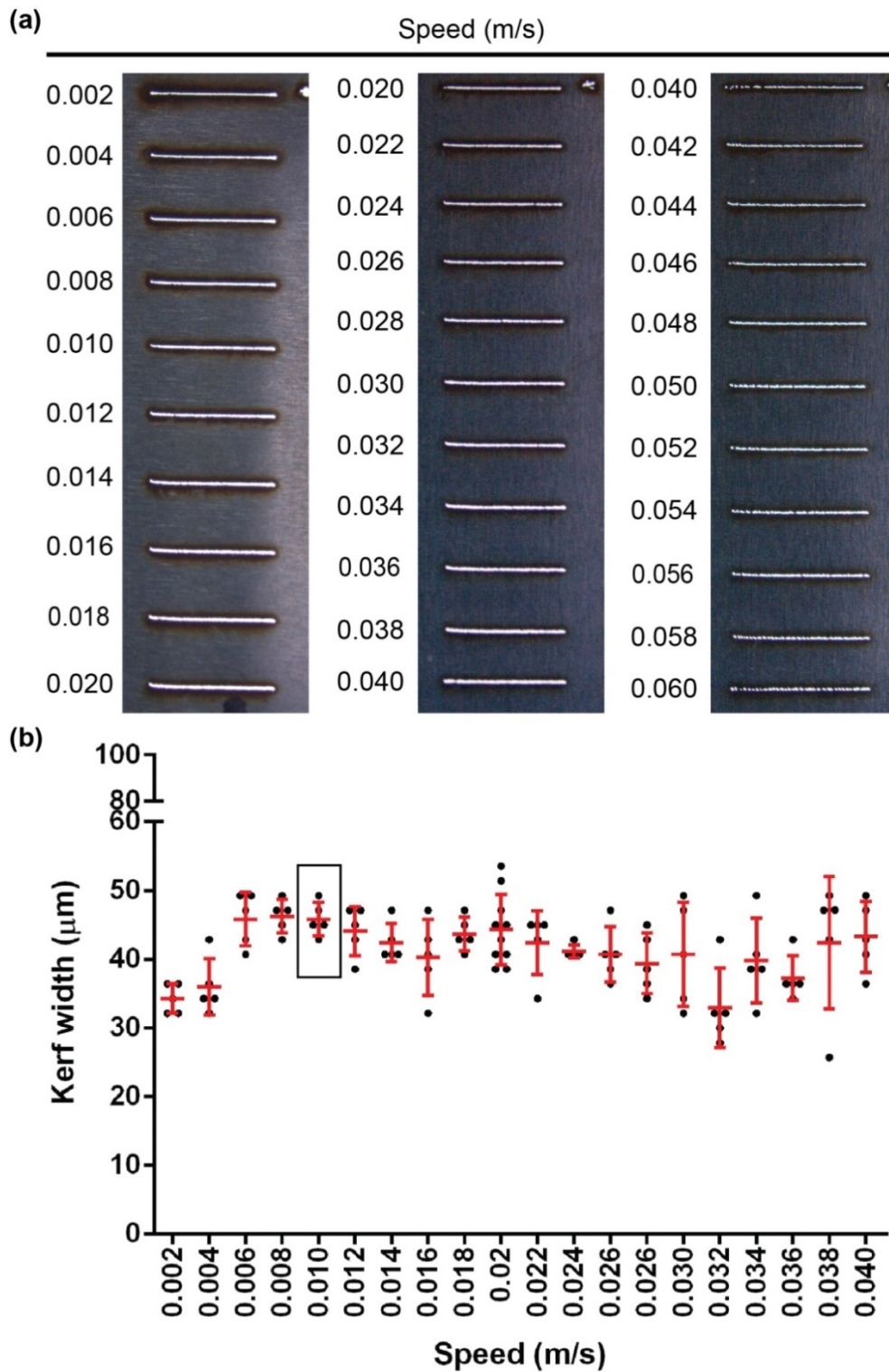


**Figure 3.8: Laser speed optimisation.**

Single set of lines were laser cut at 100% power, 300 kHz frequency and at varying speeds from 0.002 to 0.060 m/s (a). Kerf width measured at five random locations within the cut (b).

To improve the method of defining which laser speed results in better quality of cut, binary images of the optical images were generated using ImageJ. The binary image depicted in **Figure 3.9a** shows the total surface area of material that was removed from the line. The indicated red arrows in **Figure 3.9a** were positions of cuts that had smaller kerf width. Therefore, as assumed earlier, the average kerf width may not be the best parameter for identifying optimal cutting settings. Instead of quantifying the kerf width, the total surface area was quantified using the particle counting function in ImageJ. Overall, lines cut with lower speeds (0.002 – 0.008 m/s) were observed to be relatively straight and wide. Cuts above 0.026 m/s were irregular in width and wavy even though the kerf width was mostly narrower. The calculated total surface area of material that was removed within the line is shown in **Figure 3.9b**. The cutting speed that achieved complete cut with minimum dross was determined to be 0.010 m/s (**Figure 3.9b**). In summary, the line optimisation experiments defined optimal laser parameter settings of 100% power, 300 kHz frequency, and speed of 0.010 m/s.

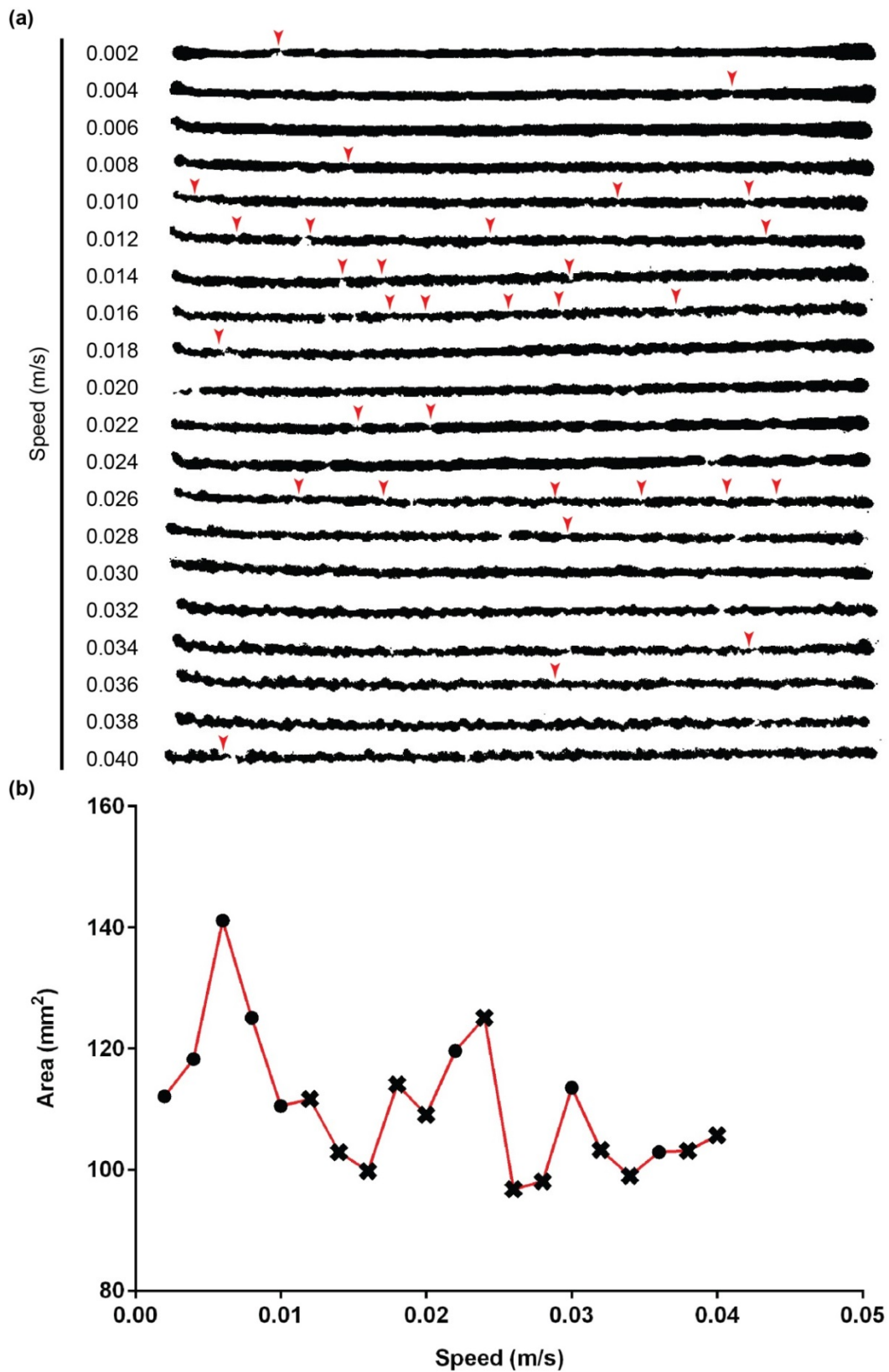


**Figure 3.9: Laser speed optimisation.**

Binary image of laser cut lines derived from previous speed test (**Figure 3.8**). Red arrows indicate areas with smaller kerf width within the line (a). Total surface area of material being removed for each line was calculated with ImageJ software (b). The black circle represents line;2 with a complete cut while the cross symbol represents incomplete cut.

### 3.3.2 Laser setting optimisation with single needle microbiopsy

The previous optimisation studies utilised a single straight line. However, the microbiopsy design consists of both straight and curved trajectories that may not result in optimal cutting quality based on the previously defined parameters. The differences in quality of cut were more evident in the power and frequency tests, and less defined in the speed test. Therefore, the first parameter that was investigated in this test was cutting speed. Single needle microbiopsy cutting die was laser cut at 100% power, 300 kHz frequency and at varying speeds between 0.002 to 0.040 m/s (**Figure 3.10a-t**). Complete cut was achieved with 0.008, and 0.012 – 0.016 m/s laser speeds as highlighted by red boxes in **Figure 3.10d** and **10f-h**. Unfortunately, complete cut at 0.010 m/s, which was identified as the optimal speed in the straight line optimisation test was not observed. One explanation for the incomplete cut at 0.010 m/s could be due to the unevenness of the stainless steel sheet that was used. The stainless steel shim was trimmed down into smaller sheets using a pair of scissor before the microbipsies were laser cut. The process of trimming might have warped the sheet.

Another set of microbiopsy cutting die at varying speeds but with power reduced to 90% was laser cut. The power was scaled down to compare the microbipsies cut at different powers and at varying speeds. The only cutting die that had complete cut were done at 0.006 m/s and 0.008 m/s (data not shown). This finding correlated with what Steen and Mazumder previously described (**Figure 3.2**) (Steen and Mazumder, 2010). Total surface area calculation was not possible as strong reflection was captured in the optical images, negatively influencing the image threshold adjustments. Kerf width measurements were obtained for microbipsies with complete cuts. Kerf width measurements ranged between  $38.15 \pm 6.2 \mu\text{m}$  to  $44.51 \pm 8.01 \mu\text{m}$  (**Figure 3.10u**). One-way ANOVA analysis indicated that the width differences between different speeds were not significant. Based on the results, cutting speed at 0.016 m/s was defined as the optimal speed given that the cut was more even across the entire laser path ( $43.04 \pm 5.7 \mu\text{m}$ ). The uniformity of the cut was partially attributed to a reduction in the amount of dross.

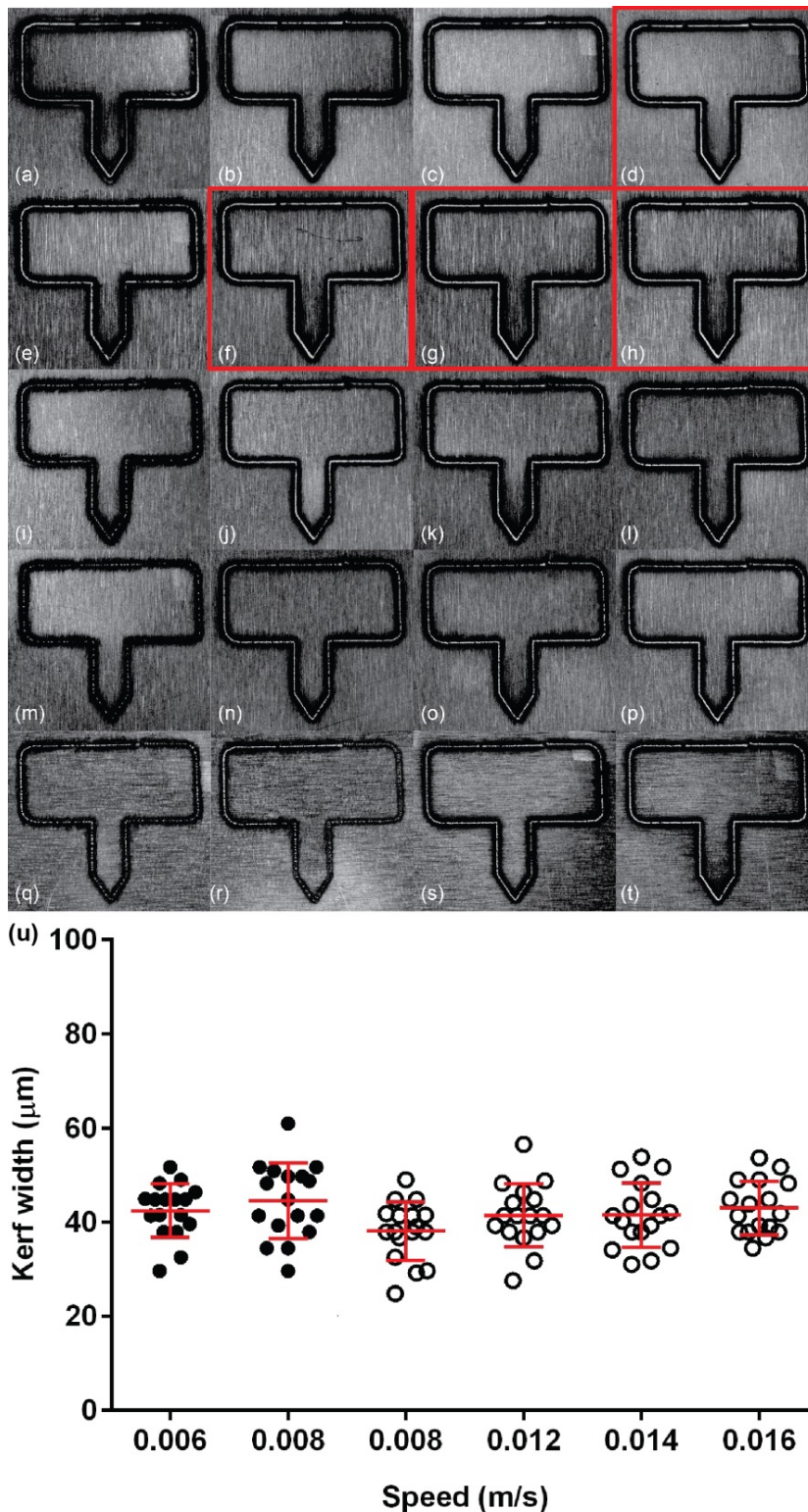


**Figure 3.10: Laser speed optimisation using single needle microbiopsy.**

Greyscale images of single needle microbiopsy that were laser cut at 100% power, 300 kHz frequency and at varying speeds (a-t). Kerf width measurements of selected microbiopsies that had complete cuts were taken at 17 different sites (u). Red bars represent SD of kerf width taken at 17 different area of the microbiopsy. Microbiopsies laser cut at a power of 90% and 100% were represented by the closed circles and open circles, respectively.

The frequency optimisation test was repeated with cutting die at varying frequencies from 0 kHz to 1000 kHz to reconfirm that 300 kHz was the optimal frequency. Laser was set at optimal power and speed of 100% and 0.016 m/s, respectively. Positive cuts for frequencies between 100 - 300 kHz, and minimal or no cut for other frequencies (**Figure 3.11a-k**) were observed. Even though the cut had the highest average kerf width when processed at a frequency of 300 kHz, the cut width was more even compared to others

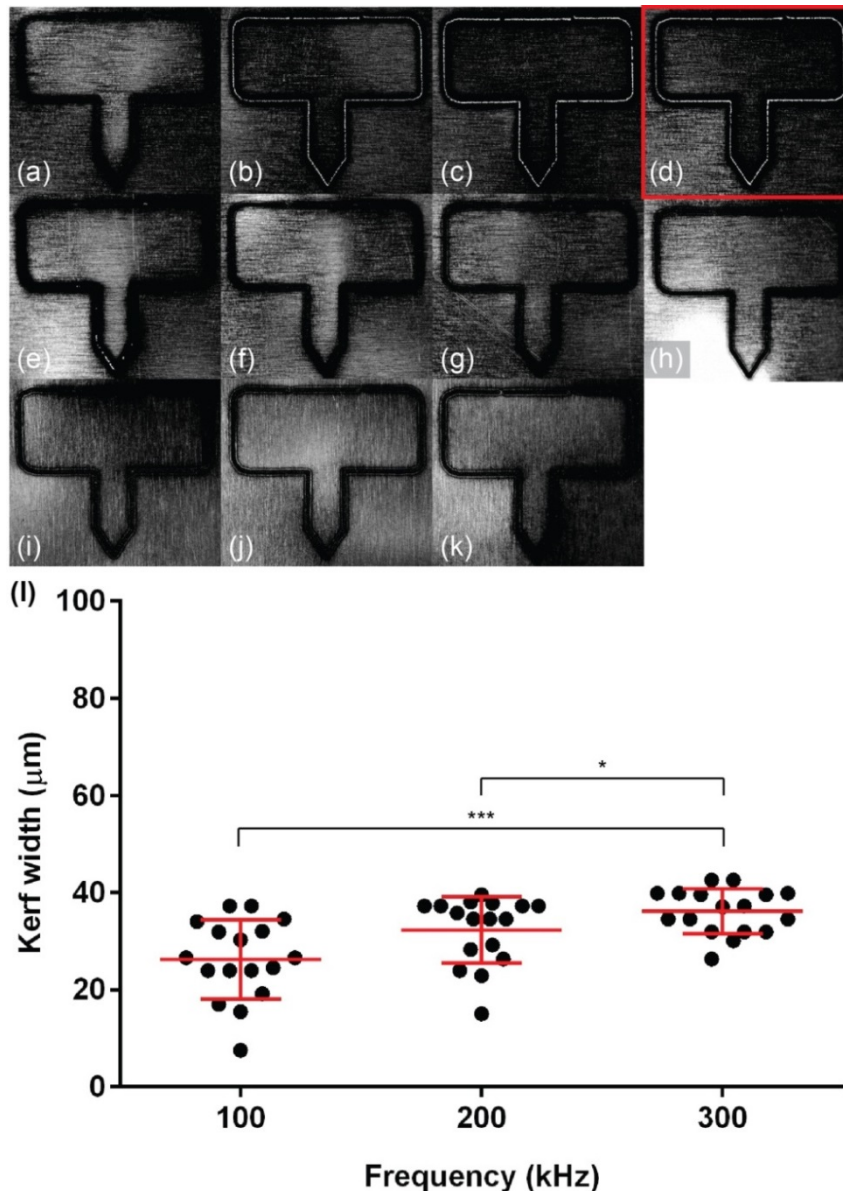


**Figure 3.11: Laser frequency optimisation using single needle microbiopsy.**

Greyscale images of single needle microbiopsy that were laser cut at 100% power, 0.016 m/s speed and at varying frequencies (a-k). Measurements of kerf width were collected at 17 different locations from microbiopsies that had positive cuts (l). Standard deviation is represented by the red bars.



( $26.24 \pm 8.19$  vs.  $32.33 \pm 6.89$  vs.  $36.12 \pm 4.63$   $\mu\text{m}$ ) (**Figure 3.11i**). Another observation noted in this test was that the cut width along the curved trajectory was narrower and had higher amount of dross at lower frequency (100 kHz) (data not shown).

The arrayed microbiopsy was considered to be the ideal configuration, given that multiple tissue biopsies can be collected from a single application. It was important to ensure that the current laser settings are optimised for efficient cutting to prevent thermal damage to the surrounding area. This may in turn cause burning and warping of the microbiopsy cutting die. Array microbiopsy cutting die was laser cut using the optimised parameter settings defined above. Warping on the right needle for all three microbiopsies when cut individually (data not shown) was observed. Similar observations were noted when microbiopsy cutting die was laser cut on individual sheets (data not shown). Subsequently, the power to 95% was reduced and maintained the other settings. The resulting microneedles were all straight and flat for all microbiopsies (n=5) (**Figure 3.12a**). This indicated that the power was slightly above optimal level for laser cutting curved or angled trajectories. Width and length measurements showed that the width and length for all microbiopsies were comparable and within  $\pm 10\%$  of the defined measurements (**Figure 3.12b**). The widths and lengths of the right needle were observed to be more variable than

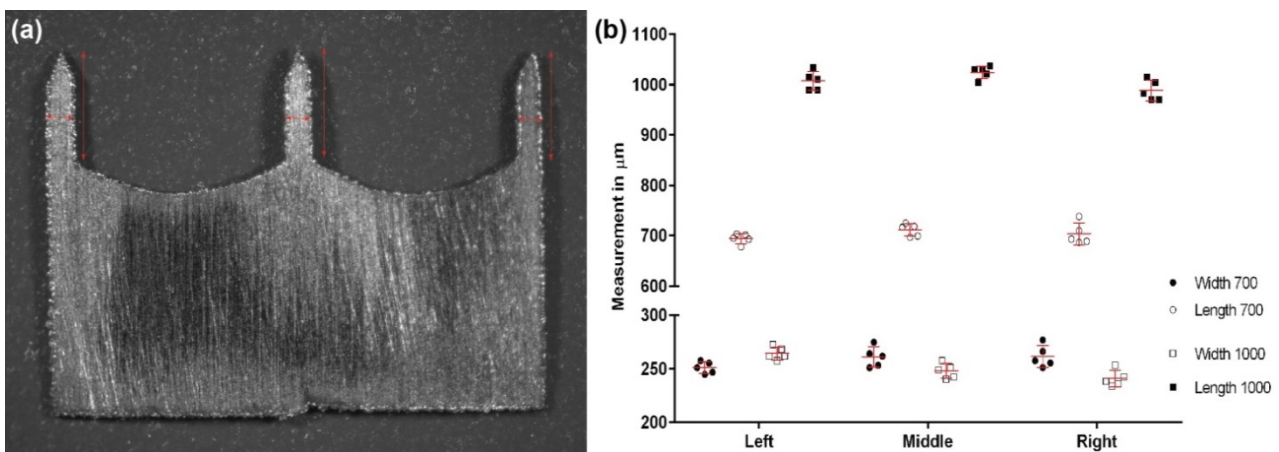


**Figure 3.12: Width and length measurements of array microbiopsies.**

Greyscale image of arrayed microbiopsy that was laser cut at 95% power, 0.016 m/s speed and 300 kHz frequency (a). Graph shows the average width and length of each needle (n=5) of arrayed microbiopsies (b). The microbiopsy had needle length of either 700  $\mu\text{m}$  or 1000  $\mu\text{m}$  with a width of 250  $\mu\text{m}$ .

the other 2 for both 700  $\mu\text{m}$  (SD: 5.47 vs 9.43 vs 10.22) and 1000  $\mu\text{m}$  (SD: 5.95 vs 6.89 vs 7.65) width microbiopsies. This might indicate slight distortion of the microbiopsy during the laser cutting process even though it was not visible to the eye.

One focus of this project was to validate the microbiopsy technology as a platform for molecular analysis of small tissue samples. The amount of tissue sample collected was dependent on various factors. For example, if an arrayed microbiopsy was applied at an angle, there is a possibility that one microneedle may collect more tissue than others. To reduce possible risk of complications arising from arrayed microbiopsy, future assessments and validations were performed using a single needle configuration microbiopsy. In the final optimisation test, the goal was to verify the reproducibility of the channel width. In this test, microbiopsies with 5 different channel widths (**Figure 3.13a-d**) were included and five microbiopsies of each width were fabricated. A single measurement of the channel width was taken from each microbiopsy and compared within each group to determine if reproducible channel width could be achieved. The channel widths of all microbiopsies were within  $\pm 10\%$  of the defined measurements (**Figure 3.13e**).

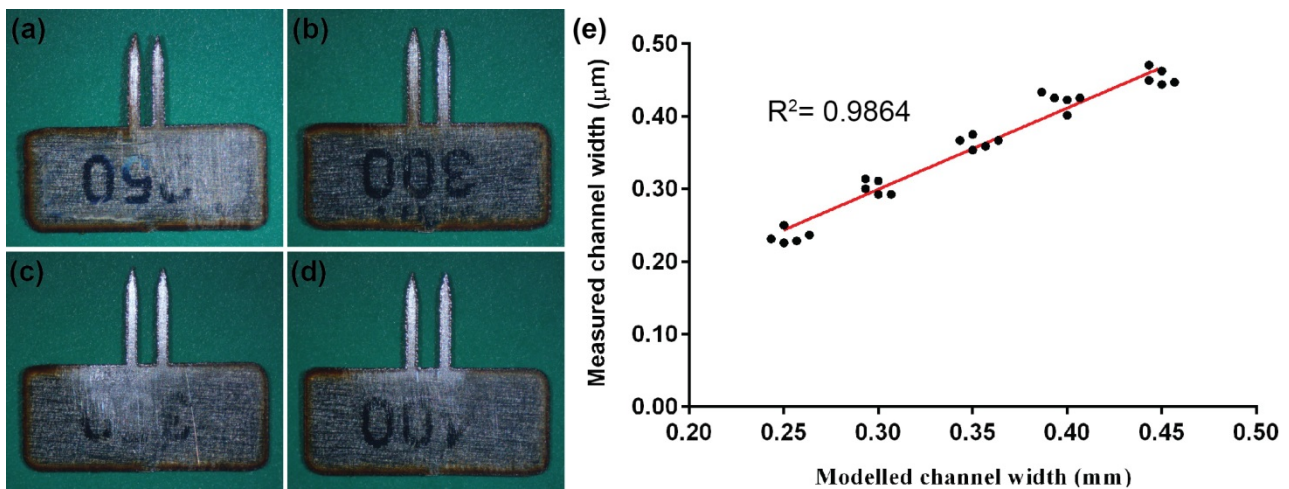


**Figure 3.13: Channel width measurements of single microbiopsies.**

Single microbiopsies of varying channel widths that were laser cut at 100% power, 0.016 m/s speed and 300 kHz frequency (a-d). Graph shows the average width measurements for microbiopsies with different channel widths ( $n=5$ ) (e). Red bar is the standard deviation of the width measurements.

### 3.3.3 Device integrity assessment

It was important to establish the functionality of the microbiopsy cutting die configurations described in **Figure 3.3**. The geometry of the inner and outer plates of the microbiopsy cutting elements were shown in **Figure 3.14a** and **14b**, respectively. The dimension of the hollow channel was approximately 0.42 mm in width and 0.87 mm in length. The microbiopsy cutting die was tested on a piece of excised human skin. No tissue was found in the channel but very small pieces of tissue were hanging on the edge of the cutting die (data not shown). The site of microbiopsy revealed a circular hole that was approximately 0.12 mm x 0.11 mm in size (**Figure 3.14c**). Reflectance confocal microscopy (RCM) identified a microbiopsy puncture site that was approximately 0.11 mm x 0.32 mm in dimension and penetrated up to 0.028 mm in depth (**Figure 3.14d**). RCM mosaics were used to detect puncture site and observe impact of microbiopsy application to the skin. The microbiopsy site was identified with presence of cellular damage (indicated by red arrow) around the puncture site. The confocal stacks indicated that microbiopsy penetration was superficial (data not shown). This might imply that the cutting elements of the microbiopsy were inefficient in piercing the skin. This could be due to a blunt cutting

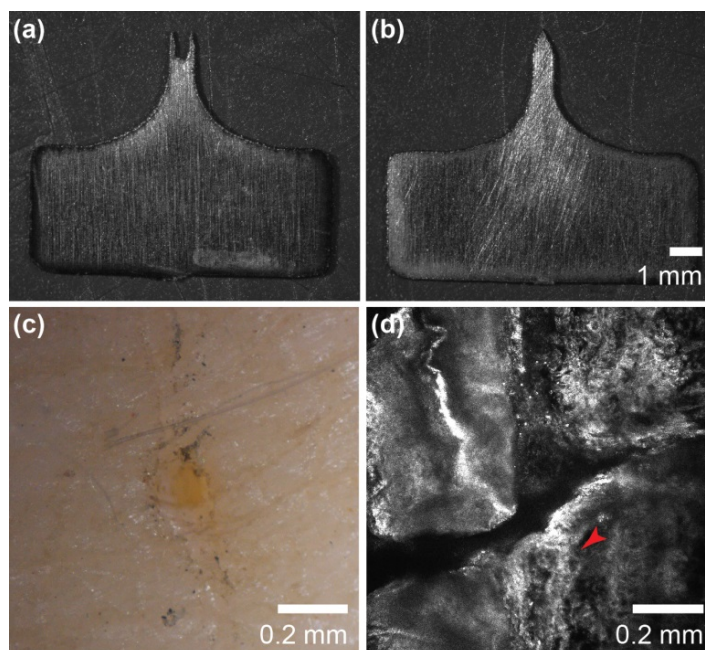


**Figure 3.14: Functionality test of microbiopsy cutting die.**

Inner plate (a) and outer plate of cutting elements that forms the microbiopsy cutting die. Optical image shows site of microbiopsy application (c). RCM image shows a puncture site at 0.028 mm below skin surface (d).

edge or that the cutting elements were too thick to penetrate the skin. This also explained the lack of tissue present in the channel of the cutting die. The average thickness of human stratum corneum can range between 0.017 mm (cheek) to 0.179 mm (palm) depending on the body site (Egawa et al., 2007). It was very likely that the cutting die just passed the rigid stratum corneum layer and penetrated superficially into viable epidermis. Therefore, only small pieces of cornified tissue was torn and removed from the skin during application.

Accordingly, a sharp tapered end of the outer cutting elements was created by filing the edges and one side of the tip with sandpaper (**Figure 3.15a** and **15b**). The microbiopsy cutting die was assembled with the tapered side of the outer cutting plate facing outwards, effectively creating a wedge (**Figure 3.15c**). This allowed the blade to cut into the skin without being pushed apart during penetration. Similar to the previous test, no tissue within the channel of the cutting die but only small pieces of tissue hanging on the edge of the cutting die (data not shown) was found. RCM mosaics identified the puncture site next to a hair follicle that was approximately 0.25mm x 0.75 mm in dimension (**Figure 3.15d**). Stacks of mosaics at 0.05 mm increments were taken to assess the penetration depth and scope of cellular damage around the application site (**Figure 3.15e** and **15f**). The RCM image taken at 0.033 mm (**Figure 3.15e**) and 0.066 mm (**Figure 3.15f**) below skin surface revealed a distinct puncture region and intact tissue within the puncture site. This indicated that the the outer cutting plates penetrated efficiently into the skin but the cutting die did not remove the tissue from the skin. This experiment showed that a sharp and thin outer cutting element may be necessary for effective penetration to get pass the rigid cornified layer. Confirmation of penetration depth was not possible using RCM due to the lack of contrast in the excised skin.

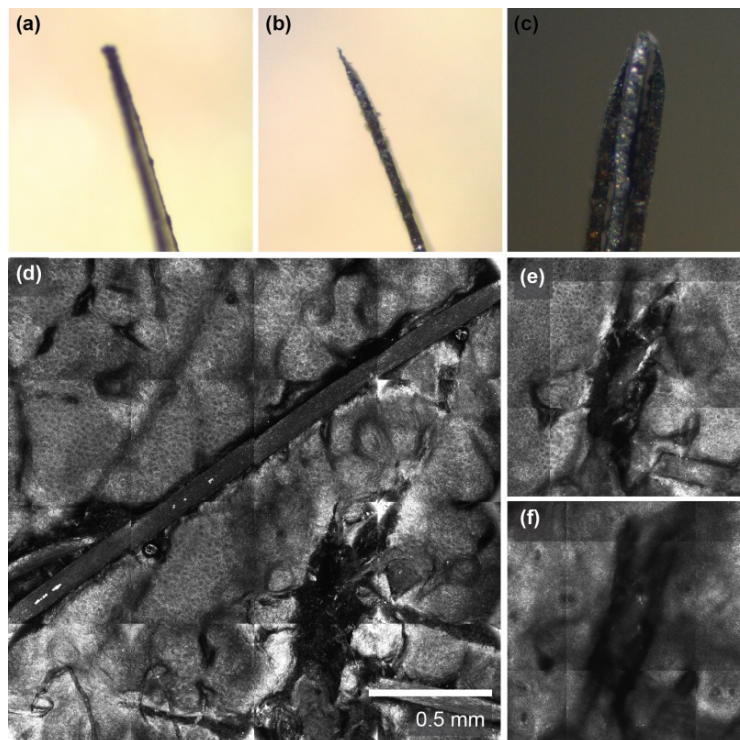


**Figure 3.15: Functionality test of tapered tip cutting die.**

Outer cutting plates were filed on one side of the tip (a) - (b) to create sharp tapered end for the cutting die (c). RCM image shows a puncture site located next to a hair follicle at a various depths below skin surface (d) – (f).

The outer plate was replaced with 0.01 mm thick 304L stainless steel to create a cutting die of similar width to the manually filed plate (**Figure 3.16a**). The hypothesis was that a thinner outer cutting blade would result in improved penetration due to less resistance during application. The microbiopsy cutting die was applied to the skin using the same applicator and speed. However, both the 0.01 mm outer cutting plates were bent post application (**Figure 3.16b**). There was no visible penetration into skin when examined under the stereo microscope. This suggested that a sharp tapered edge was the key to achieve effective skin piercing. The thickness of the outer cutting element was not the cause for superficial penetration into skin as seen in the previous experiment.

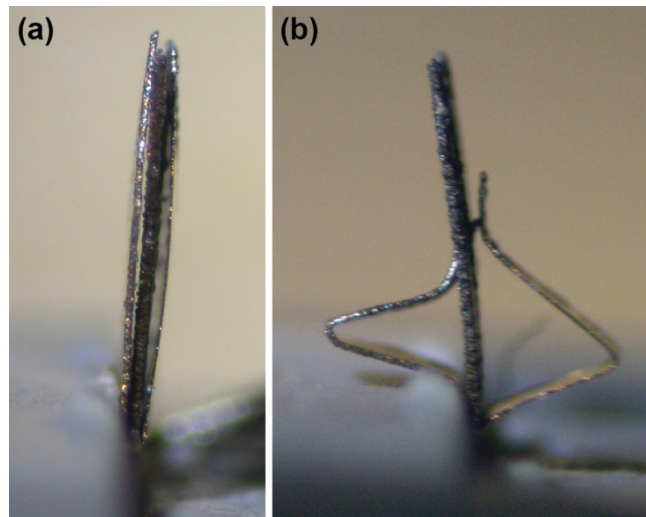


**Figure 3.16: Functionality test of cutting die with 0.01 mm thick outer plates.**

The optical images show the before (a) and after (b) microbiopsy application.

### **3.4 Conclusions**

Fabrication of the microbiopsy device was not possible without first optimising the laser cutting parameters. However, the optimisation process was not straight forward and instead consists of a complex matrix of parameters such as frequency, speed and power. Additionally, the laser parameters were unique for different type of materials and their thickness with optimised settings for one material of a certain thickness not applicable for the same material of different thickness. Furthermore, parameters were machine dependant.

Even though assisting gas pressure and beam divergence were also important factors to consider when optimising laser parameters, adjustments to these laser parameters were not possible due to the set-up of the laser system. The trends observed correlated with previous publications even though the lasers were of vastly different powers and the materials were also thicker in the industrial applications than what was used in these experiments. For example, the kerf width was reduced from  $65.67 \pm 2.44$  to  $44.10 \pm 3.25$  by decreasing the laser frequency to the optimal level of 300 kHz from 800 kHz. This improvement enabled relatively accurate microneedles to be fabricated in just a few seconds for the studies described in the following Chapters 4, 5, 6, and 7. This showed that the previous observations could be adapted for micromedical device prototyping.

These experiments were sufficient to optimise the laser parameters for the purpose microbiopsy prototype fabrication. Further optimisation of laser cutting parameters is required for mass manufacturing but this is outside the scope of this thesis.

Compared to industrial optimisation of laser cutting systems, these optimisations were limited to thin shim material and therefore not as detailed as what has been described in more sophisticated systems/applications. Others have reported the use of high resolution scanning electron microscopic images for accurate measurements of the heat affected zone (HAZ) and kerf width. Making these measurements in the context of the microbiopsy was not as relevant as the industrial applications, so the analysis was limited to optical assessment of kerf width and cross characterisation.

The findings from this Chapter have highlighted the importance of laser parameter optimisation. The conceptual path outlined in the literature was followed and applied to the principals of microbiopsy fabrication protocol using a laser etching system. This opened up the possibility for microbiopsy fabrication. The preliminary experiments have shown the potential of the first generation microbiopsy cutting die for microsampling of skin tissue. However, more optimisation was needed once functional testing began and these experiments were discussed in Chapter 4.

## Chapter 4

### *Microbiopsy optimisation and characterisation*

#### 4.1 Introduction

Skin biopsy is one of the most essential techniques in dermatology for accurate diagnosis of neoplastic or inflammatory skin diseases through histopathological assessment. This technique is performed under local anaesthetic by trained medical personnel, normally a dermatologist, to remove a skin sample 2–4 mm in diameter using a punch biopsy tool or a scalpel (**Figure 4.1**). The wound is then either sutured or left to heal. The sample is then preferably sent to a dermatopathologist for histopathological diagnosis. Pathological examination using skin biopsies often complements and/or confirms diagnosis of common neoplastic or inflammatory skin diseases (Sina et al., 2009).

An excisional biopsy, a common alternative in neoplastic skin conditions, is performed when the entire tumour is needed for histopathological examination, or when melanoma is suspected. This depends on the size and location of the lesion and can be performed using a larger 4 – 6 mm diameter punch biopsy, a deep shave biopsy, or with a fusiform excision (Pickett, 2011a). These biopsy techniques coupled with histopathology diagnosis enable accurate analysis of the disease occurrence and progression. However, the downsides of these techniques are that they require local anaesthesia and sutures in addition to the time required to carry out the procedure. Furthermore, use of a sample that is generally fixed with formalin hinders molecular analysis.

Molecular pathology is rapidly advancing as a field and will become increasingly important in dermatology. The first step to molecular analysis is DNA and RNA preparation and isolation. They are basic but important steps for many molecular analysis protocols. Individual or parallel isolation and purification of DNA, RNA and protein from mammalian cells can be done using commercially available kits and reagents. These kits utilise either anion-exchange columns (Budelier and Schorr, 2001), silica membrane columns (Moore and Dowhan, 2001a), magnetic beads (Berensmeier, 2006) or organic extraction (Moore and Dowhan, 2001a). General benefits include time-saving, straight forward process and effectiveness in isolation and purification.



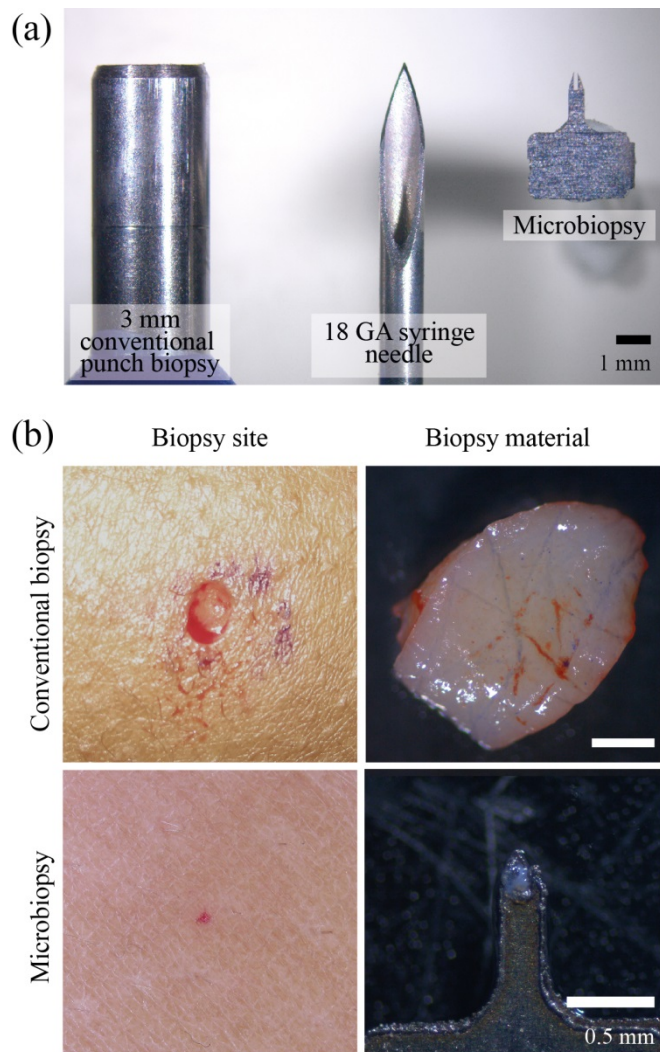


**Figure 4.1: Size comparison of needle biopsy devices and biopsy comparisons.**

A conventional biopsy punch is shown on the left, an 18 gauge syringe needle in the centre and the inner chamber of the microbiopsy device on the right, Panel (a) the microbiopsy device chamber is 0.15 mm in width with an outer width of 0.25 mm. The top row of Panel (b) contains a conventional 3 mm biopsy site and tissue, whereas the bottom panels show microbopsied skin and tissue. Reproduced from (Lin et al., 2013).

The downsides of using kits are higher cost per sample and inflexibility for isolation of samples that involve special conditions (Moore and Dowhan, 2001b, Kingston, 2001). Kit selection depends on the amount of starting material, the compatibility of sample types and the nature of downstream applications. The small size of microbiopsy samples creates challenges for downstream processing. Pre-analytical variability can cause bias and variability to downstream molecular analysis (Espina et al., 2009, Spruessel et al., 2004). Cells within the tissue biopsy can react to the sampling procedure (Spruessel et al., 2004).

Therefore, commercially available reagents used for stabilising tissue (PAXgene), and DNA and/or RNA (RNALater®) are used to preserve the integrity of the macromolecule (Gundisch et al., 2013, Staff et al., 2013, Lee et al., 2013, Pérez-Portela and Riesgo, 2013).

Molecular fingerprinting of skin disease has the potential to dramatically improve diagnostic sensitivity and open the door for personalised medicine (Greinert, 2009, Shivers et al., 2007, Ugurel et al., 2009). To date, there have been no reports on biomarker profiling of lesional samples in a prospective study. This is due to the lack of suitable technologies to perform multiple, non-destructive sampling over time. Furthermore, the iatrogenic issue of cutting out the lesion through biopsy precludes further study of that lesion. This problem exists in many medical disciplines and has led to the evolution of experimental diagnostic devices that tend to be miniature versions of their predecessors. This miniaturisation trend is enabled by several factors including improved micro-manufacturing tolerances, decreased costs and increased availability. One of the earliest micro-devices developed to obtain biopsy samples was patented by Krulevitch et al (Krulevitch P.A., 1999). They patented vascular microbiopsy/precision cutting devices fabricated by conventional machining, silicon micromachining, precision machining and injection moulding. Over the years, there have been many similar patents that report a variety of similar microbiopsy devices.

The unifying theme is that the vast majority of these patents describe micro-biopsy devices for breast or intestinal tissue sampling (Byun S., 2005, Cho D., 2011, Cosnier et al., 2009, Pflueger D.R., 2004) and importantly none were engineered for skin or skin lesions. Our group has developed a new microbiopsy platform technology that enables the collection of tiny pieces of skin using a micro-medical device that is minimally invasive and does not require local anaesthesia (IP Australia Appl. Num. 2012901490, filed on 16/04/2012). There are situations when conventional biopsies are not appropriate. Skin disease may present with multiple lesions and/or in a cosmetically sensitive area. The microbiopsy device has the potential to fill a void in dermatology where conventional biopsies are not feasible or could do more harm than good. The aims of this Chapter were to:

- AIM 1** Determine the content of microbiopsy samples
- AIM 2** Observe the wound healing kinetics of microbiopsy site
- AIM 3** Evaluate commercial extraction approaches
- AIM 4** Optimise microbiopsy application and configuration parameters

This Chapter compared conventional biopsy and microbiopsy. Characteristics of the microbiopsy tissue and microbiopsy site were evaluated. Different molecular processing methods using commercially available kits and protocols were explored to determine the optimal handling procedure for microbiopsy samples. This Chapter also discussed important application and configuration parameters of the cutting tip, which were critical for optimisation of tissue collection. To summarise briefly, the experiments included in this Chapter show that the microbiopsy sample can contain 1000 to 3000 cells corresponding to approximately 5 – 10 ng of DNA. The use of the microbiopsy did not cause any adverse reactions in volunteers. Small sample size was overcome by amplification via polymerase chain reaction (PCR) and the samples were comparable, in terms of quality and quantity, to the much larger matched conventional biopsies.

## 4.2 Materials and Methods

### 4.2.1 Fabrication of cutting tips with varying widths, geometries and micro-texturing

The cutting tips were fabricated from 304L stainless steel with varying widths using the S290-20 laser system at 100% laser power (**Chapter 3, Figure 10**), speed of 0.016 m/s (**Chapter 3, Figure 10**) and frequency of 300 kHz (conditions optimised in **Chapter 3, Figure 11**). The cutting tips used in the volunteer studies were polished and assembled according to the protocol described in section 2.1.1. However, the microbiopsy devices were sterilised in 70 % isopropanol prior to use instead of gamma irradiation. To accommodate the large amount of microbiopsies required for the studies, their fabrication was outsourced to Mastercut Technologies (Burleigh Heads, Australia). The microbiopsies supplied were cut according to my specifications. The microbiopsies that were subjected to micro-texturing were fabricated using photochemical etching and the designs with different geometries were fabricated using Mastercut's laser cutting systems. Different levels of micro-texturing were achieved in-house by adjusting the laser's cutting speed and resolution as shown in **Table 5**.

**Table 5: Laser parameters used for micro-texturing of cutting tip.**

Microbiopsy	O1	O3	O4	O5	O6	O8	M4	M6
Resolution (DPI)	125	250	380	380	500	500	380	500
Speed (m/s)	0.026	0.026	0.011	0.026	0.011	0.026	0.011	0.011

A clean microscope slide was put on top of M4 and M6 cutting tips during micro-texturing to prevent the cutting element from warping. Increasing the resolution (DPI) of the laser decreases the spacing between each laser pulse. Higher DPI produces more etching in a fixed surface area, creating a rougher surface. On the other hand, lower cutting speed can achieve a deeper etch.

#### **4.2.2 Punch biopsy and microbiopsy characterisation**

Conventional punch biopsies (Proscitech, Australia) and microbiopsies were taken from excised human skin. The punch biopsy diameters were 3 mm, 1 mm, 0.50 mm and 0.35 mm. The dimensions of the microbiopsy tested in this experiment were 0.25 mm (width) x 1 mm (length) x 0.15 mm (thickness). The excised skin was mounted on a cork board, stretched and held down by blunt syringe needles. Microbiopsies were applied to the excised skin using the standard spring from the Unistik® 2 blood lancet (Owen Mumford, UK, # 08470-0702-01).

Optical images were collected using a Stemi 2000C stereo microscope (Carl Zeiss, Microscopy GmbH, Germany) after biopsies were applied. Tissue samples extracted by either the microbiopsy or the standard punch biopsy were treated with DRAQ5™ DNA dye (5 mM, BioStatus Limited, UK, #6313) diluted in phosphate buffered saline (PBS). Nuclear labelling of microbiopsy samples were done with the tissue remaining within the chamber of the cutting tip. Microbiopsy samples were incubated in the DNA dye solution for 5 minutes; 0.35 mm and 0.50 mm punch biopsy samples for 15 minutes, and; 1 mm and 3 mm punch biopsy samples for 30 minutes. Incubation was done in the dark at room temperature. The samples were removed, rinsed and stored in PBS. The tubes were wrapped in aluminium foil to prevent photo-bleaching by light exposure. Reflectance and fluorescence confocal images were acquired using Vivascope® 2500 (Caliber Imaging & Diagnostics, Inc., USA). Single-field (0.5 mm x 0.5 mm) or mosaic (single-field images that were stitched together) vertical stacks were taken using automatic intensity control (AIC) settings. Images were acquired using L2 (fluorescence) and L3 (reflectance) filter bars at an excitation wavelength of 488 nm. Zero depth was marked at surface on fluorescence channel to ensure both reflectance and fluorescence images were taken from the same initial depth. In the repeated experiment, the tissue samples were subjected to 5-10% citric acid (Sigma-Aldrich, USA, #251275) treatment before incubating with DNA dye to enhance nuclear visibility in the reflectance channel.

### **4.2.3 Total cell count**

Microbiopsy tissue samples were imaged using confocal microscopy (Zeiss 510 META, Carl Zeiss Microscopy GmbH, Germany) at 2- $\mu$ m incremental optical sections. A three-dimensional projection of the microbiopsy with tissue sample was created using Imaris (Bitplane Scientific Software, Switzerland) from the z-stacks. ImageJ software (NIH, USA) was used to count the number of nuclei in the microbiopsy tissue samples. The grey threshold was adjusted for each image. The size of ten individual nuclei was measured to determine the average diameter and area of the cells, which was used to guide the software's automated particle analysis. The cell count per stack or block (mosaic) was estimated by dividing the sum of area over the average size per nucleus.

### **4.2.4 Histology of microbiopsy skin defect**

Excised human tissue that was subjected to microbiopsy application was embedded in Tissue-Tek® optimal cutting temperature (OCT) compound (VWR International Pty Ltd., USA, #25608-930) and cryosectioned (CM1850, Leica Microsystems Pty Ltd, Australia). Histology sections of 10  $\mu$ m thickness were fixed with 100% cold methanol (VWR International Pty Ltd., Australia, #US006360) for 10 minutes, air dried and stained with haematoxylin and eosin (Varistain Gemini ES, Thermo Fisher Scientific Inc., USA) to visualize the microbiopsy sites.

### **4.2.5 DNA isolation comparison**

Commercially available DNA isolation kits, NucleoSpin® Tissue kit (MACHEREY-NAGEL, Germany, #740952) and QIAamp DNA Micro kit (QIAGEN, GmbH, Germany, #56304) were used to compare the DNA yield from 2 mm punch biopsies and 0.20 mm microbiopsies. The punch biopsies were collected from excised human skin and stored in -80°C freezer until they were ready for processing. The samples were finely chopped using a disposable surgical scalpel blade on a microscope slide. Each tissue sample (punch biopsy or microbiopsy) was put into a Lysing Matrix D tube (MP Biomedicals, USA, #116913050) containing either 180  $\mu$ l Buffer T1 and 25  $\mu$ l Proteinase K (NucleoSpin® Tissue kit) or 180  $\mu$ l Buffer ATL and 20  $\mu$ l Proteinase K (QIAamp DNA Micro kit). Only punch biopsies were subjected to additional homogenisation using a FastPrep® FP120 (Thermo Savant, USA) at 6.5 m/s speed

for 45 seconds per cycle. Tissue disruption was completed with 3 cycles. Subsequent DNA isolation steps were carried out according to manufacturers' protocol for both kits.

This experiment was repeated with NucleoSpin® Tissue XS kit (MACHEREY-NAGEL, Germany, #740901) and QIAamp DNA Micro kit (QIAGEN, GmbH, Germany, #56304).

#### **4.2.6 Channel width pilot study**

Microbiopsy cutting tips of four different channel widths ranging from 0.05 mm to 0.20 mm were evaluated. These cutting tips were fabricated by our S290-20 laser cutting system. Microbiopsies were applied on excised human skin and repeated until three successful microbiopsies for each width were collected. The microbiopsy tissue samples were treated with 1 mM Acridine Orange (Sigma-Aldrich, USA, #A6014-25G) for 20-30 seconds to stain for both DNA and RNA. This assay allowed quantification of the total amount of nucleic acid. Each tissue sample was removed from the microbiopsy device with a clean 30-gauge syringe needle prior to imaging to avoid background noise in the reflectance channel from the metal cutting tip. Single-field fluorescence and reflectance images at 2  $\mu\text{m}$  incremental step-wise vertical stacks were acquired with Vivascope® 1500 Multilaser at an excitation wavelength of 488 nm. L1 filter bar was used. The number of nuclei from each image was counted using ImageJ software.

The experiment was repeated with the addition of 0.40 mm, 0.60 mm, 0.80 mm and 1 mm channel widths. Three microbiopsy cutting tips from each width were applied to excised human skin. DNA was extracted from each successful collection using the QIAamp DNA Micro Kit (QIAGEN, GmbH, Germany, #56304) as described in section 2.3.1. The total amount of DNA per sample was determined by the Qubit® dsDNA HS assay (refer to section 2.3.3).

#### **4.2.7 Surface roughness ( $R_A$ ) pilot study**

Four microbiopsy cutting tips of decreasing surface roughness ( $R_A$ ) on the channel edge were evaluated. The microbiopsy with the highest roughness amplitude consisted of a jagged inner channel wall. The other three  $R_A$  were fabricated with

cutting tips of 0.15 mm channel width. The cutting tip was polished with either 428 carbon steel brush (cut and polish) or fine sandpaper (smooth). It was assumed that the micro biopsy that was not subjected to polishing after laser cutting had higher roughness amplitude than the cutting tips that were polished. Three cutting tips from each test group were collected. DNA from each sample was extracted using the QIAamp DNA Micro Kit as described in section 2.3.1. DNA quantification was done using the Qubit® dsDNA HS assay (refer to section 2.3.3).

#### **4.2.8 High resolution device imaging**

A bench top scanning electron microscope (SEM) (JCM-6000 Neoscope, JEOL, USA) was used to acquire high-resolution images of the micro biopsy device. The roughness amplitude of the micro biopsy chamber was obtained by measuring the average distances of the edge to a regression-fitted straight line using MatLab (Mathworks, Australia). The Matlab equation was developed by Hames S. (PhD student within the Group).

#### **4.2.9 Quasi-static and velocity-aided biopsy application**

The conventional cylindrical punch biopsy and the micro biopsy were applied using either quasi-static or dynamic (velocity-driven) application. Static administration was achieved by manually pushing and twisting the biopsy tool into excised skin. For dynamic application, the cylindrical cutting blade of the punch biopsy was removed and attached to a modified plunger (refer to details on section 2.1.4). The number of successful and unsuccessful punch biopsies was recorded. The sites of application for the second method were imaged with the Vivascope® 1500 Multilaser. Prior to imaging, the sites of biopsy were treated with 5% citric acid as per protocol described in section 4.2.2.

#### **4.2.10 Pre-load and application velocity pilot study**

Micro biopsy cutting tip with a channel width of 0.15 mm was used in the pre-load and application velocity preliminary study. Pre-load is the force or pressure applied to the skin prior to applying the micro biopsy resulting in pre-tensioning of the skin. Three different preloads were defined for the study being none, medium and high, which corresponded to approximately 0, 10 and 20 N, respectively. Zero preload was



achieved by resting the applicator lightly on the excised skin before application. The two higher preloads were achieved by firmly pressing the applicator onto the skin prior to and during microbiopsy application. The force was controlled by placing the skin on a scale. The applicator was pressed firmly on the skin before application to achieve medium preload. The preloading application forces determined by Alex Ansaldo (research engineer) were 0 N, 10N and 20 N respectively. Increasing application velocities were achieved with the use of different compression springs and making modification to the standard plunger from the UniStik® 2 blood sampling device. The test groups included in this study were (1) standard plunger with spring from punch biopsy device, (2) plunger with a long scallop (cut) and spring from punch biopsy device, (3) standard plunger with standard spring from blood sampling device, and (4) application without spring (quasi static). The corresponding velocities of these groups were 15 m/s, 13.4 m/s, 9.4 m/s and 0 m/s. Three microbiopsy samples were collected from each test group.

The application velocity experiment was repeated to determine the upper velocity limits. This experiment was performed on the volar forearm of a single volunteer. The microbiopsy applicator (**Figure 4.2**) was designed by Alex Ansaldo and fabricated using a V-Flash® Personal 3D Printer (3D System, USA). A range of compression springs were used to achieve different application velocities. Velocity of the springs was calculated using a spring velocity calculation software developed by Alex Ansaldo. Microbiopsy cutting tip of 0.15 mm channel width was used in the experiment. The application velocities tested were 0.5 m/s, 2.3 m/s, 6.0 m/s, 8.3 m/s, 12.0 m/s and 14.2 m/s. Microbiopsy applications were carried out according to protocol described in section 2.2.2. Clinical photographs were used to document skin after microbiopsy application. The sites of microbiopsy application were examined under reflectance confocal microscopy (RCM).

DNA from each sample obtained from these preliminary experiments was extracted using the QIAamp DNA Micro Kit as described in section 2.3.1. The total amount of DNA per sample was quantified by the Qubit® dsDNA HS assay as described in section 2.3.3.

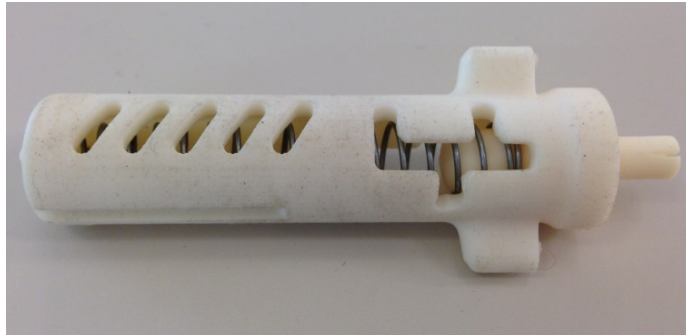


**Figure 4.2: In-house microbiopsy applicator.**

Microbiopsy applicator fabricated by 3D printing system. It consists of a housing case with three loading positioner, compression spring and a plunger with a slit at the tip to fit the microbiopsy cutting tip.

#### **4.2.11 Wound healing kinetics**

A single microbiopsy was applied onto the forearm of each volunteer (n=2). The microbiopsy site was imaged using handheld dermoscopy and reflectance confocal microscopy. Images were taken before and at various time-points (immediate, 24-hours, Day 8, Day 14, and Day 21) after microbiopsy application. Single mosaic and single-field of 2  $\mu\text{m}$ -step increment images were collected at each time point. This experiment was conducted under the approval from Metro South Human Research Ethics Committee, Princess Alexandra Hospital (HREC/11/QPAH/442).

#### **4.2.12 Measurement of pain score**

A blinded pain score evaluation was conducted among 20 volunteers who were recruited in the width and application velocity study. Each volunteer was presented with an assessment form to grade his/her expected pain score based on a numerical rating 10-point Likert scale, 0 as having no pain and 10 as pain as bad as they can imagine before the start of the experiment. The order of microbiopsy application was randomised in the study. Each microbiopsy application was performed one minute apart and the pain score recorded immediately after application. Five minutes after the final microbiopsy application, the volunteers were asked to rate the level of pain for each microbiopsy site to understand if the pain they experienced would last more than five minutes. The volunteers also provided descriptive words related to the pain they felt during and after the microbiopsy application. Zero channel width

microbiopsy and application without spring were included in the study as negative controls. Based on the findings of Gill et al. (2008), it was considered unnecessary to include the commercially available 0.35 mm conventional punch biopsy was not necessary to be included in the study based on previous study (Gill et al., 2008).

#### **4.2.13 Human volunteer study**

Two volunteer studies were conducted under Metro South Human Research Ethics Committee, Princess Alexandra Hospital approval (HREC/12/QPAH/082).

The first study investigated the influence of channel width, application velocity and surface roughness on the amount of tissue collected. The second examined the impact of micro-texturing and different geometries on the amount of tissue extracted.

#### **4.2.14 Channel width, application velocity and surface roughness study**

A total of 20 volunteers were recruited for this study. Ten microbiopsies were collected from each volunteer's forearm. Six channel widths and four application velocities were evaluated in the study. The bore size of the channel ranged between 0 mm to 0.30 mm. The tested velocities were between 1.1 m/s to 20.2 m/s. The bore size of microbiopsy used to test application velocities was 0.15 mm. Clinical images of the forearm were documented before and after microbiopsy application. Dermoscopic photographs of each microbiopsy site before and after application were collected. The photographs were collected with a Canon Power Shot G10 digital camera (Canon, Japan) and a dermatoscope attachment (Dermlite©, 3Gen, USA). Each microbiopsy was applied according to the protocol described in section 2.2.2. Presence of tissue and/or blood were confirmed under stereo microscopy and noted in the collection form. DNA was extracted from all of the microbiopsy samples using the QIAamp DNA Micro Kit (refer to section 2.3.1). Each DNA sample was eluted with 23 µl of AE buffer. The maximum amount of sample volume (20 µl) was used in the Qubit® dsDNA HS Assay (refer to section 2.3.3) to quantify the amount of DNA in each sample.

A separate study was conducted to evaluate cutting tips that had lower surface roughness than the microbiopsies fabricated with the S290-20 laser cutting system. In this study, the cutting tips fabricated with two different laser cutting systems (in-

house S290-20 and a customised industrial laser cutting system), in addition to chemical milling were compared. Four cutting tips from each test group were collected.

All samples were processed for DNA extraction. The total amount of DNA per sample was quantified using the Qubit® dsDNA HS assay (refer to section 2.3.3). Statistical analysis was performed using PRISM 6 for Windows (GraphPad Software, Inc., USA). Channel width, velocity and roughness amplitude data were presented as mean  $\pm$  SD. Pain score for channel width and velocity were presented as minimum to maximum box-and-whiskers plot. One-way ANOVA combined with a Tukey's multiple comparison post-test was performed to determine the statistical significance.

#### **4.2.15 Micro-texturing and geometry study**

Ten volunteers were recruited to test 15 different cutting tips that were either micro-textured using the in-house laser engraving system or had a different geometry from the standard cutting tip. Examinations of the microbiopsy devices post application to check for presence of tissue or blood were not done. DNA was extracted from all of the microbiopsy samples using the QIAamp DNA Micro Kit (refer to section 2.3.1). Each DNA sample was eluted with 23  $\mu$ l of AE buffer. Maximum amount of sample volume (20  $\mu$ l) were used in the Qubit® dsDNA HS Assay (refer to section 2.3.3) to quantify the amount of DNA in each sample.

#### **4.2.16 RNA isolation, quantification and quality control**

Three pieces of excised human skin samples were cut up into finer pieces and subjected to different isolation methods. For RNA isolation with TRIzol® (Life Technologies, USA, #15596-018), 500  $\mu$ l of TRIzol® reagent was added to the tissue sample. The sample was frozen at -20°C and thawed on ice repeatedly for 4 to 8 times to disrupt the tissue. Post disruption, 100  $\mu$ l of chloroform was added to the sample. The tube was then shaken vigorously. The sample was incubated at room temperature for 2-15 minutes or until a phase separation was seen. The sample was centrifuge at 12,000 x g for 15 minutes at 4°C. The mixture separated into a lower red phenol-chloroform phase, an interphase and a colourless upper aqueous phase. The aqueous phase was collected and transferred to a new microcentrifuge tube. An

equal volume of isopropanol was added and mixed well with the sample. The sample was then incubated at room temperature for 10 minutes. Centrifugation of the sample was performed at 12,000 x g for 8 minutes at 4°C. Most of the isopropanol (supernatant) was removed without disrupting the pellet. The pellet was washed using 500 µl of 75% ethanol prepared with nuclease-free water. The sample and ethanol solution was then vortexed followed by centrifugation at 7,500 x g for 5 minutes at 4°C. The majority of the ethanol solution was removed and a 10-µl pipette tip was used to remove the remaining solution without disrupting the pellet. The pellet was air dried on a Kimwipes towel (Kimberly-Clark Professional, USA, #34120) for approximately 10 minutes. Nuclease-free water (30 µl) was added to the pellet and mixed well by pipetting. The sample was then incubated at 55-60°C in a water bath for 10 minutes to solubilise the pellet.

The other isolation method evaluated was with RNeasy Mini kit (QIAGEN, GmbH, Germany, #74106). The chopped up tissue sample was further disrupted either by liquid nitrogen in a pestle and mortar or in a Lysing Matrix D tube. A small volume of liquid nitrogen was poured onto the mortar containing the tissue sample. The snap-frozen sample was then ground using the pestle. Post processing, the sample was placed in a clean microcentrifuge tube containing 350 µl of Buffer RLT using a spatula. Disruption of the tissue in a Lysing Matrix D tube was carried out as described in section 4.2.4 of this Chapter except that 350 µl or 600 µl of Buffer RLT was used. Prior to use, 10 µl of beta-mercaptoethanol (Sigma-Aldrich, USA, #M6250) was added to every 1 ml of Buffer RLT. Isolation and purification of RNA samples were carried out according to the manufacturer's protocol.

The total amount of RNA was quantified using the Qubit® RNA BR Assay (Life Technologies, USA, #Q10211) as per the manufacturer's protocol. Quality control of the samples post quantification was done using the Bioanalyzer RNA 6000 Pico Kit (Agilent Technologies, USA, #5067-1513) as per the manufacturer's protocol.

After determination that good quality total RNA could not be extracted via the protocols described earlier, a commercial kit (Arcturus® PicoPure® RNA Isolation Kit, Life Technologies, USA, #KIT0204) designed for single cell was tested.

Microbiopsies collected from excised actinic keratoses were selected to compare total RNA quality of microbiopsy to lesional samples. The total RNA was isolated from microbiopsy and lesional samples according to the protocol described in sections 2.4.1 and 2.4.2. The total RNA was quantified using the Qubit® RNA HS Assay (Life Technologies, USA, #Q32855) and RNA BR Assay following protocol described in section 2.4.3. The quality and integrity of the total RNA were determined using the Bioanalyzer RNA 6000 Pico kit.

#### **4.2.17 Molecular characterisation of lesional and microbiopsy samples**

Comparison of DNA and RNA from microbiopsy and its matched lesional samples were assessed. Identical amounts of total DNA (1.85 ng) for both lesional and microbiopsy samples were subjected to whole genomic amplification. The amplification procedure was carried according to manufacturer's instructions (REPLI-g Single Cell Kit, QIAGEN, Australia, #150345). The integrity and quality of amplified DNA were assessed using the Bioanalyzer DNA 120000 Kit (Agilent Technologies, USA, #5067-1508).

Identical amounts of total RNA (14 ng) for both lesional and microbiopsy samples were subjected to whole transcriptome amplification. The procedure was carried out using the supplied instructions (QuantiTect Whole Transcriptome Kit, QIAGEN, Australia, #207043). The cDNA obtained from the amplification process was used as a template in a polymerase chain reaction (PCR) reaction using human beta actin primers (forward: ATC TGG CAC ACC TTC TAC AAT GA; reverse: CGT CAT ACT CCT GCT TGC TGA TCC AC) (Integrated DNA Technologies, NSW, Australia). There was an initial denaturation for 2 minutes at 98°C, followed by 30 cycles of 98°C for 30s (denaturation), 67°C for 30s (annealing), and 72°C for 1 minute (extension). The cDNA and PCR products were run on a 1% agarose gel (Bio-rad Laboratories, Inc., Australia) and visualized with RedSafe (ChemBio Ltd., UK, #21141). HyperLadder™ 1 kb (Hyper- Ladder I) (Bioline, UK, #BIO-33053) was used to determine the mass of cDNA and human beta actin amplicons.

## 4.3 Results and Discussion

### 4.3.1 Characterisation of microbiopsy content and site of application

**Figure 4.3** provides a visual presentation to the reader on the varying sizes of conventional punch biopsy compared to the microbiopsy. RCM was used to visualise the

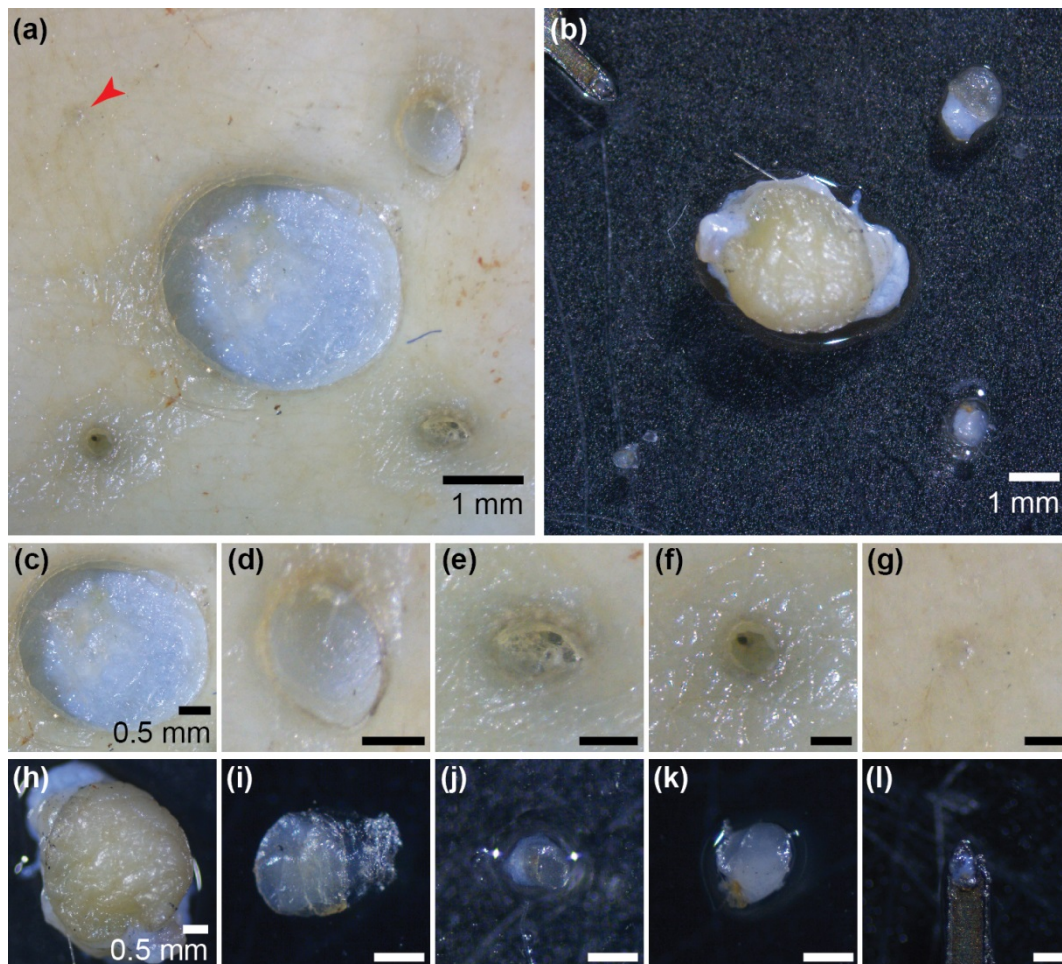


**Figure 4.3: Conventional punch biopsy and microbiopsy sites and biopsy materials.**

Site of four punch biopsies and microbiopsy application on excised human skin (a), and respective biopsy materials of varying sizes (n=2) (b). Clockwise from top left: microbiopsy, 1 mm, 0.50 mm, 0.35 mm; centre is 3 mm (a-b). Middle row shows the enlarged optical images of biopsy sites (c-g). Bottom row are the enlarged optical images of the biopsy materials (h-l).

microbiopsy application site. RCM images revealed a microbiopsy site similar to the size of a small hair follicle in the dermal papillary post microbiopsy application (**Figure 4.4a and 4.4b**). The inset shows that microbiopsy application resulted in a puncture site that was approximately  $0.10 \times 0.50$  mm in dimension (**Figure 4.4b**). Microbiopsy samples were

stained with DRAQ5™ (BioStatus Limited, UK) to highlight the nuclei. Confocal images were used to generate a 3D model of the microbiopsy sample. The usual skin strata were apparent in this model. I estimated that there were 1634 nuclei in **Figure 4.4c**. Puncture sites that were approximately  $0.22 \pm 0.12$  mm wide and  $0.26 \pm 0.09$  mm deep in excised abdominal skin from 10 histological sections were observed (**Figure 4.4d**).

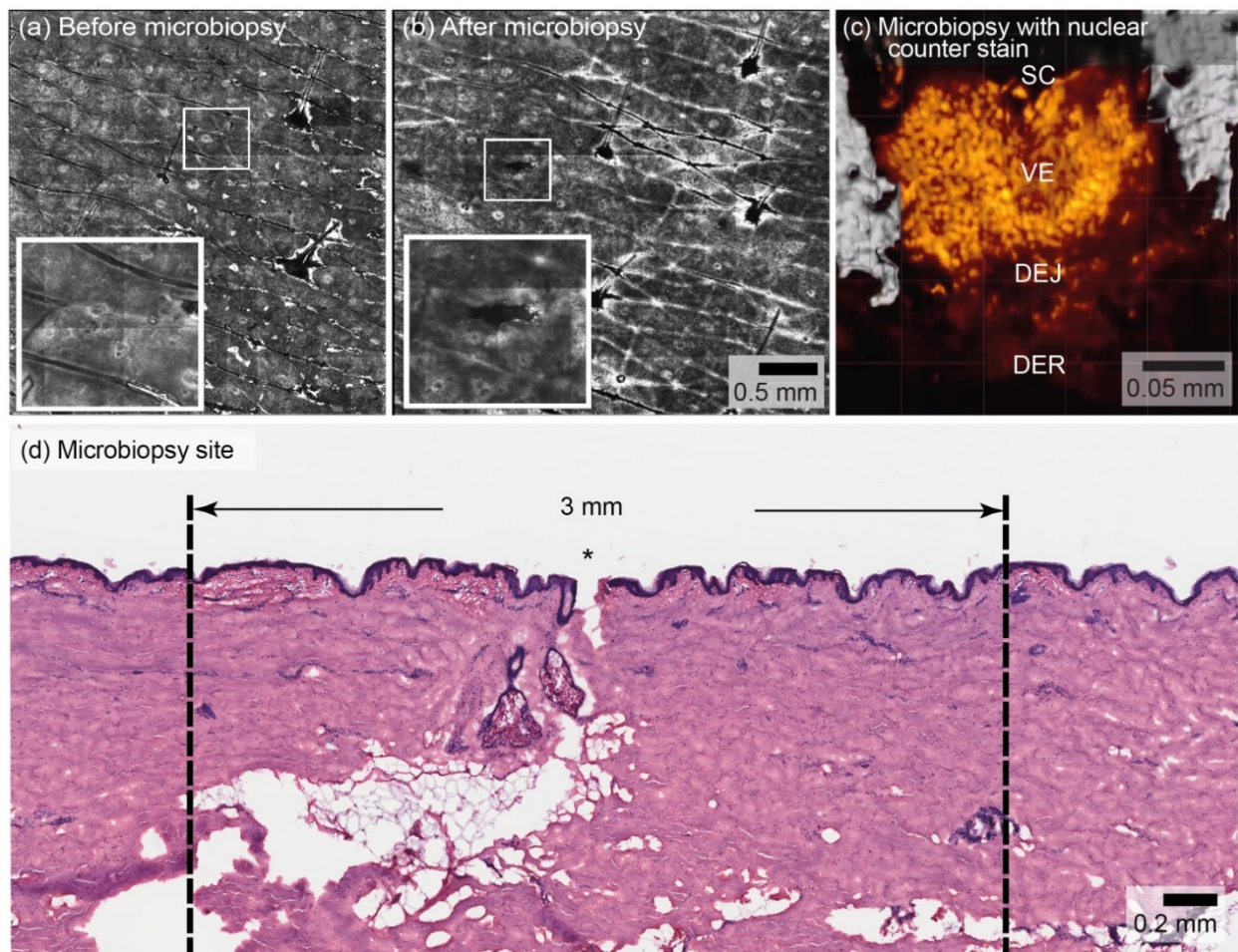


**Figure 4.4: Site of microbiopsy and microbiopsy content.**

Panels (a) and (b) are reflectance confocal microscopy mosaics of a microbiopsy site, hair follicles are featured in the centre and on the right hand side of the images for size comparison (bar indicates 0.50 mm in a and b). Panel (c) shows a 63x magnification, 3D rendering of the microbiopsy tissue with a nuclear counter stain (orange) derived from a confocal microscopy z-stack of the sample within the microbiopsy device. The stratum corneum (SC), viable epidermis (VE), dermal-epidermal junction (DEJ) and superficial dermis (DER) are labelled. This microbiopsy contained an estimated 1634 nuclei. Haematoxylin and eosin stained section of human skin after microbiopsy application shows a 0.10 mm wide and 0.25 mm deep puncture (n=10) (d). \* indicates the site of microbiopsy application. Reproduced from (Lin et al., 2013).



### 4.3.2 Quantification of cellular material

The previous experiment illustrated that increasing the size of the punch biopsy results in greater tissue yield. Therefore, it was hypothesised that increasing the chamber volume of the microbiopsy by widening the channel of the cutting element will increase the amount of tissue collected. To test this, four microbiopsy cutting tips with channel widths ranging from 0.05 mm to 0.20 mm (**Figure 4.5**) were applied to excised human skin. The tissue sample was treated with 5% citric acid with the biopsy *in situ* to improve the nuclear visibility of the samples. Tissue was observed on the edges, surface of the cutting element and within the channel of the cutting tip. Single-field images were successfully acquired for

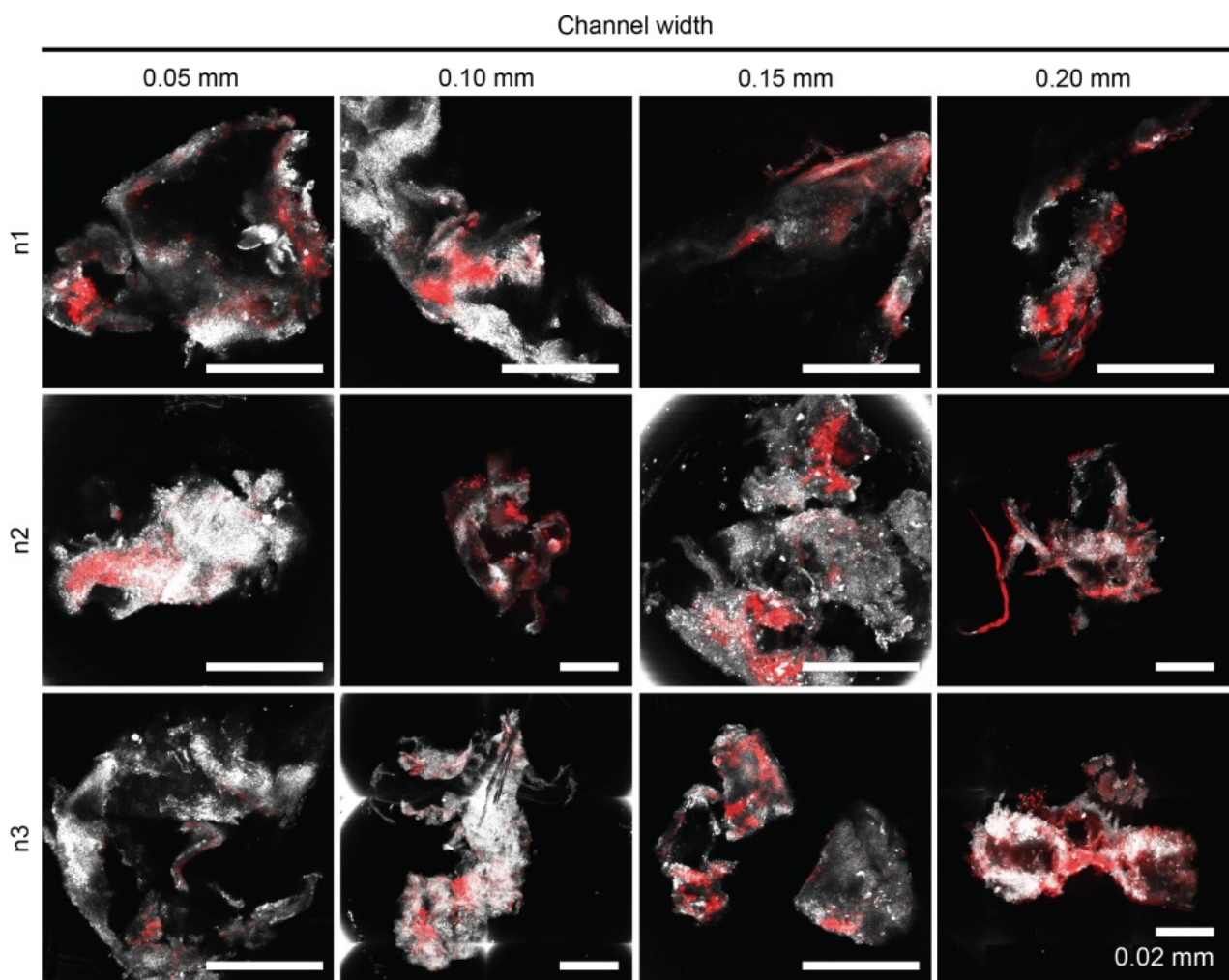


**Figure 4.5: Visualisation and quantification of tissue biopsy from microbiopsy device.**

Tissue samples were extracted using varying channel widths from 0.05 mm to 0.20 mm (left to right). Three microbiopsies from each width were applied on excised human skin. Merged fluorescence (red) and reflectance (grey) confocal images were taken either as single-field or mosaics.

most samples. Four out of 12 samples were too big and the images of the samples were acquired in cubes (z-stacks of mosaic images).

This method can provide a gross estimate of the total cell count for each tissue biopsy. However, the signal-to-noise ratio and z resolution of the confocal system were not sufficient to separate individual cells. Hence, this analysis method was not pursued to quantify amount of cellular material. An accurate quantification method to compare the amount of tissue was to quantify the DNA within each microbiopsy sample.

#### 4.3.4 DNA isolation comparison

Two commercially available DNA kits were selected to compare the total DNA yields from 2 mm punch tissue biopsy and microbiopsy sample. The total DNA yield from the QIAamp DNA Micro kit was higher in both samples compared to the NucleoSpin® Tissue kit (**Figure 4.6a**). The punch tissue biopsy was included in the study as a positive control to ensure that the kits functioned as expected. The difference could be due to the latter kit not being suitable for small tissue samples. The experiment was repeated to compare the QIAamp DNA Micro kit and another kit from NucleoSpin® that was advertised to effectively isolate DNA from small tissue samples. The number of microbiopsy tissue samples was

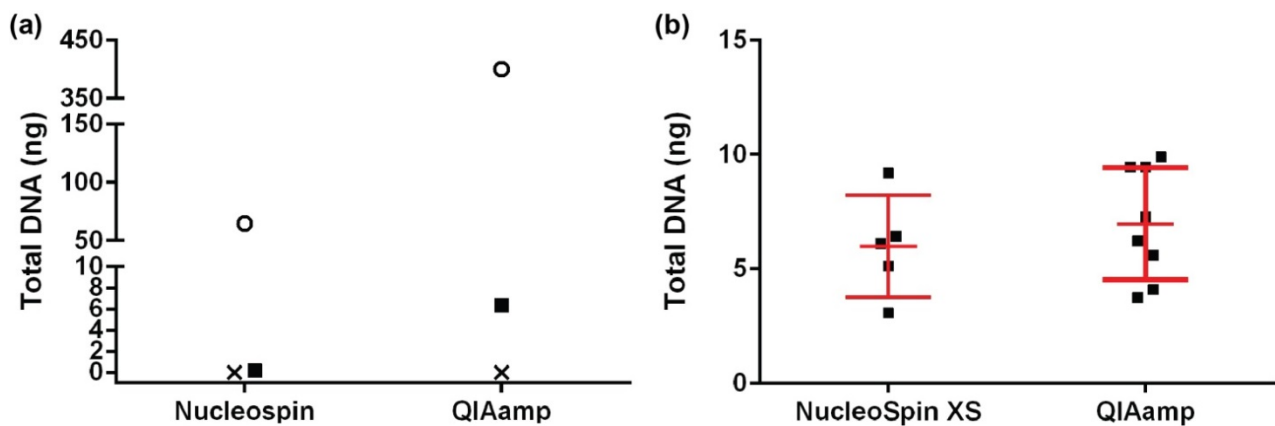


**Figure 4.6: DNA isolation kits comparison.**

Panel (a) and (b) show the comparison in total DNA yield isolated by two commercially available kits. One sample from punch biopsy and microbiopsy were compared for assessing Nucleospin kit to QIAamp kit (n=1) (a). Kits recommended for DNA isolation from small tissue samples were also compared (n=5) (b). Punch tissue biopsy of 2 mm in diameter is indicated as ●, Microbiopsy tissue biopsy with a channel width of 0.20 mm is indicated as ■, and the negative control (elution buffer) is indicated as x. Mean with standard deviation (SD) is represented by red error bar.

increased in this experiment to see the range of total DNA that could be obtained with the 0.20 mm channel microbiopsies. There was no significant difference between the average total DNA yield from the NucleoSpin® Tissue XS kit ( $5.99 \pm 2.22$  ng) and the QIAamp DNA Micro kit ( $6.97 \pm 2.46$  ng) (**Figure 4.6b**). Overall, QIAamp isolated a higher yield of DNA from the microbiopsy samples. Therefore, unless specifically mentioned all future DNA isolations were carried out using the QIAamp DNA Micro kit.

### 4.3.3 Wound healing kinetics

Immediately after microbiopsy application, local erythema developed that resolved within 24 hours. The tiny excision site from the microbiopsy healed quickly and was invisible to the naked eye after 24 hours (**Figure 4.7**). Dermoscopy and RCM were used to monitor the wound healing process at regular intervals (**Figure 4.7, center and right columns**). It was hypothesised that the microbiopsy device enables acquisition of tissue samples with minimal to no risk of infection. The healing kinetics advocates potential for minimal infection and is a safe device for biopsy collection in humans. A study by Donnelly et al. supports this hypothesis by showing that the site of microneedle array application results in significantly less microbial infiltration than puncture by a 21G hypodermic needle. They also showed that the the infiltrated microorganism did not cross the viable epidermis in the microneedle-punctured site (Donnelly et al., 2009). Even though the dimensions of each microneedle was smaller (0.25 x 0.28 mm) than the microbiopsy (0.50 x 0.80 mm), it was shown in **Figure 4.4d** that the puncture sites were only  $0.22 \pm 0.12$  mm wide and  $0.26 \pm 0.09$  mm deep and were no deeper than what one could expect from a hypodermic needle. In addition, there was no adverse reaction reported by 20 volunteers when applied with the microbiopsy device. This suggested that the process is not prone or no more prone to infection than an injection.

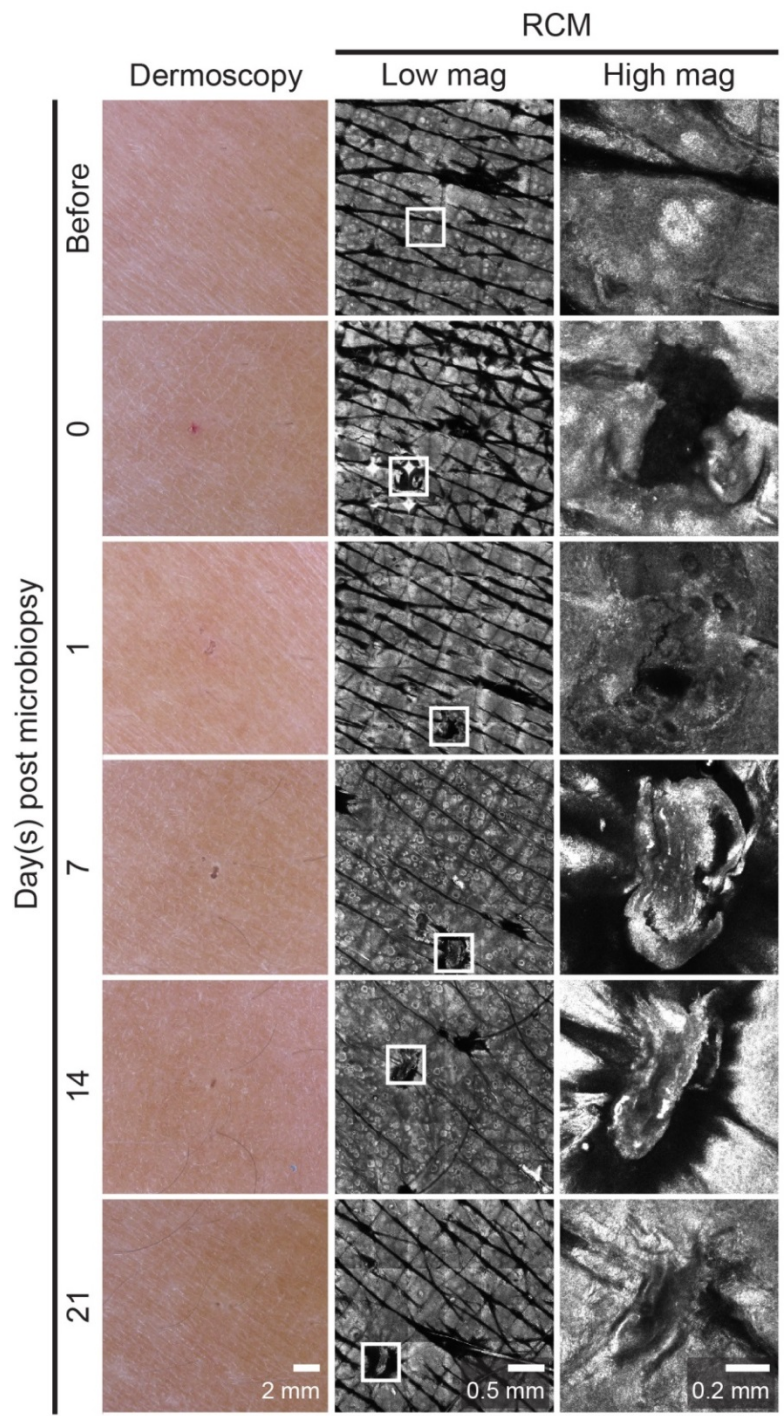


**Figure 4.7: Wound healing kinetics of microbiopsy site.**

The left column shows dermoscopic images of the microbiopsy site (n=2) over time. The middle and right column are mosaics and at 30x magnification reflectance confocal microscopy (RCM) images, respectively, of the microbiopsy site. Reproduced from (Lin et al., 2013).

#### 4.3.4 Influence of channel width on tissue extraction

It was hypothesised that optimal tissue extraction can be influenced by different geometries and configurations, application velocity, and surface roughness of the microbiopsy cutting tip. A series of preliminary experiments were conducted to determine the correlation between these factors and amount of tissue collection. Based on the previous experiment shown in **Figure 4.5**, more tissue biopsy was observed with microbiopsy cutting tips consisting of wider channel widths. A pilot study was performed by testing channel widths ranging from 0.05 mm to 1 mm (**Figure 4.8a-h**) to determine the width limit at which unsuccessful tissue collection occurred.

Microbiopsy cutting tips with a channel width of 0.05 mm collected the least amount of tissue with an average of  $4.28 \pm 2.83$  ng DNA. The cutting tips with 0.10 mm channel width had the highest amount of tissue collected ( $9.26 \pm 2.06$  ng). The cutting tips with 0.05 mm and 0.15 mm channel widths ranging had 100% collection rate (3 out of 3). Four out of six microbiopsies with a channel width of 0.10 mm resulted in successful tissue extraction. The microbiopsy extraction decreased to three out of six when the width was increased to 0.20 mm. Tissue collection was unsuccessful when channel widths were greater than 0.20 mm (**Figure 4.8i**). It was determined that there was a moderate correlation of increased total DNA with increasing channel width when there were successful tissue biopsy collections (correlation coefficient,  $r = -0.7884$ ). However, increased width results in lower successful microbiopsy extraction.

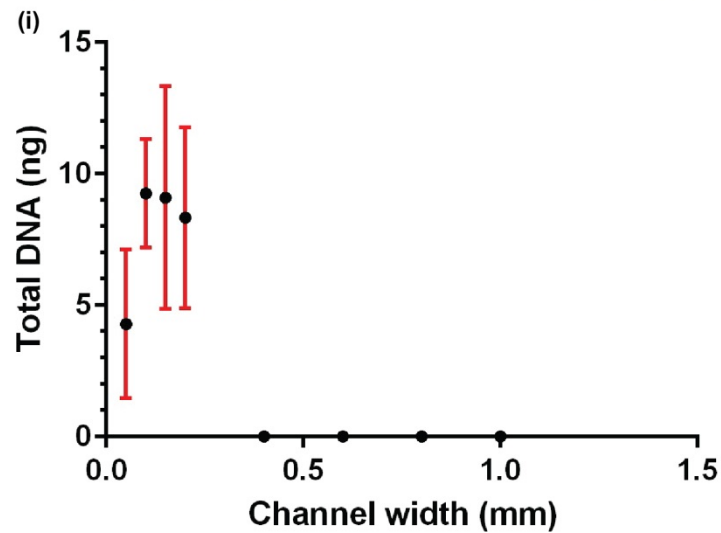
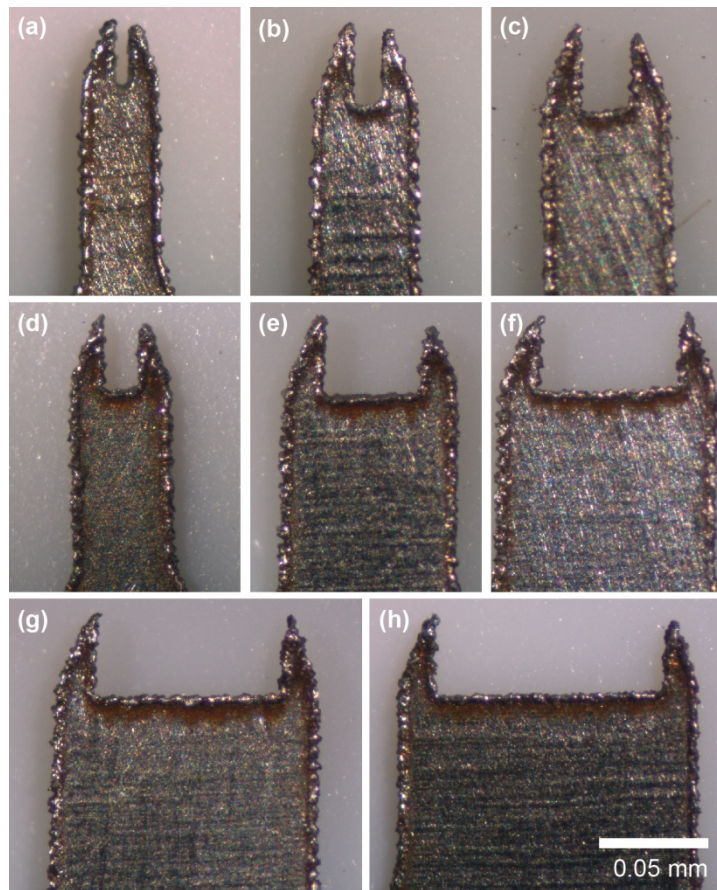


**Figure 4.8: Pilot channel width study.**

Panel (a) to (h) shows cutting tip of different channel width ranging between 0.05 mm to 1 mm. Average total DNA (n=3) was compared between different channel widths (i).

A volunteer study with 20 healthy individuals was conducted to determine the optimal channel width and application velocity. Isolated DNA mass was chosen to be the primary indicator for sample-to-sample comparisons. Tissue collection ( $4.5 \pm 1.5$  ng DNA) was observed around the rough edges of a microbiopsy device without a chamber (**Figure 4.9a**, channel width of 0 mm). Successful collection was achieved when tissue was evident within or around the device and unsuccessful if no tissue was present. Tissue was collected from all volunteers ( $n=20$ ) when a 0.15 mm channel width microbiopsy device was used. Only 13 successful collections were achieved when a 0.20 mm channel width microbiopsy device was used. This indicated that the collection rate decreased from 100% to 65% when channel width was increased by 0.05 mm. This experiment showed that a channel width of 0.15 mm resulted in the highest average amount of DNA ( $5.9 \pm 3.4$  ng), which was significantly higher than 0.25 and 0.30 mm channel widths ( $p < 0.0001$ ). There was no significant difference in the total DNA extracted between 0 to 0.20 mm channel widths (**Figure 4.9a**). High resolution images of the microbiopsy cutting tips were illustrated in **Figure 4.9b**. There was no change in the level of pain reported when microbiopsies with varying channel widths were applied (**Figure 4.9c**). The pain score study did not include the 0.35 mm conventional punch biopsy as previous studies have shown that it was the length and not the width of the microneedle that significantly influenced level of pain experienced by volunteers.

#### **4.3.5 Influence of pre-loading on tissue extraction**

It was hypothesised that a higher amount of pre-loading creates higher surface tension to the skin, which in return penetrates the cutting tip deeper into skin. By penetrating deeper into the skin, more tissue can be collected in the process. The outcome of the experiment shows that a minimum of 10 N is required for successful extraction of the microbiopsy sample. Preloading application forces higher than 10 N did not appear to increase tissue collection ( $n=1$ , 4.5 ng vs. 4.76 ng).

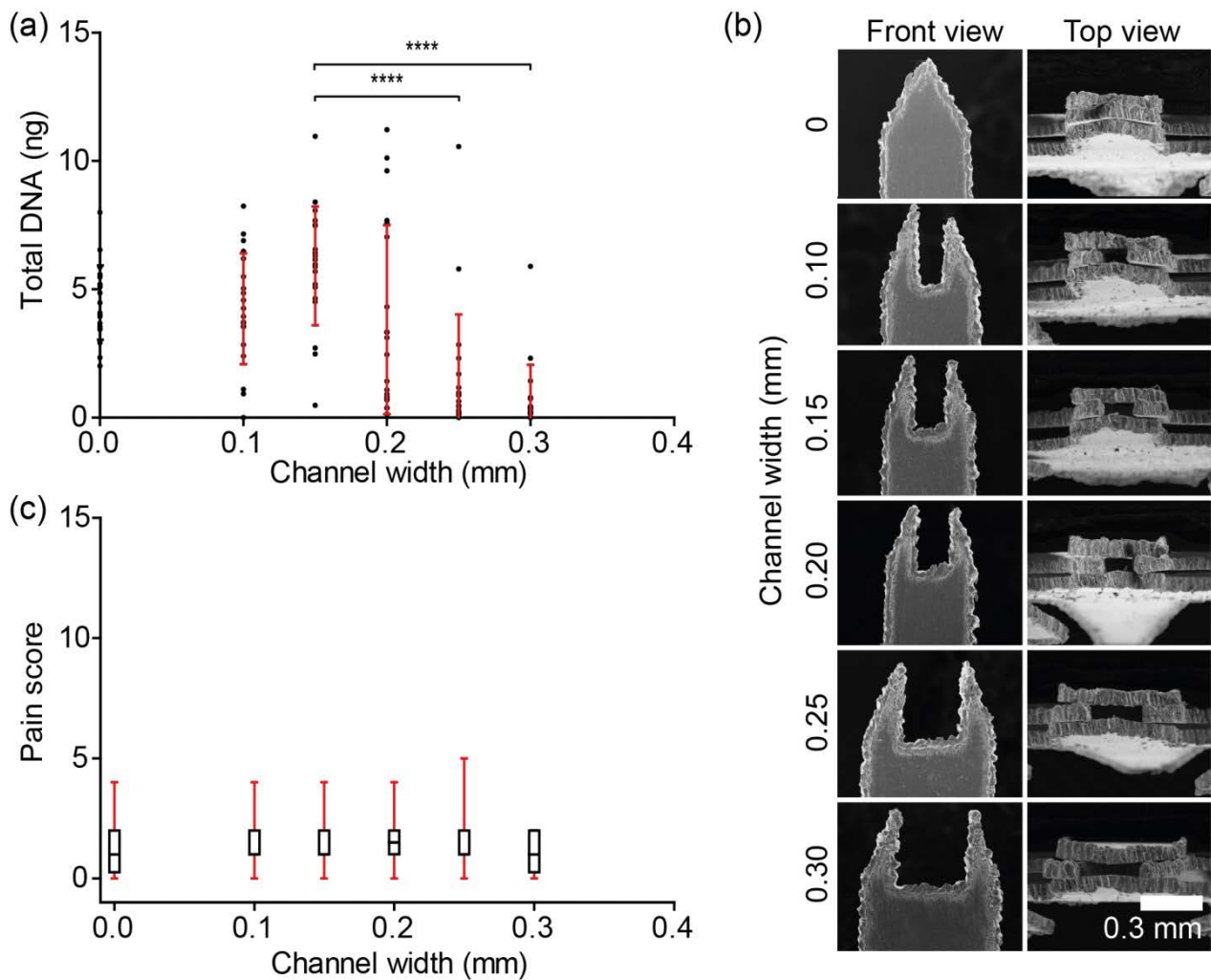


**Figure 4.9: Microbiopsy channel width optimisation in a volunteer study.**

Channel width and velocity were varied to optimise the microbiopsy device configuration. Total DNA was used as a surrogate for sample size. Panel (a) shows the DNA extracted from device with varying channel width ( $n=20$  per channel size) and that the maximum amount of DNA was collected with 0.15 mm channel width. Panel (b) displays high resolution scanning electron microscopy images showing different channel widths of the microbiopsy device. Panel (c) shows the level of pain volunteers reported when different channel width microbiopsies were used. Figure modified from (Lin et al., 2013)

#### 4.3.6 Influence of application velocity on tissue extraction

One of the questions was whether velocity-aided application of the microbiopsy was required for successful tissue biopsy. Quasi-static and velocity-aided biopsy applications were compared using both the punch biopsies and the microbiopsy. Tissue biopsy collection was defined as successful if there was presence of tissue within the device after



application. In the quasi-static experiment, all the punch biopsies (n=3 for each group, 0.35 mm, 0.50 mm, 1 mm and 3 mm) successfully collected tissue. However, no tissue was observed within the microbiopsy cutting tips in this experiment (data not shown). The results from dynamic application showed that one out of three 0.35 mm and 1 mm punch biopsies successfully extracted tissue while two out of three tissue biopsies were collected using the 0.5 mm punch biopsy. The success rate for tissue extraction with the microbiopsy device in this experiment was 100% (n=3). The potential to extract tissue from velocity-aided punch biopsy was found to be variable compared to the microbiopsy. This is expected as it was shown in Section 4.3.5 that the success rate decreased as the width of cutting tip increases. Reflectance confocal microscopy was used to examine the site of unsuccessful biopsy applications. Confocal images showed that the skin was penetrated by the punch biopsy at the application sites but tissue biopsies remained intact. There was 0% success rate for the 3 mm velocity-aided punch biopsy.

The comparison between quasi-static and dynamic microbiopsy application emphasised the importance of velocity on microbiopsy extraction. The velocity was further investigated by varying the speed using different compression springs and adjusting the height where the spring sits before the device was loaded. Microbiopsy cutting tips did not penetrate the skin when applied under quasi-static application. The highest amount of DNA was obtained at 15 m/s ( $6.75 \pm 1.22$  ng) followed by 13.4 m/s ( $4.94 \pm 2.83$  ng) and 9.4 m/s ( $2.47 \pm 1.55$  ng). All groups except the standard spring had 100% collection rate (three out of three). Only two microbiopsies from the standard spring group successfully obtained tissue sample. Although the study demonstrated an increase in velocity resulted in increased tissue extraction it was limited by the lack of identical plungers. Hence, in order to expand the range of application velocities in the study, an alternate applicator and plungers were fabricated. Also, the range of velocity tested was too small to identify the upper limit of application velocity. In order to expand the range of application velocity, proper device applicator and plunger had to be fabricated.

Following fabrication of an alternate microbiopsy applicator suitable for varying administration velocity (described in Section 4.2.10), six different velocities were tested. Dermoscopy and reflectance confocal images showed that the microbiopsy did not penetrate the skin when applied at 0.5 m/s and 2.3 m/s. Superficial skin penetration was seen when the microbiopsy was applied at 6.0 m/s. There was no tissue found in those

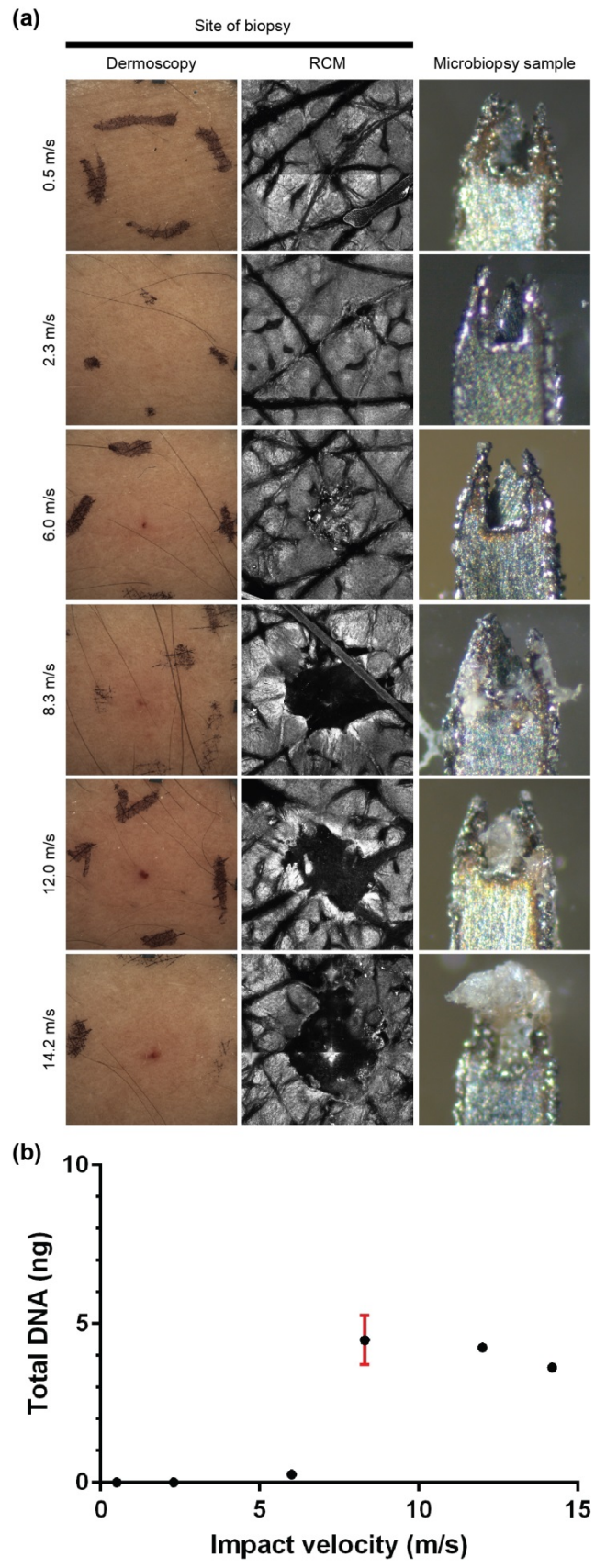


**Figure 4.10: Pilot application velocity study.**

Panel (a) shows dermoscopic (left panels) and reflectance confocal (middle panels) images of application sites and the tissue biopsies collected from each group (right panels). Total DNA 99 extracted from each application velocity (b). The red error bar is the SD.

microbiopsies when examined under stereo microscopy (**Figure 4.10a**). Successful tissue collection was obtained when microbiopsies were applied at minimum a speed of 8.3 m/s (4.49 ng). The amount of DNA plateaued between 3.62 ng to 4.25 ng when application velocity was higher than 8.3 m/s (**Figure 4.10b**).

The study was repeated in a volunteer study (n=20). Microbiopsy application velocity was evaluated by using defined applicator springs to achieve velocities between 0 to 20.2 m/s (**Figure 4.11a**). Only negligible amounts of DNA were recovered when the device was applied at less than 9.2 m/s. However, there was a 7.5-fold increase ( $0.8 \pm 0.8$  to  $6.0 \pm 3.0$  ng) in DNA recovered when the application velocity was increased from 9.2 m/s to 16.6 m/s ( $p < 0.0001$ ). An additional increase to 20.2 m/s increase in application velocity did not result in significant increases in DNA collection.

The level of pain and variation increased when microbiopsies were applied at increasing velocities but there was no significant relationship between increased velocity and the amount of pain experienced (**Figure 4.11b**). All of the volunteers had a pain score of 0 at 5 minutes after the final microbiopsy application (data not shown). The volunteers scored pain between 0 to 10 with an average score of  $1.5 \pm 1.1$ , when the 0.15 mm channel width microbiopsy was applied at 20.2 m/s.

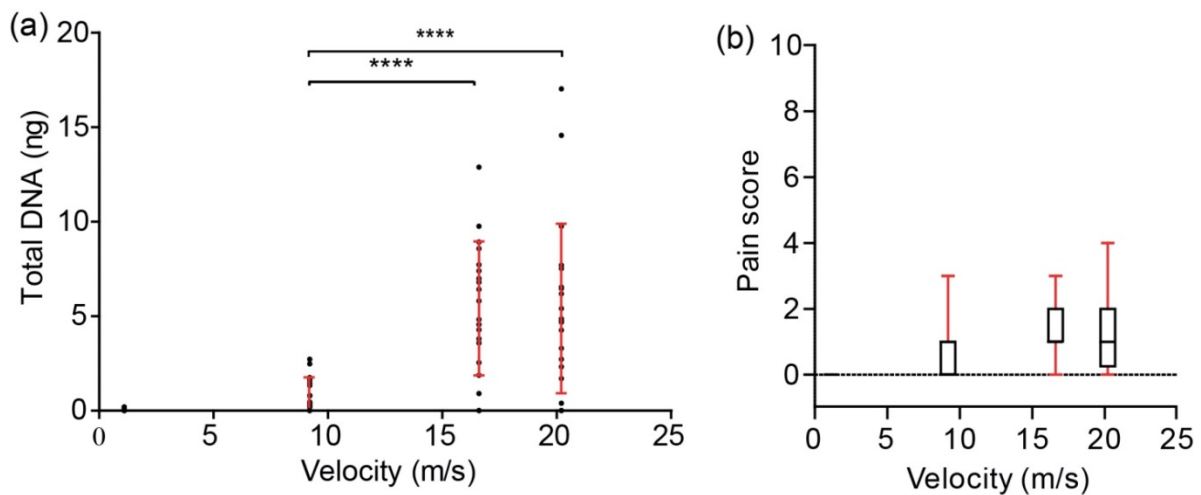


**Figure 4.11: Application velocity optimisation.**

Panel (d) shows the varying velocity applied and that the maximum amount of DNA was collected when the device was applied at 16.6 m/s. Panel (e) shows the level of pain volunteers reported when application velocity was varied. The red error bars represent the SD. Figure modified from (Lin et al., 2013)

### 4.3.7 Influence of surface roughness on tissue extraction

Surface roughness was hypothesized to increase friction between the sample and microbiopsy. Rougher edges were produced by having jagged lines within the channel edge. Smoother edges were achieved by performing a polishing step to the cutting tips after laser cutting (**Figure 4.12a-d**). There was no significant difference in increased total DNA with increasing surface roughness in this test (**Figure 4.12e**). One reason to explain this outcome is that polishing was only applied on the surface of the cutting tips and not within the channel edge. The roughness amplitude of the main surface should have minimal to no impact on tissue collection given that surface contact with skin during application only happens on the edges of the cutting tip. In addition, the roughness of the

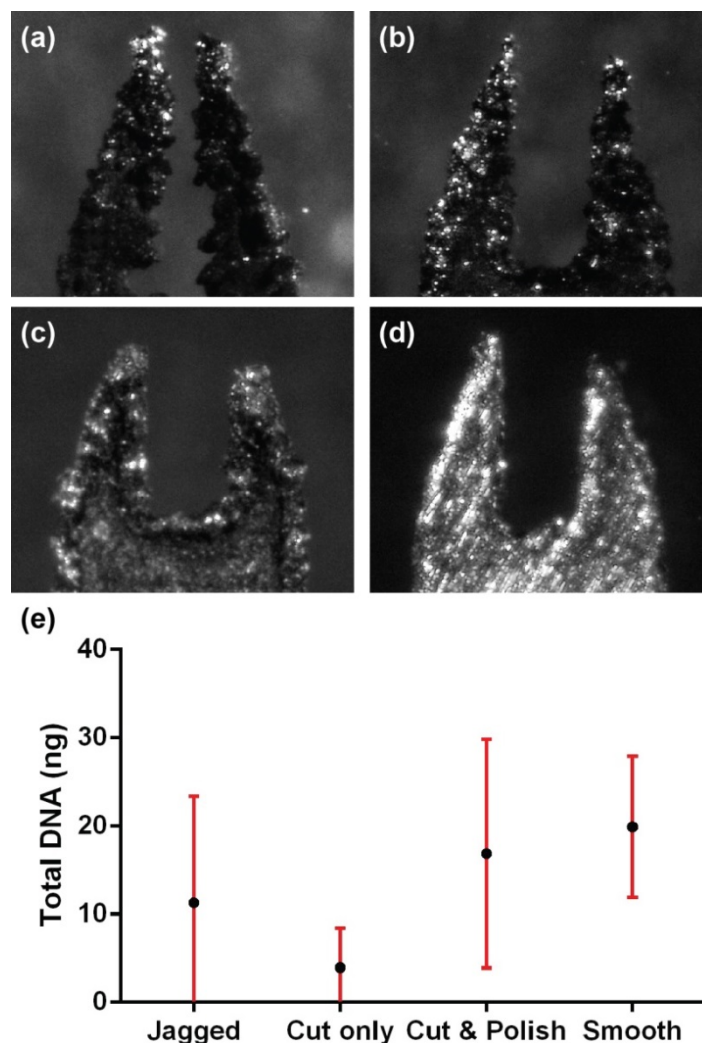


**Figure 4.12: Pilot surface roughness study.**

Panel (a) to (d) shows cutting tip of different surface roughness. Average total DNA (n=4) was compared between different groups (e). SD is represented by the red error bar.

edges was only assessed visually and not quantified in this pilot. Therefore, this may not be an accurate representation on how roughness amplitude may affect tissue collection.

The findings from the channel width study showed that successful collection was achieved using microbiopsy cutting tips without a centre chamber (**Figure 4.9a**,  $4.5 \pm 1.4$  ng from channel width 0 mm). Therefore, it was hypothesized that the surface roughness of the cutting tip edge might play an important role in tissue collection. Microbiopsy devices with varying roughness amplitudes ( $R_A$ ) were compared and resulting in a trend of increasing total DNA extracted with increasing  $R_A$  (**Figure 4.13a**) ( $n=20$  for  $5.36 R_A$  and  $n=5$  for  $0.92$  and  $1.32$ ). The SEM images of the inner chamber edge were used to measure the  $R_A$ . These measurements ranged from relatively smooth ( $R_A 0.92$ ) to rough ( $R_A 5.36$ ) (**Figure 4.13b, side view**).

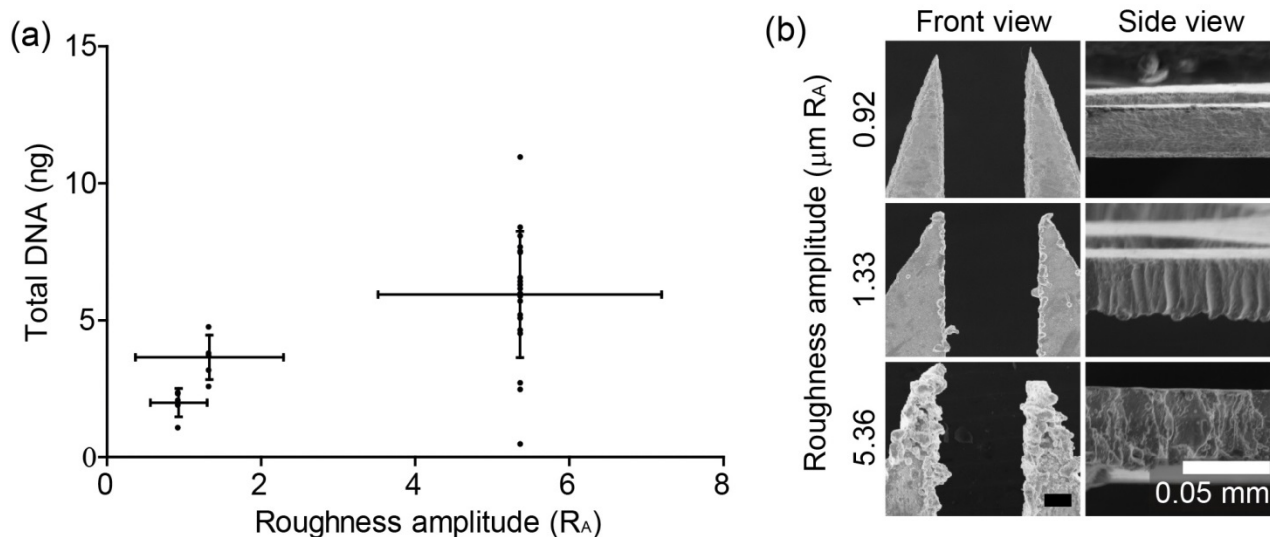


**Figure 4.13: Roughness amplitude optimisation.**

Panel (a) shows that microbiopsy devices with higher roughness amplitude channels are capable of collecting more DNA. Panel (b) contains high resolution scanning electron microscopy images showing different channel widths and roughness of the microbiopsy device. Reproduced from (Lin et al., 2013).

#### 4.3.8 Influence of geometry and surface texturing on tissue extraction

The previous static and velocity-aided punch biopsy application experiments demonstrated that geometry of the cutting tips might influence the success of extracting tissue. In this volunteer study, 18 microbiopsies were tested on each volunteer. Out of the 18 microbiopsies, ten were of different geometry (**Figure 4.14, G1B to G2A**) and eight were surface textured on the outer cutting elements (**Figure 4.14, 01 to M6**). Based on previous usage experience, the microbiopsy that was identified with the highest total amount of DNA in the earlier volunteer study could have unsuccessful tissue collection. Therefore, the optimal microbiopsy design in the current study was defined as the one that resulted in the most reproducible tissue extraction efficiency (highest total amount of DNA and smallest SD). Microbiopsy cutting tips with a short hook shape (G1B, G2B, G2E) and standard G2A had the least variability in amount of tissue collected (**Figure 4.14, graph**). Tissue collection using other geometries had inconsistent results. Of those four cutting tip, G2A had the least variability ( $3.06 \pm 0.76$  ng). Out of the surface textured microbiopsies, 01 had the most reproducible outcome ( $2.91 \pm 0.91$  ng). G2A was identified as the optimal microbiopsy as it had higher total DNA than 01.

A new laser was commissioned by Mastercut Technologies after the first volunteer study. Roughness amplitude of the laser cut edge was re-assessed to ensure that this was not a contributing factor to the total DNA variability in the geometry study. The roughness amplitude of cutting tips fabricated by the existing laser in Mastercut Technologies was  $0.92 \mu\text{m}$ .

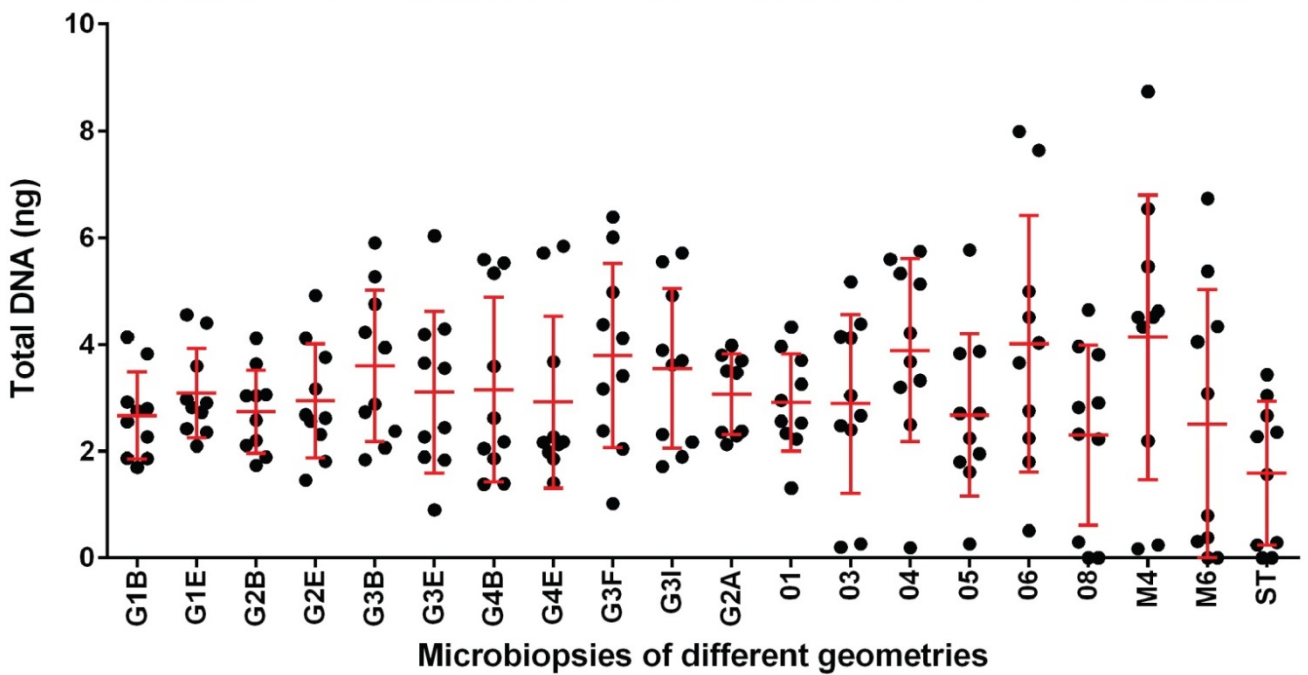
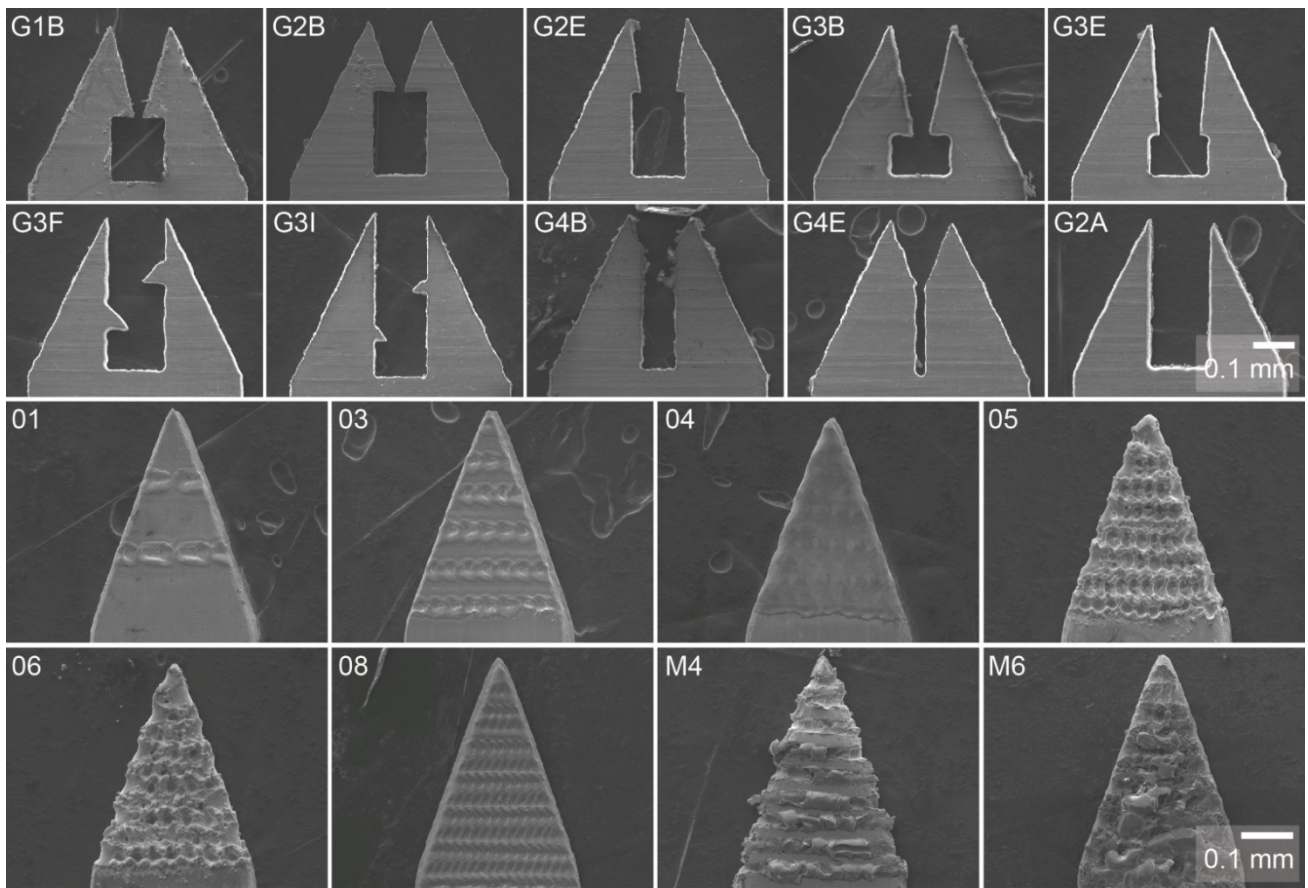


**Figure 4.14: Geometry and surface texturing optimisation.**

Scanning electron microscopy (SEM) showed high resolution images of the microbiopsy cutting tip with different geometries (G1B to G2A, row 1 and 2) and those that were surface-textured on the outer cutting elements (01 to M6, row 3 and 4). Mean with SD (red error bar) of total DNA isolated from each group were illustrated in the graph.

#### 4.3.9 Microbiopsy RNA isolation optimisation

Only 1-5% of total RNA consists of messenger RNAs (mRNA) while the rest are comprised of ribosomal RNAs (80-85%), low molecular weight RNAs and small nuclear RNAs (15-20%). For small tissue samples like the microbiopsy, it is critical to determine the most efficient method for good quality RNA extraction. The ideal quality of RNA for most downstream applications is determined as RIN 8-10. The RNA yield from frozen human skin using different extraction methods was compared. RNA yield can vary depending on quantity of tissue sample. Excised human skin of similar weight was used to compare the efficiency of different extraction methods. RNA yield of 2.53 µg was obtained using the TRIzol® reagent and 0.44 µg using pestle and mortar disruption and the RNeasy Mini kit. The amount of RNA was too low for detection when the FastPrep® instrument and the RNeasy Mini kit were used together. This could be due to insufficient amount of RLT Plus lysis buffer during the disruption step. Sample was lost when disruption step was done with pestle and mortar. This explains the low RNA yield outcome using this method. I repeated the experiment comparing the TRIzol® reagent and the FastPrep® instrument with the RNeasy Mini kit. The RNA yields were 0.66 µg and 0.13 µg, respectively. RNA yields from both experiments using the TRIzol® reagent were relatively similar and higher than sample isolated with the RNeasy Mini kit. The RIN for both TRIzol®-extracted sample was 2.6, and <1 for RNA extracted using pestle mortar and FastPrep® instrument. The tube containing tissue sample and lysis buffer was observed to be warm during disruption step with FastPrep® instrument. The samples also had two freeze-thaw cycles before quality analysis. These may have contributed to RNA degradation. Both methods did not appear to isolate RNA of sufficient quality.

In order to make relevant comparison of total RNA quality, microbiopsy and its matched lesional sample were included in this experiment. A commercial kit, Arcturus® PicoPure® RNA Isolation Kit, which was designed to isolate total RNA from single cell was used. The quality of RNA for four out of five microbiopsy samples compared to their matched lesions was comparable but slightly lower. This was expected as microbiopsy samples were collected 20 to 30 minutes after lesions were excised. Changes to the integrity of RNA within minutes post excision was expected as reported by Spruessel et al. (Spruessel et al., 2004). Similar variability in integrity of the lesions that were preserved using RNALater® reported by Pérez-Portela and Riesgo (Pérez-Portela and Riesgo, 2013) was



also observed. The RIN ranged from 2.6 to 7.2 for the lesions and 1.2 to 7.6 for the microbiopsy tissue samples.

Representative Bioanalyzer results for the conventional biopsy (RIN 6.50) and microbiopsy (RIN 5.10) are shown in **Figure 4.15, Total RNA**. The results showed that there are similarities and differences in the RNA bands, which may be due to the large amount of tissue sampled with conventional biopsy and the relatively small number of cells sampled with the microbiopsy. The small sample size is an inherent limitation of the microbiopsy device. To mitigate this, a pilot experiment was conducted where the microbiopsy sample was subjected to whole transcriptome amplification for RNA analysis. A skin sample with the same amount of starting material (14 ng) was included as an amplification control in the experiment. A 2000-fold increase in cDNA from both samples based on total RNA and cDNA measurements was noted. The cDNAs were of comparable quality and quantity (**Figure 4.15, Transcriptome Amplification to cDNA**). Subsequently, PCR was used to amplify human beta-actin mRNA. Two identical bands at 800 bp with comparable PCR product quality both lanes were observed (**Figure 4.15, Actin PCR**).

Berglund et al. (2007) reported that their optimised methodology yielded an average  $1.4 \pm 0.4$   $\mu\text{g}$  of consistently high quality RNA (8.4–8.9 RIN) from 3 mm skin punch biopsies (Berglund et al., 2007). Another group reported that they had isolated an average of 1.5  $\mu\text{g}$  of RNA with an average RIN value of 8.1 from half of a 4 mm punch biopsy skin sample (n=97) (Bruning et al., 2011). The average total RNA yielded from the microbiopsy device was  $9.0 \pm 10.1$  ng (n=5). Even though far less RNA with the microbiopsy device was isolated, this proof-of-concept study supports the hypothesis that this limitation can be addressed using commercial amplification kits and PCR (**Figure 4.15**) for investigating the molecular basis of skin disease. Through the course of these experiments, RNA integrity values that ranged between 1.2 and 7.6 were observed with the microbiopsy. These values correlated with matched conventional shave biopsies. In some cases the values were quite low (e.g. RIN 5.1 in **Figure 4.15**) and would not be considered for whole transcriptome approaches. Sampling for RNA analysis can be difficult and optimizing this application for the microbiopsy is one of our priorities as we move forward with this technology.

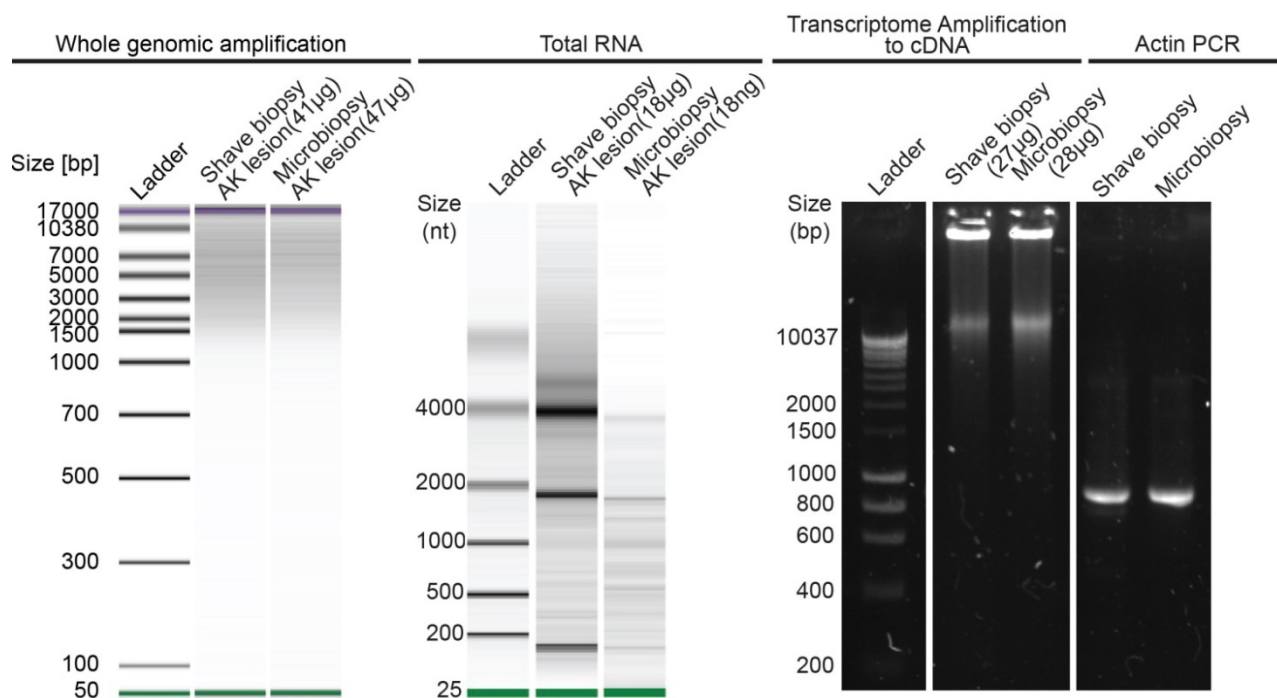


**Figure 4.15: Molecular characterisation of conventional shave biopsies and microbiopsies.**

The left panel shows the Bioanalyzer readout from amplified DNA from a conventional actinic keratosis (AK) shave biopsy next to the microbiopsy DNA sample obtained from the same AK lesion. The right panel compares the RNA quality of a shave biopsy and normal skin microbiopsy that were subjected to total transcriptome amplification to generate cDNA. The cDNA was then used as a template for a PCR reaction containing actin specific primers with an expected product at 800 bp. Figure modified from (Lin et al., 2013).

## 4.4 Conclusions

Characterisation experiments have shown that a typical microbiopsy sample contained approximately 1000 to 3000 cells. Image analysis was used to estimate the number of cells based on counting nuclei, as the viable epidermis has relatively few multinucleated cells. This approach was fast and non-destructive to the samples but was limited by only estimating the number of cells. Total DNA was eventually used as a marker to determine the amount of microbiopsy tissue that was collected. The microbiopsy was optimised through testing various application (velocity) and configuration (i.e. channel width, surface roughness, geometry designs and surface texturing) parameters in volunteers. The first volunteer study included testing a range of application velocities between 1.1 m/s to 20.2

m/s; microbiopsy with channel widths ranging from 0 mm to 0.30 mm and surface roughness from 0.92  $\mu\text{m}$  to 5.36  $\mu\text{m}$ . In the second volunteer study, ten different geometries and eight different surface textured microbiopsies were tested. Total DNA and RNA from microbiopsy samples can be isolated effectively using commercial kits designed for small samples. The quality and integrity of microbiopsy samples can be affected by the pre-analytical process (i.e. how tissue was collected and stored). The RIN of microbiopsy samples isolated using the same kit ranged from 1.2 to 7.6. To conclude, the outcome of this Chapter firstly identified G2A microbiopsy with a channel width of 0.15 mm as the optimal design for reproducible tissue collection. Optimal application velocity was determined as 16.6 m/s. Secondly, isolation of total DNA and RNA with commercial kits ranged from 2.12 ng to 9.90 ng and 1.09 ng to 25.52 ng, respectively. Finally, the problem of small sample size for extensive downstream molecular analyses was overcome through amplification where a 2000-fold increase in cDNA from 14 ng of starting material was observed.

There are several benefits of microbiopsy over a ready-made 0.35 mm punch biopsy that is also in the submillimetre size range as the microbiopsy device. One apparent benefit is that microbiopsy samples can be safely collected in volunteers without the need to administer local anaesthetics unlike the approach with conventional punch biopsy. There was also no report of adverse reaction from the application of microbiopsies. Considering that the channel width of the microbiopsy is at least half the size of the 0.35 mm punch biopsy, the healing process for a microbiopsy application site would have been quicker than an area that had been biopsied by the punch biopsy. The current cost of making one microbiopsy in a small laboratory scale is approximately \$10 and is 1.5 times the price of a single punch biopsy. However, it is anticipated that the cost will be reduced once the production is scaled-up. In terms of diagnostic utility, both devices are unsuitable for histopathological analysis given their sizes.

## Chapter 5

### *Genotyping and mutation profiling applications*

#### 5.1 Introduction

In Chapter 4, the characterisation of the microbiopsy content and the quality compared to conventional punch biopsy tissue was examined. It was hypothesised that microbiopsy technology is a minimally invasive approach to assess conventional biomarkers for skin diseases. The primary focus of this Chapter was to assess the Microbiopsy technology for molecular analysis of pigmented and non-pigmented skin lesions. These proof-of-concept experiments tied to clinical skin disease research described here were published as three articles in JAMA Dermatology journal. The following four aims were addressed:

- AIM 1** Assess the suitability of microbiopsy extracted samples for genotyping
- AIM 2** Determine the effects of microbiopsy application on histopathologic diagnosis in melanocytic skin lesions
- AIM 3** Evaluation of BRAF and NRAS mutation profiles in pigmented lesions
- AIM 4** Profile somatic mutation status of significant p53/Rb pathway genes in non-pigmented lesions

The diagnosis of skin lesions can be confounded by the quality of clinical information and morphological nature of the histopathologic interpretation (Ferrara et al., 2009). Considering that histopathological analysis is the current gold standard for diagnosing dermatological diseases, it is critical that microbiopsies will not jeopardise downstream histopathology assessment. Conventional chemical fixation of the lesions after being excised can hinder downstream molecular analysis. The microbiopsy device provides the opportunity to acquire a small tissue sample for molecular analysis without the need to remove the entire lesion.

Validating the microbiopsy device in these skin lesions is critical for future translation of this technology into clinical practice. There is significant interest and need for a better understanding of the underlying genetic basis of disease development and progression in both melanoma and non-melanoma skin cancer.

The B-Raf proto-oncogene (BRAF) is expressed in many human cells including the melanocytes. The occurrences of BRAF mutations are approximately 70% - 82% in naevi and 50% - 60% in melanomas (Davies et al., 2002, Pollock et al., 2003). The most prevalent BRAF mutation is a valine to glutamine substitution that occurs at position 600 (V600E, 74% - 90%), followed by V600K (16% - 29%) (Thomas, 2006). These mutation sites account for 95% of all BRAF mutations. It is speculated that the BRAF mutation plays an important role in the genetic basis of melanoma development and progression. This series of morphological changes begin as a benign naevus and then becomes a melanoma through the formation of a dysplastic naevus as described by the Clark model (Bennett, 2003).

The discovery of BRAF as an important oncogene in disease progression has led to development of targeted molecular therapies such as BRAF inhibitors. These therapies have significantly, but importantly, only temporarily, improved the survival of patients with advanced melanoma and have shown promising outcomes in the treatment of other diseases (Girotti et al., 2014, Nguyen et al., 2014, Berghoff and Preusser, 2014). BRAF<sup>V600E</sup> inhibitors blocked tumor growth and induced partial or complete regression in metastatic melanoma (Flaherty et al., 2010). Considering that the BRAF<sup>V600E</sup> mutation is highly prevalent in benign naevi (Pollock et al., 2003), it is of no surprise to see changes to existing melanocytic naevi and the appearance of new naevi during kinase inhibitor therapy (Haenssle et al., 2012, Dalle et al., 2011, Perier-Muzet et al., 2014). New primary melanomas arising from naevi that are rapidly changing or proliferating during the early stages of vemurafenib therapy were found to be BRAF wild type (Dalle et al., 2011, Perier-Muzet et al., 2014, Zimmer et al., 2012). Clearly, the outcome of the targeted therapy depends if the mutation is present within the naevus and there is a need to develop personalised treatment for individual patients. It is likely that there will be targeted inhibitors for local skin treatment in the future. The development of the microbiopsy as a companion diagnostic for such therapeutics would be beneficial.

Similar to melanocytic skin lesions, actinic keratoses (AK) are thought to progress into squamous cell carcinoma (SCC). However, the majority of the actinic keratoses do not go on to become SCC (Feldman and Fleischer, 2011, Fuchs and Marmur, 2007). Molecular profiling of AK, SCC and normal skin suggested that the dysplastic lesions and carcinomas share certain differentially expressed genes (Hameetman et al., 2013, Padilla et al., 2010).

To date, there has been no report on biomarker profiling of lesional samples in a prospective study given the lack of suitable technologies to perform multiple sampling over time. The microbiopsy technology platform is capable of collecting multiple micro-size samples that can be potentially used for biomarker profiling of these lesions. Given the sample size differences, it is crucial to validate the molecular profiles from both microbiopsies and shave biopsies.

The Chapter begins with discussion on preliminary experiments to optimise and validate the potential of the microbiopsy device for DNA genotyping. Disease formation and progression is a complex process. In order to shed light on the role of relevant mutations in disease progression, microbiopsy samples were acquired from suspicious dysplastic lesions for molecular analysis. Three independent case studies were conducted to evaluate the mutation status of BRAF and Neuroblastoma RAS viral oncogene homolog (NRAS) genes in dysplastic melanocytic lesions. The data from these three case studies were published in JAMA Dermatology, a leading Dermatology journal (McClenahan et al., 2014, Banan et al., 2013, Tan et al., 2015). The last experiment of this Chapter described the somatic mutation profiling of significant genes related to p53/Rb pathway in dysplastic non-pigmented skin lesions.

## **5.2 Materials and Methods**

### **5.2.1 Melanocortin 1 receptor (MC1R) and Oculocutaneous albinism II (OCA2) genotyping**

These experiments were conducted with approval from Metro South Human Research Ethics Committee in Princess Alexandra Hospital (HREC/12/QPAH/082) and The University of Queensland Human Ethics Review Committee (Approval number: 2012000648).

The subjects were recruited from an ongoing clinical study at the Dermatology Department of Princess Alexandra Hospital (HREC/09/QPAH/162). One microbiopsy was collected from the forearm of each subject. A total of five subjects, four Caucasians and one Asian, were included in these preliminary genotyping experiments. DNA was extracted according to protocol described in Section 2.3.1. Nested PCR and Sanger sequencing were performed by Kasturee Jagirdar to determine the genetic variant of MC1R gene (Box et al., 2001, Box et al., 1997).

Given that four out of five samples had insufficient amounts of DNA for MC1R genotyping, Two to three microbiopsy samples was re-collected from each of these four subjects and pooled for analysis. The usual amount of DNA they used in these reactions was 100 ng, thus the need to pool samples. In addition, a single microbiopsy sample was collected from each subject for OCA2 genotyping. DNA from the saliva samples that were collected for the clinical study were used as controls. TaqMan-based genotyping was again performed by Kasturee Jagirdar for OCA2 genotyping (rs12913832) (Sturm et al., 2008). MC1R genotyping was repeated with amplified DNA samples obtained from a small clinical study described in Section 5.2.2. DNA from matched peri-lesional samples was also included in this experiment.

Samples post sequencing reaction were sent to the Australian Equine Genetics Research Centre (Queensland, Australia) for sequencing analysis. Chromatographs were analysed using Sequencer version 5.2 (Gene Codes Corporation, USA).

### **5.2.2 Small clinical study on pigmented skin lesions**

Five patients that presented with dysplastic naevus were recruited and consented from the Dermatology Department by a clinical researcher (Dr. Paras Banan). The study was

conducted under the approval of the Metro South Human Research Ethics Committee in Princess Alexandra Hospital (HREC/11/QPAH/363) and The University of Queensland Human Ethics Review Committee (Approval number: 2011001201). A total of five dysplastic naevi were included in this case study. Clinical and dermoscopic photographs were obtained using a Canon Power Shot G10 digital camera (Canon, USA) with a dermatoscope attachment (Dermlite©, 3Gen, USA). Photographs were collected before excision and after the lesions were excised. The excised lesion was bisected by Dr. Paras Banan. Half of the lesion was sent for routine histopathologic analysis. Microbiopsy samples were collected from the other halved lesion as per the protocol described in Section 2.2.3. The halved lesion that was applied with microbiopsies was sent to a dermatopathologist (Dr. Duncan Lambie) for histopathological assessment including microbiopsy damage assessment. The sites of microbiopsy application were numbered and samples labelled accordingly (**Figure 5.1**). The lesion that was applied with microbiopsies was sectioned by the Department of Anatomical Pathology in Princess Alexandra Hospital according to routine protocols.

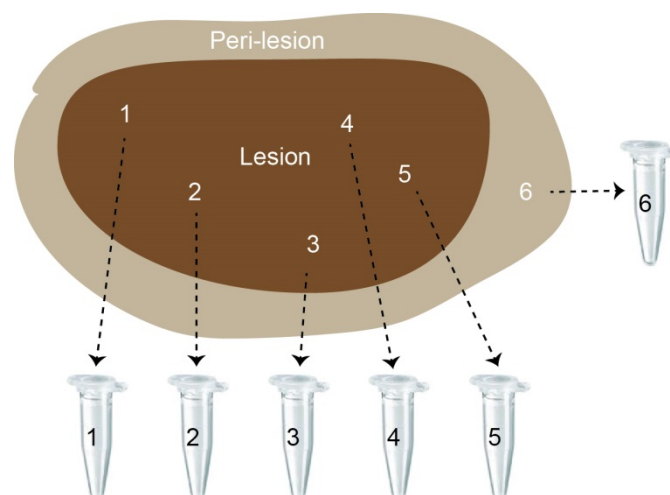


**Figure 5.1: Microbiopsy sample collection and site documentation.**

This is an illustration showing a piece of excised pigmented lesion that was applied with six microbiopsies. The sites of application were documented and microbiopsy samples were stored in their respective tubes.

At least five microbiopsies were collected from each excised lesion and kept in RNase/DNase-free microfuge tubes containing RNAlater® RNA Stabilization Solution (Life Technologies, USA, #AM7024). Microbiopsy samples were stored at -80°C until the



samples were processed. Microbiopsy samples from two out of five lesions were excluded in the study as the locations of microbiopsy application were not evident. Three microbiopsy samples were selected for downstream molecular analysis. DNA was extracted from the microbiopsy samples and quantified according to the protocol described in Sections 2.3.1 and 2.3.3. DNA samples were subjected to whole genomic amplification according to protocol described in Section 2.3.4. A 15-fold dilution was prepared using 2 µl of each amplified DNA sample prior to quantification. DNA quantification was performed using Qubit® dsDNA BR assay (Life Technologies, USA, #Q32853) according to the manufacturer's instructions. The quality and integrity of amplified DNA products was confirmed as per protocol described in Section 2.3.5. Amplified DNA samples were stored in 1.5 ml microcentrifuge tubes at -80°C. A small piece of the peri-lesional tissue was collected from each naevi as a control. DNA was extracted according to protocol described in Section 2.3.2.

Bi-directional Sanger sequencing of BRAF Exon 15 and NRAS Exon 2 were performed based on the protocol described by Richter et al. and Tschandl et al. (Richter et al., 2013, Tschandl et al., 2013). PCR amplification was performed in a 25 µl reaction mixture containing 5X Taq reaction buffer (200 mM Tris pH 8.4, 500 mM potassium chloride), 5% dimethyl sulfoxide (DMSO), 10 mM deoxynucleotide triphosphates (dTNPs), 50 mM magnesium chloride (MgCl<sub>2</sub>), 25 pmol/µl forward (F) and reverse (R) primers, 1.25 U of Taq DNA Polymerase, Native (Life Technologies, USA, #18038018) and 50 ng/sample of genomic DNA template. Forward and reverse primers used in the PCR amplification of BRAF Exon 15 were: F-5'-TCATAATGCTTGCTCTGATAGGA-3' and R-5'-GGCCAAAATTTAATCAGTGGA-3'. Forward and reverse primers used in the PCR amplification of NRAS Exon 2 were: F-5'-GATTCTTACAGAAAACAAGTG-3' and R-5'-ATGACTTGCTATTATTGATGG-3'. PCR amplification was carried out with an initial denaturation at 94°C for 5 minutes, followed by a 40-cycled template denaturation for 40 seconds at 94°C; primer annealing at 60°C for 40 seconds and primer extension for 1 minute at 72°C, and completed with a final elongation at 72°C for 7 minutes. The settings for NRAS Exon 2 PCR amplification were similar to BRAF PCR amplification settings, except that the primer annealing temperature was reduced to 58°C. Positive (saliva-derived DNA) and negative (nuclease-free water) controls were also examined under the same PCR conditions.

The presence of amplified PCR products were confirmed by gel electrophoresis using 2% agarose gel stained with 1x SYBR® Safe DNA Gel Stain (Life Technologies, USA, #S33102). Amplified products were extracted from bands resolved on the gel and purified using QIAquick Gel Extraction Kit (QIAGEN GmbH, Germany, #28704). Amplified products were subjected to sequencing reaction using BigDye® Terminator v3.1 Cycle Sequencing Kit (Life Technologies, USA, #4337455), 3.2 pmol/μl forward BRAF or NRAS primers and 10 ng/sample DNA template (GeneWorks Pty Ltd, Australia). Samples, post sequencing reaction, were sent to the Australian Equine Genetics Research Centre (Queensland, Australia) for sequencing analysis. Chromatographs were analysed using Sequencer version 5.2 (Gene Codes Corporation, USA).

### **5.2.3 Case Study 1 – BRAF mutation status in regressing and stable naevi**

This was a case study on a 30-year-old male patient who participated in a naevus surveillance study within the Dermatology Department of Princess Alexandra Hospital. The study was conducted with approval from Metro South Human Research Ethics Committee in Princess Alexandra Hospital (2009/126 and HREC/11/QPAH/363) and The University of Queensland Human Ethics Review Committee (Approval number: 2009001307 and 2011001201). The patient developed metastatic melanoma and was enrolled in a clinical trial where participants were given either a BRAF inhibitor (dabrafenib) drug only or a combination therapy with a MEK inhibitor (trametinib). Full-body and dermoscopic photographs were taken with a FotoFinder system (FotoFinder Systems, Inc., Germany). Naevi that were more than 2 mm on the back and 5 mm on the rest of the body were documented by the imaging system. Imaging was repeated another five times over a period of 27 months at approximately 7-month intervals.

Two naevi were selected for excision and BRAF and NRAS mutation status screening. One of the naevi regressed over time and the other remained similar throughout the monitoring period. Six microbiopsies were collected from each naevus as per the protocol described in Section 2.2.3. Five out of six microbiopsies were collected from the naevus and one from the peri-lesional region. The microbiopsy application sites were documented. All 12 microbiopsies from both naevi were processed and analysed according to the procedures described earlier.

#### **5.2.4 Case Study 2 – Targeted microbiopsy sampling**

This was a case study on a 58-year-old male patient who presented with an unevenly pigmented lesion on the left lower back that had recently changed in appearance. The study was conducted under the approval of the Metro South Human Research Ethics Committee in Princess Alexandra Hospital (HREC/11/QPAH/363) and The University of Queensland Human Ethics Review Committee (Approval number: 2011001201).

Clinical and dermoscopic photographs were obtained before and after excision using a Canon Power Shot G10 digital camera with a dermatoscope. Three different regions of interest were identified within the lesion from the dermoscopic photograph.

A targeting cassette made from a modified Tissue-Tek® Cyromold® mold (VWR International Pty Ltd., USA, #25608-916) was used as an aiming guide for microbiopsy collection. The accuracy of the targeting cassette was defined by a research engineer (Ross Flewell-Smith). A minimum of three microbiopsies were applied to each region. Microbiopsy devices were opened up and examined to check for the presence of tissue. Successful collections were kept in RNase/DNase-free microfuge tubes containing 180 µl of Buffer ATL from QIAamp DNA Micro Kit (QIAGEN GmbH, Germany, #56304). A total of nine microbiopsy samples collected from this case study were processed and analysed according to the procedures described earlier. Twenty micrometer stepwise stacks of reflectance confocal mosaics made up of 500 x 500 µm field of view images were collected before and after microbiopsy application.

Aliquots of DNA sample sets from the microbiopsies were sent to an independent sequencing facility (IMVS, SA Pathology, Australia) to perform quantitative BRAF<sup>V600E</sup> single nucleotide polymorphism (SNP) genotype analysis using matrix-assisted laser desorption ionization time-of-flight (MALDI-TOF) mass spectrometry assay. Genomic DNA from human saliva and MM96L melanoma cell line were used as negative and positive controls, respectively. The positive controls consisted of samples with different ratio of mutant to wild type DNA.

#### **5.2.5 Somatic mutation profiling**

Four sets of matched microbiopsies and lesional samples were included in this experiment. Clinical and dermoscopic photographs were collected before and after lesions

were excised. Five microbiopsies were collected from the bisected lesions after they were excised. *Ex vivo* microbiopsy collections were performed according to protocol described in Section 2.2.3. This study was conducted under the approval of the Metro South Human Research Ethics Committee in Princess Alexandra Hospital (HREC/11/QPAH/236) and The University of Queensland Human Ethics Review Committee (Approval number: 2011001386). Human neonatal foreskin was included in the experiment as wild type control samples. The foreskin tissue was provided by A/Prof. Nick Saunders.

Three out of five microbiopsies were selected for somatic mutation profiling using p53/Rb Pathway Mutation PCR Array (Sabiosciences, QIAGEN GmbH, Germany, #SMH-011ARE-12). The kit is a real-time PCR-based array that profiles over 70 mutation hotspots in Serine/threonine protein kinase (ATM), Cyclin-dependent kinase inhibitor 2A (CDKN2A) and Tumor protein p53 (TP53) genes. DNA from microbiopsies was extracted, amplified and tested for integrity and quality following protocols described in Sections 2.3.1, 2.3.4 and 2.3.5. DNA manipulations of halved lesions were also performed according to protocols described in Sections 2.3.2 to 2.3.5. Unamplified lesional and foreskin DNA samples were included as controls in the real-time assay to determine false positives and negative results from the amplification process. Real-time PCR was performed according to the manufacturer's instructions (qBiomarker Somatic Mutation PCR Array version August 2012, Page 22 – 28). Data analysis was performed on an integrated web-based software package (Qiagen GmbH, Germany) (<http://pcrdataanalysis.sabiosciences.com/mutation/somaticpcrarraydataanalysis.php>) using the delta-delta Ct ( $\Delta\Delta Ct$ ) method.

Real-time PCR data was compared to RNA sequencing (RNA-Seq) data for two out of four samples (VH006 and VH009). The sequencing and bioinformatics analysis were conducted in the laboratory of A/Prof. Marcel Dinger at the Garvan Institute of Medical Research Sydney, Australia.

## 5.3 Results and Discussion

### 5.3.1 MC1R and OCA2 genotyping of single and pooled microbiopsy samples

Only one out of five samples (#305AR) was successful for MC1R genotyping when a single microbiopsy was used. Subject 305AR was wild type for MC1R gene (**Table 6**). Unsuccessful genotyping was likely due to insufficient genomic DNA to seed the reaction. The average total DNA from each single microbiopsy sample was between 7 – 9 ng, and approximately 25 - 50 ng of DNA was required for MC1R genotyping.

The experiment was repeated with pooled samples from four out of five subjects. MC1R genotyping was successful for one out of four pooled samples (#303TP). This subject was heterozygous for V92M variant. The genotypes from saliva samples compared to matched microbiopsy samples were identical for both subjects (**Table 6**). This shows that samples can be pooled to improve rate of success but was still insufficient for MC1R genotyping. Two out of four samples (303TP and 305AR) were successfully genotyped for OCA2 gene when a single microbiopsy was used. The genotypes were also identical when comparing microbiopsy sample to saliva sample (**Table 6**).

**Table 6: Genotype outcome comparing microbiopsy and saliva samples.**

Volunteer ID	MC1R genotype		OCA2 genotype	
	<i>Microbiopsy</i>	<i>Saliva</i>	<i>Microbiopsy</i>	<i>Saliva</i>
302PS	Unsuccessful	Wild type	Unsuccessful	C / C
303TP	V92M+/-	V92M+/-	C / C	C / C
304LL	Unsuccessful	R163Q-/-	Not done	T / T
305AR	Wild type	Wild type	C / C	C / C
306CP	Unsuccessful	R151C+/-	Unsuccessful	C / C

MC1R genotyping was also performed using three amplified DNA samples collected from a small clinical study described in the next few sections. It was hypothesized that limited

molecular material can be overcome with amplification and will not affect outcome of genotyping. All three samples were successfully genotyped. One of the patients was wild type for MC1R gene and the other two patients had two variant alleles within the gene. The genotypes from the amplified DNA matched their respective peri-lesional skin samples. Allelic drop-out may occur during amplification process. Hence, non-amplified DNA from peri-lesional skin was included in the study to validate that there was no allelic drop-out as a result of whole genomic amplification by REPLI-g Single Cell Kit.

### **5.3.2 Effects of microbiopsy application on histopathological diagnosis**

The average dimension of four microbiopsy defects identified from the sections was  $113 \pm 50 \mu\text{m}$  wide and  $146 \pm 37 \mu\text{m}$  deep. The microbiopsy defects were similar but not identical to the artefacts arising from processing of the tissue sections from the halved lesions that were not applied with microbiopsies. The dimensions of the processing artefacts ranged from  $20 - 2100 \mu\text{m}$  wide and  $70 - 600 \mu\text{m}$  deep. Histopathological diagnoses of each pair of halved lesions were examined separately. The outcomes of the diagnosis were identical in all lesions. The diagnoses of the five naevi included compound naevus, junctional lentiginous naevus, compound dysplastic naevus, junctional dysplastic naevus and solar lentigo.

A total of 29 microbiopsies were applied to the five naevi. However, not all microbiopsy defects were found. In this section, two out of five naevi were presented. An example of a compound dysplastic naevus is shown in **Figure 5.2a**. The naevus was identified on the left flank of an 88-year-old male patient who had a history of metastatic melanoma. A deep shave excision was performed and the lesion was bisected by the registrar on duty. Five microbiopsies were applied to the bisected lesion (**Figure 5.2b**) and microbiopsy samples were stored in 1.5 ml nuclease-free microcentrifuge tubes containing RNALater® solution to preserve the integrity of the samples. A microbiopsy defect was identified within the melanocytic region. The dimension of this defect was approximately  $132 \times 74 \mu\text{m}$  (**Figure 5.2c** and **5.2d**).

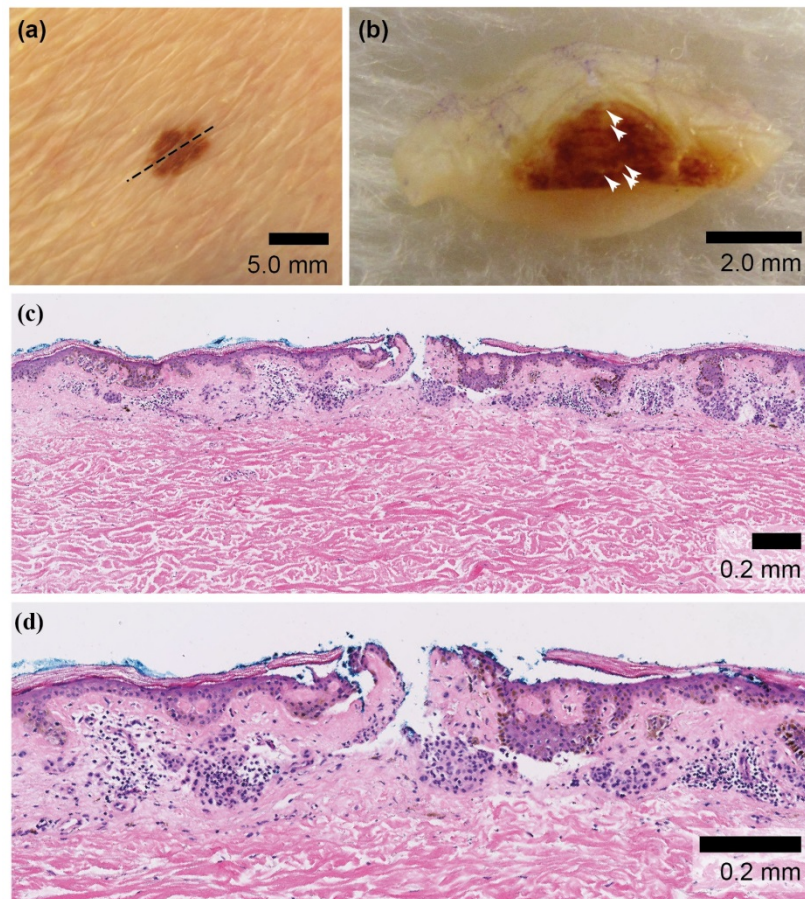


**Figure 5.2: Clinical and histomicrograph of a compound dysplastic naevus.**

Clinical photograph of a compound dysplastic naevus (a) that was bisected and applied with microbiopsy device (b) White arrow represents the sites of microbiopsy application. Panel (c) and (d) shows a microbiopsy defect at low and high magnifications, respectively. Figure modified with permission from (Banan et al., 2013) Copyright 2013, American Medical Association.

Another 56-year-old female patient who was presented with a changing naevus on the left scapula was recruited in the study. The diagnosis was a junctional lentiginous naevus (**Figure 5.3a**). The lesion was excised and bisected prior to microbiopsy application (**Figure 5.3b**). The microbiopsy defect was observed outside the lesional region and had penetrated the superficial dermis. The size of the defect was approximately 145 x 201  $\mu\text{m}$  (**Figure 5.3c and 5.3d**).

The severity of the defects due to microbiopsy application was comparable to artifacts commonly seen in routine sectioned specimens. Given that the diagnosis outcomes for all five naevi were identical, the defects contributed by microbiopsy application did not appear to hinder the diagnosis process. In addition, ordering multiple levels of tissue sectioning

can overcome the potential diagnostic complications with histopathological assessment in microbiopsied lesions. Given the small defect size observed in the histomicrographs, it was foreseen that the use of microbiopsy should not affect the diagnostic process even in equivocal cases. The data have shown that the application of microbiopsies did not interfere with the downstream histopathology diagnosis of those lesions.

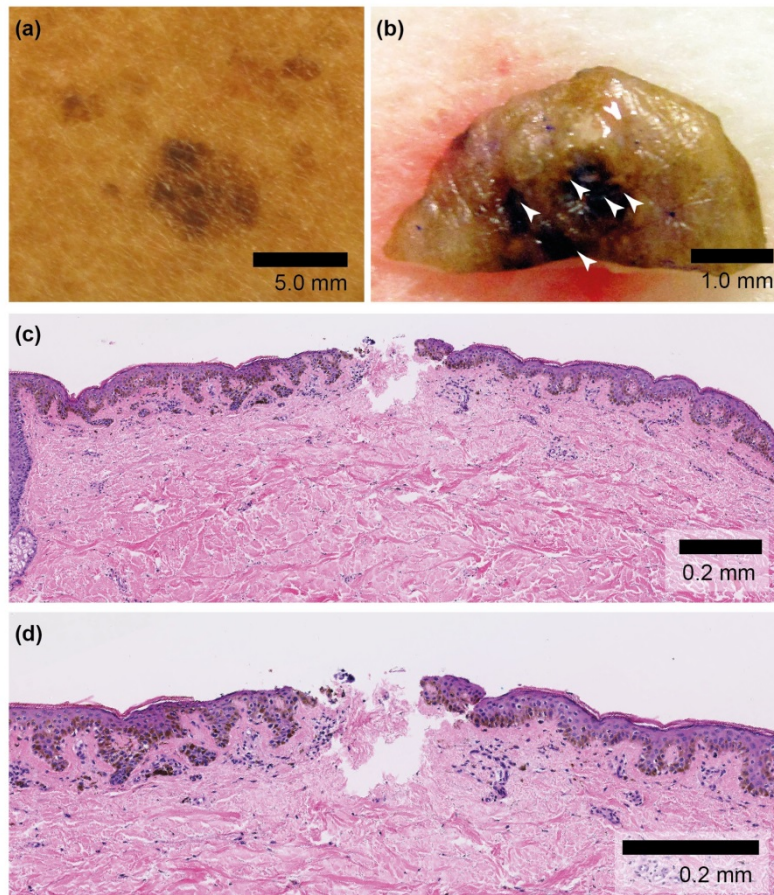


**Figure 5.3: Clinical and histomicrograph of a junctional lentiginous naevus.**

Clinical photograph of a junctional lentiginous naevus (a) that was bisected and applied with microbiopsy device (b) White arrow represents the sites of microbiopsy application. Panel (c) and (d) shows a microbiopsy defect at low and high magnifications, respectively. Figure modified with permission from (Banan et al., 2013) Copyright 2013, American Medical Association.



### 5.3.3 Detection of BRAF Exon 15 and NRAS Exon 2 mutations

The microbiopsy samples collected in the same study were processed for mutational status analysis of BRAF Exon 15 and NRAS Exon 2. A dysplastic naevus located on the chest of a 76-year-old woman (**Figure 5.4a**) was removed surgically and bisected before microbiopsy samples and peri-lesional tissue was collected (**Figure 5.4b**). One of the microbiopsy sites identified from the histopathological sections was outside the lesional region (**Figure 5.4c**). No BRAF or NRAS mutations were detected from the matched peri-lesional skin and all three of the microbiopsy samples taken within the lesion (**Figure 5.4d**).

The second case study was a dysplastic naevus that was surgically removed from the left flank of an 88-year-old man. The lesion was bisected before microbiopsies were applied on one half. All three microbiopsy tissue samples collected from the compound dysplastic naevus had BRAF<sup>V600E</sup> mutation and wild type for NRAS Exon 2 (**Figure 5.5**). The matched peri-lesional skin was also identified as wild type for both BRAF Exon 15 and NRAS Exon 2 (**Figure 5.5**). Histopathological assessment confirmed both lesions as compound dysplastic naevi.

The third lesion that was histopathologically diagnosed as a junctional lentiginous naevus was wild type for both BRAF Exon 15 and NRAS Exon 2 from all samples (data not shown). In conclusion, six out of nine microbiopsy tissue samples from two different dysplastic naevi were determined as wild type for BRAF Exon 15 and the remaining three microbiopsies from another lesion had BRAF<sup>V600E</sup> mutation. All three matched peri-lesional skin samples that were included as control from all three naevi were wild type. This confirmed that BRAF<sup>V600E</sup> mutation that was detected in microbiopsy samples were indeed mutations found in melanocytes within the lesional tissue. Similar to the previous lesion, wild type NRAS Exon 2 were detected from all samples. This result is expected given that the percentage of reported NRAS mutations in melanocytic lesions or melanoma is 10-20% (Lee et al., 2011, Zebary et al., 2014).

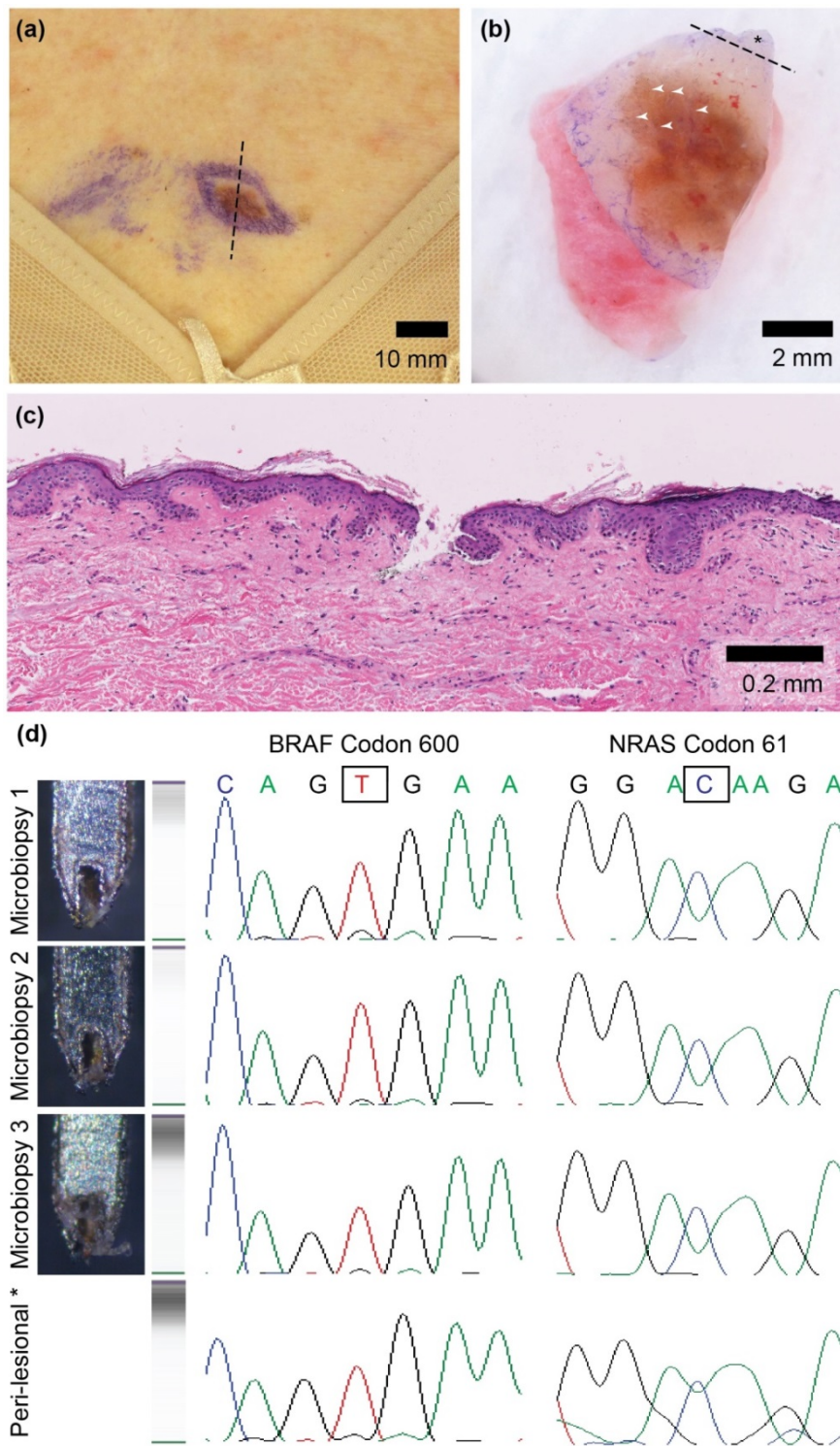


**Figure 5.4: BRAF<sup>V600E</sup> negative case study.**

Clinically dysplastic naevus identified on chest of 76-year-old female patient was excised surgically (a). Five unguided microbiopsy applications (indicated by white arrowheads) were applied on naevus post excision and matched peri-lesional skin (indicated by asterisk) was included as BRAF<sup>V600E</sup>-negative control (b). One of the microbiopsy sites was identified in the non-lesional region (c). All samples including peri-lesional skin were negative for BRAF and NRAS mutations (n=3) (d).

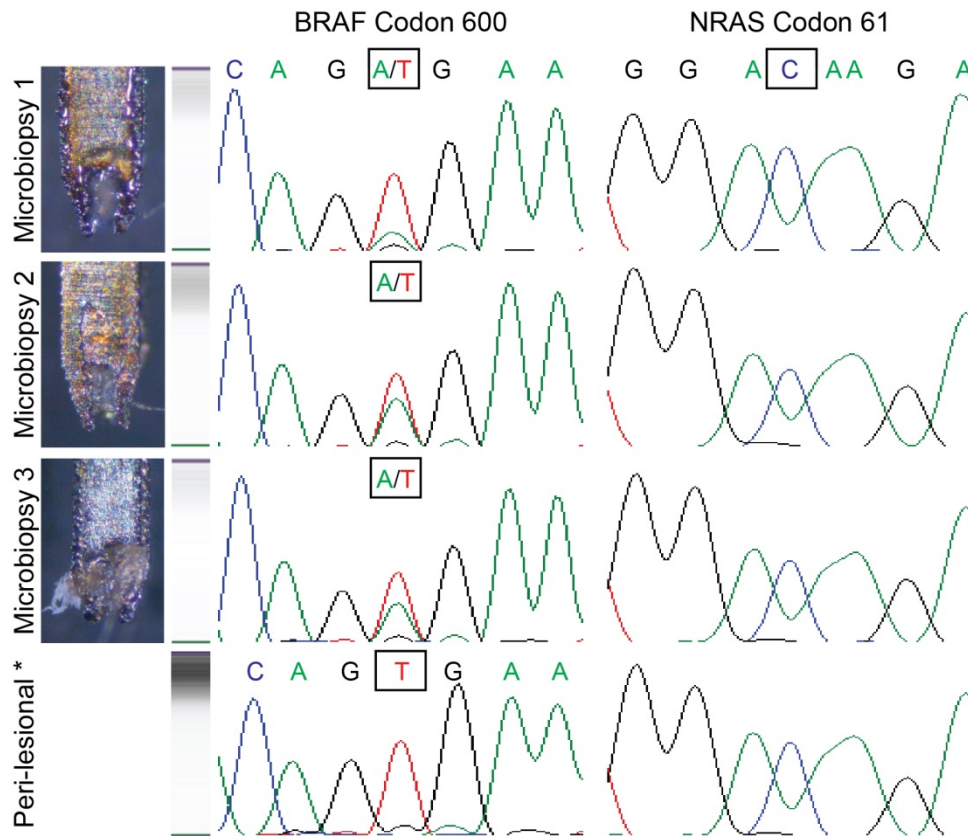


**Figure 5.5: BRAF<sup>V600E</sup> positive case study.**

All microbiopsy samples were positive for BRAF<sup>V600E</sup> but negative for NRAS mutations (n=3), while peri-lesional skin were negative for both BRAF and NRAS mutations (n=1).

### 5.3.4 BRAF<sup>V600E</sup> Mutation status in regressed and stable naevi

A case study from an ongoing study was selected to demonstrate the feasibility and benefit of the microbiopsy for determining the mutation status of changing naevi in individuals. A total of 31 naevi on the body of a 30-year-old male melanoma patient (129BR) were monitored over 27 months. Of these, 25 naevi were larger than 2 mm and ten were greater than 5 mm. Based on the dermoscopic photographs, there were no significant changes to the naevi 14 months after the study had started. Significant dermoscopic changes to 16 naevi (51%) were observed six months after he commenced participation in the inhibitor drug trial. Examples of naevi that had significant dermoscopic changes and those that were stable were illustrated in **Figure 5.6**. The changes observed in those naevi were regression, and decrease in size and level of pigmentation. Flattening of raised naevi was observed in this study, which has also been reported by others (Haenssle et al., 2012).

During the final imaging at the 27-month visit, only five naevi were observed to have regressed since the previous visit. Increased pigmentation was not observed in any naevi and no new naevus was identified. The patient was reported to have excellent systemic response to the therapy with the exception of a node near the pancreas that remained unchanged.

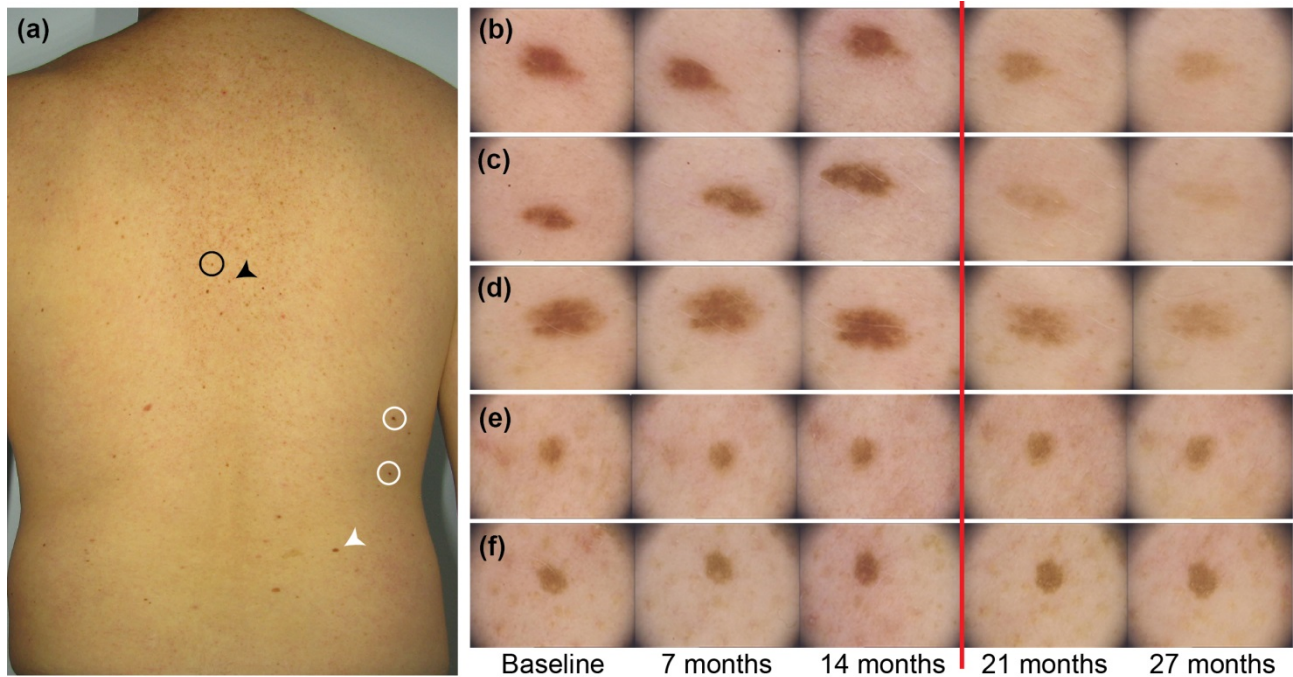


**Figure 5.6: Surveillance of naevi in male patient on clinical trial with BRAF inhibitor and/or MEK inhibitor drugs.**

Clinical photograph of the patient's back showing regressed (white circles and arrow) (n=3) and stable (black circle and arrow) (n=2) naevi. Excised naevi that were included in the case study are indicated by the arrows (a). Panel (b) to (d) represent naevi that has significant dermoscopic changes observed at 21-month visit. Panel (e) and (f) show naevi that they were stable throughout the monitoring period. The red line indicates the commencement of the clinical trial. Figure modified with permission from (McClenahan et al., 2014) Copyright 2014, American Medical Association.

The changes and appearance of new naevi over time can be influenced by UV radiation (Hofmann-Wellenhof et al., 1997), hormone changes associated with pregnancy and targeted therapy (Haenssle et al., 2012). The influence of UV exposure was not considered as the major factor as regressing and stable naevi in the patient was observed at the same body site. Pregnancy-related factor was also ruled out. Therefore, it was hypothesized that changing naevi had a positive BRAF<sup>V600E</sup> mutation, which had responded to the targeted therapy.

Microbiopsy sampling was performed for detection of BRAF<sup>V600E</sup> mutation in a changing and an unchanging naevus (**Figure 5.7a** and **5.7b**). Sanger sequencing showed that the regressing lesion was heterozygous for BRAF<sup>V600E</sup> mutation (**Figure 5.7c**). Two out of five microbiopsies collected within the naevus was positive for BRAF<sup>V600E</sup> mutation. On the other hand, no BRAF mutation was detected in the stable naevus (**Figure 5.7d**). Perilesional samples were also collected from both naevi as negative controls. Similar to the previous study, the samples were also screened for NRAS mutation within Exon 2 but no mutation was detected for both naevi (data not shown).

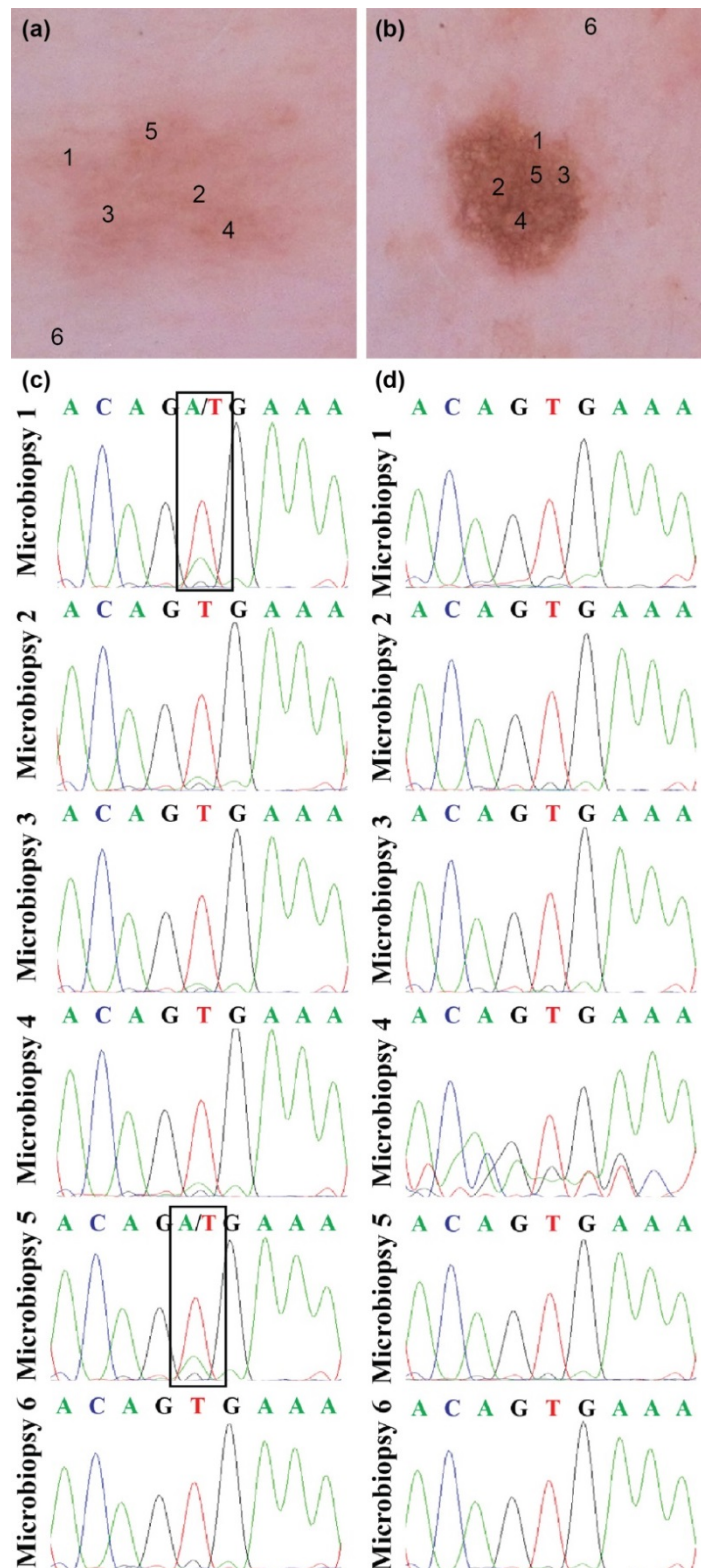


**Figure 5.7: BRAF<sup>V600E</sup> mutation status in regressed and stable naevi.**

Dermoscopic photograph of regressing (a) and stable (b) naevi. Sites of microbiopsy application within the lesional region were chronologically labelled from 1 – 5. Microbiopsy 6 was taken on the peri-lesional area. Positive BRAFV600E mutations were identified in Microbiopsy 1 and 5 of the regressing naevus (c). No BRAF mutation was detected in the peri-lesional area and in the unchanging naevus (d). Figure modified with permission from (McClenahan et al., 2014) Copyright 2014, American Medical Association.

### 5.3.5 Unguided and guided tissue sampling

The initial microbiopsy design introduced within the Thesis consisted of a micro-sized biopsy cutting tip that is attached to a modified spring-loaded blood lancet applicator (Unistik, Owen Mumford, UK). The microbiopsy device is loaded (**Figure 5.8a**) and fired at high speed into the skin with sampling accuracy to certain extent (**Figure 5.8a** and **8b**). The current unguided microbiopsy device has limited targeting accuracy and was unable to achieve consistent sampling within regions of interest approximately 1 mm in diameter (**Figure 5.8b**). Ross Flewell-Smith determined from the application spread test that the unguided microbiopsy sampling has a targeting accuracy of  $0.29 \pm 0.32$  mm (horizontally) by  $1.05 \pm 0.56$  mm (vertically) (**Figure 5.8c**).

The use of a dermoscope and a targeting cassette (indicated by a black arrowhead) were incorporated to improve on the targeting accuracy of the microbiopsy device (**Figure 5.8d**). The hand-held dermoscope can help to align the targeting cassette within a 1 mm diameter hole to enable improved sampling accuracy. After the targeting cassette is aligned on the region of interest, the microbiopsy is placed on top of the cassette and standard microbiopsy sampling procedures are followed (**Figure 5.8d**). Targeted tissue sampling within the region of interest  $\leq 1$  mm in size (**Figure 5.8e**) was achieved when the microbiopsy was used in conjunction with the targeting cassette. The application spread test confirmed that the targeting accuracy with the use of a dermoscope and targeting cassette was  $0.19 \pm 0.11$  mm (horizontally) by  $0.66 \pm 0.24$  mm (vertically) (**Figure 5.8f**). The addition of a targeting cassette and dermoscope improved horizontal and vertical targeting accuracy by 4.8- and 1.6-fold, respectively. This device is designed to enable precise tissue sampling that can be performed repeatedly without damaging the lesion. In the next experiment, I validated the use of this device as a targeted tool for more precise sampling in melanocytic lesions.

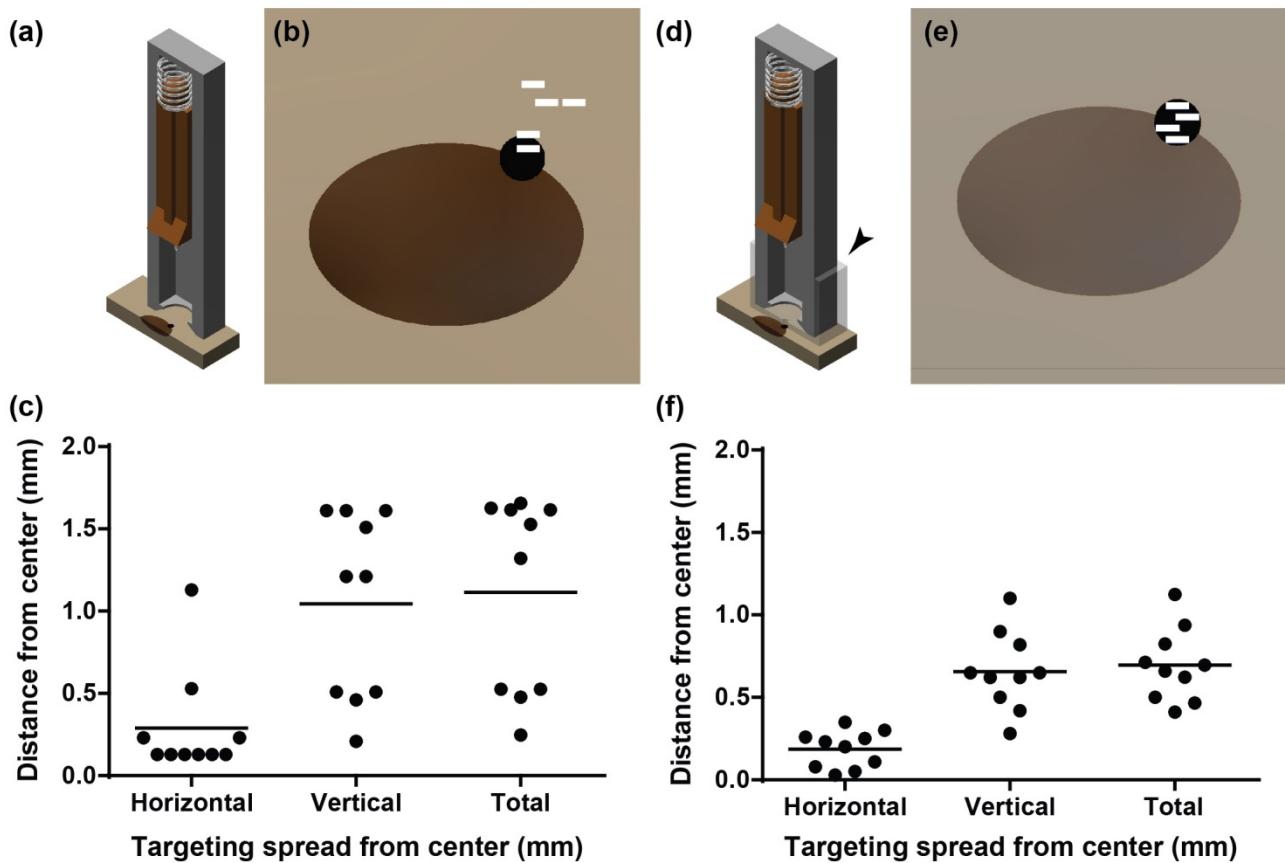


**Figure 5.8: The targeted skin microbiopsy.**

Non-guided microbiopsy device (a) when applied to the skin, collects tissue samples on or around region of interest (b) that has an average targeting accuracy of 0.29 mm horizontally and 1.05 mm vertically (n=10) (c). Microbiopsy guided with a targeting cassette (indicated by black arrowhead) (d) can collect tissue samples more accurately within region of interest (e) and has an average targeting accuracy of 0.06 mm horizontally and 0.66 mm vertically (n=10) (f).

### 5.3.6 Targeted sampling from regions of interest within lesion

To establish the feasibility of precise sampling ( $\leq 1$  mm) in a small region of interest within a lesion, a clinically interesting case study of an atypical melanocytic naevus that will allow us to study three individual regions within the lesion will be discussed.



A 5 x 3 mm clinically diagnosed atypical lentiginous melanocytic lesion identified on the left lower back of a 58-year old male was excised through shave biopsy (**Figure 5.9a**). This clinical case had allowed assessment for the precision of tissue sampling from three different regions of interest identified within the lesion (**Figure 5.9b**). Three microbiopsies were applied within the 1 mm dotted outline of each area as highlighted in **Figure 5.9a**. DNA was isolated from each microbiopsy sample independently and processed for whole genomic amplification. The amplification was even and unbiased (data not shown) across

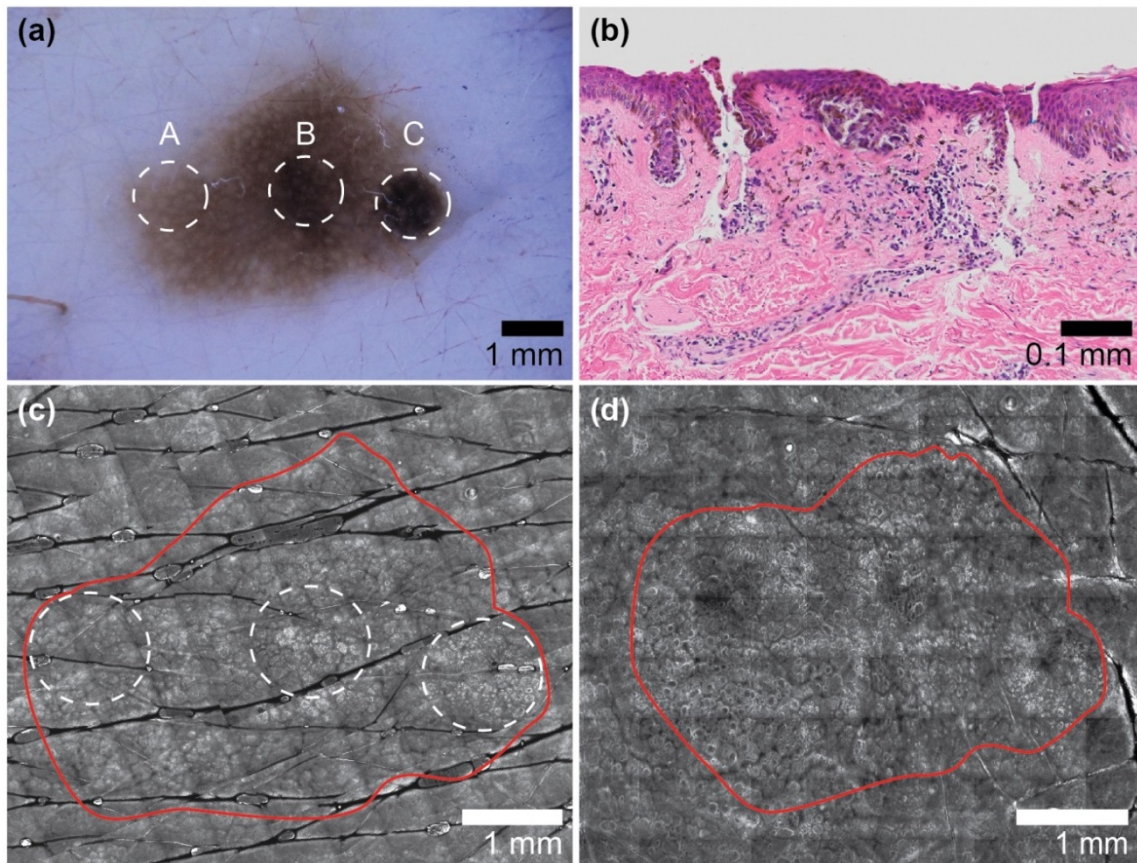


**Figure 5.9: Case study demonstrating precision microbiopsy sampling.**

A 5 x 3 mm dysplastic naevus that has clinically different regions (A-C) within the lesion was diagnosed as lentiginous naevus on the lower left back of a 56-year-old male patient. Three microbiopsies were applied within each white dotted circle indicated as region A, B and C (a). Two microbiopsy sites were identified from one of the histopathological sections within region C (b). The reflectance confocal microscopy mosaics show the sites of application before (c) and after (d) microbiopsy. The red outline and white dotted outlines on the images represent the outline of the naevus and the site of microbiopsy applications on the three regions that are identified to be clinically different.

all samples and amplified DNA output ranges between 40-66 µg. Histopathological sections revealed two microbiopsy sites within region C (**Figure 5.9b**). The reflectance confocal mosaics of the lesion taken at the dermal-epidermal junction dermis (approximately 60 µm in depth) before (**Figure 5.9c**) and after microbiopsy application (**Figure 5.9d**) was compared, and microbiopsy sites were observed within the region of interest.

Results from Sanger sequencing showed that two out of three regions have heterogeneous BRAF<sup>V600E</sup> mutation, while no mutation was detected in the microbiopsy samples from region C (**Figure 5.10**). Also detected were BRAF<sup>V600E</sup> and a rare BRAF<sup>S605R</sup> mutation in one of the microbiopsies and a BRAF<sup>S605R</sup> mutation in another area within region A. Two BRAF mutations were detected in one microbiopsy and only BRAF<sup>V600E</sup> was detected in another area within region B. Both regions had a single microbiopsy that detected wild type BRAF.

On the other hand, microbiopsy samples obtained from region C that was diagnosed as melanoma *in-situ* were all BRAF wild type. One may speculate that this could be due to insufficient sampling of melanocytes that carry BRAF mutations or that only a small percentage of the melanocytes that carry BRAF mutations were present in the melanoma *in-situ*. Therefore, the microbiopsy may not be able to detect positive BRAF<sup>V600E</sup> mutation if less than 25% of the melanocytes carry BRAF mutations (Richter et al., 2013). Similar to other lesions, NRAS Exon 2 mutations were not able to be detected in any of the microbiopsy samples (data not shown).

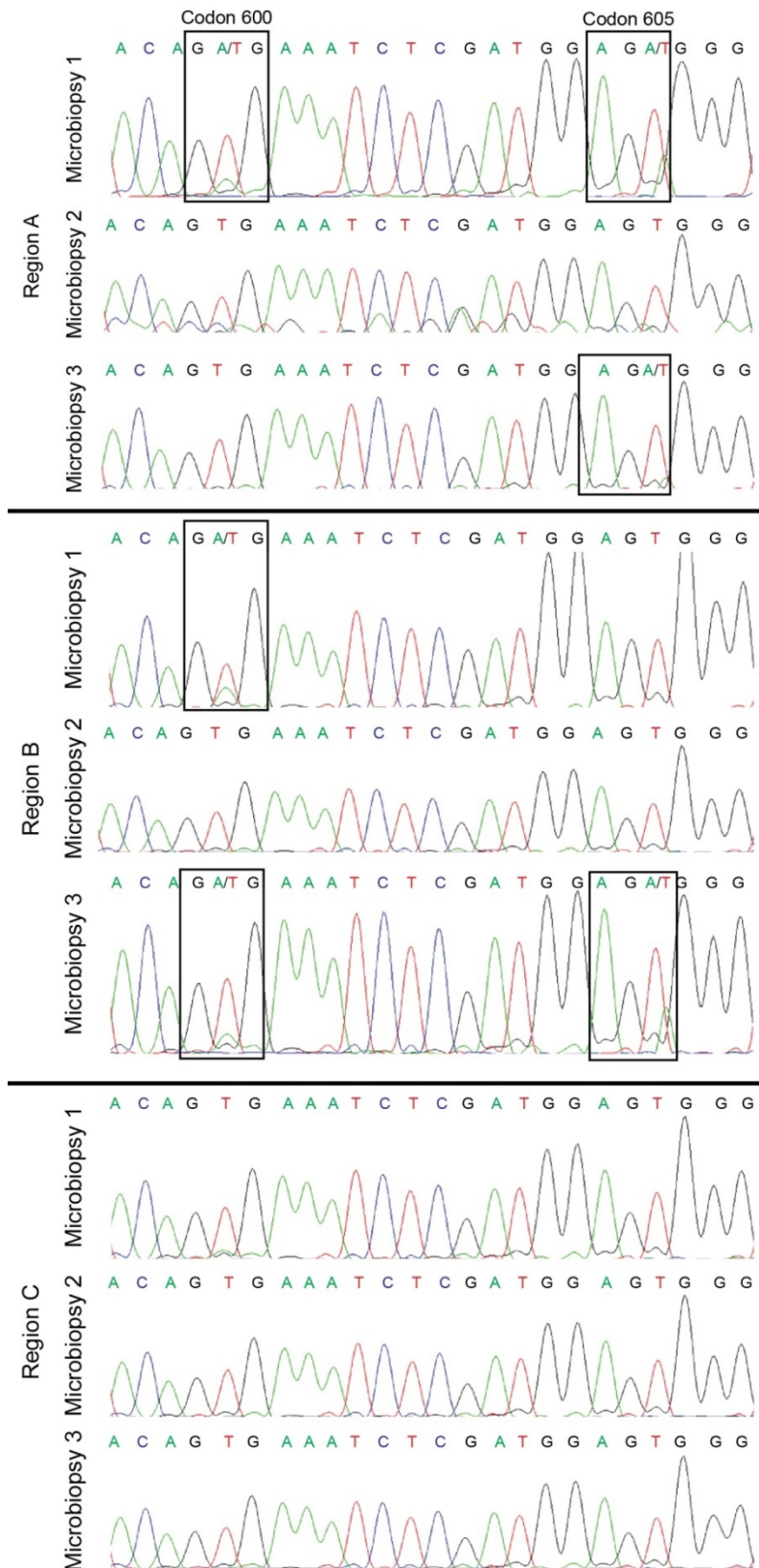


**Figure 5.10: BRAF mutations from microbiopsy samples.**

Two BRAF mutations within Exon 15 were identified from the microbiopsy samples taken from three regions of interest, a common BRAF<sup>V600E</sup> and a rarer BRAF<sup>S605R</sup> mutation. Both mutations were found in at least one out of three microbiopsy samples in region A and B. No BRAF mutation was detected in any of the microbiopsy samples from region C (n=3 per region).

The sensitivity of Sanger sequencing was previously tested by Kasturee Jagirdar using genomic DNA from human saliva (negative control) and samples from a melanoma cell line with different concentrations of BRAF<sup>V600E</sup> mutation (positive controls) (**Figure 5.11a**). An identical set of samples (n=9), in addition to samples of known BRAF<sup>V600E</sup> mutation ratios were sent to a sequencing facility for independent quantitation of BRAF<sup>V600E</sup> mutation analysis. The assay detected 6% of BRAF<sup>V600E</sup> mutation in one out of three microbiopsies from both region A and B. BRAF<sup>V600E</sup> mutation was not detected in microbiopsies from region C (**Figure 5.11b**). The results from Sanger sequencing and MALDI-TOF assay were relatively similar except for region B. It was observed that positive BRAF<sup>V600E</sup> mutations in two out of three microbiopsies with Sanger sequencing but only

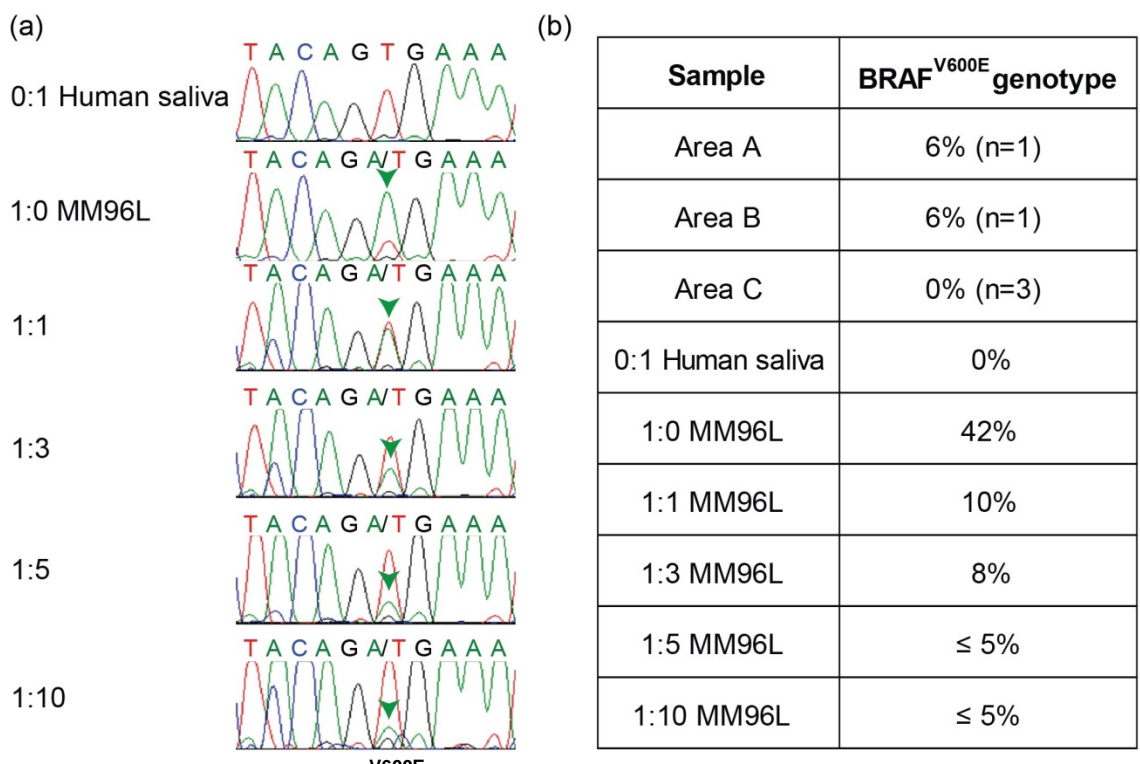


**Figure 5.11: Quantitating BRAF<sup>V600E</sup> mutations from microbiopsy samples.**

Genomic DNA from human saliva and DNA containing different mutant to wild type ratios extracted from MM96L melanoma cell line were used as controls to test the sensitivity of Sanger sequencing to detect BRAF<sup>V600E</sup>. BRAF<sup>V600E</sup> is detected as A/T in the chromatographs. The green arrows highlight the peak of BRAF<sup>V600E</sup> signal (a). The amount of BRAF<sup>V600E</sup> mutation in microbiopsies taken from the three distinct regions and the controls were independently quantified using MALDI-TOF assay by a sequencing facility (b). Reproduced with permission from (Tan et al., 2015) Copyright 2015, American Medical Association.

one out of three was detected with MALDI-TOF assay. Results based on the positive controls suggested that MALDI-TOF assay was not as sensitive. This explained the difference in detection outcome.

Tschandl et al. (2013) investigated the number of positive BRAF mutations in melanoma that arise from a pre-existing naevi. They performed one or more laser capture microdissections on 5 µm thick formalin fixed paraffin embedded histology sections to selectively obtain cells from the naevus or the melanoma. Sanger sequencing was performed to detect BRAF mutations within Exon 15 and immunohistochemistry was included to confirm the mutations. They observed five out of 46 cases (10.9%) of melanoma with wild type BRAF adjacent to a pre-existing naevus with BRAF<sup>V600E</sup> mutation (Tschandl et al., 2013). They concluded that the findings based on phenotypic and genotypic analysis did not concur with the existing concept of stepwise tumor progression. On contrary, the phenotypic features of our lesion matched Clark's progressive clinic-pathologic model even though this is challenged by the conflicting genetic profile of the lesion. Otherwise, the case study well-demonstrated the benefits of microbiopsy device for *in vivo* sampling to provide insights in heterogeneity of melanocytic lesions. One may reason that either the microbiopsy did not sample at the right location or melanocytes were not sampled from the melanoma in-situ, thus leading to a wild type sequence. However, this proof-of-concept study did illustrate the potential of the device for future melanoma diagnosis. Ongoing work in the laboratory is focused on detecting the presence of melanocyte markers in conjunction to mutation analysis.

### **5.3.7 Somatic mutation status in non-pigmented skin lesions**

Microbiopsy and its matched non-pigmented lesions (n=4) were compared for genetic signatures using a real-time p53/Rb PCR Array kit. This PCR assay is capable of detecting down to 1% of somatic mutations from the background of wild type genomic DNA using amplification refractory mutation system (ARMS®) technology. DNA from non-sun exposed foreskin was used in this experiment as the wild type control. The diagnosis of all four samples was intraepithelial carcinoma (IEC). **Table 7** shows the summary of positive mutation calls identified by the analysis software. A total of 17 positive mutations (18.8%) were detected in 20 samples. The most prevalent p53 mutation occurred at codon 535 consisting of a C – T substitution, where 20% of the samples had this point mutation. No RB1 mutation was detected in any of the samples.

Only one out of four sample sets (AKSFS15) detected a G>A at codon 330 of CDKN2A gene in both lesions and microbiopsies (100% match). Most mutations were detected within the TP53 gene in this experiment. None of the sample sets (amplified DNA from lesion and microbiopsies) had a 100% match when compared to the non-amplified lesional sample. Comparing only microbiopsy to its non-amplified lesional sample, only one out of four (AKSFS30) had a 100% match. In the sample set from AKSFS15, there were one 100% and two 50% matches in the microbiopsy samples. It was observed that only one out of four lesional samples that was subjected to whole genomic amplification matched its non-amplified lesional samples. This suggested that amplifying DNA can create false positive mutation signals possibly by creating mutations during the amplification process. Borderline mutation call, which represents mutation that is present at low percentage, was also identified by the analysis software. It is represented by the +/- symbol in **Appendix 1**.

There were 15 different borderline mutations identified among the 20 samples (microbiopsies and lesions). The most common mutations among the samples were all within TP53 gene (c. 422G>A, c.535C>T and c.844C>T). At least seven out of 20 samples (35 – 45%) have one or more of these mutations detected from the assay. Only one microbiopsy had a 100% match to the non-amplified lesional sample. Overall, using amplified DNA samples resulted in the increased detection of borderline mutations regardless of the sample source (microbiopsy or lesion). Up to eight borderline mutation calls were identified in an amplified DNA sample while none was detected in the non-amplified lesional sample. Unfortunately, there is no sample remaining to confirm the mutations detected in this experiment. In the future, I would like to do a prospective study in photodamaged and non-photodamaged skin but it is beyond the scope of this Thesis.

**Table 7: Summary of positive mutation calls in p53/Rb pathway PCR array.**

Sample	Mutation found	Gene	Cosmic ID	Nucleotide change	Amino acid residue	No. of mutation	% match to non-amplified lesion
AKSFS15-L1 NA	Yes	CDKN2A	12547	c.330G>A	p.W110	1	
AKSFS15-L1 Amp	Yes	CDKN2A	12547	c.330G>A	p.W110	1	100%
AKSFS15-MB2	Yes	CDKN2A, TP53	12547, 43635	c.330G>A, c.536A>T	p.W110, p.H179L	2	50%
AKSFS15-MB3	Yes	CDKN2A	12547	c.330G>A	p.W110	1	100%
AKSFS15-MB4	Yes	CDKN2A, TP53	12547, 10768	c.330G>A, c.535C>T	p.W110, p.H179Y	2	50%
<hr/>							
AKSFS30-L2 NA	No	-	-	-	-	0	
AKSFS30-L2 Amp	Yes	TP53	10768, 10939	c.535C>T, c.832C>T	p.H179Y, p.P278S	2	0%
AKSFS30-MB1	No	-	-	-	-	0	100%
AKSFS30-MB2	No	-	-	-	-	0	100%
AKSFS30-MB3	No	-	-	-	-	0	100%
<hr/>							
VH006-L1 NA	No	-	-	-	-	0	
VH006-L1 Amp	Yes	TP53	10768	c.535C>T	p.H179Y	1	0%
VH006-MB1	Yes	ATM	21624	c.9139C>T	p.R3047*	1	0%
VH006-MB2	No	-	-	-	-	0	100%
VH006-MB4	Yes	TP53	10727	c.438G>A	P.W146*	1	0%
<hr/>							
VH009-L1 NA	No	-	-	-	-	-	
VH009-L1 Amp	Yes	TP53	43635, 10863	c.536A>T, c.833C>T	p.H179L, p.P278L	2	0%
VH009-MB1	Yes	TP53	1081, 43708, 43609, 10727, 10690, 10687, 10768, 43635, 11089, 10704, 10726	c.404G>T, c.422G>A, c.856G>A, c.451C>T, c.461G>T, c.469G>T, c.476C>T	p.C135Y, p.C141Y, p.W146*, p.W146*, p.R158H, p.C176Y, p.H179Y, p.H179L, p.I195T, p.R282W, p.E286K	11	0%
VH009-MB2	No	-	-	-	-	-	100%
VH009-MB3	Yes	TP53	43947, 10659	c.614A>G, c.817C>T	p.Y205C, p.R273C	2	0.0%

NA: non-amplified DNA from lesion, Amp: amplified DNA from lesion, MB: microbiopsy

There is currently no published data on the use of this kit for mutational profiling. Transcriptome wide SNP analysis results from the RNA-Seq data using methods that were described previously by Quinn et al. (Quinn et al., 2013) were performed. Comparison of data from both RNA-Seq and p53/Rb real-time PCR were made to look for mutations that were detected by both assays. A total of seven and five distinct loci were reported for sample VH006 and VH009, respectively, at CDKN2A, ATM, TP53 and RB1 gene regions. The read depth and coverage of these gene regions were summarized in **Table 8**. Unfortunately, none of these mutations corresponded to the 90 cosmic mutations found on 74 distinct sites assayed by the p53/Rb PCR Array kit.

**Table 8: Average gene coverage and read depth of ATM, CDKN2A, RB1 and TP53 genes.**

Sample	ATM		CDKN2A		RB1		TP53	
	Gene coverage	Read depth	Gene coverage	Read depth	Gene coverage	Read depth	Gene coverage	Read depth
VH006	<b>97%</b>	<b>24.05</b>	<b>100%</b>	<b>27.29</b>	<b>9%</b>	<b>3.10</b>	<b>100%</b>	<b>22.88</b>
VH009	<b>95%</b>	<b>9.00</b>	<b>100%</b>	<b>15.86</b>	<b>12%</b>	<b>2.00</b>	<b>100%</b>	<b>13.63</b>

The lack of concordance between results from the RNA-Seq assay and the p53/Rb PCR Array kit can be largely attributed to intrinsic differences between the technologies of the two assays. The p53/Rb PCR Array kit is a DNA-based assay designed to pick up specific mutations from these gene regions. Unlike the p53/Rb PCR Array, RNA-Seq technology measures the abundance of different mRNA species, which may vary between gene and samples (Wang et al., 2009). Hence, any mutations of poor transcription activity that lie within regions will not be detected using RNA-Seq (Mercer et al., 2012).



## 5.4 Conclusions

The genotyping experiments established the framework for downstream processing of microbiopsy samples to carry out a range of molecular analytical techniques. The success of MC1R and OCA2 genotyping using microbiopsies was confounded by quantity of sample used for techniques suited for much larger samples. This limitation was overcome when DNA sample was amplified, although with some limitations.

The sub-millimetre microbiopsy demonstrated its potential for repeated micro-tissue sampling in excised melanocytic lesions without interfering downstream histopathological analysis. The defects from microbiopsy application found in the histology sections were similar to artefacts caused by routine sample processing. However, it is important to recognise that a more clinically relevant question is whether previous microbiopsy application sites might contain residual inflammation as this may impact histopathological interpretation of difficult dysplastic lesions or early melanomas. Exploring this question is an exciting area of research that needs to be done prior to widespread use of the device. Such a clinical trial would need to include a substantial number of cases to address the question. In the future I see molecular diagnosis replacing histopathological assessment, but until that vision is realized, this is an important question.

Positive BRAF<sup>V600E</sup> mutation in microbiopsy samples were successfully detected through Sanger sequencing. Rarer BRAF mutations (S605R) were detected in the microbiopsy samples collected from the dysplastic naevus adjacent to a melanoma *in-situ*. No NRAS mutation was identified in all samples including the lesions. Multiplex mutation profiling has become a common technique in research settings to characterise a disease. PCR amplification is usually required for multiplex assays. Microbiopsy samples were successfully profiled for significant mutations in the p53/Rb pathway. A total of 17 positive and 15 borderline mutations were identified in the samples. The overall results have, however, highlighted the consequence of introducing mutations when samples were subjected to genomic amplification. In conclusion, these proof-of-concept studies have demonstrated that the guided skin microbiopsy device has the potential to study *in vivo* molecular changes within a targeted area over time, which were impossible in the past.

## Chapter 6

### *Microbiopsy – a new approach for live cell assay*

#### 6.1 Introduction

The skin is a major target for a wide range of therapeutics and cosmeceuticals. However, analysis of active pharmaceutical ingredients or excipients with the skin often requires tissue extraction followed by downstream analysis. Current approaches, in particular those related to the cosmeceutical arena are limited to restrictive regulations on animal testing and the fact it is often not deemed ethical or practical to use conventional biopsy techniques to assess the effect of cosmetics. It has been demonstrated in Chapter 4 that cell imaging can be performed on tissue acquired by the microbiopsy device. Furthermore, considering that small skin tissue samples can be acquired using the microbiopsy without the need of local anaesthetic or scarring, this technology platform can have significant benefits in the area of animal-free cosmeceutical testing.

One of the most common topical formulation ingredients are UV-filters zinc oxide and titanium dioxide nanoparticles. However, there is evidence that zinc-oxide and titanium dioxide nanoparticles could induce free radicals in the presence of sunlight, which may cause damage to skin cells (Anreddy et al., 2013). Yet, the relevance of this data and of others within a clinical context remains debatable. The question is to know whether these nanoparticles would penetrate into viable skin cells in people. The focus of this Chapter was to explore microbiopsy potential for assessing the effects of zinc-oxide nanoparticles (ZnO-NP) on viable tissue within volunteers. The aims were to:

- AIM 1** Establish microbiopsy tissue sample staining and imaging with live tissue
- AIM 2** Live cell assay development for assessing oxidative stress in viable tissue
- AIM 3** Determine the potential of ZnO-NP to induce oxidative stress in intact and barrier compromised skin

Nanotoxicology investigation in volunteers is generally carried out using minimally invasive imaging technology such as fluorescence lifetime imaging microscopy (FLIM). This technique has been previously established in the lab, and was used to monitor metabolic

changes in ZnO-NP treated volunteer's skin (Lin et al., 2011). Nanoparticles are discrete objects ranging from a size of 1 nm to 100 nm. ZnO-NP commonly used in sunscreens range from 5 to 50 nm but often aggregate forming larger sizes. The commercial success of such formulations is reflected by these products remaining in the market for more than 30 years (Wang and Tooley, 2011). Today, ZnO-NP continues to be incorporated not just into sunscreens but also in a diverse range of cosmeceutical products. Preference for these nanoparticles is, however, not universal. There have been suggestions that these nanoparticles are small enough to penetrate damaged skin resulting in immune perturbation (Nel et al., 2006).

Nanoparticles have greater relative surface area compared to micro-sized particles. This allows more atoms to be exposed to the environment resulting in unique properties (Nel et al., 2006). Nanoparticles often form larger clusters through interaction with one another leading to decreased relative surface area. Therefore, elucidating the probability of nanoparticles as individual entities to cause cytotoxic effects remains an academic area of study. The clinical relevance of this topic is limited because of the rapid adsorption of biological material that occurs through corona formation on the nanoparticle surface when it is introduced to a biological environment. The current data suggests that the nanoparticle aggregate corona plays a major role in cellular uptake (Xia et al., 2011, Monteiro-Riviere et al., 2013). This may be a crucial difference between *in vitro* and clinical experimental outcomes.

Multiple ZnO-NP sunscreen studies have been carried out to elucidate the fate of ZnO-NP within the skin after being applied. The results from these studies were confounded by varying experimental models with authors using a range of *in vitro*, *ex vivo* and *in vivo* animal models (Sharma et al., 2009, Xia et al., 2011, Anreddy et al., 2013, Nel et al., 2006, Jeng and Swanson, 2006, Rasmussen et al., 2010). Few were done in human volunteers. However, a majority of those that were, came from our Group, where I have been involved with both the research design and implementation investigating the effects of ZnO-NP exposure on changes to cell metabolic activities. (Gulson et al., 2010, Leite-Silva et al., 2013, Lin et al., 2011, Raphael et al., 2013). Clinical experiments remain the most relevant but the most challenging to do. *In vitro* studies have illustrated the cytotoxicity effects of ZnO-NP on cells. Sharma et al. (2009) showed that ZnO-NP even at a low concentration of 0.008 µg/ml had damaging effects on DNA (Sharma et al., 2009). Others concurred that

oxidative stress appeared to be the key inducer for cytotoxic effects (Jeng and Swanson, 2006, Rasmussen et al., 2010). In contrast, the clinical safety concerns for ZnO-NP are minimal based on current reports from clinical and *ex vivo* studies (Raphael et al., 2013, Leite-Silva et al., 2013, Gulson et al., 2010, Lin et al., 2011) demonstration poor nanoparticle tissue infiltration.

In this Chapter, the changes in oxidative stress induced by ZnO-NP exposure to intact and barrier compromised human skin (**Figure 6.1**) were investigated. Intact or barrier disrupted skin was treated with ZnO-NP suspended in a caprylic capric triglycerides (CCT) solution. Skin barrier disruption was achieved using tape-stripping resulting in obvious clinical differences (increased erythema / moisture content) compared to intact regions (**Figure 6.1b**). ZnO-NP were applied to the contralateral forearm to reduce the possibility of cross-contamination. After treatment incubation, the microbiopsy was applied to the treated areas resulting in a micro-scale extraction site (**Figure 6.1c**, arrow head). The tissue was collected within the microbiopsy (**Figure 6.1d**) and used for downstream analysis of reactive oxygen and nitrogen species, and mitochondrial superoxide production.

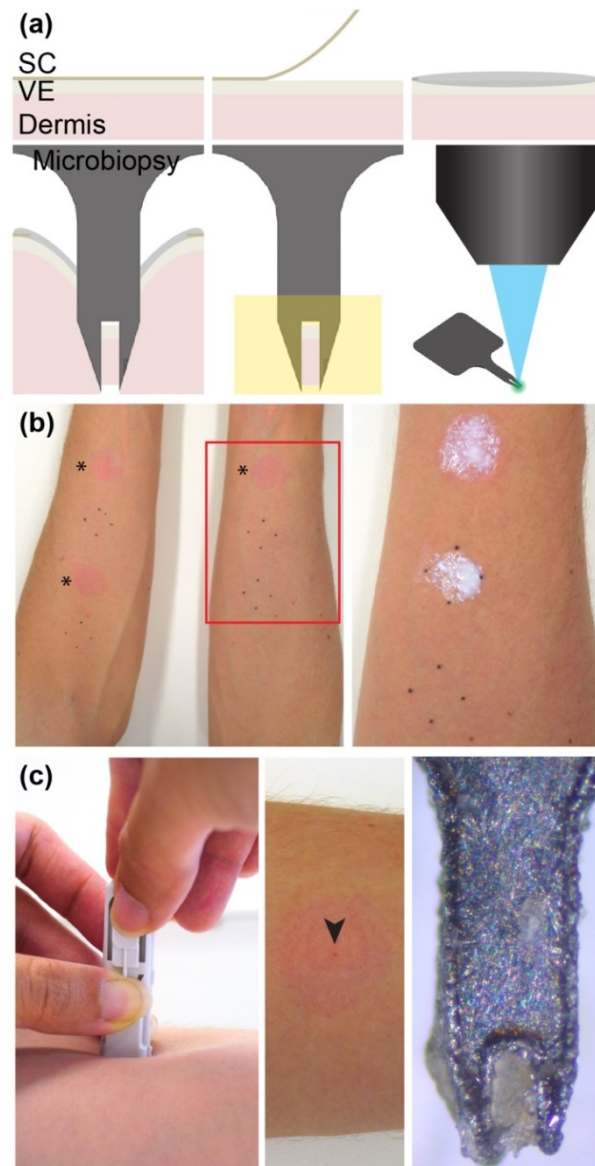


**Figure 6.1: Schematic and clinical photographs showing ZnO-NP administration to volunteers followed by microbiopsy enabled oxidative stress analysis.**

Top left panel show the three layered structure of the skin (SC – stratum corneum, VE – viable epidermis and dermis) (Panel (a), left). The SC was removed using tape-stripping to expose the viable epidermis (Panel (a), middle). ZnO-NPs were applied topically to intact and tape-stripped skin (Panel (b), right). The tissue was then stained for oxidative stress followed by fluorescence confocal microscopy analysis (a, right). Clinical photographs of a volunteer arm that has been tape-stripped (Panel (b), left and center). The asterisks show the areas that have been tape-stripped. ZnO-NP treatment was done on the separate forearm to prevent any risk of cross-contamination (Panel (b), right). Clinical photographs showing the microbiopsy procedure (Panel (c), left). The middle panel shows minimally invasive nature of the microbiopsy (Panel (c), middle). The microbiopsy site is indicated by the arrowhead. The tissue is collected in the microscopy chamber ready to oxidative stress analysis (Panel (c), right).

## **6.2 Materials and Methods**

### **6.2.1 Study volunteers**

Six volunteers were recruited in this study approved by the Metro South Health Human Research Ethics Committee (HREC/12/QPAH/251) and the University of Queensland Human Research Ethics Committee (Approval number: 2012000992). All volunteers gave informed consent and signed a Participant Information and Consent Form before the study commenced. Equal numbers of male and female volunteers were recruited.

### **6.2.2 Tape-stripping and Trans-epidermal water loss (TEWL)**

Tape-stripping was used to disrupt the skin barrier. Commercially available 3M Scotch® 810 Magic™ adhesive tape (3M Australia, Australia) with a width of 12.7 mm was used to remove the skin layers. The tape was applied to the ventral forearm and even pressure was applied across the tape using a metal roller to ensure that uniform adhesion of the tape on the skin was achieved. The adhesive tape was stripped off quickly from the skin after the metal roller was pressed over twice.

Each volunteer was requested to sit in the laboratory for 10 minutes before the start of the study while the process of the experiment was discussed. This approach is to prevent the influence of sweating on the increased TEWL measurements. Single TEWL measurement was taken periodically on tape-stripped skin during the tape-stripping process with a closed chamber VapoMeter (Delfin Technologies, Finland). The tape-stripping procedure was repeated with a new piece of tape until trans-epidermal water loss (TEWL) increased greater than 20 g/m<sup>2</sup>h.

### **6.2.3 Zinc-oxide nanoparticle (ZnO-NP) preparation and application**

Micronised zinc-oxide nanoparticle (ZnO-NP) with a hydrophobic coating (Z-Cote® HP 1, BASF, Germany) was applied to intact and tape-stripped skin in volunteers. The average size of ZnO-NP determined by transmission electron microscopy was approximately 60 nm (data not shown). The manufacturer reported a guaranteed size of less than 200 nm as the aggregation of such small particles is very common during synthesis. The concentration of ZnO-NP in commercially available sunscreens can vary depending on the sun protection factor of the product. A commercially available SPF 30+ sunscreen from Cancer Council contains 200 mg/g ZnO-NP while the SPF 50+ sunscreen contains 50 mg/g. The

concentrations of ZnO-NP tested in previous studies varied from 2% to 60%. The total amount of ZnO-NP applied can vary but the dose was consistent across most studies at 2 mg/cm<sup>2</sup>.

In this experiment, 100 mg of ZnO-NP powder was suspended into 1 ml caprylic capric triglycerides (CCT) solution. The solution was mixed thoroughly using a vortex mixer at a speed of 8 a.u. for 1 minute. Further mixing was performed using a FXP10MH Sonicator (Unisonics Australia, Australia) at 30°C for 20 minutes. Vortex mixing was repeated for another minute after sonication. The ZnO-NP solution was applied at a final concentration of 100 mg/ml. There were three 2 x 2 cm treatment areas mapped out on each forearm, with a total of six treatment areas for each volunteer (**Figure 6.1**). Tape-stripped and intact skin were treated with either ZnO-NP at a dosage of 2 mg/cm<sup>2</sup> (for a total of 8 mg on the site) or CCT solution over a total area of 4 cm<sup>2</sup> per treatment site. Treatment duration was two hours. Untreated sites were included as a negative treatment control. ZnO-NP was applied on the contralateral forearm to prevent cross contamination of treatment sites. No adverse reactions or effects were observed after all treatments.

#### **6.2.4 Microbiopsy sample collection**

Type G2A microbiopsy cutting die fabricated by our S290 laser system was used in this study. The microbiopsy device fabrication was carried out as per protocol described in Section 2.1. Two microbiopsies were collected from each treatment group after being treated for two hours. Microbiopsy tissue collection was performed as per protocol described in Section 2.2.2 except that samples were immersed in Hank's Balanced Salt Solution (HBSS). Preparation of in-house HBSS was carried out as per protocol adopted from theLabRat.com website (<http://www.thelabrat.com/protocols/Hanks.shtml>). Microbiopsy sample was stored at 37°C water bath prior to fluorogenic probe labelling. No adverse effects were observed following microbiopsy application.

#### **6.2.5 Reactive Oxygen and Nitrogen species and Mitochondrial Superoxide assessment**

Samples were incubated in a water bath at 37°C throughout the entire staining process except during washing steps. Negative control samples were obtained from tape-stripped and intact, untreated sites. Negative control samples were incubated in 8-well chamber slides (Nunc™ Lab-Tek™ II Chambered Coverglass, Thermo Fisher Scientific Inc,

Australia, #155409) containing 300 µl HBSS and maintained at 37°C throughout the staining process. Positive control samples were obtained from the same areas but were subjected to 60 minutes of incubation with 200 µM Luperox® TBH70X (Sigma-Aldrich, USA, #458139) prior to fluorogenic probe labelling. *tert*-Butyl hydroperoxide (*t*BHP) solution was used to induce oxidative stress and reactive oxygen species (ROS). *t*BHP solution was washed off twice with HBSS prior to labelling.

CellROX® Green reagent (Life Technologies, USA, #C10444) and MitoSOX™ Red mitochondrial superoxide indicator (Life Technologies, USA, #M36008) were used to assess the level of oxidative stress and superoxide in microbiopsy tissue samples. CellROX® is a live cell dye that measures ROS in the nucleus and mitochondria. MitoSOX™ is another live cell dye that measures superoxide only in the mitochondria. Staining was carried out in 8-well chamber slides according to manufacturer's instructions. The cell nuclei were counterstained with 10 mg/ml Hoechst 33342 trihydrochloride, trihydrate (Life Technologies, USA, #H3570) at 1:1000 dilution for 10 minutes.

### **6.2.6 Confocal Microscopy**

The microbiopsy cutting die was opened up using clean sharp tip forceps (ProSciTech Pty Ltd, Australia) prior to imaging. A separate pair of forceps was used to handle cutting die containing ZnO treated tissue sample to prevent cross contamination. Confocal images of the tissue sample were obtained with a Zeiss 510 Meta confocal microscope (Carl Zeiss Microscopy GmbH, Germany). Excitation wavelength of 488 nm was used for both CellROX® and MitoSOX™ indicators. The confocal images were taken using an optical power of 25x, and a constant gain of 529 and 488 for CellROX® and MitoSOX™, respectively. The field of view for each confocal image was 359.3 µm x 359.3 µm. Stacks of confocal images at 5 µm-incremental steps were obtained for each sample. The number of steps acquired for each sample varied, depending on the thickness of the sample.

### **6.2.7 Image analysis and statistical analysis**

Fluorescence raw integrated density was acquired from each confocal image using ImageJ analysis software (National Institutes of Health, USA). The number of cell nuclei were counted based on Hoechst 33342 signal. The method of cell counting was performed as per procedure described in Section 4.2.3. Normalised fluorescence signal of CellROX® and MitoSOX™ was determined by calculating the raw integrated density per nuclei.



Statistical analysis was performed using one-way ANOVA with Tukey's multiple comparison test (GraphPad Prism 6, Graphpad Software Inc., USA). Paired two-tailed *t*-test was used to determine the significant difference between tape-stripped and intact skin.

### 6.3 Results and Discussion

Stratum corneum removal resulted in increased water loss through the skin. Therefore, TEWL was used to assess barrier integrity post tape-stripping. The average TEWL reading of intact skin based on single measurement from six volunteers was  $5.4 \pm 1.3$  g/m<sup>2</sup>h. Tape-stripped sites had significantly higher average TEWL reading of  $22.5 \pm 4.7$  g/m<sup>2</sup>h compared to the intact skin ( $p \leq 0.0001$ ). Following TEWL acquisition, the skin (in both intact and disrupted states) was either treated with CCT, ZnO-NP in CCT or left untreated for two hours. The treatment area was then untouched until microbiopsy sampling (**Figure 6.1**).

The microbiopsied samples were stained and the level of fluorescence produced by the oxidation of the cell permeable dyes was measured. The overall level of reactive oxygen and nitrogen species resulted in no obvious visual difference between intact and tape-stripped skin (**Figure 6.2a & 6.2b**, respectively). Both groups of untreated skin resulted in negligible oxidative stress signals. In contrast, the *t*BHP positive controls generated relatively high oxidative stress signal. ZnO-NP and CCT treatment resulted in comparable signals to the untreated skin. The same trends were observed following mitochondrial superoxide analysis (intact – **Figure 6.3a**, tape-stripped – **Figure 6.3b**).

The normalised fluorescence signal was then measured by dividing the level of integrated density per nuclei in each microbiopsy sample. Higher oxidative stress was correlated with higher levels of normalised fluorescence signal in the sample. The fluorescence signals from positive and untreated controls were compared in both assays.

Microbiopsy sample from *t*BHP treated intact skin had fluorescence signal with a significant 2.1-fold ( $p \leq 0.01$ ) increase compared to the untreated intact skin. Likewise, tape-stripped skin treated with *t*BHP also had a significant increase (2.5-fold) in fluorescence signal compared to untreated tape-stripped skin (**Figure 6.4a**). Overall, the positive control (*t*BHP) resulted in significantly higher signal than all other groups of intact skin ( $p = 0.0026$ ,  $p = 0.0014$  and  $p = 0.0007$ , respectively). Tape-stripped skin treated with *t*BHP followed the same trend ( $p = 0.0010$ ,  $p = 0.0027$  and  $p = 0.0023$ , respectively).

Similar observations were seen in the mitochondrial superoxide assay where both the *t*BHP treated samples were significantly higher than untreated samples taken from intact

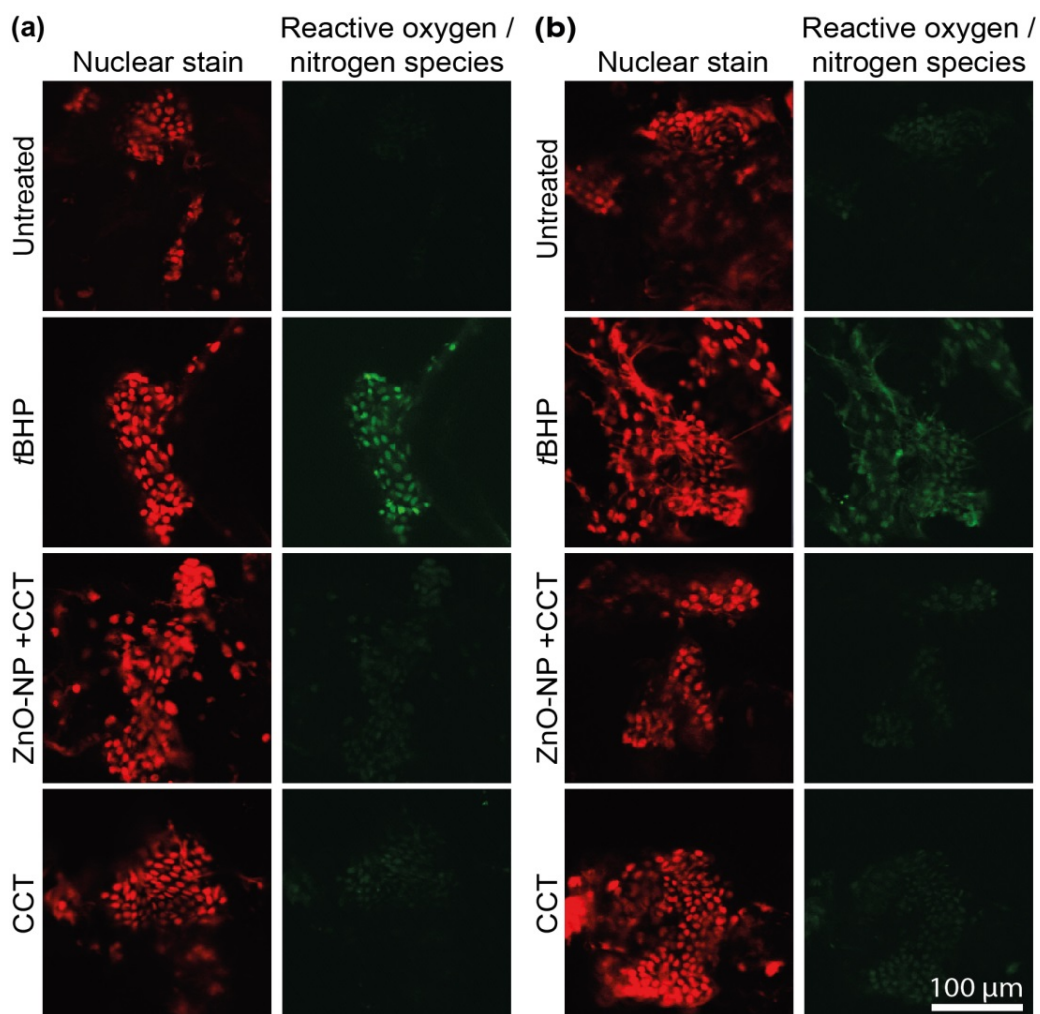


**Figure 6.2: Confocal microscopy images of microbiopsies.**

Reactive oxygen and nitrogen species assay on intact skin (n=6) (a). Reactive oxygen and nitrogen species assay on tape-stripped skin (n=6) (b). Degree of oxidative stress corresponds to intensity of fluorescent signal (green). Cell nucleus counterstained with Hoechst 33342 (red).

and tape-stripped skin (2.0- and 2.3-fold increase) (**Figure 6.4b**). The positive control resulted in significantly higher signal than untreated, ZnO-NP and buffer (CCT) in intact skin ( $p = 0.0051$ ,  $p = 0.0063$  and  $p = 0.0006$ , respectively). Tape-stripped skin, once again, followed the same trend ( $p < 0.0001$ ,  $p = 0.0001$  and  $p < 0.0001$ , respectively).

There was no difference in fluorescence signal from untreated and ZnO-NP treated samples taken from both intact and tape-stripped skin. The relative difference in reactive oxygen and nitrogen species analysis in ZnO-NP treated samples compared to untreated samples from intact skin was 0.9-fold and for tape-stripped skin 1.1-fold. A similar outcome

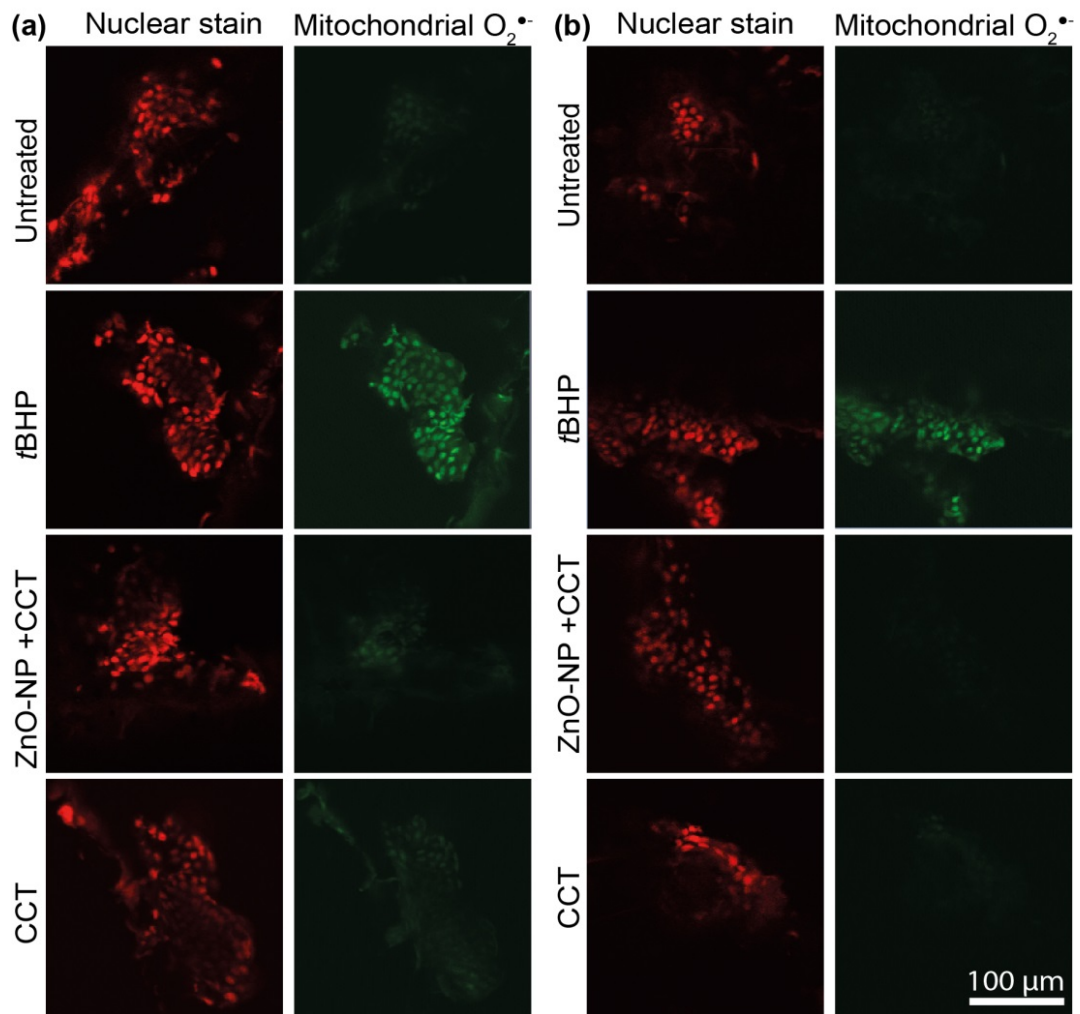


**Figure 6.3: Confocal microscopy images of microbiopsies.**

Mitochondrial superoxide assay on intact skin (n=6) (a). Mitochondrial superoxide assay on tape-stripped skin (n=6) (b). Degree of oxidative stress corresponds to intensity of fluorescent signal (green). Cell nucleus counterstained with Hoechst 33342 (red).

was observed in the mitochondrial superoxide assay, where a 1.0- and 1.2-fold change for intact and tape-stripped skin, respectively, was noted (**Figure 6.4b**).

When compared to the positive control, the intact skin treated with ZnO-NP produced reactive oxygen and nitrogen species and mitochondrial superoxide signal that was significantly lower ( $p \leq 0.01$ ) (2.3- and 2.0-fold decrease) (**Figure 6.4**). Similarly, ZnO-NP treated tape-stripped skin resulted in signal significantly lower ( $p \leq 0.001$ ) than tBHP treated tape-stripped skin for both assays (2.2- and 2.0-fold decrease, respectively).

Finally, ZnO-NP and CCT treatment were compared in terms of induced oxidative stress in both intact and tape-stripped skin. No significant differences were seen in either the reactive oxygen and nitrogen species or the mitochondrial superoxide signals (**Figure 6.4**). CCT treated intact and tape-stripped skin produced fluorescence signals that were also significantly lower than tBHP treated skin ( $p \leq 0.001$  and  $p \leq 0.0001$ , respectively).

There were a few major trends observed from the results of this study. Firstly, comparisons between the controls for the intact and the tape-stripped groups showed no significant difference in the oxidative stress. The results suggested that neither tape-stripping nor nanoparticle treatment on barrier disrupted skin induced detectable levels of oxidative stress. Secondly, the oxidative stress induced fluorescence signals were not significantly different to each other when treated with either ZnO-NP or CCT in both intact and tape-stripped skin. Thirdly, tBHP treatment resulted in signal that was significantly greater than ZnO-NP and CCT treated groups. Finally, increase in oxidative stress was not observed with ZnO-NP treatment.

The potential of ZnO-NP to induce cytotoxicity have been shown repeatedly in many *in vitro* studies. The most well-known mechanism is caused by the imbalance between the formation of ROS and the antioxidant radical quenching, leading to oxidative stress in cells. Quantifying this dynamic status is extremely challenging and dependent on a complex environment with multiple confounding factors. However, it is an important area with ROS affecting a range of biological processes including cellular viability, cellular growth and proliferation, tissue repair and regeneration, inflammatory and immune processes, and the regulation of various haemodynamic and haemostatic forces.

Sharma et al. (2009) demonstrated that human epidermal cells went through significant oxidative stress after the cells were treated with 0.8 µg/ml of ZnO-NP for 6 hours (Sharma et al., 2009). They reported indications of oxidative stress from the cells by monitoring levels of oxidative stress related markers. The concentration of ZnO-NP passing through the skin barrier and into the viable epidermis can vary. Tape-stripping did not induce an increase in oxidative stress in this study despite any potential increase in the number of nanoparticles interacting with keratinocytes. Therefore, it might not be completely relevant to compare the outcome from an *in vivo* study to an *in vitro* study.

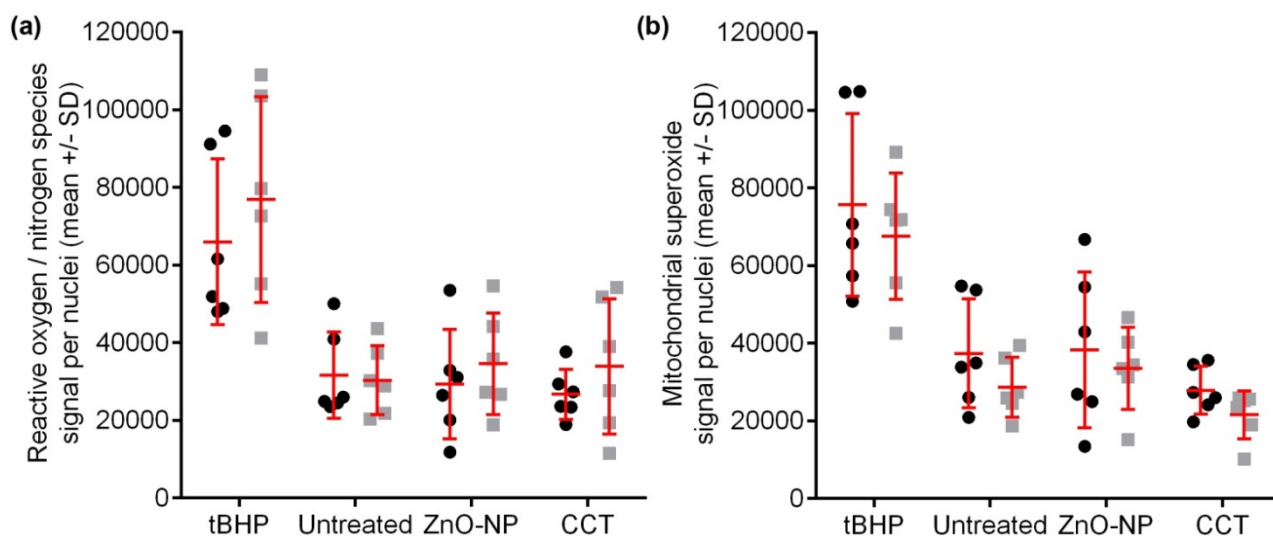


**Figure 6.4: Analysis of oxidative stress in volunteers of cells exposed to topical application of ZnO-NPs.**

Raw integrated density of fluorescence per nuclei in intact skin (n=6) and tape-stripped skin (n=6) (a). No significant differences were observed between the treatment groups, excluding the tBHP treatment group. Raw integrated density of fluorescence from the microchondrial superoxide probe per nuclei in intact and tape-stripped skin (b). No significant differences were observed between the treatment groups examined, with the exception of tBHP treatment. Intact and tape-stripped skin are represented by black closed circle and grey closed square, respectively.

There were a few groups who studied the impact of ZnO-NP exposure on metabolic changes in the skin. One of the studies also investigated changes in nicotinamide adenine dinucleotide phosphate (NAD(P)H) levels using fluorescence lifetime imaging microscopy (FLIM) (Leite-Silva et al., 2013) established in our lab. FLIM is a non-invasive technique facilitating real-time investigation of metabolic and oxidative state of the cell (Labouta et al., 2011, Lin et al., 2011). Leite-Silva et al. (2013) were studying the effects of coated and uncoated ZnO-NP of different formulations on penetration into the viable epidermis in human volunteers. The study also employed a similar treatment dosage at 2 mg/cm<sup>2</sup> but for a longer treatment time of 6 hours. They found limited penetration of both coated and uncoated ZnO-NP into stratum granulosum through the skin furrows. Yet, no signs of metabolic or morphological changes to the keratinocytes were detected (Leite-Silva et al., 2013). The method that Leite-Silva et al. (2013) employed was slightly different from what was done in this volunteer study. However, the outcome and interpretations from both studies were consistent and support the hypothesis that ZnO-NP do not induce cell toxicity

in an *in vivo* environment. The outcome from both studies suggests extrapolation of *in vitro* cell line based outcomes should not be the sole basis for cytotoxicity regulatory decisions. Overall, there is little doubt that the gold standard for assessment of topical formulations should be investigated in *in vivo* using human volunteers.

Considering that it is the skin barrier properties that protect the viable cells from any toxic nanoparticle effects, one can postulate that the cells will be susceptible to these effects once the barrier is compromised. In the volunteer study, stripping was performed to remove the stratum corneum and expose cells within the viable epidermis to ZnO-NP. The thickness of stratum corneum varies among individuals and body-site. Therefore, TEWL was used to assure all subjects had similar levels of skin barrier disruption.

It was also assessed if tape-stripping and ZnO-NP can together increases oxidative stress. The average fluorescence signals for both groups did not differ significantly in both assays. This suggested that either the cells within the viable epidermis tolerate well to the oxidative insult or there was no insult to begin with. One may also postulate that despite removal of stratum corneum through tape-stripping, the viable epidermis remains an effective barrier. The outcome of this study correlated with the findings that was published previously (Lin et al., 2011). The study in 2011 was investigating the effect of ZnO-NP on changes in level of NAD(P)H in intact and barrier disrupted skin in volunteers. The detectable concentrations of ZnO-NP in the stratum corneum of intact and tape-stripped skin after 4 hours were  $5.16 \pm 3.85$  mg/ml and  $34.03 \pm 15.13$  mg/ml, respectively. A significant increase of NAD(P)H/keratin signal in the ZnO-NP treated viable epidermis of tape-stripped skin when compared to vehicle-only treated skin was reported in the study. However, there was no enhanced penetration or significant ZnO-NP signal within detectable limits in the viable epidermis of tape-stripped skin treated with ZnO-NP.

## 6.4 Conclusions

In summary, viable skin tissue were extracted using the microbiopsy device to perform live cell assays for detection of oxidative stress in volunteers. There was no observable increase in fluorescence level when tape-stripping was applied to the skin. There was no evidence from the study that oxidative stress was induced in skin treated with ZnO-NP when compared to untreated tissue in both intact and barrier disrupted skin. The findings showed that barrier disruption followed by ZnO-NP exposure did not result in an observable increase in oxidative stress. The outcome of these experiments supported previously published results that ZnO-NP did not cause any metabolic changes to viable cells. This Chapter illustrated the potential of using the microbiopsy device as a novel approach to assess viable tissue for live cells assay. In the following Chapter, empirical applications of the microbiopsy as a future molecular diagnostic tool are described.



## Chapter 7

### ***The feasibility of advanced analytical platforms for molecular analysis***

#### **7.1 Introduction**

Since a decade ago, there has been increasing interest in personalised human genome sequencing to acquire information that can predict disease and provide tailored treatment for individuals. The advancement of computational and sequencing technologies has resulted in the falling price per genome sequencing from billions to thousands. The cost of personal genomic sequencing is anticipated to drop even further in the near future (Mattick et al., 2014). In parallel, the emerging field of proteomics and commercially available high throughput technologies has provided powerful tools to study diseases. These new technologies are becoming common place in research and sampling plays a crucial role. In this Chapter, the focus was to explore the possibility of using the microbiopsy samples in different omics technologies with the aims being:

- AIM 1** Tandem mass spectrometry (MS/MS) identification of selected cytokines of microbiopsy samples
- AIM 2** Gene expression profiling of single microbiopsy using direct digital detection technology platform
- AIM 3** Generation of indexed cDNA library from microbiopsy samples using SMARTer® Stranded RNA-Seq Kit

One of the exploratory omics technologies was proteomic characterisation of microbiopsy skin samples using mass spectrometry. Conventional liquid chromatography-tandem mass spectrometry (LC-MS/MS) offers better analytical specificity for low molecular weight analytes than immunoassays (Grebe and Singh, 2011). Despite that, conventional LC-MS/MS approaches are limited by detection sensitivity and sample throughput (Grebe and Singh, 2011). This limitation has led to many peptides remaining unidentified with this technology.

The targeted MS approach was developed to overcome these sampling limitations and facilitate the identification of peptides, proteins and/or post-translational modifications (Gillette and Carr, 2013). The development of triple quadrupole has permitted targeted MS analysis. The mass spectrometers commonly used in current clinical practice are mostly single- or triple-quadrupole mass filter spectrometers coupled with liquid chromatography (LC). A quadrupole is a set of four electrodes that are electrically connected in opposite pairs and applied with a constant (DC) voltage and an alternating (AC) voltage to create alternating electric field. The alternating electric field filters ions of specified size as they maintain constant drift and transit across the field without colliding with the electrode (Burns et al., 2005).

Triple quadrupole mass spectrometer (QqQ) is a form of MS/MS method. Small molecules, peptides or metabolites known as analytes are commonly analysed in clinical proteomics research using the MS/MS approach. Clinical proteomics research uses targeted MS approaches to facilitate diagnosis for early detection of disease, determine prognosis, direct therapy, or monitor disease activities.

In both conventional and targeted MS approaches, analytes are converted to gas-phase ions by an ionization source. Ionized peptides are then filtered by their mass and fragmented (Q2) by inducing collisional excitation of the ions with a neutral gas. Fragmented ions are passed through another mass analyser and scanned. The identity of the peptide is established by parent and fragment masses. The amino acid sequences are derived from tandem mass spectra, and peptide identification is performed through database search engines (Gillette and Carr, 2013). **Figure 7.1** compares conventional and targeted MS. The targeted MS method provides absolute structural specificity of selected analytes. Relative or absolute quantification of the analytes can also be established with isotopically-labelled internal standards of known quantities.

Proteomic profiling for identification of peptides may be limited with small samples as amplification could not be performed to increase detection signals. Direct digital detection is a cutting edge technology to detect molecules without the need to convert or amplify the targets. The molecular targets developed for their analysis platform were identified in discovery experiments using new-generation sequencing (NGS) approach. **Figure 7.2** illustrates the overview of the technology process.

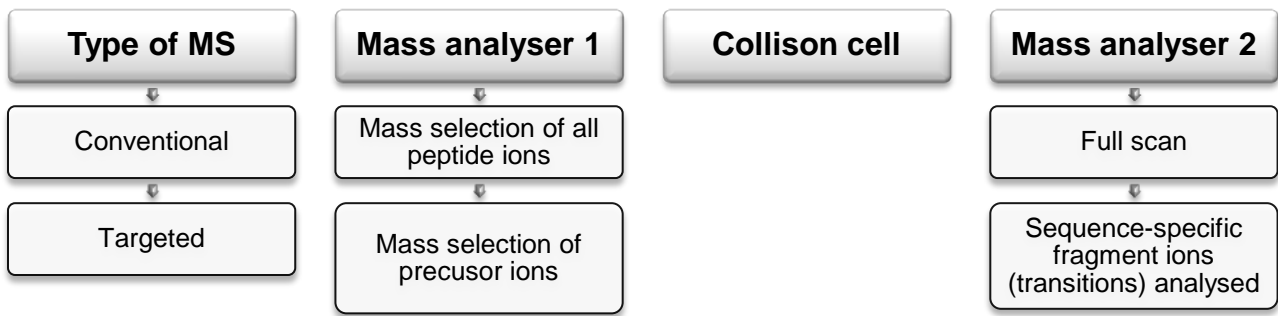


**Figure 7.1: Comparison of conventional and targeted MS.**

Flow chart illustrates the differences between conventional data-dependent and targeted MS. The process differences between the two approaches happen in the second mass analyser. In targeted MS, only ions of interest which is also known as precursor ions are filtered and analysed in Q1. Post fragmentation, sequence-specific fragment ions (transitions) are filtered and analysed in Q3.

This technology was first introduced in 2008 (Geiss et al., 2008). The authors reported that direct gene expression profiling could be achieved without enzymatic reactions or bias, which are common in existing gene expression technologies. A seven position and a four color barcode system was established that could create a max of 16,384 different barcodes unique to individual mRNA targets. Each unique seven dye-coupled RNA segment corresponded to a single code. The reporter probe consisted of a gene-specific sequence and a unique RNA segment that was ligated to the backbone. The capture probe was a ligated product containing a unique sequence-specific oligonucleotide for each gene and a biotinylated universal sequence. Purification of the hybridised probe-target complex was performed using magnetic beads and excess probes were removed to prevent binding and imaging interference. Sample processing steps post hybridisation were handled by a liquid-handling robot (nCounter® Prep Station). Automated imaging and data collection was done by the Digital Analyzer. Approximately 10 mm<sup>2</sup> of the binding surface for each sample, which corresponded to 600 fields-of-view was imaged at a resolution of 1376 x 1024 pixels.

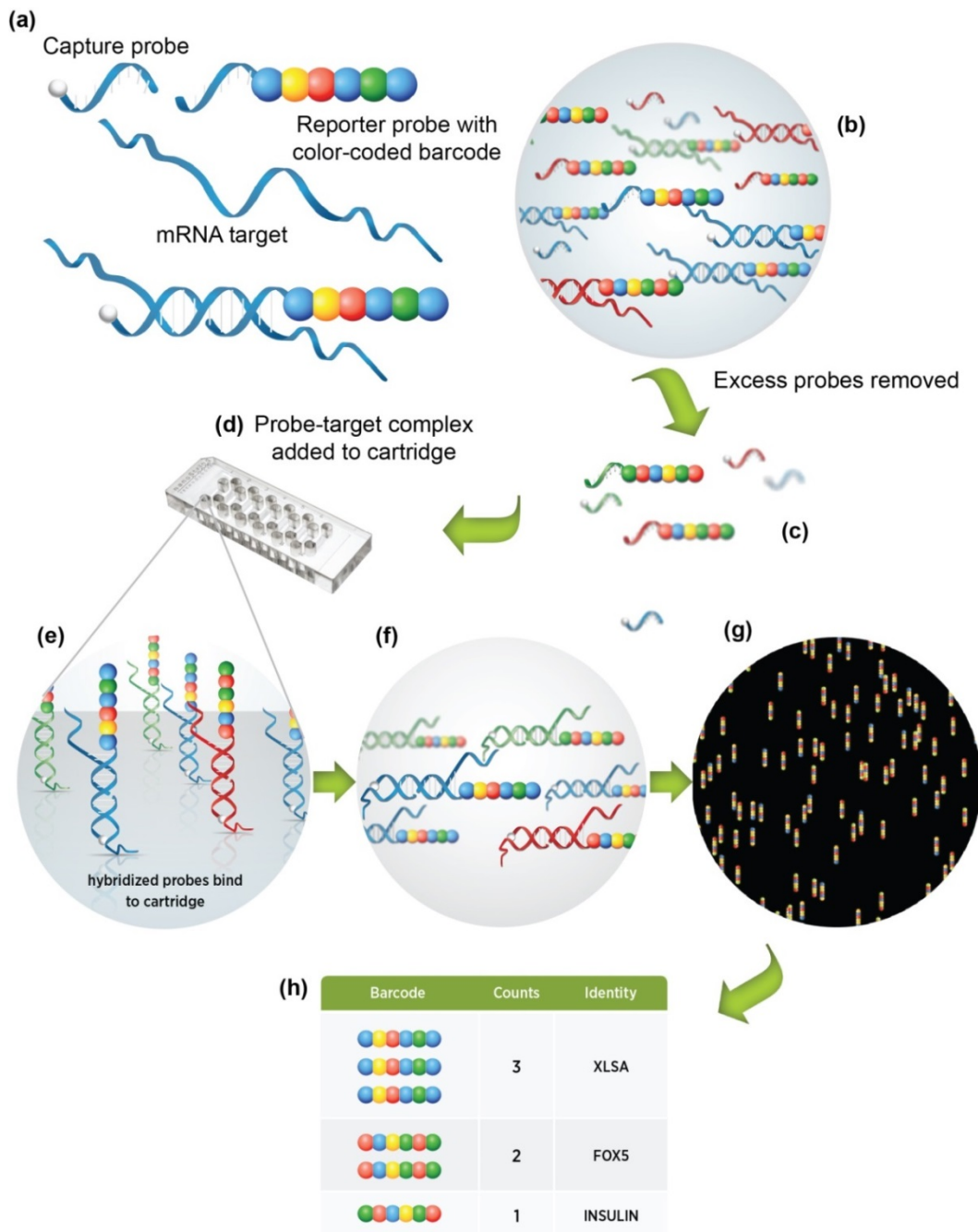


**Figure 7.2: Schematic of digital mRNA profiling technology.**

Total mRNA is mixed with capture and reporter probes that carry color-coded barcode unique to a single target molecule (a). The probes hybridised directly to a molecular target in solution (b). Excess probes are removed (c) and the probe-target complex is added to the cartridge using the automated sample processing station (d). The hybridised complexes are bound (e) and immobilised (f) on the cartridge. The immobilised complexes are aligned on the cartridge as illustrated by the false-color image (g). The cartridge is transferred to the digital analyser for barcode counting and data organisation (h). Figure modified with permission from (NanoString Technologies, 2014) Copyright 2014, Nanostring Technologies, Inc. All rights reserved.

They compared the nCounter® results to microarrays (Affymetrix U133Plus2 array) and quantitative reverse-transcriptase PCR (qRT-PCR) of the MAQC gene set results. They detected 17 to 35 more genes with their technology compared to the microarrays when identical non-amplified sample input was used. The nCounter® analysis system was reported as a sensitive and reproducible technology, which had a 0.1 - 0.5 fM detection limit and achieved an average correlation coefficient ( $R^2$ ) of 0.999. The nCounter® system showed good correlation with both microarray ( $R^2 = 0.79$ ) and qRT-PCR ( $R^2 = 0.95$ ), and was more sensitive than the microarrays but had similar accuracy and sensitivity to qRT-PCR (Geiss et al., 2008).

Geiss et al (2008) highlighted four advantages of their nCounter® technology over microarrays and qRT-PCR. The four advantages being: 1) direct quantification without gene-specific or 3' biases given that no amplification of sample was required; 2) higher sensitivity with lower amounts of sample input when compared to the microarrays; 3) digital readout of mRNA transcript counts showed less background noise and provided more definite downstream analysis, and finally 4) less time, effort and sample requirement was needed for the nCounter® system (Geiss et al., 2008).

Moving forward with the micro-device validation, the focus of this Chapter was to explore the feasibility of molecular analysis using advanced analytical platforms. The protein content was determined and cytokine of interest was identified using state-of-the-art tandem mass spectrometry. The relative quantification of microbiopsy samples using quantitative reverse-transcriptase PCR and digital gene expression profiling using a 48-MAQC human gene set was also examined. Finally, cDNA library preparation from microbiopsy samples for future discovery experiments using new-generation sequencing technology was also explored.

## **7.2 Materials and Methods**

### **7.2.1 Protein extraction from microbiopsy sample**

Microbiopsy sample collection from a volunteer was performed according to protocol described in Section 2.1.6. Up to ten microbiopsies were collected from the volar forearm of a volunteer. Each microbiopsy was opened up and tissue sample was removed from the chamber using a disposable 30-gauge syringe needle. This procedure was done under a Stemi 2000C stereo microscope (Carl Zeiss Microscopy GmbH, Germany). Microbiopsy tissue samples were pooled into a nuclease-free 1.5 ml microcentrifuge tube containing 100 µl of in-house RIPA buffer (50 mM Tris pH 7.5, 1% Triton X-100, 0.5% deoxycholate, 0.1% sodium dodecyl sulphate, 150 mM sodium chloride, 10 mM sodium fluoride, 1x protease inhibitors, 0.5 mM 4- benzenesulfonyl fluoride hydrochloride, 1 mM sodium pyrophosphate, 0.5 mM sodium vanadate) provided by the TRI Proteomics Core Facility. The microbiopsy tissue samples together with the RIPA buffer were kept on ice throughout the extraction process. The pooled samples were incubated in the RIPA buffer for 30 minutes to no more than an hour. The tissue samples were disrupted by passing the samples through a 100-µl pipette tip. The tissue samples were then subjected to sonication to lyse the samples further. The samples was put into the FXP10MH Sonicator (Unisonics Australia, Australia) for 1 minute and cooled on ice. This sonication step was repeated after the sample was chilled and until the sample was lysed completely. The sample was centrifuged at 16,873 x g (maximum speed) for 5 minutes at 4°C. The supernatant containing the extracted proteins was collected without disrupting the pellet.

### **7.2.2 Protein extraction from COS cells**

Adherent monkey kidney tissue derived COS cells were rinsed with sterile phosphate buffered saline (PBS). The cells were detached using 0.5% trypsin at 37°C for 5 minutes. Fresh Gibco® RPMI medium (Life Technologies, USA, #11875-093) was added to further detach adhering cells. Equal volume of 0.4% Trypan Blue (Life Technologies, USA, #15250061) was mixed into 20 µl of suspension cells for cell counting. Ten-fold serial dilution was performed, and cells were pelleted for protein extraction using 100 µl of RIPA buffer.

### **7.2.3 Protein quantification**

The quantity of protein in the pooled microbiopsy sample was determined using Pierce Micro BCA Protein Assay Kit (Thermo Fisher Scientific Inc., Australia, #23235). Protein standards (BSA) and working reagents were prepared according to the manufacturer's instructions. Microplate procedure was followed to determine the concentration of the extracted proteins from microbiopsy tissue samples.

### **7.2.4 Protein separation using polyacrylamide gel electrophoresis (SDS-PAGE)**

The SDS-PAGE acrylamide gel was made up of 4% stacking gel and 10% resolving gel. The gels were prepared according to the in-house recipe provided by the TRI Proteomic Core Facility. The gel was run with 1 x SFS running buffer (provided by the facility) at 150 W for one hour. The Precision Plus Protein™ Dual Color Standards (Bio-Rad Laboratories, Inc., USA, #161-0374) was used to identify molecular mass of the targeted protein. The sample was premixed with 5 x SDS-Page sample buffer (10% SDS, 0.25 M dithiothreitol, 0.2 M Tris pH 6.8, 0.1% bromophenol blue, 50% glycerol). Two separate SDS-PAGE gels were processed. Approximately 30 – 40 µl of the sample was run for an extended period to achieve a better separation of the protein. The remaining 45 µl of the sample was used to run a short 8 mm gel that was subsequently processed for mass spectrometry analysis. Triple quadrupole (QqQ) hybrid liquid chromatography mass spectrometry (LC-MS) was performed by the facility to identify a specific range of peptides in skin tissue. Mass spectrometry data was generated and analysed by the facility.

### **7.2.5 Quantitative reverse-transcriptase PCR (qRT-PCR)**

Freshly excised healthy skin was collected and prepared according to procedure described in Section 2.1.5. The excised skin was cut into smaller pieces weighing approximately 25 mg each. The RNA from excised healthy skin was used as standard curves for two qRT-PCR experiments. Serial dilutions were performed to obtain varying concentrations for the standard curves.

In the first experiment, two sets of single microbiopsies, pooled of two and five samples (n=6) were collected from the volar forearm of a volunteer as per protocol described in Section 2.1.6. In the second experiment, two sets of microbiopsies from the normal skin and a raised melanocytic naevi located on the volunteer's forearm were collected. The volunteer was consented with written consent forms approved by the Metro South Human

Research Ethics Committee in Princess Alexandra Hospital (HREC/13/QPAH/551) and The University of Queensland Human Research Ethics Committee (Approval number: 2013001551).

The samples were processed for RNA as per protocol described in Sections 2.3.1 and 2.3.2. On-column Dnase digestion was incorporated in the isolation protocol using RNase-Free DNase Set (QIAGEN GmbH, Germany, #79254). The RNA samples from the excised skin samples were then quantified and assessed for quality as per protocol described in Sections 2.3.3 and 2.3.4. RNA from micro biopsy samples were not quantified with Qubit® assay but quality assessment was carried out together with the RNA samples from the excised skin. Four microliters from each micro biopsy samples were used for cDNA synthesis. Total RNA from the excised skin was included in the cDNA synthesis procedure as a no amplification control. First-strand cDNA was synthesized by reverse transcription using SensiFAST™ cDNA Synthesis Kit (Bioline, UK, #BIO-65053). A three- to five-points standard curve was prepared using cDNA from the excised skin. SYBR® Green-based (SensiFAST™ Probe No-ROX Kit, Bioline, UK, #BIO-86005) qRT-PCR was used to determine the quantity of micro biopsy samples in this experiment. PCR master mix was prepared according to supplied instructions. Forward and reverse primers were used in the PCR amplification of RPLPO housekeeping gene were: F-5'-ATCAACGGGTACAAACGAGTC-3' and R-5'-CAGATGGATCAGCCAAGAAGG-3' (Sigma-Aldrich,USA) (Minner and Poumay, 2009). Forward and reverse primers were used in the PCR amplification of tyrosinase gene were: F-5'- TCTTCTCCTCTTGGCAGATTGT-3' and R-5'-CAGTAAGTGGACTAGCAAATCCTTC-3' (Sigma-Aldrich,USA) (Gkalpakiotis et al., 2010). The PCR cycling conditions were set at 95°C for 2 minutes for initial denaturation, followed by a 40-cycled template denaturation at 95°C for 5 seconds, primer annealing at 60 - 65°C for 10 seconds and primer extension for 5 – 20 seconds at 72°C. qRT-PCR was performed in technical duplicates in both experiments. The result was analysed using Rotor-Gene 6000 Series Software 1.7 (Corbett Life Science, QIAGEN GmbH, Germany). Any sample that was not amplified properly during qRT-PCR was excluded from the analysis.

### **7.2.6 Gene expression analysis via nCounter® assay**

The recommended sample and starting material for this gene expression assay is 100 ng of total RNA. The aim of this experiment was to validate if unamplified micro biopsy RNA



samples and amplified cDNA sample (100 ng) using Whole Transcriptome Amplification kit could be used for nCounter® Customer Assay Evaluation (CAE) Kit (NanoString® Technologies Inc., USA, # GXA-CAE-12). The amplified cDNA sample used was generated from the previous experiment described in **Chapter 4, Figure 4.15**.

Two microbiopsy samples were obtained from a volunteer and incubated in 100 µl of Extraction Buffer from Arcturus® PicoPure® RNA Isolation kit (Life Technologies, USA, # KIT0204) for 30 mins at 42°C. Post incubation, the sample was kept on ice to prevent degradation of RNA samples. Unpurified RNA samples can be analysed using nCounter® assays as advised by the manufacturer. Given that RNA samples can be lost during the column purification, downstream processing using the Arcturus® PicoPure® RNA Isolation kit was not performed. Two to five microliters of each sample were used to quantify the concentration of cDNA and RNA samples using the Qubit® DNA BR and RNA BR assays (refer to Sections 2.2.3 and 2.3.3), respectively. Dilutions were made to each sample to make up 100 ng of starting material for the experiment. Further dilutions were made to diluted RNA samples to achieve 10 ng, 5 ng and 1 ng.

Overnight hybridisation of capture probes and reporter probes at 65°C were carried out according to manufacturer's instructions. The samples were then transferred to the nCounter® Prep Station where excess probes were removed and the probe/target complexes were aligned and attached to the nCounter® cartridge. This was an automated sample processing step by the Prep Station. Digital data were acquired by the nCounter® Digital Analyzer where 48 color-coded barcodes unique to their respective target molecule were counted and tabulated. The data was normalised by the positive controls included in the assay using nSolver Analysis software version 1.1 (NanoString® Technologies Inc., USA)

### **7.2.7 cDNA library preparation for Illumina® sequencing platforms**

Two pooled microbiopsy samples were collected from each volunteer (n=2). The volunteers were consented under the same Human Ethics Study as described in Section 7.2.4. Total RNA was isolated from the samples using Nucleospin RNA XS Kit (Macherey-Nagel GmbH & Co. KG, Germany, #740902.10) according to the manufacturer's instructions. Total RNA (7 ng) from a lesional sample with RNA Integrity Number (RIN) number of 8.5 was included in the experiment to compare the cDNA library of the

microbiopsy samples. Integrity and quality of the microbiopsy samples were analysed according to the protocol described in Section 2.3.4. However, the RIN number of the samples could not be determined. Therefore, the microbiopsy samples were treated as medium to low quality samples in this experiment. The Ribo-Zero Magnetic Kit (Epicentre®, USA, #MRZH116) was used to remove ribosomal RNA (rRNA) according to a modified protocol from Clontech Laboratories, Inc. The samples were first subjected to fragmentation and conversion to single-stranded cDNA. The samples were then purified using SPRI AMPure Beads and amplified into RNA-Seq libraries. The generated cDNA libraries were then purified and assessed for quality following Agilent's High Sensitivity DNA Kit's protocol (Agilent Technologies, USA, #5067-4626). The preparation of cDNA libraries were carried out according to the manufacturer's instructions.

## 7.3 Results and Discussion

### 7.3.1 Targeted mass spectrometry approach for peptide identification

Total protein was isolated independently from two individual microbiopsy samples in a preliminary experiment. One sample had approximately 1.45  $\mu\text{g}$  of total protein and the other was below the detection limit of the kit. A series of ten-fold serial dilutions ( $10^2$ ,  $10^3$ ,  $10^4$ ,  $10^5$ , and  $10^6$  cells) were included in the experiment to estimate the cell count obtained from a microbiopsy sample. It was calculated that the microbiopsy extracted approximately  $10^2$  to  $10^3$  cells from the tissue. The estimated cell count was slightly lower than what was observed in **Figure 4.4** of **Chapter 4**. However, this is of no surprise given that sample variation is common with microbiopsy sampling as observed in the volunteer studies (**Chapter 4**).

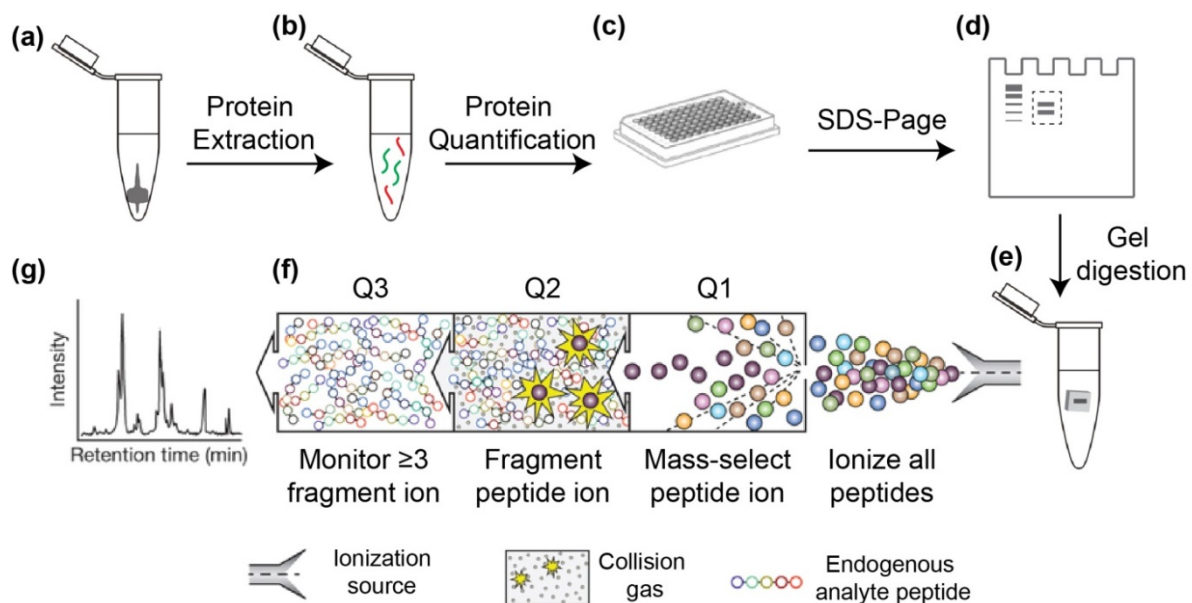


**Figure 7.3: Schematics of protein handling and analysis.**

Microbiopsy sample was collected in microcentrifuge tube containing in-house RIPA buffer (a). Total protein is isolated from microbiopsy samples (b) and quantified using microplate procedure of Pierce Micro BCA Protein Kit (c). The protein masses were separated using SDS-Page (d) and digested (e) for targeted tandem MS analysis (f). The MS spectra was analysed for identification and relative quantification of the cytokines (g). Figure modified with permission from (Gillette and Carr, 2013) Copyright 2013, Nature Publishing Group.

The identification of selected cytokines using the microbiopsy technology was performed for a collaborative project. The general work flow of this experiment is illustrated in **Figure 7.3**. The total protein was extracted from single, and pooling of two and five microbiopsy samples, respectively. Post protein quantification suggested insufficient protein for all three samples to perform downstream MS/MS analysis. The experiment was repeated with a pooled sample of ten microbiopsies. The total protein extracted was approximately 4 µg. Half of the total extracted protein sample was used for SDS-Page gel analyses and the other half was given to a proteomic core facility for tandem mass spectrometry analysis. A total of 27 cytokines were screened, and of which 22 were identified using 0.2 µg of total protein (**Table 9**). Relative quantification of six cytokines (CD56, CXCL2, CD11c, CD103, IL36g and Periostin) was performed (**Table 10**).

The mass-charge-ratio ( $m/z$ ) of the parent protein was analysed in Q1 while transitions were analysed in Q3. Ion with the highest intensity signal is known as the 'quantifier' while additional ions are known as qualifier. Compound identification was calculated based on the quantifier/qualifier ratio. The 'area' represents the signal intensity of the fragment ions. **Table 10** shows the list of peptides that were semi-quantitated using the parent mass. Comparison in relative quantity of identified cytokines within the sample was limited by the lack of isotopically-labelled internal standards of known quantities. Precision and confidence in peptide identification were confounded as a consequence of the absence of internal standards. This preliminary analysis supported the possibility of microbiopsy samples for screening of relevant proteomic biomarkers for skin diseases.

**Table 9: List of proteins detected from a pooled microbiopsy sample.**

<b>Accession number</b>	<b>Protein name</b>	<b>Gene name</b>
<b>P38570</b>	Integrin alpha-E (CD103)	ITGAE
<b>A2VCQ7</b>	EGFR protein	EGFR
<b>P01579</b>	Interferon gamma (IFN-g)	IFNG
<b>P01584</b>	Interleukin-1 beta (IL1B)	IL1B
<b>P01730</b>	T-cell surface glycoprotein (CD4)	CD4
<b>P05231</b>	Interleukin-6 (IL6)	IL6
<b>P08571</b>	Monocyte differentiation antigen CD14 (CD14)	CD14
<b>P08575</b>	Receptor-type tyrosine-protein phosphatase C	PTPRC
<b>P09693</b>	T-cell surface glycoprotein CD3 gamma chain (CD3)	CD3G
<b>P10966</b>	T-cell surface glycoprotein CD8 beta chain (CD8)	CD8B
<b>P11215</b>	Integrin alpha-M (CD11b)	ITGAM
<b>P11836</b>	B-lymphocyte antigen CD20 (CD20)	MS4A1
<b>P13591</b>	Neural cell adhesion molecule 1 (CD56)	NCAM1
<b>P19875</b>	C-X-C motif chemokine 2 (CXCL2)	CXCL2
<b>P20702</b>	Integrin alpha-X (CD11c)	ITGAX
<b>P51671</b>	Eotaxin	CCL11
<b>P59665</b>	Neutrophil defensin 1	DEFA1
<b>Q15063</b>	Periostin	POSTN
<b>Q6UZ82</b>	Monocyte chemoattractant protein-1	MCP1
<b>Q9NZH8</b>	Interleukin-36 gamma (IL36g)	IL36G
<b>Q9UBH0</b>	Interleukin-36 receptor antagonist protein (IL36Ra)	IL36RN
<b>Q9UJ71</b>	C-type lectin domain family 4 member K (CD207)	CD207

**Table 10: Relative quantification of identified peptides.**

Protein name	Peptide	Q1 m/z	Quantifier		Qualifier	
			Q3 m/z	Area	Q3 m/z	Area
Neural cell adhesion molecule 1 (CD56)	GLGEISAASEFK	604.8	510.3	2722	470.3	1627
C-X-C motif chemokine 2 (CXCL2)	ATLSAAPSNPR	542.8	570.3	33860	515.3	19806
Integrin alpha-X (CD11c)	FGAALTVLGDVNGDK	738.9	1017.5	1015	773.5	809
Integrin alpha-E (CD103)	VQNITQVGSVTK	637.4	248.2	3577	228.1	1925
Interleukin-36 gamma (IL36g)	IMDLYGQPEPVKPFIFYR	738.4	245.1	11879	696.9	8167
Periostin	AAAITSDILEALGR	700.9	214.1	1531	1074.6	1391

### 7.3.2 High sensitivity total RNA quantification via qRT-PCR

Quantitative mRNA profiling of single cells has been established by a few groups (Stahlberg and Bengtsson, 2010, Bengtsson et al., 2008, Taniguchi et al., 2009). RNA quantification using Qubit® HS RNA assay had not been successful for every microbiopsy sample. Even though mRNA is only 1-3% of total RNA, an accurate estimation of sample quantity can be performed using tissue-specific housekeeping genes. RPLP0 was validated as one of the most stable housekeeping genes in keratinocytes, which is the most abundant cell type in skin (Minner and Poumay, 2009). Relative quantification of the microbiopsy samples was performed using standard curves with known quantities.

The integrity and quality of RNA for standard curves was 6.9 (RIN). The RIN of the microbiopsy samples ranged from 5.5 to 6.6 with an average of  $6.18 \pm 0.43$ . The calculated cDNA quantity per reaction by the software was comparable to the actual input of known quantities. The cDNA starting material for the standard curves were 25 ng, 2.5 ng and 0.25 ng, and the average calculated quantity were  $24.48 \pm 0.37$ ,  $2.62 \pm 0.37$  and  $0.25 \pm 0.02$  ng, respectively. The mRNA expression level of RPLP0 of the microbiopsy samples were within standard curves 2 and 3 (**Figure 7.4**). The average cDNA of single microbiopsies were  $0.73 \pm 0.58$  ng (n=2) and the two-pooled samples were  $0.61 \pm 0.31$  ng (n=2). The cDNA quantity of a five-pooled sample was  $2.07 \pm 0.18$  ng (n=1). The other pooled sample with five microbiopsies did not amplify properly during qRT-PCR and was excluded in the analysis. Calculations showed that average total RNA from single, two-

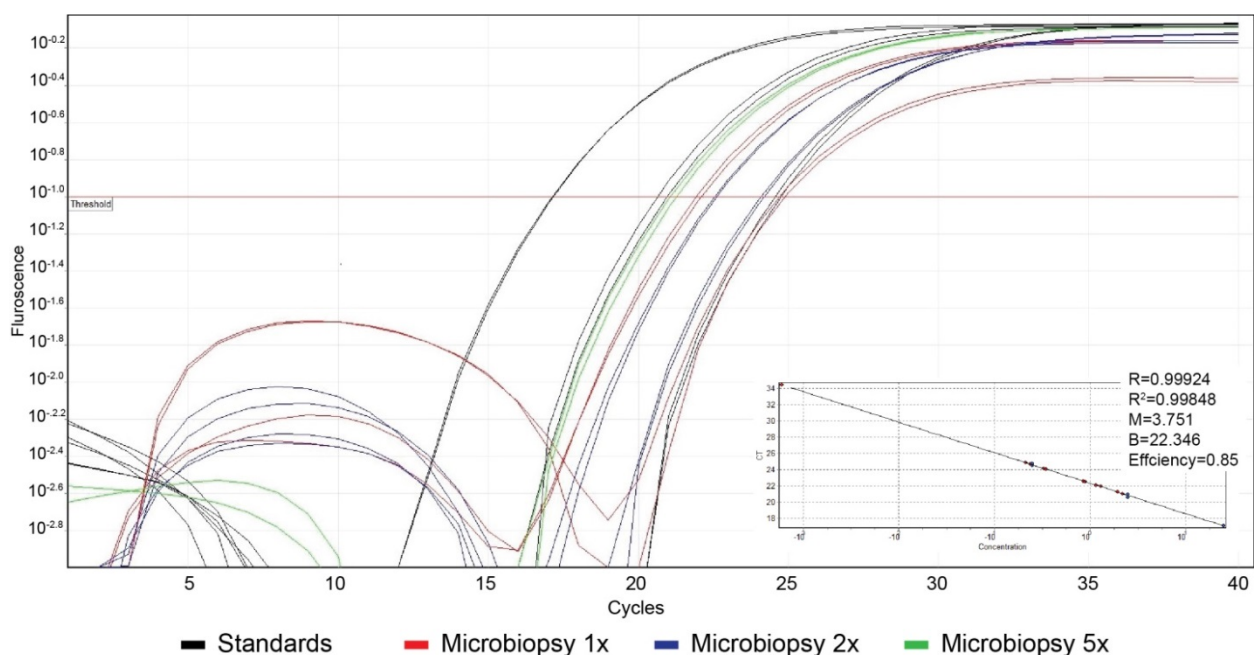


**Figure 7.4: Detection and quantification of RPLP0 in microbiopsies.**

Amplification plot shows three-point standard curves to quantify housekeeping RPLP0 gene in two sets of microbiopsy samples collected from normal skin area. The microbiopsy groups include single, pooled of two and five samples. The average fluorescence curve of the standards and the samples are represented in this plot. The inset on the bottom right shows the efficiency curve of the standards.

pooled and five-pooled microbiopsies were  $7.99 \pm 7.83$  ng,  $6.66 \pm 4.18$  ng and 22.8 ng, respectively. RNA from the single microbiopsy was within the range reported in **Chapter 4** while the average per microbiopsy for pooled samples was slightly lower ( $5.16 \pm 4.33$  ng).

The starting cDNA quantified by Qubit® were similar to the calculated quantity reported by the software. The mRNA expression level of RPLP0 of the microbiopsy samples ranged from 0.032 to 0.80 ng (**Figure 7.5**). The  $R^2$  and PCR efficiency were similar between both runs ( $R^2= 0.99924$  vs.  $0.99684$ , efficiency=  $0.85$  vs.  $0.81$ ). Total RNA from the raised melanocytic naevus ( $8.91 \pm 0.31$  ng) was higher than the normal skin region ( $1.41 \pm 0.08$  ng). Presence of tyrosinase was assessed to validate if melanocytes were contained in the microbiopsy samples. Positive tyrosinase was detected in the microbiopsy collected from the melanocytic naevus but not from the normal skin. This is plausible given that one can expect more melanocytes within a melanocytic naevus than in a non-melanocytic region. Complete data of the qRT-PCR experiments were reported in **Appendix 2**.

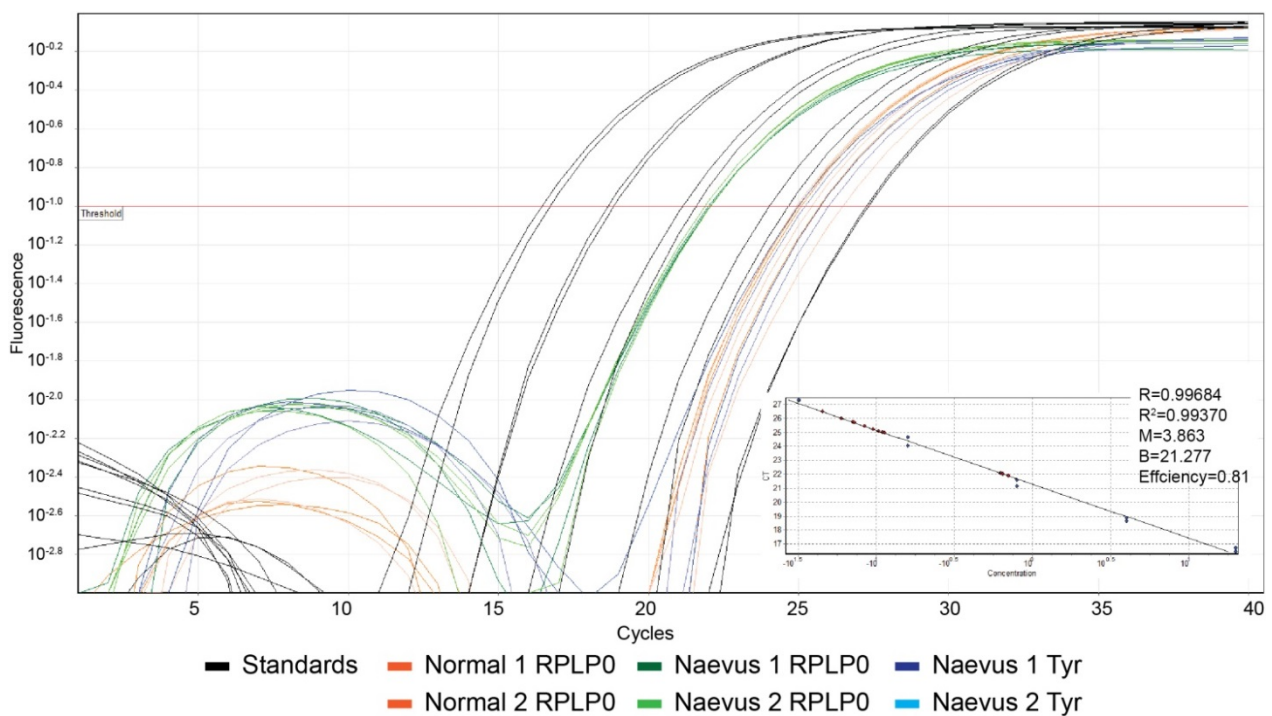


**Figure 7.5: Detection and quantification of RPLP0 and tyrosinase genes in microbiopsies.**

Amplification plot shows five-point standard curves to quantify housekeeping RPLP0 and tyrosinase genes in two sets of microbiopsy samples collected from normal skin area and a melanocytic naevi. The average fluorescence curve of the standards and the samples are represented in this plot. The inset on the bottom right shows the efficiency curve of the standards.



### 7.3.3 Detection limits of NanoString® technologies using microbiopsy samples

It was presented in a scientific report by Bhargava et al. that technical variations were observed in low input libraries regardless of the amplification methods (Bhargava et al., 2014). They reported a reduction in transcriptome coverage when the amount of sample was progressively reduced from 1 ng to 100 pg to 50 pg to 25 pg. It was anticipated that genes expressing low levels might be below detectable limit when amount of sample input was lower than recommended. In this experiment, the mRNA input was decreased to the range of a single microbiopsy sample size (1 to 10 ng). There were 42 out of 48 human

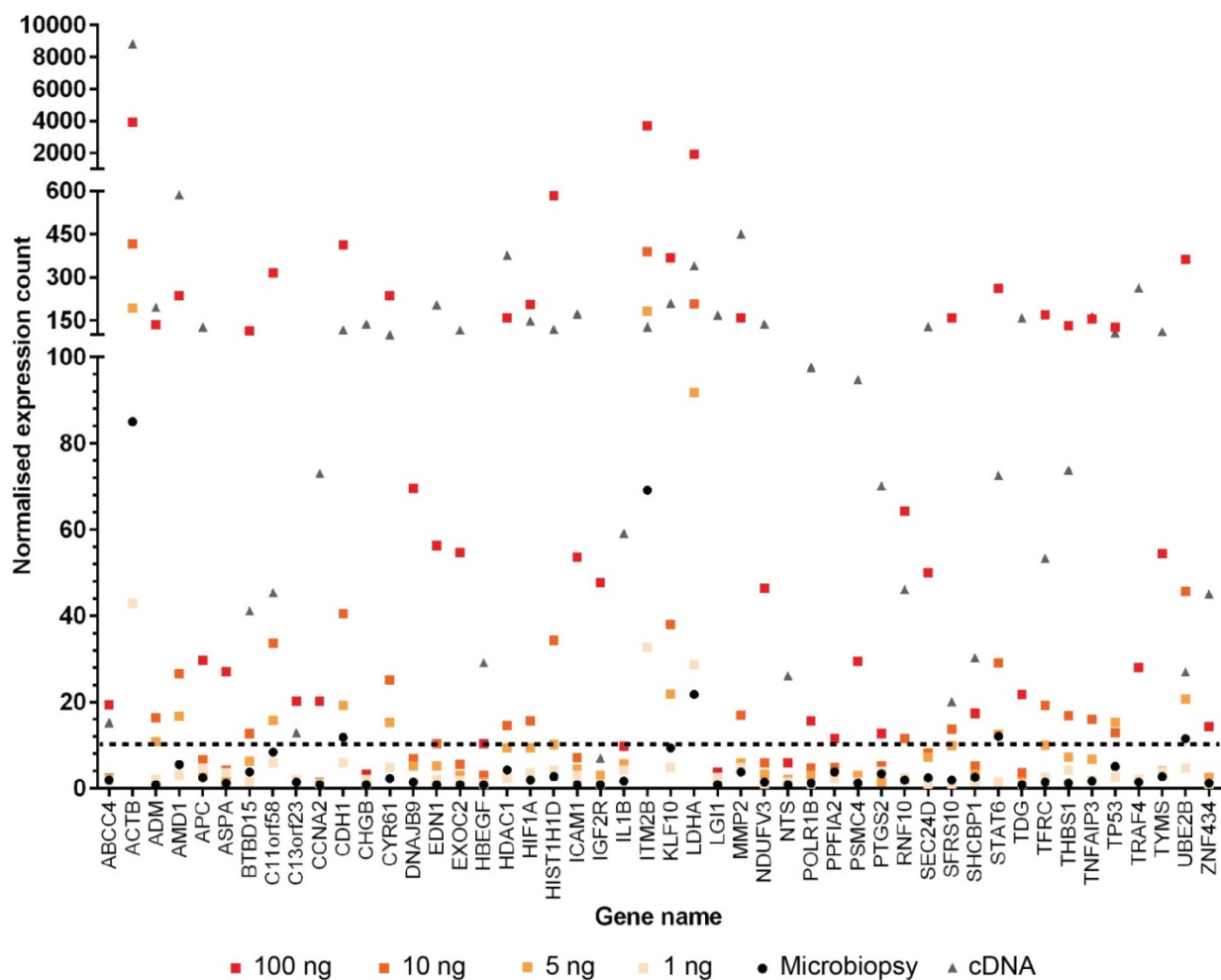


**Figure 7.6: Multiplex gene expression count using NanoString® technology.**

Digital counting of 48 human gene expression of each sample group (n=2) was acquired and tabulated. The raw count data was normalised with positive controls using nSolver software. The number of normalised count is shown on the y-axis and the name of genes that was evaluated is represented on the x-axis. The dotted black line represents the limit for detectable expression of gene.

MAQC genes (87.5%) that were above the detection threshold (black dotted line) when the recommended quantity of 100 ng of RNA was used (**Figure 7.6**). The number of detectable genes decreased from 42 to 22 (45.8%) to 10 (20.8%) when the samples were reduced from 100 ng to 10 ng to 5 ng. Only three out of 48 genes (6.25%) were detected in 1 ng and microbiopsy samples. Forty-seven genes (97.9%) were identified in the cDNA sample (100 ng) from a microbiopsy that was subjected to whole transcriptome amplification.

The MAQC genes were segregated into four different categories based on their expression profiles in 100 ng of mRNA (**Figure 7.7**). The number of gene expression counts decreased when the starting sample was reduced regardless of the expression profiles of the genes. These trends were consistent across genes that are highly expressed (**Figure 7.7a**), expressed in high to med (**Figure 7.7b**) and med to low (**Figure 7.7c**) levels. The expression counts were more variable in genes that were expressed in low levels across all samples (**Figure 7.7d**).

This experiment indicated that gene expression profiling of single, non-amplified microbiopsy samples was not feasible with NanoString® nCounter® gene expression assay. So to use this approach, additional microbiopsies would need to be pooled or amplified. The other option would be to use the single cell assay kit, which utilized an amplification step.

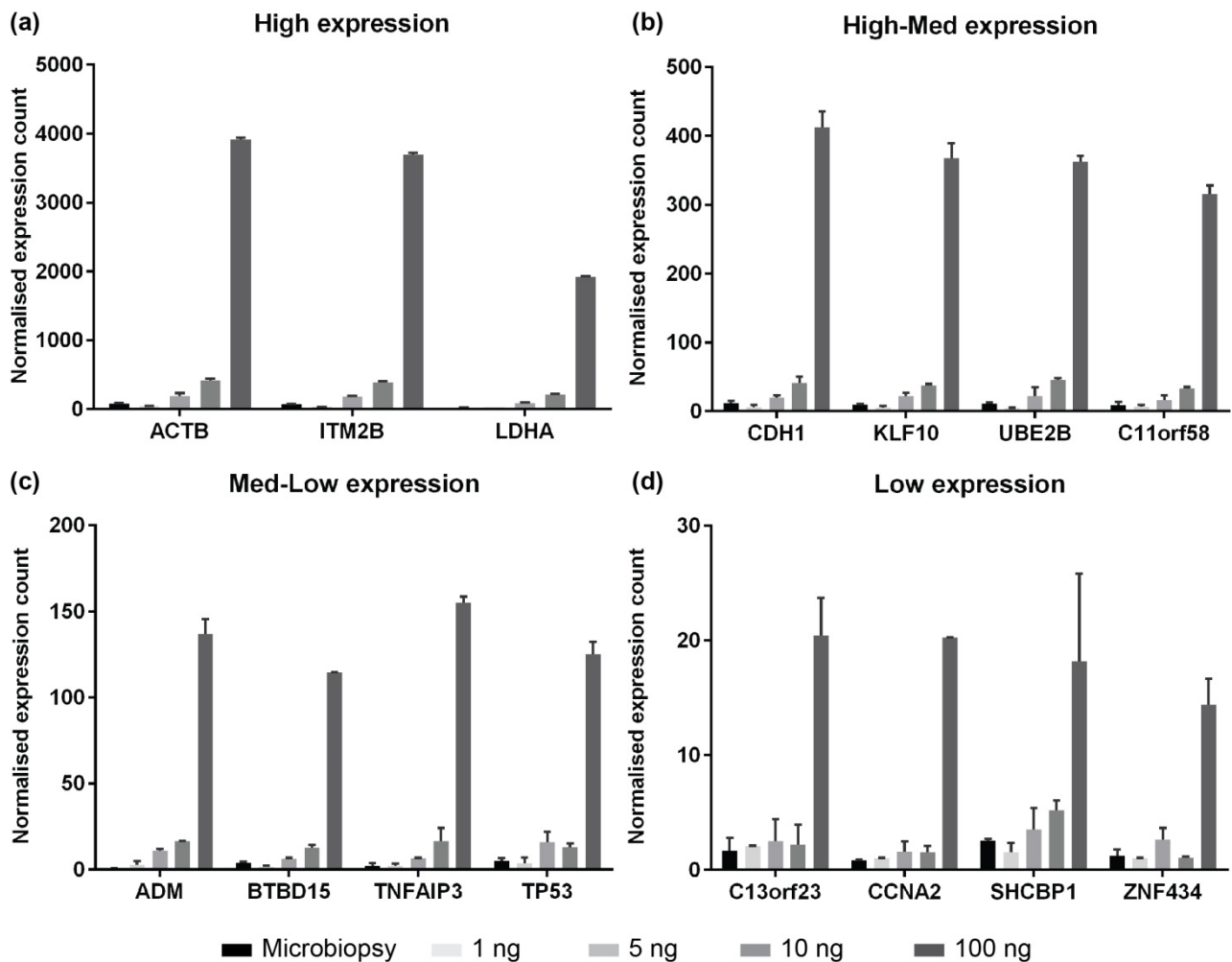


**Figure 7.7: Comparison of microbiopsy and sample input in varying concentrations across different levels of gene expression.**

The bar charts show comparisons of microbiopsy and starting material of varying concentrations (n=2) per test group, including 1 ng, 5 ng, 10 ng and 100 ng across representative genes of different expression levels. The genes are categorised into four groups: high (a), high to med (b), med to low (c) and low expression levels genes.

### 7.3.4 Generation of indexed cDNA library

Clontech SMARTer Stranded RNA-Seq Kit was selected for producing cDNA libraries as it was designed to generate full transcriptome coverage and was suitable for samples of both high and low RNA integrity. In addition, this kit provided a streamlined library preparation workflow to produce compatible indexed cDNA libraries for Illumina sequencing platforms.

Complimentary DNA libraries were detected within 150 to 1000 bp for both microbiopsy samples. The cDNA library product of my samples did not have a distinct peak but were observed as double humps in both samples (**Figure 8**). It has been suggested in a NGS community forum that this was a consequence of excess amplification of the cDNA library during PCR and can result in high duplicate rates post sequencing (Jelsoft Enterprises Ltd., 2014). The cDNA library product from the lesion appeared to be insufficiently fragmented given the presence of a broad range peak at high molecular mass (**Figure 7.8**, black arrowhead). The kit is designed to generate RNA-seq libraries at a final concentration of greater than 7.5 nM and all of the microbiopsy samples were of the right final concentration, ranging from 7.76 to 61.68 nM.

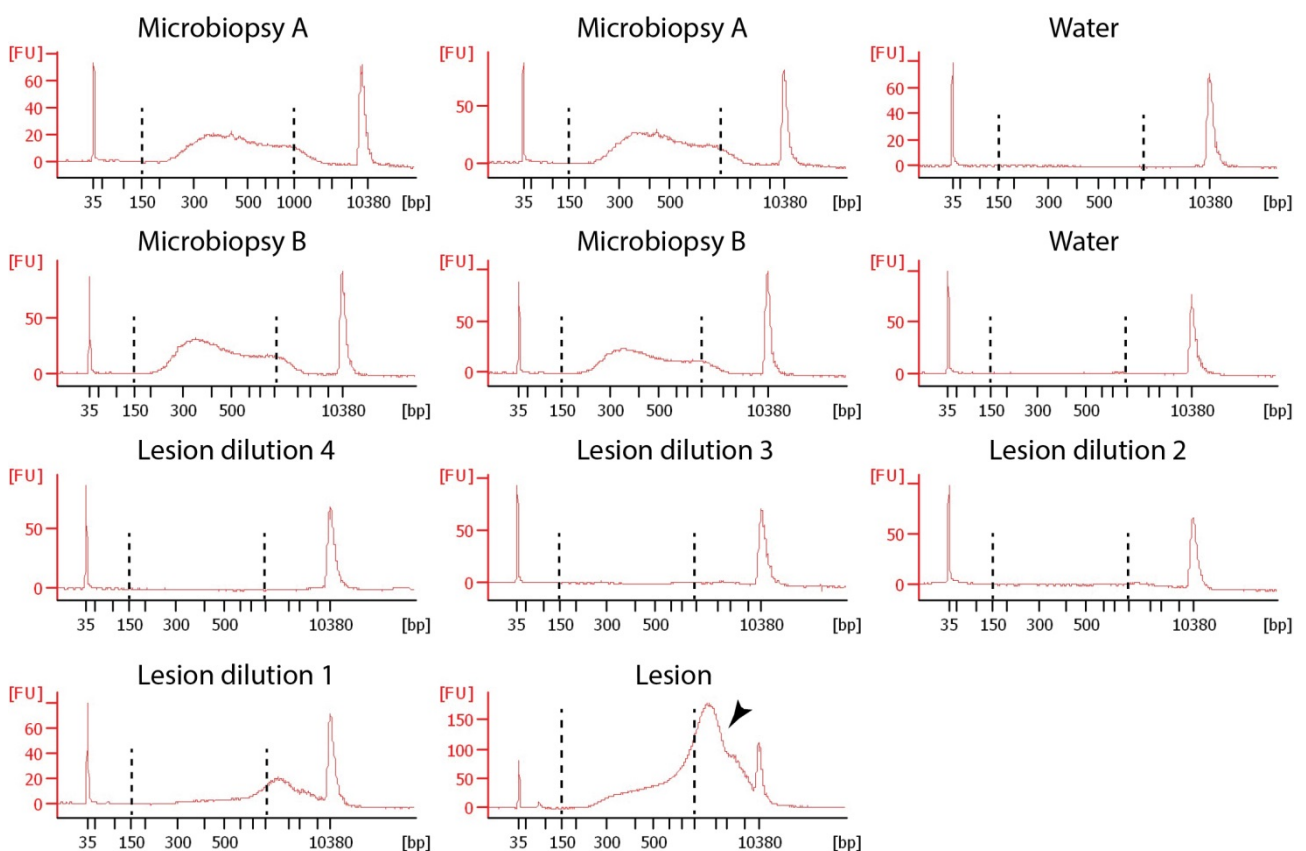


**Figure 7.8: cDNA library synthesis validation.**

Bioanalyzer High Sensitivity DNA data of cDNA samples from two sets of pooled microbiopsy samples and actinic keratosis lesion. Serial dilutions of the lesional cDNA (n=1) were tested from lowest to highest concentration in the analysis. Successful cDNA library synthesis was marked by a distinct peak bridging 150 to 1000 base pairs as indicated by the dotted black lines. Black arrowhead indicates sample of high molecular mass.

## 7.4 Conclusions

The aim of this Chapter was to explore cutting edge molecular technologies to characterise microbiopsy samples. Proteomics is a rapidly growing area of research that could be used to investigate a number of dermatological conditions. The average microbiopsy samples were found to contain  $0.93 \pm 0.74 \mu\text{g}$ . These samples were successfully analysed with liquid chromatography-tandem mass spectrometry (LC-MS/MS) and 22 cytokines have been identified.

Another state-of-the-art technology available in the market to study skin disease signature is the digital analysis of gene expression profiles by NanoString® Technologies Inc. qRT-PCR was used to provide a more accurate quantification of the total RNA in microbiopsy samples by profiling the skin-specific RPLP0 housekeeping gene. The presence of melanocytes in microbiopsy samples was confirmed with positive tyrosinase expression in qRT-PCR. The suggested starting mRNA sample for this kit is 100 ng. The percentage of detectable genes decreased by 41.7% when the amount of starting mRNA was reduced from 100 to 10 ng. Only three out of 48 genes were detected with microbiopsy and 1 ng sample input, i.e. the percentage of detectable genes in these samples was decreased by 81.25% when compared to the recommended starting mRNA.

Complementary DNA libraries were successfully generated using SMARTer® Stranded RNA-Seq Kit. Even though the library products were not of ideal quality, this can be easily corrected by further optimisation of the protocol for processing microbiopsy samples. The success in generating cDNA libraries of the microbiopsy samples opens up opportunity for a wide variety of prospective studies. This Chapter provided a good snapshot of downstream omics technologies that can be analysed with microbiopsy samples.

Technical variations are one of the most important issues to address for small sample input. It is yet to be validated how much technical variation one can expect from microbiopsy samples and the accuracy of biological information the microbiopsy sample represents. The future molecular validation work for this device will be to compare it against single cell and conventional tissue biopsy in various omics technologies. This will provide clarity to the relevance of biological information from the microbiopsy sample when compared to single cell and whole lesions.

## Chapter 8

### *General Discussion, Conclusions and Future Directions*

Current sampling approaches adopted in clinical and research practice are confounded by the need for local anaesthetic and suture, along with possible risks of infection and pain experienced by patients during the process. There is a clear need for an alternative method to enable minimally invasive sampling in the field of dermatology to fill the gap for both clinical and research use. As discussed previously, there are many fabrication methods available, but not all were suitable in this context mainly due to the cost of operation and the feasibility of using this process in a laboratory environment.

Three strategies were put in place to approach this research project. 1) To identify a feasible fabrication method suitable for use in the laboratory settings that will enable reproducible fabrication of the microbiopsy at low operational cost. Laser cutting was ultimately chosen as the fabrication technique to produce the microbiopsy devices. 2) To characterise and optimise the microbiopsy prototypes, and benchmark it to the conventional biopsy as the gold standard. 3) To explore and validate the functionalities of this device for molecular analysis in various downstream omics technologies and assays. The overall development process of the microbiopsy platform is illustrated in **Figure 8.1**.

This Chapter addresses the pros and cons of current sampling approaches, followed by factors influencing the choice of fabrication methods and microneedle material. The testing models employed during the device optimisation stage, and the advantage and considerations of these models will also be addressed. Finally, possible improvements to the current device and potential applications of this device in dermato-oncology and research settings, and future plans for integration with existing technology/platforms are proposed.

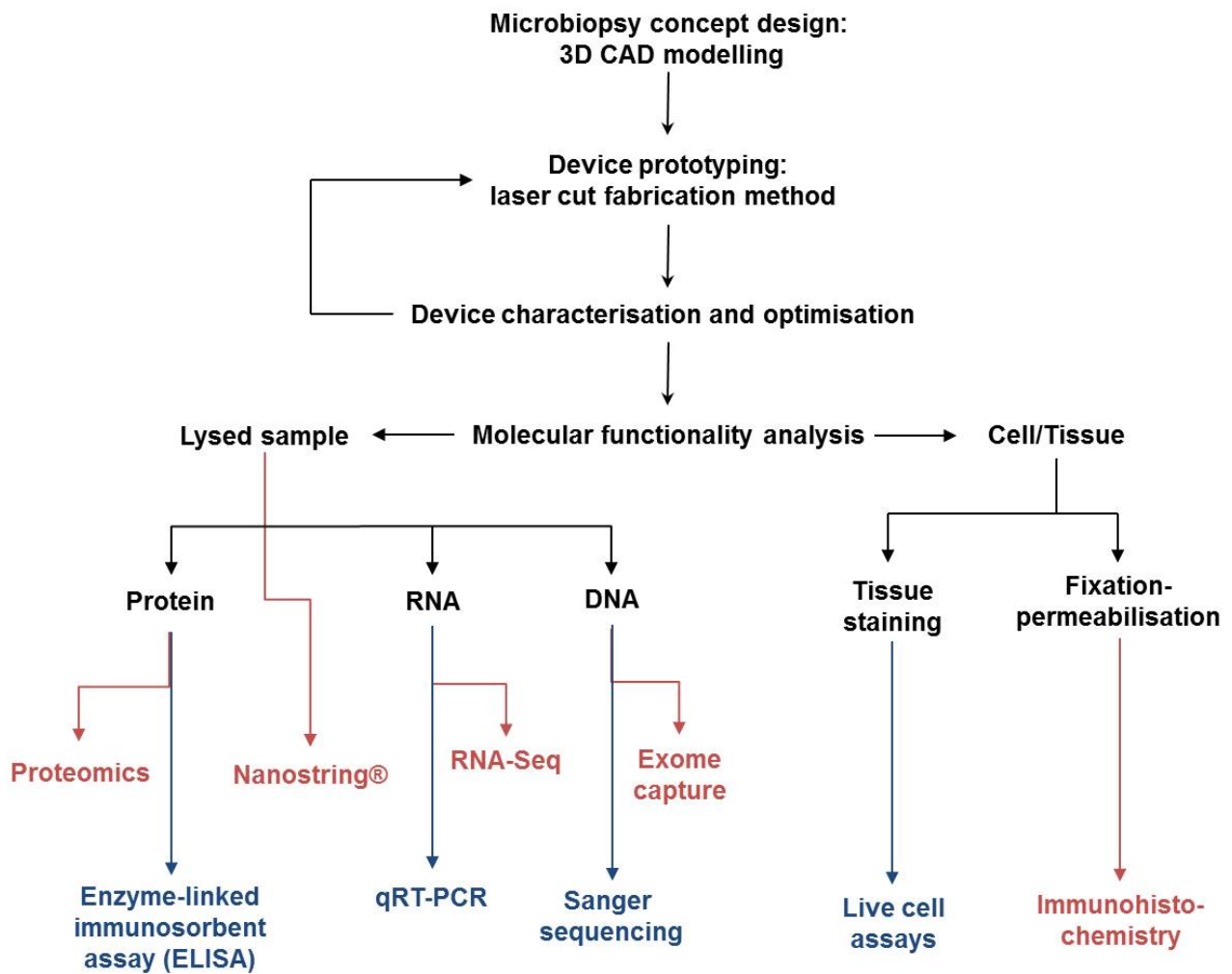


**Figure 8.1: Developmental process of the microbiopsy device.**

The flowchart highlights the process of developing the device, starting from conceptual design by 3D CAD modelling, followed by prototype construction, characterisation and optimisation, to the functionality assessment of the microbiopsy. Red text: requires further characterisation, Blue text: functionality assays completed.

## 8.1 Comparisons of current sampling approaches

Current sampling approaches for genetic analysis include blood, saliva and cheek swabs. The issue with blood sampling (phlebotomy) is the invasive and painful nature of the procedure, which has resulted in needle phobia in people. This condition has been reported to affect treatment compliance in patients with chronic disease such as diabetes when multiple monitoring of glucose level per day is required.

Saliva collection, in contrast, is non-invasive and does not risk needle-stick injuries. An added benefit of this sampling method is that samples can be self-collected by patients. As a result, this was perceived as a more appealing approach for sample collection. Even though many salivary biomarkers were comparable to that of blood or urine samples, this approach is limited by inconsistency in results and several methodological concerns during sampling process (Koh and Koh, 2007). Examples of these issues include risk of cross contamination by blood and environmental exposure, and stability problems contributed by storage duration. Buccal cell collection using either cheek swabs or cytobrushes is a simple and quick technique, which is also commonly used for non-invasive sampling of DNA. The downside of using these samples was the lower quality of DNA compared to whole saliva sample (Rogers et al., 2007). Molecular samples extracted from frozen microbiopsy samples that were stored at  $-70^{\circ}\text{C}$  for over 12 months were shown to be of relatively good quality. This advocated that the storage duration had minimal impact on the quality of microbiopsy samples. This highlights another advantage of microbiopsy sampling over saliva collection. Microbiopsy sampling also has the capacity for repeated sampling and longitudinal studies. The time taken to collect multiple samples is moreover significantly reduced with microbiopsy devices when compared to blood or saliva sampling.

The use of sample from all the sampling techniques discussed earlier is limited to only DNA analysis. Due to the specificity of the sample location obtained by the microbiopsy, DNA, RNA and protein studies can be used for somatic profiling at both transcriptional and translational level relating to the disease. The samples from blood, saliva or buccal cells, with respect to skin, can only be used for germline mutation profiling. Microbiopsy-based sampling approach collects a few cells with minimal to no pain and damage to site of application. This signifies that collection can be made repeatedly and molecular changes



in an individual can be monitored over time. The usefulness of this approach can also be extended to the monitoring of toxic chemicals and sun exposure in high risk people.

## **8.2 Fabrication of the microbiopsy device**

There are many microneedles (MN) methods developed in recent years due to the advances in rapid prototyping technologies, and the appeal of minimally invasive procedures. Scalability for mass production is an issue relevant to these technologies due to high cost of production contributed by the requirement for cleanroom facilities, expensive equipment and the engagement of services to handle hazardous chemical waste. Therefore, the goal of the project was to design a device that was minimally invasive, but also easy to use, low-cost and has scalable potential.

Traditionally, the production of MN was achieved by hand pulling glass pipettes. Not only was this process expensive and time consuming, the resulting MNs demonstrated poor fracture properties. Microfabrication techniques, also known as MEMS (originally used for the production of microprocessors) was effectively employed by Henry et al. to microfabricate MN for drug delivery purpose (Henry et al., 1998). Even though these microfabrication processes for making silicon MN has the potential for scaling, but the cost of production remains prohibitive compared to commonly used materials. This is because the processes are highly specialised, complex and multistep (Ziaie et al., 2004).

The choice of using stainless steel in our design was supported by the lower fabrication cost, while equally effective skin penetration (Verbaan et al., 2008). Medical apparatus made out of metal, particularly stainless steel, have a long standing history in medical use. This was also the other benefit for using stainless steel as the regulatory path to approval will be considerably cut down.

Fabrication techniques compatible with stainless steel are electroplating and laser cutting. Electroplating supports a wide array of geometrical designs (including hollow solid MNs), but suffers from poor resolution. On top of that, MN produced by this method has poor fracture resistance and are relatively thin walled (Gittard et al., 2010). The choice of using laser cutting was influenced by the speed and accuracy of the technique, generating relatively good resolution for sub-millimetre objects. We have demonstrated that laser cutting was easy to operate, and a low-cost and scalable operation.

### **8.3 Microbiopsy characterisation and optimisation**

There are several areas to further improve the functions of the microbiopsy. One is to enable direct imaging and immunohistochemistry analysis. To image the sample with the current device, one will have to unfold the cutting tip to gain access to the tissue. During this process, the histological structure of the tissue will be disrupted and often makes image analysis difficult as images from multiple areas need to be combined to represent the sample. Microbiopsies made of transparent polymer or silicon can resolve this issue. Emerging fabrication technologies like two-photon polymerisation have the potential to mass manufacture microbiopsy devices of high resolution made of transparent polymer material without the high cost of maintaining the operation. The presence of blood can sometimes pose as a confounding factor in certain analysis when only tissue samples are required. A possible solution would be to coat the microbiopsy's cutting tip with a hydrophobic film to allow extraction of tissue without contaminating the sample with blood.

The depth of microbiopsy penetration was characterised in the human and mouse skin models, which each model showing advantages and limitations. For example, in the mouse skin and excised human skin, cross-sectional analysis of histological sections for accurate measurement of the application site was possible. The drawback of the mouse model is that the skin is thinner, and the probability of the microbiopsy cutting tip penetrating the skin completely is high. Hence, characterising the penetration depth of microbiopsy application will not be ideal using the mouse model. There are important considerations for using human explants. For example, the surface tension of excised human skin can vary depending on how much it was stretched during the experiment. This can potentially affect the way the device penetrates the skin and how deep it can infiltrate. Therefore, it is important to have an applicator that helps to flatten the skin surface and maintain a mechanically reproducible application site.

The functionality of the microbiopsy device was also compared in healthy and diseased skin such as in actinic keratoses where the stratum corneum is significantly thickened due to the hyperkeratotic condition. Varying amount of tissue collected was observed throughout the collection period even though the same batch of cutting tips was used. The number of successful collection can vary from four out of five to two out of five on different AK lesions. It was believed that the severity of the hyperkeratosis had affected the

outcome. This was no different to healthy skin models as every individual may have difference in thickness of their stratum corneum. The access of a consistent model may provide more rapid and accurate manner by eliminating structural variability in those models. One approach will be to use of computer modelling for the characterisation and optimisation of the microbiopsy.

#### **8.4 Microbiopsy applications in dermato-oncology.**

High-throughput technologies such as genomic sequencing and together with bioinformatics have the potential to influence the health care planning and prevention. These technologies provide molecular stratification of the disease to determine treatment pathways and the ability to optimise drug options and dosages in an individual. It is foreseen that the personalised medicine will play a strong role in the future of oncology. Personalised oncology is a new diagnostic and individualised treatment-based approach to address the problems of intra- and inter-tumor heterogeneity. It is conceivable that the development of targeted drug in the near future will make this approach commonplace, although relevant molecular signatures and targets must first be identified. The submillimeter skin microbiopsy offers a targeted sampling solution to help address these intra- and inter-tumor heterogeneity issues in squamous cell carcinoma (SCC) and melanoma.

In today's clinical practice, US FDA-approved signalling pathway inhibitors are used to target metastatic melanoma that harbours the BRAFV600E mutation. The issue is that not all melanomas have this mutation and many develop resistance to the drug (Nazarian et al., 2010). Combination inhibitors drug therapy has shown promising results. The current clinical reality is that the primary melanoma lesion is excised before tumor genomic profile is extracted. One cannot define the optimum combination unless possible therapeutic resistance has been predefined. In the future, microbiopsies can be taken from every clinically suspicious naevi or primary melanoma to either assess for prognosis biomarkers or to determine the probabilities of transformation before metastasis occurs.

This principle can also be applied in the arena of non-melanoma skin cancer where the prevalence is much higher, especially in organ transplant patients (Bangash and Colegio, 2012). Many of the sun-damaged and immunocompromised patients can present with numerous precancerous actinic keratoses (AK), where some of which will progressively

become SCC. The task to select a few most suspicious lesions out of this many for biopsy and histopathology can be daunting. It can also be cosmetically challenging when AK is present on areas like the face. The microbiopsy-based sampling approach could yield molecular signatures to detect presence of neoplastic transformation without the need for conventional biopsy. Crucially, this improvement in patient care is only possible if there are validated biomarkers and development of new targeted therapies.

## **8.5 Microbiopsy applications in the research arena**

The skin provides easily access for research in many areas, yet many of these research are limited by a common confounding factor – the lack of a suitable sampling tool that will enable repeated sampling over time. One example is the research in the field of molecular skin pathology. A repeated collection from multiple lesions in an animal model or a given patient, which was previously unfeasible, is now possible with the microbiopsy device. This enables researchers to study the molecular mechanisms of disease more closely, as it progresses. This also suggests that the outstanding question of how valuable molecular profiling is to the treatment process can now be answered with the device.

Mutations of the oncogenes can provide clues for prediction of the disease course while the immune system inexorably plays an important role in the suppression of skin cancer. By combining oncogene mutations, expression and immune profiling, one can obtain comprehensive overview of the processes leading to disease progression and predict the efficacy of small molecules used during immunotherapy. This area of research may be necessary for stratifying skin cancer, predicting risk of disease and determining the effectiveness of the therapy. Given today's rapid advances in nanomedicine and bioengineering, this approach can theoretically be carried out with a single microbiopsy.

The capacity of the microbiopsy device to sample viable cell from the skin enabled a unique approach for *in vivo* live cell-based assay that has, to the best of my knowledge, not been performed by any research group. This means new paradigms for analysing products that can be topically delivered to the skin. For example, the functionality and toxicology of a particular vaccine, drug or chemical can now be performed on human volunteers. Current testing systems are either done using cell lines, on explants (excised skin) or in animal models, but the most relevant model remains to be the human volunteer. Furthermore, current techniques (e.g. microdialysis and suction blistering) that are

considered minimally invasive still carry higher risks of infection compared to the microbiopsy due to the deeper and wider surface area of sampling.

Biobanking involves the collection and storage of biological samples in a biorepository to support research studies. It is now considered an important and valuable research tool for the validation and translation of research into medical diagnoses and treatment. The challenges in biobanking sampling are the ethical concerns, and balancing the rights of individuals versus the interests of the research society. The pitfalls associated with conventional biopsy have resulted in potential donors turning away from sample donations. It is foreseen that microbiopsies will become a functional option for biobanking of all skin diseases to move forward clinical and translational medicine in dermatology.

The microbiopsy device has a unique application in the area of vector-borne diseases. Pilot field testing has been conducted in Ethiopia and Ghana for detection of skin/blood parasites causing visceral leishmaniasis and river blindness. These parasites are spread by blood-feeding vectors such as sand flies and black flies. In the study of its transmission, a method called xenodiagnosis is traditionally performed by exposing infected individuals to insectary-reared vectors to determine the infectivity of the host. The application of this technique to mass screen large rural communities in impoverished countries like Ethiopia and Ghana is limited due to logistical and ethical complications. Serendipitously, it was discovered that the cutting tip of the microbiopsy resembles the mouthparts of the vector-of-interest. Hence, the microbiopsy could substitute the vector by mimicking the transmission during blood feeding. The pilot study showed promising results of microbiopsy application in this area of research wherein only one out of eight subjects had a false positive outcome. This alternate method helps to improve logistic capacity, and increase patient compliance, particularly in rural areas, and also minimises any potential experimental variability.

## **8.6 Smart-integration of microbiopsy**

The existing problem observed with the microbiopsy device is the sample handling procedure. The microbiopsy's cutting tip containing the biopsy sample is typically removed from the applicator plunger by a clean pair of forceps. This handling process introduces the risks of samples contamination. To reduce this risk, direct handling of the cutting tip should be avoided. One approach to overcome this is to integrate the microbiopsy

sampling tool into micro-total analysis systems (Asiello and Baeumner, 2011). These systems are established using isothermal nuclei acid amplification technology platform. Combining the sample preparation and miniaturising amplification reactions prevents risk of contamination, requires fewer manual steps and can significantly reduce the use of expensive reagents. This type of isothermal microsystems is portable and can be useful for rapid on-site diagnosis of pathogens and parasites, particularly in field conditions in rural countries. These systems have the potential for streamlining near patient diagnosis and treatment planning in a clinical setting. There are existing systems with and without sample preparation integrations but none works for whole tissue. The microbiopsy device fills the technology gap in dermatology research that has the potential to be translated into a diagnostic device in the future.

Biosensing is another conceivable future application of microiopsy. One of the most common biosensor is used for glucose monitoring in diabetes patients. Biosensor offers real-time and label-free measurement and detection of biological elements. This technology is not new and rapid advanced have been made since the 1990s to detect a variety of biological materials (Cornell et al., 1997). An example of biosensor that made out to the market is the Medtronic MiniMed. This device has an integrated insulin pump that accurately detects, monitor and maintain optimal glucose level by controlled delivery of insulin to meet the body's needs. It is anticipated that moving forward, the next-generation of microbiopsy technology would have an integrated miniaturized diagnostic component where direct diagnosis is detected on the microbiopsy device. An analogy of such a diagnostic device is the pregnancy test kit, where sample collection and diagnostic information is integrated. It is envisioned that consumers as the end-users would be able to purchase these devices easily off-the-shelves in a pharmacy.

## **8.7 Conclusions**

Fabrication of these devices using laser cutting techniques is quick and of low operation cost with scalable potential, making it a commercially viable alternative to current biopsy tools. This device fills the need for an alternative sampling approach that is minimally-invasive for both research and clinical settings. More importantly, it is a simple and easy-to-use device that can be easily adopted in clinics or used by patients themselves. Given its pain-free and suture-free application, the microbiopsy can improve patient care and

compliance for early detection of skin diseases. Adequate amounts of nucleic acids were successfully obtained from human tissues, and together with current amplification technologies, this platform can essentially be applied to any downstream molecular analysis application. The potential of this device is not limited to bedside testing of common skin diseases, but also the diagnosis of infectious diseases in the field. It is foreseen that the microbiopsy can enable elaboration of molecular profiling to facilitate early detection of diseases and aid in the identification of therapeutic targets. The anticipated long-term benefits of using microbiopsies in the research and clinical settings are earlier and more accurate detection of neoplastic skin diseases, enabling targeted skin cancer therapy.

## References

- 3GEN. 2014. *Pocket dermoscopy devices* [Online]. Available: <http://dermlite.com/collections/pocket-dermoscopy-devices> [Accessed 25 November 2014].
- ALAMOUTI, B. & FUNK, J. 2003. Retinal thickness decreases with age: an OCT study. *British Journal of Ophthalmology*, 87, 899-901.
- ANDERL, H., ZUR NEDDEN, D., MUHLBAUER, W., TWERDY, K., ZANON, E., WICKE, K. & KNAPP, R. 1994. CT-guided stereolithography as a new tool in craniofacial surgery. *Br J Plast Surg*, 47, 60-4.
- ANDERSON, R. R. 1991. Polarized light examination and photography of the skin. *Arch Dermatol*, 127, 1000-5.
- ANREDDY, R. N., YELLU, N. R. & DEVARAKONDA, K. R. 2013. Oxidative biomarkers to assess the nanoparticle-induced oxidative stress. *Methods in molecular biology*, 1028, 205-19.
- ASIELLO, P. J. & BAEUMNER, A. J. 2011. Miniaturized isothermal nucleic acid amplification, a review. *Lab on a Chip*, 11, 1420-1430.
- AUSTRALIAN CANCER NETWORK MELANOMA GUIDELINES REVISION WORKING PARTY 2008. Clinical practice guidelines for the management of melanoma in Australia and New Zealand.
- AXINTE, D., SRINIVASU, D., KONG, M. & BUTLER-SMITH, P. 2009. Abrasive waterjet cutting of polycrystalline diamond: A preliminary investigation. *International Journal of Machine Tools and Manufacture*, 49, 797-803.
- AZMIR, M. A. & AHSAN, A. K. 2009. A study of abrasive water jet machining process on glass/epoxy composite laminate. *Journal of Materials Processing Technology*, 209, 6168-6173.
- BANAN, P., LIN, L. L., LAMBIE, D., PROW, T. & SOYER, H. P. 2013. Effects of ex vivo skin microbiopsy on histopathologic diagnosis in melanocytic skin lesions. *JAMA Dermatol*, 149, 1107-9.
- BENFELDT, E., SERUP, J. & MENNE, T. 1999. Microdialysis vs. suction blister technique for in vivo sampling of pharmacokinetics in the human dermis. *Acta Derm Venereol*, 79, 338-42.
- BENGTSSON, M., HEMBERG, M., RORSMAN, P. & STAHLBERG, A. 2008. Quantification of mRNA in single cells and modelling of RT-qPCR induced noise. *BMC Mol Biol*, 9, 63.
- BENNETT, D. C. 2003. Human melanocyte senescence and melanoma susceptibility genes. *Oncogene*, 22, 3063-9.
- BENVENUTO-ANDRADE, C., DUSZA, S. W., AGERO, A. L., SCOPE, A., RAJADHYAKSHA, M., HALPERN, A. C. & MARGHOUB, A. A. 2007. Differences between polarized light dermoscopy and immersion contact dermoscopy for the evaluation of skin lesions. *Arch Dermatol*, 143, 329-38.
- BERENSMEIER, S. 2006. Magnetic particles for the separation and purification of nucleic acids. *Applied Microbiology and Biotechnology*, 73, 495-504.
- BERGHOFF, A. S. & PREUSSER, M. 2014. BRAF alterations in brain tumours: molecular pathology and therapeutic opportunities. *Curr Opin Neurol*, 27, 689-96.
- BERGLUND, S. R., SCHWIETERT, C. W., JONES, A. A., STERN, R. L., LEHMANN, J. & GOLDBERG, Z. 2007. Optimized methodology for sequential extraction of RNA and protein from small human skin biopsies. *The Journal of investigative dermatology*, 127, 349-53.
- BHARGAVA, V., HEAD, S. R., ORDOUKHANIAN, P., MERCOLA, M. & SUBRAMANIAM, S. 2014. Technical variations in low-input RNA-seq methodologies. *Sci Rep*, 4, 3678.
- BOLOGNIA, J., RAPINI, R. P. & JORIZZO, J. L. 2003. *Dermatology*, Mosby.
- BOLOGNIA, J. L., JORIZZO, J. L. & SCHAFFER, J. V. 2012. *Dermatology*, Elsevier Health Sciences UK.
- BOONE, M. A., MARNEFFE, A., SUPPA, M., MIYAMOTO, M., ALARCON, I., HOFMANN-WELLENHOF, R., MALVEHY, J., PELLACANI, G. & DEL MARMOL, V. 2015. High-definition optical coherence tomography algorithm for the discrimination of actinic keratosis from normal skin and from squamous cell carcinoma. *J Eur Acad Dermatol Venereol*.



- BOX, N. F., DUFFY, D. L., CHEN, W., STARK, M., MARTIN, N. G., STURM, R. A. & HAYWARD, N. K. 2001. MC1R genotype modifies risk of melanoma in families segregating CDKN2A mutations. *Am J Hum Genet*, 69, 765-73.
- BOX, N. F., WYETH, J. R., O'GORMAN, L. E., MARTIN, N. G. & STURM, R. A. 1997. Characterization of melanocyte stimulating hormone receptor variant alleles in twins with red hair. *Hum Mol Genet*, 6, 1891-7.
- BRUNING, O., RODENBURG, W., RADONIC, T., ZWINDERMAN, A. H., DE, V. A., BREIT, T. M. & DE, J. M. 2011. RNA isolation for transcriptomics of human and mouse small skin biopsies. *BMC research notes*, 4, 438.
- BUDELIER, K. & SCHORR, J. 2001. Purification of DNA by Anion-Exchange Chromatography. *Current Protocols in Molecular Biology*. John Wiley & Sons, Inc.
- BURNS, D. M., TAYLOR, S. & GIBSON, J. R. 2005. Quadrupole mass filter. Google Patents.
- BYUN S., L. J., PAIK S, LEE A., KOO K, PARK S., PARK J., CHOI B, SEO J.M., KIM K., CHUNG H., SONG S.Y., JEON D. AND CHO D. 2005. Barbed micro-spikes for micro-scale biopsy. *Journal of Micromechanics and Microengineering*, 15, 1279-1284.
- CHO D., P. S. K., LEE A.R, PAIK S.J, JEONG M.J, CHOI H.M, LIM J.M. 2011. *Catheter capable of being equipped with micro biopsy tool*.
- CHUA, C. K., LEONG, K. F. & LIM, C. S. 2010. *Rapid Prototyping: Principles and Applications*, World Scientific.
- CONTALDO, M., AGOZZINO, M., MOSCARELLA, E., ESPOSITO, S., SERPICO, R. & ARDIGO, M. 2013. In vivo characterization of healthy oral mucosa by reflectance confocal microscopy: a translational research for optical biopsy. *Ultrastruct Pathol*, 37, 151-8.
- CORNELL, B. A., BRAACH-MAKSVYTIS, V. L. B., KING, L. G., OSMAN, P. D. J., RAGUSE, B., WIECZOREK, L. & PACE, R. J. 1997. A biosensor that uses ion-channel switches. *Nature*, 387, 580-583.
- COSNIER, M. L., MARTIN, F., BOUAMRANI, A., BERGER, F. & CAILLAT, P. 2009. A minimally invasive microdevice for molecular sampling and analysis. *IEEE transactions on bio-medical engineering*, 56, 2898-904.
- CUSTOMPARTNET. 2008. *Laminated object manufacturing* [Online]. Available: <http://www.custompartnet.com/wu/laminated-object-manufacturing> [Accessed 03 February 2015 2015].
- D'URSO, P. S., BARKER, T. M., EARWAKER, W. J., BRUCE, L. J., ATKINSON, R. L., LANIGAN, M. W., ARVIER, J. F. & EFFENEY, D. J. 1999a. Stereolithographic biomodelling in cranio-maxillofacial surgery: a prospective trial. *J Craniomaxillofac Surg*, 27, 30-7.
- D'URSO, P. S., THOMPSON, R. G., ATKINSON, R. L., WEIDMANN, M. J., REDMOND, M. J., HALL, B. I., JEAUVONS, S. J., BENSON, M. D. & EARWAKER, W. J. 1999b. Cerebrovascular biomodelling: a technical note. *Surg Neurol*, 52, 490-500.
- DAHOTRE, N. B. & HARIMKAR, S. 2008. *Laser Fabrication and Machining of Materials*, Springer.
- DALLE, S., POULALHON, N. & THOMAS, L. 2011. Vemurafenib in melanoma with BRAF V600E mutation. *N Engl J Med*, 365, 1448-9; author reply 1450.
- DAVIES, H., BIGNELL, G. R., COX, C., STEPHENS, P., EDKINS, S., CLEGG, S., TEAGUE, J., WOFFENDIN, H., GARNETT, M. J., BOTTOMLEY, W., DAVIS, N., DICKS, E., EWING, R., FLOYD, Y., GRAY, K., HALL, S., HAWES, R., HUGHES, J., KOSMIDOU, V., MENZIES, A., MOULD, C., PARKER, A., STEVENS, C., WATT, S., HOOPER, S., WILSON, R., JAYATILAKE, H., GUSTERSON, B. A., COOPER, C., SHIPLEY, J., HARGRAVE, D., PRITCHARD-JONES, K., MAITLAND, N., CHENEVIX-TRENCH, G., RIGGINS, G. J., BIGNER, D. D., PALMIERI, G., COSSU, A., FLANAGAN, A., NICHOLSON, A., HO, J. W., LEUNG, S. Y., YUEN, S. T., WEBER, B. L., SEIGLER, H. F., DARROW, T. L., PATERSON, H., MARAIS, R., MARSHALL, C. J., WOOSTER, R., STRATTON, M. R. & FUTREAL, P. A. 2002. Mutations of the BRAF gene in human cancer. *Nature*, 417, 949-54.
- DE GIORGI, V., STANTE, M., MASSI, D., MAVILIA, L., CAPPUGI, P. & CARLI, P. 2005. Possible histopathologic correlates of dermoscopic features in pigmented melanocytic lesions identified by means of optical coherence tomography. *Exp Dermatol*, 14, 56-9.

- DONNELLY, R. F., SINGH, T. R., TUNNEY, M. M., MORROW, D. I., MCCARRON, P. A., O'MAHONY, C. & WOOLFSON, A. D. 2009. Microneedle arrays allow lower microbial penetration than hypodermic needles in vitro. *Pharm Res*, 26, 2513-22.
- EGAWA, M., HIRAO, T. & TAKAHASHI, M. 2007. In vivo estimation of stratum corneum thickness from water concentration profiles obtained with Raman spectroscopy. *Acta Derm Venereol*, 87, 4-8.
- ESCOBAR-CHAVEZ, J. J., MERINO-SANJUÁN, V., LÓPEZ-CERVANTES, M., URBAN-MORLAN, Z., PINON-SEGUNDO, E., QUINTANAR-GUERRERO, D. & GANEM-QUINTANAR, A. 2008. The tape-stripping technique as a method for drug quantification in skin. *Journal of Pharmacy & Pharmaceutical Sciences*, 11, 104-130.
- ESPINA, V., MUELLER, C., EDMISTON, K., SCIRO, M., PETRICOIN, E. F. & LIOTTA, L. A. 2009. Tissue is alive: New technologies are needed to address the problems of protein biomarker pre-analytical variability. *PROTEOMICS – Clinical Applications*, 3, 874-882.
- FEIT, N. E., DUSZA, S. W. & MARGHOOB, A. A. 2004. Melanomas detected with the aid of total cutaneous photography. *British Journal of Dermatology*, 150, 706-714.
- FELDMAN, S. R. & FLEISCHER, A. B., JR. 2011. Progression of actinic keratosis to squamous cell carcinoma revisited: clinical and treatment implications. *Cutis*, 87, 201-7.
- FERRARA, G., ARGENYI, Z., ARGENZIANO, G., CERIO, R., CERRONI, L., DI BLASI, A., FEUDALE, E. A., GIORGIO, C. M., MASSONE, C., NAPPI, O., TOMASINI, C., URSO, C., ZALAUDEK, I., KITTLER, H. & SOYER, H. P. 2009. The influence of clinical information in the histopathologic diagnosis of melanocytic skin neoplasms. *PLoS One*, 4, e5375.
- FERRARI, B., PUPELLI, G., FARNETANI, F., DE CARVALHO, N. T., LONGO, C., REGGIANI, C., ARGENZIANO, G. & PELLACANI, G. 2014. Dermoscopic difficult lesions: an objective evaluation of reflectance confocal microscopy impact for accurate diagnosis. *J Eur Acad Dermatol Venereol*.
- FLAHERTY, K. T., PUZANOV, I., KIM, K. B., RIBAS, A., MCARTHUR, G. A., SOSMAN, J. A., O'DWYER, P. J., LEE, R. J., GRIPPO, J. F., NOLOP, K. & CHAPMAN, P. B. 2010. Inhibition of mutated, activated BRAF in metastatic melanoma. *N Engl J Med*, 363, 809-19.
- FRANSEN, M., KARAHALIOS, A., SHARMA, N., ENGLISH, D. R., GILES, G. G. & SINCLAIR, R. D. 2012. Non-melanoma skin cancer in Australia. *Med J Aust*, 197, 565-8.
- FUCHS, A. & MARMUR, E. 2007. The kinetics of skin cancer: progression of actinic keratosis to squamous cell carcinoma. *Dermatol Surg*, 33, 1099-101.
- GAMBICHLER, T., JAEDICKE, V. & TERRAS, S. 2011. Optical coherence tomography in dermatology: technical and clinical aspects. *Arch Dermatol Res*, 303, 457-73.
- GAMBICHLER, T., REGENITER, P., BECHARA, F. G., ORLIKOV, A., VASA, R., MOUSSA, G., STUCKER, M., ALTMAYER, P. & HOFFMANN, K. 2007. Characterization of benign and malignant melanocytic skin lesions using optical coherence tomography in vivo. *J Am Acad Dermatol*, 57, 629-37.
- GAYNOR, A. T., MEISEL, N. A., WILLIAMS, C. B. & GUEST, J. K. 2014. Multiple-Material Topology Optimization of Compliant Mechanisms Created Via PolyJet Three-Dimensional Printing. *Journal of Manufacturing Science and Engineering*, 136, 061015-061015.
- GEISS, G. K., BUMGARNER, R. E., BIRDITT, B., DAHL, T., DOWIDAR, N., DUNAWAY, D. L., FELL, H. P., FERREE, S., GEORGE, R. D., GROGAN, T., JAMES, J. J., MAYSURIA, M., MITTON, J. D., OLIVERI, P., OSBORN, J. L., PENG, T., RATCLIFFE, A. L., WEBSTER, P. J., DAVIDSON, E. H., HOOD, L. & DIMITROV, K. 2008. Direct multiplexed measurement of gene expression with color-coded probe pairs. *Nat Biotechnol*, 26, 317-25.
- GENE, S. 2007. Rapid Prototyping Processes. *Rapid Prototyping and Engineering Applications*. CRC Press.
- GERGER, A., HOFMANN-WELLENHOF, R., LANGSENLEHNER, U., RICHTIG, E., KOLLER, S., WEGER, W., AHLGRIMM-SIESS, V., HORN, M., SAMONIGG, H. & SMOLLE, J. 2008. In vivo confocal laser scanning microscopy of melanocytic skin tumours: diagnostic applicability using unselected tumour images. *British Journal of Dermatology*, 158, 329-333.
- GILL, H. S., DENSON, D. D., BURRIS, B. A. & PRAUSNITZ, M. R. 2008. Effect of microneedle design on pain in human volunteers. *Clin J Pain*, 24, 585-94.

- GILLETTE, M. A. & CARR, S. A. 2013. Quantitative analysis of peptides and proteins in biomedicine by targeted mass spectrometry. *Nat Methods*, 10, 28-34.
- GIROTTI, M. R., SATURNO, G., LORIGAN, P. & MARAIS, R. 2014. No longer an untreatable disease: how targeted and immunotherapies have changed the management of melanoma patients. *Mol Oncol*, 8, 1140-58.
- GITTARD, S. D. & NARAYAN, R. J. 2010. Laser direct writing of micro- and nano-scale medical devices. *Expert Rev Med Devices*, 7, 343-56.
- GITTARD, S. D., OVSIANIKOV, A., CHICHKOV, B. N., DORAISWAMY, A. & NARAYAN, R. J. 2010. Two Photon Polymerization of Microneedles for Transdermal Drug Delivery. *Expert opinion on drug delivery*, 7, 513-533.
- GKALPAKIOTIS, S., ARENBERGER, P., KREMEN, J. & ARENBERGEROVA, M. 2010. Quantitative detection of melanoma-associated antigens by multimarker real-time RT-PCR for molecular staging: results of a 5 years study. *Exp Dermatol*, 19, 994-9.
- GOMAA, Y. A., GARLAND, M. J., MCINNES, F., EL-KHORDAGUI, L. K., WILSON, C. & DONNELLY, R. F. 2012. Laser-engineered dissolving microneedles for active transdermal delivery of nadroparin calcium. *Eur J Pharm Biopharm*, 82, 299-307.
- GONZALEZ, S., RAJADHYAKSHA, M., RUBINSTEIN, G. & ANDERSON, R. R. 1999. Characterization of psoriasis in vivo by reflectance confocal microscopy. *J Med*, 30, 337-56.
- GONZALEZ, S. & TANNOUS, Z. 2002. Real-time, in vivo confocal reflectance microscopy of basal cell carcinoma. *J Am Acad Dermatol*, 47, 869-74.
- GOODSON, A. G. & GROSSMAN, D. 2009. Strategies for early melanoma detection: Approaches to the patient with nevi. *J Am Acad Dermatol*, 60, 719-35; quiz 736-8.
- GOSS J. & MANN N. 2005. Health system expenditures on cancer and other neoplasms in Australia, 2000-01. Australian Institute of Health and Welfare Canberra
- GREBE, S. K. & SINGH, R. J. 2011. LC-MS/MS in the Clinical Laboratory - Where to From Here? *Clin Biochem Rev*, 32, 5-31.
- GREENEMEIER, L. 2013. To print the impossible. *Sci Am*, 308, 44-7.
- GREINERT, R. 2009. Skin cancer: new markers for better prevention. *Pathobiology : journal of immunopathology, molecular and cellular biology*, 76, 64-81.
- GRIMM, T. 2003. Fused deposition modeling: a technology evaluation. *Time Compression-Technologies*.
- GRULICH, A. E., BATAILLE, V., SWERDLOW, A. J., NEWTON-BISHOP, J. A., CUZICK, J., HERSEY, P. & MCCARTHY, W. H. 1996. Naevi and pigmentary characteristics as risk factors for melanoma in a high-risk population: a case-control study in New South Wales, Australia. *Int J Cancer*, 67, 485-91.
- GUITERA, P., PELLACANI, G., LONGO, C., SEIDENARI, S., AVRAMIDIS, M. & MENZIES, S. W. 2009. In vivo reflectance confocal microscopy enhances secondary evaluation of melanocytic lesions. *J Invest Dermatol*, 129, 131-8.
- GULSON, B., MCCALL, M., KORSCH, M., GOMEZ, L., CASEY, P., OYTAM, Y., TAYLOR, A., MCCULLOCH, M., TROTTER, J., KINSLEY, L. & GREENOAK, G. 2010. Small Amounts of Zinc from Zinc Oxide Particles in Sunscreens Applied Outdoors Are Absorbed through Human Skin. *Toxicological Sciences*, 118, 140-149.
- GUNDISCH, S., SCHOTT, C., WOLFF, C., TRAN, K., BEESE, C., VIERTLER, C., ZATLOUKAL, K. & BECKER, K. F. 2013. The PAXgene((R)) tissue system preserves phosphoproteins in human tissue specimens and enables comprehensive protein biomarker research. *PLoS One*, 8, e60638.
- HAENSSLE, H. A., KRAUS, S. L., BREHMER, F., KRETSCHMER, L., VOLKER, B., ASPER, H., KAPP, A. & GUTZMER, R. 2012. Dynamic changes in nevi of a patient with melanoma treated with vemurafenib: importance of sequential dermoscopy. *Arch Dermatol*, 148, 1183-5.
- HALLOCK, G. G. & LUTZ, D. A. 1998. Prospective study of the accuracy of the surgeon's diagnosis in 2000 excised skin tumors. *Plast Reconstr Surg*, 101, 1255-61.

- HALLORAN, J. W., TOMECKOVA, V., GENTRY, S., DAS, S., CILINO, P., YUAN, D., GUO, R., RUDRARAJU, A., SHAO, P., WU, T., ALABI, T. R., BAKER, W., LEGDZINA, D., WOLSKI, D., ZIMBECK, W. R. & LONG, D. 2011. Photopolymerization of powder suspensions for shaping ceramics. *Journal of the European Ceramic Society*, 31, 2613-2619.
- HAMEETMAN, L., COMMANDEUR, S., BAVINCK, J. N., WISGERHOF, H. C., DE GRUIJL, F. R., WILLEMZE, R., MULLENDERS, L., TENSEN, C. P. & VRIELING, H. 2013. Molecular profiling of cutaneous squamous cell carcinomas and actinic keratoses from organ transplant recipients. *BMC Cancer*, 13, 58.
- HENRY, O. Y., FRAGOSO, A., BENI, V., LABORIA, N., SANCHEZ, J. L., LATTA, D., VON GERMAR, F., DRESE, K., KATAKIS, I. & O'SULLIVAN, C. K. 2009. Design and testing of a packaged microfluidic cell for the multiplexed electrochemical detection of cancer markers. *Electrophoresis*, 30, 3398-405.
- HENRY, S., MCALLISTER, D. V., ALLEN, M. G. & PRAUSNITZ, M. R. 1998. Microfabricated microneedles: a novel approach to transdermal drug delivery. *J Pharm Sci*, 87, 922-5.
- HINZ, T., EHLER, L. K., VOTH, H., FORTMEIER, I., HOELLER, T., HORNUNG, T. & SCHMID-WENDTNER, M. H. 2011. Assessment of tumor thickness in melanocytic skin lesions: comparison of optical coherence tomography, 20-MHz ultrasound and histopathology. *Dermatology*, 223, 161-8.
- HOFMANN-WELLENHOF, R., WOLF, P., SMOLLE, J., REIMANN-WEBER, A., SOYER, H. P. & KERL, H. 1997. Influence of UVB therapy on dermoscopic features of acquired melanocytic nevi. *J Am Acad Dermatol*, 37, 559-63.
- JELSOFT ENTERPRISES LTD. 2014. *SeqAnswers* [Online]. Available: <http://seqanswers.com/> [Accessed 19 November 2014].
- JENG, H. A. & SWANSON, J. 2006. Toxicity of metal oxide nanoparticles in mammalian cells. *J Environ Sci Health A Tox Hazard Subst Environ Eng*, 41, 2699-711.
- KARDYNAL, A. & OLSZEWSKA, M. 2014. Modern non-invasive diagnostic techniques in the detection of early cutaneous melanoma. *Journal of Dermatological Case Reports*, 8, 1-8.
- KELES, O. & ONER, U. 2012. Laser Cutting Process: Influence of Workpiece Thickness and Laser Pulse Frequency on the Cut Quality. *Arabian Journal for Science and Engineering*, 37, 2277-2286.
- KIM, H., CHOI, J. W. & WICKER, R. 2010. Scheduling and process planning for multiple material stereolithography. *Rapid Prototyping Journal*, 16, 232-240.
- KIM, M. S., HANSGEN, A. R., WINK, O., QUAIFFE, R. A. & CARROLL, J. D. 2008. Rapid prototyping: a new tool in understanding and treating structural heart disease. *Circulation*, 117, 2388-94.
- KINGSTON, R. E. 2001. Preparation and Analysis of RNA. *Current Protocols in Molecular Biology*. John Wiley & Sons, Inc.
- KOH, D. S. Q. & KOH, G. C. H. 2007. The use of salivary biomarkers in occupational and environmental medicine. *Occupational and Environmental Medicine*, 64, 202-210.
- KONG, C. 2014. Water-Jet Cutting. Springer Berlin Heidelberg.
- KONG, M., AXINTE, D. & VOICE, W. 2011. Challenges in using waterjet machining of NiTi shape memory alloys: an analysis of controlled-depth milling. *Journal of Materials Processing Technology*, 211, 959-971.
- KOST, J., MITRAGOTRI, S., GABBAY, R. A., PISHKO, M. & LANGER, R. 2000. Transdermal monitoring of glucose and other analytes using ultrasound. *Nat Med*, 6, 347-50.
- KRULEVITCH P.A., L. A. P., NORTHRUP M.A., BENETT W.J. 1999. *Microbiopsy/Precision cutting devices*. United States patent application 08/887780.
- KRULEVITCH, P. A., LEE, A. P., NORTHRUP, M. A. & BENETT, W. J. 1999. *Microbiopsy/precision cutting devices*. Google Patents.
- KRUTH, J.-P., WANG, X., LAOUI, T. & FROYEN, L. 2003. Lasers and materials in selective laser sintering. *Assembly Automation*, 23, 357-371.
- KULEKCI, M. K. 2002. Processes and apparatus developments in industrial waterjet applications. *International Journal of Machine Tools and Manufacture*, 42, 1297-1306.

- LABOUTA, H. I., LIU, D. C., LIN, L. L., BUTLER, M. K., GRICE, J. E., RAPHAEL, A. P., KRAUS, T., EL-KHORDAGUI, L. K., SOYER, H. P., ROBERTS, M. S., SCHNEIDER, M. & PROW, T. W. 2011. Gold nanoparticle penetration and reduced metabolism in human skin by toluene. *Pharm Res*, 28, 2931-44.
- LEE, J. H., CHOI, J. W. & KIM, Y. S. 2011. Frequencies of BRAF and NRAS mutations are different in histological types and sites of origin of cutaneous melanoma: a meta-analysis. *Br J Dermatol*, 164, 776-84.
- LEE, S. J. J., SACHS, E. & CIMA, M. 1995. Layer position accuracy in powder-based rapid prototyping. *Rapid Prototyping Journal*, 1, 24-37.
- LEE, S. M., SCHELCHER, C., GASHI, S., SCHREIBER, S., THASLER, R. M., JAUCH, K. W. & THASLER, W. E. 2013. RNA stability in human liver: comparison of different processing times, temperatures and methods. *Mol Biotechnol*, 53, 1-8.
- LEITE-SILVA, V. R., LE LAMER, M., SANCHEZ, W. Y., LIU, D. C., SANCHEZ, W. H., MORROW, I., MARTIN, D., SILVA, H. D., PROW, T. W., GRICE, J. E. & ROBERTS, M. S. 2013. The effect of formulation on the penetration of coated and uncoated zinc oxide nanoparticles into the viable epidermis of human skin in vivo. *Eur J Pharm Biopharm*, 84, 297-308.
- LIM, M. C., HOH, S.-T., FOSTER, P. J., LIM, T.-H., CHEW, S.-J., SEAH, S. K. & AUNG, T. 2005. Use of optical coherence tomography to assess variations in macular retinal thickness in myopia. *Investigative ophthalmology & visual science*, 46, 974-978.
- LIN, L. L., GRICE, J. E., BUTLER, M. K., ZVYAGIN, A. V., BECKER, W., ROBERTSON, T. A., SOYER, H. P., ROBERTS, M. S. & PROW, T. W. 2011. Time-correlated single photon counting for simultaneous monitoring of zinc oxide nanoparticles and NAD(P)H in intact and barrier-disrupted volunteer skin. *Pharm Res*, 28, 2920-30.
- LIN, L. L., PROW, T. W., RAPHAEL, A. P., HARROLD III, R. L., PRIMIERO, C. A., ANSALDO, A. B. & SOYER, H. P. 2013. Microbiopsy engineered for minimally invasive and suture-free sub-millimetre skin sampling. *F1000Res*, 2, 120.
- LIU, F. W. 2007. *Rapid Prototyping and Engineering Applications: A Toolbox for Prototype Development*, CRC Press.
- LONGO, C., LALLAS, A., KYRGIDIS, A., RABINOVITZ, H., MOSCARELLA, E., CIARDO, S., ZALAUDEK, I., OLIVIERO, M., LOSI, A., GONZALEZ, S., GUITERA, P., PIANA, S., ARGENZIANO, G. & PELLACANI, G. 2014a. Classifying distinct basal cell carcinoma subtype by means of dermatoscopy and reflectance confocal microscopy. *J Am Acad Dermatol*, 71, 716-724 e1.
- LONGO, C., LALLAS, A., KYRGIDIS, A., RABINOVITZ, H., MOSCARELLA, E., CIARDO, S., ZALAUDEK, I., OLIVIERO, M., LOSI, A., GONZALEZ, S., GUITERA, P., PIANA, S., ARGENZIANO, G. & PELLACANI, G. 2014b. Classifying distinct basal cell carcinoma subtype by means of dermatoscopy and reflectance confocal microscopy. *Journal of the American Academy of Dermatology*, 71, 716-724.e1.
- LU, Y. & CHEN, S. C. 2004. Micro and nano-fabrication of biodegradable polymers for drug delivery. *Adv Drug Deliv Rev*, 56, 1621-33.
- MANKOVICH, N. J., CHEESEMAN, A. M. & STOKER, N. G. 1990. The display of three-dimensional anatomy with stereolithographic models. *J Digit Imaging*, 3, 200-3.
- MARTINEZ, A. W., PHILLIPS, S. T., WILEY, B. J., GUPTA, M. & WHITESIDES, G. M. 2008. FLASH: a rapid method for prototyping paper-based microfluidic devices. *Lab Chip*, 8, 2146-50.
- MASSIN, P., ERGINAY, A., HAOUCHINE, B., MEHIDI, A. B., PAQUES, M. & GAUDRIC, A. 2001. Retinal thickness in healthy and diabetic subjects measured using optical coherence tomography mapping software. *European journal of ophthalmology*, 12, 102-108.
- MATTICK, J. S., DZIADEK, M. A., TERRILL, B. N., KAPLAN, W., SPIGELMAN, A. D., BOWLING, F. G. & DINGER, M. E. 2014. The impact of genomics on the future of medicine and health. *Med J Aust*, 201, 17-20.
- MCCLENAHAN, P., LIN, L. L., TAN, J. M., FLEWELL-SMITH, R., SCHAIDER, H., JAGIRDAR, K., ATKINSON, V., LAMBIE, D., PROW, T. W., STURM, R. A. & SOYER, H. P. 2014.

- BRAFV600E mutation status of involuting and stable nevi in dabrafenib therapy with or without trametinib. *JAMA Dermatol*, 150, 1079-82.
- MERCER, T. R., GERHARDT, D. J., DINGER, M. E., CRAWFORD, J., TRAPNELL, C., JEDDELOH, J. A., MATTICK, J. S. & RINN, J. L. 2012. Targeted RNA sequencing reveals the deep complexity of the human transcriptome. *Nat Biotechnol*, 30, 99-104.
- MINNER, F. & POUMAY, Y. 2009. Candidate housekeeping genes require evaluation before their selection for studies of human epidermal keratinocytes. *J Invest Dermatol*, 129, 770-3.
- MINNS, R. J., BIBB, R., BANKS, R. & SUTTON, R. A. 2003. The use of a reconstructed three-dimensional solid model from CT to aid the surgical management of a total knee arthroplasty: a case study. *Med Eng Phys*, 25, 523-6.
- MONTEIRO-RIVIERE, N. A., SAMBERG, M. E., OLDENBURG, S. J. & RIVIERE, J. E. 2013. Protein binding modulates the cellular uptake of silver nanoparticles into human cells: implications for in vitro to in vivo extrapolations? *Toxicol Lett*, 220, 286-93.
- MOORE, D. & DOWHAN, D. 2001a. Purification and Concentration of DNA from Aqueous Solutions. *Current Protocols in Molecular Biology*. John Wiley & Sons, Inc.
- MOORE, D. D. & DOWHAN, D. 2001b. Preparation and Analysis of DNA. *Current Protocols in Molecular Biology*. John Wiley & Sons, Inc.
- MORHENN, V. B., CHANG, E. Y. & RHEINS, L. A. 1999. A noninvasive method for quantifying and distinguishing inflammatory skin reactions. *J Am Acad Dermatol*, 41, 687-92.
- MUKERJEE, E. V., COLLINS, S. D., ISSEROFF, R. R. & SMITH, R. L. 2004. Microneedle array for transdermal biological fluid extraction and in situ analysis. *Sensors and Actuators A: Physical*, 114, 267-275.
- NAIR, A. B., KUMRIA, R., AL-DHUBIAB, B. E., ATTIMARAD, M. & HARSHA, S. 2014. Noninvasive Sampling of Gabapentin by Reverse Iontophoresis. *Pharm Res*.
- NANOSTRING TECHNOLOGIES, I. 2014. *Digital Color-coded Barcode Technology* [Online]. Available: <http://www.nanostring.com/applications/technology>.
- NAZARIAN, R., SHI, H., WANG, Q., KONG, X., KOYA, R. C., LEE, H., CHEN, Z., LEE, M.-K., ATTAR, N. & SAZEGAR, H. 2010. Melanomas acquire resistance to B-RAF (V600E) inhibition by RTK or N-RAS upregulation. *Nature*, 468, 973-977.
- NEL, A., XIA, T., MADLER, L. & LI, N. 2006. Toxic potential of materials at the nanolevel. *Science*, 311, 622-7.
- NGUYEN, K. S., NEAL, J. W. & WAKELEE, H. 2014. Review of the current targeted therapies for non-small-cell lung cancer. *World J Clin Oncol*, 5, 576-87.
- NORI, S., RIUS-DIAZ, F., CUEVAS, J., GOLDGEIER, M., JAEN, P., TORRES, A. & GONZALEZ, S. 2004. Sensitivity and specificity of reflectance-mode confocal microscopy for in vivo diagnosis of basal cell carcinoma: a multicenter study. *J Am Acad Dermatol*, 51, 923-30.
- PADILLA, R. S., SEBASTIAN, S., JIANG, Z., NINDL, I. & LARSON, R. 2010. Gene expression patterns of normal human skin, actinic keratosis, and squamous cell carcinoma: a spectrum of disease progression. *Arch Dermatol*, 146, 288-93.
- PALIWAL, S., HWANG, B. H., TSAI, K. Y. & MITRAGOTRI, S. 2013. Diagnostic opportunities based on skin biomarkers. *Eur J Pharm Sci*, 50, 546-56.
- PALIWAL, S., OGURA, M. & MITRAGOTRI, S. 2010. Rapid sampling of molecules via skin for diagnostic and forensic applications. *Pharm Res*, 27, 1255-63.
- PELLACANI, G., GUITERA, P., LONGO, C., AVRAMIDIS, M., SEIDENARI, S. & MENZIES, S. 2007. The impact of in vivo reflectance confocal microscopy for the diagnostic accuracy of melanoma and equivocal melanocytic lesions. *J Invest Dermatol*, 127, 2759-65.
- PELLACANI, G., PEPE, P., CASARI, A. & LONGO, C. 2014. Reflectance confocal microscopy as a second-level examination in skin oncology improves diagnostic accuracy and saves unnecessary excisions: a longitudinal prospective study. *Br J Dermatol*, 171, 1044-51.
- PEPPELMAN, M., NGUYEN, K. P., HOOGEDOORN, L., VAN ERP, P. E. & GERRITSEN, M. J. 2014. Reflectance confocal microscopy: non-invasive distinction between actinic keratosis and squamous cell carcinoma. *J Eur Acad Dermatol Venereol*.

- PÉREZ-PORTELA, R. & RIESGO, A. 2013. Optimizing preservation protocols to extract high-quality RNA from different tissues of echinoderms for next-generation sequencing. *Molecular Ecology Resources*, 13, 884-889.
- PERIER-MUZET, M., THOMAS, L., POULALHON, N., DEBARBIEUX, S., BRINGUIER, P. P., DURU, G., DEPAEPE, L., BALME, B. & DALLE, S. 2014. Melanoma patients under vemurafenib: prospective follow-up of melanocytic lesions by digital dermoscopy. *J Invest Dermatol*, 134, 1351-8.
- PFLUEGER, D. 2002. Micro-invasive tissue removal device. Google Patents.
- PFLUEGER D.R., C. S. J. 2004. *Micro-invasive breast biopsy device*.
- PICKETT, H. 2011a. Shave and punch biopsy for skin lesions. *American family physician*, 84, 995-1002.
- PICKETT, H. 2011b. Shave and punch biopsy for skin lesions. *Am Fam Physician*, 84, 995-1002.
- PISTON, D. W., FELLERS, T. J. & DAVIDSON, M. W. 2013. *Fundamentals and Applications in Multiphoton Excitation Microscopy* [Online]. Available: <http://www.microscopyu.com/articles/fluorescence/multiphoton/multiphotonintro.html> [Accessed 27 November 2014 2014].
- POLLOCK, P. M., HARPER, U. L., HANSEN, K. S., YUDT, L. M., STARK, M., ROBBINS, C. M., MOSES, T. Y., HOSTETTER, G., WAGNER, U., KAKAREKA, J., SALEM, G., POHIDA, T., HEENAN, P., DURAY, P., KALLIONIEMI, O., HAYWARD, N. K., TRENT, J. M. & MELTZER, P. S. 2003. High frequency of BRAF mutations in nevi. *Nat Genet*, 33, 19-20.
- POWELL, J. 1998. *CO<sub>2</sub> laser cutting*, London, Springer.
- PROW, T. W. U., 18 ATLANDI STREETSUNNYBANK, QUEENSLAND 4109, AU), SOYER, H. PETER (58 NEWBOLT STREET, HOLLAND PARK, QUEENSLAND 4121, AU), ANSALDO, ALEX (42 NOELA STREET, COORPAROO, QUEENSLAND 4151, AU). 2013. *A MICROBIOPSY DEVICE*. WO/2013/155557.
- QUINN, E. M., CORMICAN, P., KENNY, E. M., HILL, M., ANNEY, R., GILL, M., CORVIN, A. P. & MORRIS, D. W. 2013. Development of strategies for SNP detection in RNA-seq data: application to lymphoblastoid cell lines and evaluation using 1000 Genomes data. *PLoS One*, 8, e58815.
- RAJADHYAKSHA, M., GROSSMAN, M., ESTEROWITZ, D., WEBB, R. H. & ANDERSON, R. R. 1995. In vivo confocal scanning laser microscopy of human skin: melanin provides strong contrast. *J Invest Dermatol*, 104, 946-52.
- RAO, G., GUY, R. H., GLIKFELD, P., LACOURSE, W. R., LEUNG, L., TAMADA, J., POTTS, R. O. & AZIMI, N. 1995. Reverse iontophoresis: noninvasive glucose monitoring in vivo in humans. *Pharm Res*, 12, 1869-73.
- RAPHAEL, A. P., SUNDH, D., GRICE, J. E., ROBERTS, M. S., SOYER, H. P. & PROW, T. W. 2013. Zinc oxide nanoparticle removal from wounded human skin. *Nanomedicine (Lond)*, 8, 1751-61.
- RASMUSSEN, J. W., MARTINEZ, E., LOUKA, P. & WINGETT, D. G. 2010. Zinc oxide nanoparticles for selective destruction of tumor cells and potential for drug delivery applications. *Expert Opin Drug Deliv*, 7, 1063-77.
- RASOOLY, A., BRUCK, H. A. & KOSTOV, Y. 2013. An ELISA Lab-on-a-Chip (ELISA-LOC). *Methods Mol Biol*, 949, 451-71.
- RICHTER, A., GRIEU, F., CARRELLO, A., AMANUEL, B., NAMDARIAN, K., RYNSKA, A., LUCAS, A., MICHAEL, V., BELL, A., FOX, S. B., HEWITT, C. A., DO, H., MCARTHUR, G. A., WONG, S. Q., DOBROVIC, A. & IACOPETTA, B. 2013. A multisite blinded study for the detection of BRAF mutations in formalin-fixed, paraffin-embedded malignant melanoma. *Sci Rep*, 3, 1659.
- RISHPON, A., KIM, N., SCOPE, A., PORGES, L., OLIVIERO, M. C., BRAUN, R. P., MARGHOOB, A. A., FOX, C. A. & RABINOVITZ, H. S. 2009. Reflectance confocal microscopy criteria for squamous cell carcinomas and actinic keratoses. *Arch Dermatol*, 145, 766-72.
- RISSER, J., PRESSLEY, Z., VELEDAR, E., WASHINGTON, C. & CHEN, S. C. 2007. The impact of total body photography on biopsy rate in patients from a pigmented lesion clinic. *Journal of the American Academy of Dermatology*, 57, 428-434.

- ROBISON, A. D. & FINKELSTEIN, I. J. 2014. Rapid prototyping of multichannel microfluidic devices for single-molecule DNA curtain imaging. *Anal Chem*, 86, 4157-63.
- ROGERS, N. L., COLE, S. A., LAN, H.-C., CROSSA, A. & DEMERATH, E. W. 2007. New saliva DNA collection method compared to buccal cell collection techniques for epidemiological studies. *American Journal of Human Biology*, 19, 319-326.
- RUSSO SPENA, P., DE MADDIS, M. & LOMBARDI, F. 2014. Cut quality assessment of CO2 laser cutting of twinning-induced plasticity steel sheets. *Proceedings of the Institution of Mechanical Engineers, Part B: Journal of Engineering Manufacture*.
- SAILER, H. F., HAERS, P. E., ZOLLIKOFER, C. P., WARNKE, T., CARLS, F. R. & STUCKI, P. 1998. The value of stereolithographic models for preoperative diagnosis of craniofacial deformities and planning of surgical corrections. *Int J Oral Maxillofac Surg*, 27, 327-33.
- SALERNI, G., CARRERA, C., LOVATTO, L., PUIG-BUTILLE, J. A., BADENAS, C., PLANA, E., PUIG, S. & MALVEHY, J. 2012. Benefits of total body photography and digital dermatoscopy ("two-step method of digital follow-up") in the early diagnosis of melanoma in patients at high risk for melanoma. *Journal of the American Academy of Dermatology*, 67, e17-e27.
- SALERNI, G., TERAN, T., ALONSO, C. & FERNANDEZ-BUSSY, R. 2014. The role of dermoscopy and digital dermoscopy follow-up in the clinical diagnosis of melanoma: clinical and dermoscopic features of 99 consecutive primary melanomas. *Dermatol Pract Concept*, 4, 39-46.
- SCHMELZ, M., LUZ, O., AVERBECK, B. & BICKEL, A. 1997. Plasma extravasation and neuropeptide release in human skin as measured by intradermal microdialysis. *Neurosci Lett*, 230, 117-20.
- SCHROLNBERGER, C., BRUNNER, M., MAYER, B. X., EICHLER, H. G. & MULLER, M. 2001. Application of the minimal trauma tissue biopsy to transdermal clinical pharmacokinetic studies. *J Control Release*, 75, 297-306.
- SCHULLER-RAVOO, S., ZANT, E., FEIJEN, J. & GRIJPMA, D. W. 2014. Preparation of a designed poly(trimethylene carbonate) microvascular network by stereolithography. *Adv Healthc Mater*, 3, 2004-11.
- SEGURA, S., PUIG, S., CARRERA, C., PALOU, J. & MALVEHY, J. 2009. Development of a two-step method for the diagnosis of melanoma by reflectance confocal microscopy. *J Am Acad Dermatol*, 61, 216-29.
- SHARMA, V., SHUKLA, R. K., SAXENA, N., PARMAR, D., DAS, M. & DHAWAN, A. 2009. DNA damaging potential of zinc oxide nanoparticles in human epidermal cells. *Toxicol Lett*, 185, 211-8.
- SHIVERS, S., JAKUB, J., PENDAS, S. & REINTGEN, D. 2007. Molecular staging for patients with malignant melanoma. *Expert Rev Anticancer Ther*, 7, 1665-74.
- SINA, B., KAO, G. F., DENG, A. C. & GASPARI, A. A. 2009. Skin biopsy for inflammatory and common neoplastic skin diseases: optimum time, best location and preferred techniques. A critical review. *J Cutan Pathol*, 36, 505-10.
- SMITH, L. E., HEARNDEN, V., LU, Z., SMALLWOOD, R., HUNTER, K. D., MATCHER, S. J., THORNHILL, M. H., MURDOCH, C. & MACNEIL, S. 2011. Evaluating the use of optical coherence tomography for the detection of epithelial cancers in vitro. *Journal of Biomedical Optics*, 16, 116015-1160158.
- SOYER, H. P., ARGENZIANO, G., HOFMANN-WELLENHOF, R. & ZALAUDEK, I. 2011. *Dermoscopy: The Essentials*, Elsevier Health Sciences UK.
- SPRUESSEL, A., STEIMANN, G., JUNG, M., LEE, S. A., CARR, T., FENTZ, A. K., SPANGENBERG, J., ZORNIG, C., JUHL, H. H. & DAVID, K. A. 2004. Tissue ischemia time affects gene and protein expression patterns within minutes following surgical tumor excision. *Biotechniques*, 36, 1030-7.
- STAFF, S., KUJALA, P., KARHU, R., ROKMAN, A., ILVESARO, J., KARES, S. & ISOLA, J. 2013. Preservation of nucleic acids and tissue morphology in paraffin-embedded clinical samples: comparison of five molecular fixatives. *J Clin Pathol*, 66, 807-10.



- STAHLBERG, A. & BENGTSSON, M. 2010. Single-cell gene expression profiling using reverse transcription quantitative real-time PCR. *Methods*, 50, 282-8.
- STEEN, W. M. & MAZUMDER, J. 2010. Laser Material Processing, 4th Edition. *Laser Material Processing, 4th Edition*, 1-558.
- STURM, R. A., DUFFY, D. L., ZHAO, Z. Z., LEITE, F. P., STARK, M. S., HAYWARD, N. K., MARTIN, N. G. & MONTGOMERY, G. W. 2008. A single SNP in an evolutionary conserved region within intron 86 of the HERC2 gene determines human blue-brown eye color. *Am J Hum Genet*, 82, 424-31.
- SWANSON, N. A., LEE, K. K., GORMAN, A. & LEE, H. N. 2002. Biopsy techniques. Diagnosis of melanoma. *Dermatol Clin*, 20, 677-80.
- TAN, J. M., LIN, L. L., LAMBIE, D., FLEWELL-SMITH, R., JAGIRDAR, K., SCHAIDER, H., STURM, R. A., PROW, T. W. & SOYER, H. P. 2015. BRAF Wild-Type Melanoma in Situ Arising In a BRAF V600E Mutant Dysplastic Nevus. *JAMA Dermatol*.
- TANIGUCHI, K., KAJIYAMA, T. & KAMBARA, H. 2009. Quantitative analysis of gene expression in a single cell by qPCR. *Nat Methods*, 6, 503-6.
- TAYLOR, C. R. 2000. The total test approach to standardization of immunohistochemistry. *Arch Pathol Lab Med*, 124, 945-51.
- THOMAS, N. E. 2006. BRAF somatic mutations in malignant melanoma and melanocytic naevi. *Melanoma Res*, 16, 97-103.
- TSCHANDL, P., BERGHOF, A. S., PREUSSER, M., BURGSTALLER-MUEHLBACHER, S., PEHAMBERGER, H., OKAMOTO, I. & KITTLER, H. 2013. NRAS and BRAF mutations in melanoma-associated nevi and uninvolved nevi. *PLoS One*, 8, e69639.
- UGUREL, S., UTIKAL, J. & BECKER, J. C. 2009. Tumor biomarkers in melanoma. *Cancer control : journal of the Moffitt Cancer Center*, 16, 219-24.
- ULRICH, M., MALTUSCH, A., RIUS-DIAZ, F., ROWERT-HUBER, J., GONZALEZ, S., STERRY, W., STOCKFLETH, E. & ASTNER, S. 2008. Clinical applicability of in vivo reflectance confocal microscopy for the diagnosis of actinic keratoses. *Dermatol Surg*, 34, 610-9.
- USLAN, I. 2005. CO2 laser cutting: kerf width variation during cutting. *Proceedings of the Institution of Mechanical Engineers Part B-Journal of Engineering Manufacture*, 219, 571-577.
- VERBAAN, F. J., BAL, S. M., VAN DEN BERG, D. J., DIJKSMAN, J. A., VAN HECKE, M., VERPOORTEN, H., VAN DEN BERG, A., LUTTGE, R. & BOUWSTRA, J. A. 2008. Improved piercing of microneedle arrays in dermatomed human skin by an impact insertion method. *Journal of Controlled Release*, 128, 80-88.
- VILUMSONE-NEMES, I. 2012. *Industrial Cutting of Textile Materials*, Elsevier Science.
- WACHSMAN, W., MORHENN, V., PALMER, T., WALLS, L., HATA, T., ZALLA, J., SCHEINBERG, R., SOFEN, H., MRAZ, S., GROSS, K., RABINOVITZ, H., POLSKY, D. & CHANG, S. 2011. Noninvasive genomic detection of melanoma. *Br J Dermatol*, 164, 797-806.
- WALZIK, M. P., VOLLMAR, V., LACHNIT, T., DIETZ, H., HAUG, S., BACHMANN, H., FATH, M., ASCHENBRENNER, D., ABOLPOUR MOFRAD, S., FRIEDRICH, O. & GILBERT, D. F. 2015. A portable low-cost long-term live-cell imaging platform for biomedical research and education. *Biosens Bioelectron*, 64, 639-49.
- WANG, J. 2000. An Experimental Analysis and Optimisation of the CO2 Laser Cutting Process for Metallic Coated Sheet Steels. *The International Journal of Advanced Manufacturing Technology*, 16, 334-340.
- WANG, J. 2003. *Abrasive waterjet machining of engineering materials*, Trans Tech Publications Ltd.
- WANG, S. Q., DUSZA, S. W., SCOPE, A., BRAUN, R. P., KOPF, A. W. & MARGHOUB, A. A. 2008. Differences in Dermoscopic Images from Nonpolarized Dermoscope and Polarized Dermoscope Influence the Diagnostic Accuracy and Confidence Level: A Pilot Study. *Dermatologic Surgery*, 34, 1389-1395.
- WANG, S. Q. & TOOLEY, I. R. 2011. Photoprotection in the era of nanotechnology. *Semin Cutan Med Surg*, 30, 210-3.

- WANG, Z., GERSTEIN, M. & SNYDER, M. 2009. RNA-Seq: a revolutionary tool for transcriptomics. *Nat Rev Genet*, 10, 57-63.
- WEIBEL, D. B., DILUZIO, W. R. & WHITESIDES, G. M. 2007. Microfabrication meets microbiology. *Nat Rev Microbiol*, 5, 209-18.
- WINDER, J. & BIBB, R. 2005. Medical rapid prototyping technologies: state of the art and current limitations for application in oral and maxillofacial surgery. *J Oral Maxillofac Surg*, 63, 1006-15.
- WONG, K. V. & HERNANDEZ, A. 2012. A Review of Additive Manufacturing. *ISRN Mechanical Engineering*, 2012, 10.
- WURM, E. M., LONGO, C., CURCHIN, C., SOYER, H. P., PROW, T. W. & PELLACANI, G. 2012. In vivo assessment of chronological ageing and photoageing in forearm skin using reflectance confocal microscopy. *Br J Dermatol*, 167, 270-9.
- XIA, X. R., MONTEIRO-RIVIERE, N. A., MATHUR, S., SONG, X., XIAO, L., OLDENBERG, S. J., FADEEL, B. & RIVIERE, J. E. 2011. Mapping the surface adsorption forces of nanomaterials in biological systems. *ACS Nano*, 5, 9074-81.
- YILBAŞ, B. S. 1996. Experimental investigation into CO2 laser cutting parameters. *Journal of Materials Processing Technology*, 58, 323-330.
- YILBAS, B. S., AKHTAR, S. S., BAYRAKTAR, E. & GASEM, Z. 2012. Laser cutting of thin aluminum and silicon alloy: Influence of laser power on kerf width. *Advanced Materials Research*.
- ZEBARY, A., OMHOLT, K., VAN DOORN, R., GHIORZO, P., HARBST, K., HERTZMAN JOHANSSON, C., HOIOM, V., JONSSON, G., PJANOVA, D., PUIG, S., SCARRA, G. B., HARLAND, M., OLSSON, H., EGYHAZI BRAGE, S., PALMER, J., KANTER-LEWENSOHN, L., VASSILAKI, I., HAYWARD, N. K., NEWTON-BISHOP, J., GRUIS, N. A., HANSSON, J. & MELANOMA GENETICS, C. 2014. Somatic BRAF and NRAS mutations in familial melanomas with known germline CDKN2A status: a GenoMEL study. *J Invest Dermatol*, 134, 287-90.
- ZIAIE, B., BALDI, A., LEI, M., GU, Y. & SIEGEL, R. A. 2004. Hard and soft micromachining for BioMEMS: review of techniques and examples of applications in microfluidics and drug delivery. *Advanced Drug Delivery Reviews*, 56, 145-172.
- ZIMMER, L., HILLEN, U., LIVINGSTONE, E., LACOUTURE, M. E., BUSAM, K., CARVAJAL, R. D., EGBERTS, F., HAUSCHILD, A., KASHANI-SABET, M., GOLDINGER, S. M., DUMMER, R., LONG, G. V., MCARTHUR, G., SCHERAG, A., SUCKER, A. & SCHADENDORF, D. 2012. Atypical melanocytic proliferations and new primary melanomas in patients with advanced melanoma undergoing selective BRAF inhibition. *J Clin Oncol*, 30, 2375-83.
- ZUBER, T. J. 2002. Punch biopsy of the skin. *Am Fam Physician*, 65, 1155-8, 1161-2, 1164.
- ZUBER, T. J. 2003. Fusiform excision. *Am Fam Physician*, 67, 1539-44, 1547-8, 1550.

## Appendices

### Appendix 1 – p53/Rb Pathway Mutation PCR Array Genotype Call (n=4)

Position	Gene	COSMIC ID	nt change	AA change	AKSFS15-L1 NA	AKSFS15-L1 A	AKSFS15-L1 MB2	AKSFS15-L1 MB3	AKSFS15-L1 MB4
A01	ATM	21826	c.2572T>C	p.F858L	-	-	-	-	-
A02	ATM	12951	c.7325A>C	p.Q2442P	-	-	-	-	-
A03	ATM	20404	c.7328G>A	p.R2443Q	-	-	-	-	-
A04	ATM	21642	c.9022C>T	p.R3008C	-	-	-	-	-
A05	ATM	21626	c.9023G>A	p.R3008H	-	-	-	-	-
A06	ATM	21624	c.9139C>T	p.R3047*	-	-	-	-	-
A07	CDKN2A	13653	c.128G>T	p.S43I	-	-	-	-	-
A08	CDKN2A	12743	c.143C>T	p.P48L	-	-	-	-	-
A09	CDKN2A	12484	c.322G>A	p.D108N	-	-	-	-	-
A10	CDKN2A	13520	c.322G>C	p.D108H	-	-	-	-	-
A11	CDKN2A	13489	c.322G>T	p.D108Y	-	-	-	-	-
A12	CDKN2A	12481	c.329G>A	p.W110*	-	-	-	-	-

B01	CDKN2A	12547	c.330G>A	p.W110*	+	+	+	+	+
B02	CDKN2A	12476	c.341C>T	p.P114L	-	-	-	-	-
B03	CDKN2A	12479	c.358G>T	p.E120*	-	-	-	-	-
B04	RB1	887	c.1654C>T	p.R552*	-	-	-	-	-
B05	RB1	888	c.1666C>T	p.R556*	-	-	-	-	-
B06	RB1	861	c.1981C>T	p.R661W	-	-	-	-	-
B07	TP53	11073	c.1024C>T	p.R342*	-	-	-	-	-
B08	TP53	11582	c.395A>G	p.K132R	-	-	-	-	-
B09	TP53	10801	c.404G>A	p.C135Y	-	-	-	-	-
B10	TP53	10647	c.404G>T	p.C135F	-	-	-	-	-
B11	TP53	43708	c.422G>A	p.C141Y	-	-	-	-	-
B12	TP53	43609	c.437G>A	p.W146*	-	-	-	-	-
C01	TP53	10727	c.438G>A	p.W146*	-	-	-	-	+/-
C02	TP53	10905	c.451C>T	p.P151S	-	-	-	-	-
C03	TP53	10790	c.455C>T	p.P152L	-	-	-	-	-
C04	TP53	6815	c.461G>T	p.G154V	-	-	-	-	-

C05	TP53	10670	c.469G>T	p.V157F	-	-	-	-	-
C06	TP53	10690	c.473G>A	p.R158H	-	-	-	-	-
C07	TP53	10714	c.473G>T	p.R158L	-	-	-	-	-
C08	TP53	11148	c.476C>T	p.A159V	-	-	-	-	-
C09	TP53	10739	c.481G>A	p.A161T	-	-	-	-	-
C10	TP53	10808	c.488A>G	p.Y163C	-	-	-	-	-
C11	TP53	11084	c.517G>A	p.V173M	-	-	-	-	-
C12	TP53	43559	c.517G>T	p.V173L	-	-	-	-	-
D01	TP53	10648	c.524G>A	p.R175H	-	-	-	-	-
D02	TP53	10687	c.527G>A	p.C176Y	-	-	-	-	-
D03	TP53	10645	c.527G>T	p.C176F	-	-	-	-	-
D04	TP53	10768	c.535C>T	p.H179Y	-	+/-	+/-	-	+
D05	TP53	10889	c.536A>G	p.H179R	-	-	-	-	-
D06	TP53	43635	c.536A>T	p.H179L	-	-	+	-	-
D07	TP53	10733	c.574C>T	p.Q192*	-	-	-	-	-
D08	TP53	10742	c.578A>G	p.H193R	-	-	-	-	-

D09	TP53	11066	c.578A>T	p.H193L	-	-	-	-	-
D10	TP53	11089	c.584T>C	p.I195T	-	-	-	-	-
D11	TP53	10705	c.586C>T	p.R196*	-	-	-	-	-
D12	TP53	43947	c.614A>G	p.Y205C	-	-	-	-	-
E01	TP53	10654	c.637C>T	p.R213*	-	-	-	-	-
E02	TP53	43687	c.641A>G	p.H214R	-	-	-	-	-
E03	TP53	10667	c.646G>A	p.V216M	-	-	-	-	-
E04	TP53	10758	c.659A>G	p.Y220C	-	-	-	-	-
E05	TP53	10725	c.701A>G	p.Y234C	-	-	-	-	-
E06	TP53	10731	c.707A>G	p.Y236C	-	-	-	-	-
E07	TP53	10834	c.711G>A	p.M237I	-	-	-	-	-
E08	TP53	11059	c.713G>A	p.C238Y	-	-	-	-	-
E09	TP53	10777	c.715A>G	p.N239D	-	-	-	-	-
E10	TP53	10812	c.722C>T	p.S241F	-	-	+/-	-	-
E11	TP53	10646	c.725G>A	p.C242Y	-	-	-	-	-
E12	TP53	10810	c.725G>T	p.C242F	-	-	-	-	-

F01	TP53	10941	c.730G>A	p.G244S	-	-	-	-	-
F02	TP53	11524	c.730G>T	p.G244C	-	-	-	-	-
F03	TP53	10883	c.731G>A	p.G244D	-	-	-	-	-
F04	TP53	6932	c.733G>A	p.G245S	-	-	-	-	-
F05	TP53	11081	c.733G>T	p.G245C	-	-	-	-	-
F06	TP53	43606	c.734G>A	p.G245D	-	-	-	-	-
F07	TP53	11196	c.734G>T	p.G245V	-	-	-	-	-
F08	TP53	10656	c.742C>T	p.R248W	-	-	-	-	-
F09	TP53	10662	c.743G>A	p.R248Q	-	-	-	-	-
F10	TP53	6549	c.743G>T	p.R248L	-	-	-	-	-
F11	TP53	10817	c.747G>T	p.R249S	-	-	-	-	-
F12	TP53	10771	c.749C>T	p.P250L	-	-	-	-	-
G01	TP53	10988	c.772G>A	p.E258K	-	-	-	-	-
G02	TP53	10867	c.797G>A	p.G266E	-	-	-	-	-
G03	TP53	10891	c.814G>A	p.V272M	-	-	-	-	-
G04	TP53	10659	c.817C>T	p.R273C	-	-	-	-	-

G05	TP53	10660	c.818G>A	p.R273H	-	-	-	-	-
G06	TP53	10779	c.818G>T	p.R273L	-	-	-	-	-
G07	TP53	10893	c.824G>A	p.C275Y	-	-	-	-	-
G08	TP53	10701	c.824G>T	p.C275F	-	-	-	-	-
G09	TP53	10939	c.832C>T	p.P278S	-	-	+/-	-	-
G10	TP53	10863	c.833C>T	p.P278L	-	-	+	-	-
G11	TP53	43714	c.836G>A	p.G279E	-	-	-	-	-
G12	TP53	10728	c.839G>A	p.R280K	-	-	-	-	-
H01	TP53	10724	c.839G>C	p.R280T	-	-	-	-	-
H02	TP53	10704	c.844C>T	p.R282W	-	+/-	-	-	+/-
H03	TP53	10722	c.853G>A	p.E285K	-	-	-	-	-
H04	TP53	10726	c.856G>A	p.E286K	-	-	-	-	-
H05	TP53	10856	c.880G>T	p.E294*	-	-	-	-	-
H06	TP53	10710	c.892G>T	p.E298*	-	-	-	-	-



Position	Gene	COSMIC ID	nt change	AA change	AKSFS30-L2 NA	AKSFS30-L2 A	AKSFS30-L2 MB 1	AKSFS30-L2 MB 2	AKSFS30-L2 MB 3
A01	ATM	21826	c.2572T>C	p.F858L	-	-	-	-	-
A02	ATM	12951	c.7325A>C	p.Q2442P	-	-	-	-	-
A03	ATM	20404	c.7328G>A	p.R2443Q	-	-	-	-	-
A04	ATM	21642	c.9022C>T	p.R3008C	-	-	-	-	-
A05	ATM	21626	c.9023G>A	p.R3008H	-	-	-	-	-
A06	ATM	21624	c.9139C>T	p.R3047*	-	-	-	-	-
A07	CDKN2A	13653	c.128G>T	p.S43I	-	-	-	-	-
A08	CDKN2A	12743	c.143C>T	p.P48L	-	-	-	-	-
A09	CDKN2A	12484	c.322G>A	p.D108N	-	-	-	-	-
A10	CDKN2A	13520	c.322G>C	p.D108H	-	-	-	-	-
A11	CDKN2A	13489	c.322G>T	p.D108Y	-	-	-	-	-
A12	CDKN2A	12481	c.329G>A	p.W110*	-	-	-	-	-
B01	CDKN2A	12547	c.330G>A	p.W110*	-	-	-	-	-
B02	CDKN2A	12476	c.341C>T	p.P114L	-	-	-	-	-
B03	CDKN2A	12479	c.358G>T	p.E120*	-	-	-	-	-

B04	RB1	887	c.1654C>T	p.R552*	-	-	-	-	-
B05	RB1	888	c.1666C>T	p.R556*	-	-	-	-	-
B06	RB1	861	c.1981C>T	p.R661W	-	-	-	-	-
B07	TP53	11073	c.1024C>T	p.R342*	-	-	-	-	-
B08	TP53	11582	c.395A>G	p.K132R	-	-	-	-	-
B09	TP53	10801	c.404G>A	p.C135Y	-	-	-	-	-
B10	TP53	10647	c.404G>T	p.C135F	-	-	-	-	-
B11	TP53	43708	c.422G>A	p.C141Y	-	+/-	+/-	-	+/-
B12	TP53	43609	c.437G>A	p.W146*	-	-	-	-	-
C01	TP53	10727	c.438G>A	p.W146*	-	-	-	-	+/-
C02	TP53	10905	c.451C>T	p.P151S	-	-	-	-	-
C03	TP53	10790	c.455C>T	p.P152L	-	-	-	-	-
C04	TP53	6815	c.461G>T	p.G154V	-	-	-	-	-
C05	TP53	10670	c.469G>T	p.V157F	-	-	-	-	-
C06	TP53	10690	c.473G>A	p.R158H	-	-	-	-	-
C07	TP53	10714	c.473G>T	p.R158L	-	-	-	-	-

C08	TP53	11148	c.476C>T	p.A159V	-	-	-	-	-
C09	TP53	10739	c.481G>A	p.A161T	-	-	-	-	-
C10	TP53	10808	c.488A>G	p.Y163C	-	-	-	-	-
C11	TP53	11084	c.517G>A	p.V173M	-	-	-	-	-
C12	TP53	43559	c.517G>T	p.V173L	-	-	-	-	-
D01	TP53	10648	c.524G>A	p.R175H	-	-	-	-	-
D02	TP53	10687	c.527G>A	p.C176Y	-	-	-	-	-
D03	TP53	10645	c.527G>T	p.C176F	-	-	-	-	-
D04	TP53	10768	c.535C>T	p.H179Y	-	+	+/-	+/-	+/-
D05	TP53	10889	c.536A>G	p.H179R	-	-	-	-	-
D06	TP53	43635	c.536A>T	p.H179L	-	+/-	+/-	+/-	-
D07	TP53	10733	c.574C>T	p.Q192*	-	-	-	-	-
D08	TP53	10742	c.578A>G	p.H193R	-	-	-	-	-
D09	TP53	11066	c.578A>T	p.H193L	-	-	-	-	-
D10	TP53	11089	c.584T>C	p.I195T	-	-	-	-	-
D11	TP53	10705	c.586C>T	p.R196*	-	-	-	-	-

D12	TP53	43947	c.614A>G	p.Y205C	-	-	-	-	-
E01	TP53	10654	c.637C>T	p.R213*	-	-	-	-	-
E02	TP53	43687	c.641A>G	p.H214R	-	-	-	-	-
E03	TP53	10667	c.646G>A	p.V216M	-	-	-	-	-
E04	TP53	10758	c.659A>G	p.Y220C	-	-	-	-	-
E05	TP53	10725	c.701A>G	p.Y234C	-	-	-	-	-
E06	TP53	10731	c.707A>G	p.Y236C	-	-	-	-	-
E07	TP53	10834	c.711G>A	p.M237I	-	-	-	-	-
E08	TP53	11059	c.713G>A	p.C238Y	-	-	-	-	-
E09	TP53	10777	c.715A>G	p.N239D	-	-	-	-	-
E10	TP53	10812	c.722C>T	p.S241F	-	-	+/-	-	-
E11	TP53	10646	c.725G>A	p.C242Y	-	-	-	-	-
E12	TP53	10810	c.725G>T	p.C242F	-	-	-	-	-
F01	TP53	10941	c.730G>A	p.G244S	-	-	-	-	-
F02	TP53	11524	c.730G>T	p.G244C	-	-	-	-	-
F03	TP53	10883	c.731G>A	p.G244D	-	-	-	-	-

F04	TP53	6932	c.733G>A	p.G245S	-	-	-	-	-
F05	TP53	11081	c.733G>T	p.G245C	-	-	-	-	-
F06	TP53	43606	c.734G>A	p.G245D	-	-	-	-	-
F07	TP53	11196	c.734G>T	p.G245V	-	-	-	-	-
F08	TP53	10656	c.742C>T	p.R248W	-	-	-	-	-
F09	TP53	10662	c.743G>A	p.R248Q	-	-	-	-	-
F10	TP53	6549	c.743G>T	p.R248L	-	-	-	-	-
F11	TP53	10817	c.747G>T	p.R249S	-	-	-	-	-
F12	TP53	10771	c.749C>T	p.P250L	-	-	-	-	-
G01	TP53	10988	c.772G>A	p.E258K	-	-	-	-	-
G02	TP53	10867	c.797G>A	p.G266E	-	-	-	-	-
G03	TP53	10891	c.814G>A	p.V272M	-	-	-	-	-
G04	TP53	10659	c.817C>T	p.R273C	-	-	-	-	-
G05	TP53	10660	c.818G>A	p.R273H	-	-	-	-	-
G06	TP53	10779	c.818G>T	p.R273L	-	-	-	-	-
G07	TP53	10893	c.824G>A	p.C275Y	-	-	-	-	-

G08	TP53	10701	c.824G>T	p.C275F	-	-	-	-	-
G09	TP53	10939	c.832C>T	p.P278S	-	+	-	-	-
G10	TP53	10863	c.833C>T	p.P278L	-	+/-	-	-	-
G11	TP53	43714	c.836G>A	p.G279E	-	-	-	-	-
G12	TP53	10728	c.839G>A	p.R280K	-	-	-	-	-
H01	TP53	10724	c.839G>C	p.R280T	-	-	-	-	-
H02	TP53	10704	c.844C>T	p.R282W	-	+/-	-	-	-
H03	TP53	10722	c.853G>A	p.E285K	-	-	-	-	-
H04	TP53	10726	c.856G>A	p.E286K	-	-	-	-	-
H05	TP53	10856	c.880G>T	p.E294*	-	-	-	-	-
H06	TP53	10710	c.892G>T	p.E298*	-	-	-	-	-

Position	Gene	COSMIC ID	nt change	AA change	VH006-RJW-L1 NA	VH006-RJW-L1 A	VH006-RJW-L1 MB1	VH006-RJW-L1 MB2	VH006-RJW-L1 MB4
A01	ATM	21826	c.2572T>C	p.F858L	-	-	-	-	-
A02	ATM	12951	c.7325A>C	p.Q2442P	-	-	-	-	-
A03	ATM	20404	c.7328G>A	p.R2443Q	-	-	-	-	-
A04	ATM	21642	c.9022C>T	p.R3008C	-	-	-	-	-
A05	ATM	21626	c.9023G>A	p.R3008H	-	-	-	-	-
A06	ATM	21624	c.9139C>T	p.R3047*	-	-	+	-	-
A07	CDKN2A	13653	c.128G>T	p.S43I	-	-	-	-	-
A08	CDKN2A	12743	c.143C>T	p.P48L	-	-	-	-	-
A09	CDKN2A	12484	c.322G>A	p.D108N	-	-	-	-	-
A10	CDKN2A	13520	c.322G>C	p.D108H	-	-	-	-	-
A11	CDKN2A	13489	c.322G>T	p.D108Y	-	-	-	-	-
A12	CDKN2A	12481	c.329G>A	p.W110*	-	-	-	-	-
B01	CDKN2A	12547	c.330G>A	p.W110*	-	-	-	-	-
B02	CDKN2A	12476	c.341C>T	p.P114L	-	-	-	-	-

B03	CDKN2A	12479	c.358G>T	p.E120*	-	+/-	-	-	-
B04	RB1	887	c.1654C>T	p.R552*	-	-	-	-	-
B05	RB1	888	c.1666C>T	p.R556*	-	-	-	-	-
B06	RB1	861	c.1981C>T	p.R661W	-	-	-	-	-
B07	TP53	11073	c.1024C>T	p.R342*	-	-	-	-	-
B08	TP53	11582	c.395A>G	p.K132R	-	-	-	-	-
B09	TP53	10801	c.404G>A	p.C135Y	-	-	-	-	-
B10	TP53	10647	c.404G>T	p.C135F	-	-	-	-	-
B11	TP53	43708	c.422G>A	p.C141Y	-	+/-	-	+/-	-
B12	TP53	43609	c.437G>A	p.W146*	-	-	-	-	-
C01	TP53	10727	c.438G>A	p.W146*	-	+/-	-	+/-	+
C02	TP53	10905	c.451C>T	p.P151S	-	-	-	-	-
C03	TP53	10790	c.455C>T	p.P152L	-	-	-	-	-
C04	TP53	6815	c.461G>T	p.G154V	-	-	-	-	-
C05	TP53	10670	c.469G>T	p.V157F	-	-	-	-	-
C06	TP53	10690	c.473G>A	p.R158H	-	-	-	-	-



C07	TP53	10714	c.473G>T	p.R158L	-	-	-	-	-
C08	TP53	11148	c.476C>T	p.A159V	-	-	-	-	-
C09	TP53	10739	c.481G>A	p.A161T	-	-	-	-	-
C10	TP53	10808	c.488A>G	p.Y163C	-	-	-	-	-
C11	TP53	11084	c.517G>A	p.V173M	-	-	-	-	-
C12	TP53	43559	c.517G>T	p.V173L	-	-	-	-	-
D01	TP53	10648	c.524G>A	p.R175H	-	-	-	-	-
D02	TP53	10687	c.527G>A	p.C176Y	-	-	-	-	-
D03	TP53	10645	c.527G>T	p.C176F	-	-	-	-	-
D04	TP53	10768	c.535C>T	p.H179Y	-	+	-	+/-	+/-
D05	TP53	10889	c.536A>G	p.H179R	-	-	-	-	-
D06	TP53	43635	c.536A>T	p.H179L	-	+/-	-	-	+/-
D07	TP53	10733	c.574C>T	p.Q192*	-	-	-	-	-
D08	TP53	10742	c.578A>G	p.H193R	-	-	-	-	-
D09	TP53	11066	c.578A>T	p.H193L	-	-	-	-	-
D10	TP53	11089	c.584T>C	p.I195T	-	-	-	-	-

D11	TP53	10705	c.586C>T	p.R196*	-	-	-	-	-
D12	TP53	43947	c.614A>G	p.Y205C	-	-	-	-	-
E01	TP53	10654	c.637C>T	p.R213*	-	-	-	-	-
E02	TP53	43687	c.641A>G	p.H214R	-	-	-	-	-
E03	TP53	10667	c.646G>A	p.V216M	-	-	-	-	-
E04	TP53	10758	c.659A>G	p.Y220C	-	-	-	-	-
E05	TP53	10725	c.701A>G	p.Y234C	-	-	-	-	-
E06	TP53	10731	c.707A>G	p.Y236C	-	-	-	-	-
E07	TP53	10834	c.711G>A	p.M237I	-	-	-	-	-
E08	TP53	11059	c.713G>A	p.C238Y	-	-	-	-	-
E09	TP53	10777	c.715A>G	p.N239D	-	-	-	-	-
E10	TP53	10812	c.722C>T	p.S241F	-	-	-	-	-
E11	TP53	10646	c.725G>A	p.C242Y	-	-	-	-	-
E12	TP53	10810	c.725G>T	p.C242F	-	-	-	-	-
F01	TP53	10941	c.730G>A	p.G244S	-	-	-	-	-
F02	TP53	11524	c.730G>T	p.G244C	-	-	-	-	-

F03	TP53	10883	c.731G>A	p.G244D	-	-	-	-	-
F04	TP53	6932	c.733G>A	p.G245S	-	-	-	-	-
F05	TP53	11081	c.733G>T	p.G245C	-	-	-	-	-
F06	TP53	43606	c.734G>A	p.G245D	-	-	-	-	-
F07	TP53	11196	c.734G>T	p.G245V	-	-	-	-	-
F08	TP53	10656	c.742C>T	p.R248W	-	-	-	-	-
F09	TP53	10662	c.743G>A	p.R248Q	-	-	-	-	-
F10	TP53	6549	c.743G>T	p.R248L	-	-	-	-	-
F11	TP53	10817	c.747G>T	p.R249S	-	-	-	-	-
F12	TP53	10771	c.749C>T	p.P250L	-	-	-	-	-
G01	TP53	10988	c.772G>A	p.E258K	-	-	-	-	-
G02	TP53	10867	c.797G>A	p.G266E	-	-	-	-	-
G03	TP53	10891	c.814G>A	p.V272M	-	-	-	-	-
G04	TP53	10659	c.817C>T	p.R273C	-	-	-	-	-
G05	TP53	10660	c.818G>A	p.R273H	-	-	-	-	-
G06	TP53	10779	c.818G>T	p.R273L	-	-	-	-	-

G07	TP53	10893	c.824G>A	p.C275Y	-	-	-	-	-
G08	TP53	10701	c.824G>T	p.C275F	-	-	-	-	-
G09	TP53	10939	c.832C>T	p.P278S	-	-	+/-	-	-
G10	TP53	10863	c.833C>T	p.P278L	-	+/-	-	+/-	+/-
G11	TP53	43714	c.836G>A	p.G279E	-	-	-	-	-
G12	TP53	10728	c.839G>A	p.R280K	-	-	-	-	-
H01	TP53	10724	c.839G>C	p.R280T	-	-	-	-	-
H02	TP53	10704	c.844C>T	p.R282W	-	-	+/-	+/-	-
H03	TP53	10722	c.853G>A	p.E285K	-	-	-	-	-
H04	TP53	10726	c.856G>A	p.E286K	-	-	-	-	-
H05	TP53	10856	c.880G>T	p.E294*	-	-	-	-	-
H06	TP53	10710	c.892G>T	p.E298*	-	-	-	-	-

Position	Gene	COSMIC ID	nt change	AA change	VH009-AKH-L1 NA	VH009-AKH-L1 A	VH009-AKH-L1 MB1	VH009-AKH-L1 MB2	VH009-AKH-L1 MB3
A01	ATM	21826	c.2572T>C	p.F858L	-	-	-	-	-
A02	ATM	12951	c.7325A>C	p.Q2442P	-	-	-	-	-
A03	ATM	20404	c.7328G>A	p.R2443Q	-	-	-	-	-
A04	ATM	21642	c.9022C>T	p.R3008C	-	-	-	-	-
A05	ATM	21626	c.9023G>A	p.R3008H	-	-	-	-	-
A06	ATM	21624	c.9139C>T	p.R3047*	-	-	-	-	-
A07	CDKN2A	13653	c.128G>T	p.S43I	-	-	-	-	-
A08	CDKN2A	12743	c.143C>T	p.P48L	-	-	-	-	-
A09	CDKN2A	12484	c.322G>A	p.D108N	-	-	-	-	-
A10	CDKN2A	13520	c.322G>C	p.D108H	-	-	-	-	-
A11	CDKN2A	13489	c.322G>T	p.D108Y	-	-	-	-	-
A12	CDKN2A	12481	c.329G>A	p.W110*	-	-	-	-	-
B01	CDKN2A	12547	c.330G>A	p.W110*	-	-	-	-	-
B02	CDKN2A	12476	c.341C>T	p.P114L	-	-	-	-	-

B03	CDKN2A	12479	c.358G>T	p.E120*	-	-	-	-	-
B04	RB1	887	c.1654C>T	p.R552*	-	-	-	-	-
B05	RB1	888	c.1666C>T	p.R556*	-	-	-	-	-
B06	RB1	861	c.1981C>T	p.R661W	-	-	-	-	-
B07	TP53	11073	c.1024C>T	p.R342*	-	-	-	-	-
B08	TP53	11582	c.395A>G	p.K132R	-	-	+/-	-	-
B09	TP53	10801	c.404G>A	p.C135Y	-	+/-	+	-	-
B10	TP53	10647	c.404G>T	p.C135F	-	-	-	-	-
B11	TP53	43708	c.422G>A	p.C141Y	-	+/-	+	-	+/-
B12	TP53	43609	c.437G>A	p.W146*	-	-	+	-	-
C01	TP53	10727	c.438G>A	p.W146*	-	+/-	+	-	-
C02	TP53	10905	c.451C>T	p.P151S	-	-	-	-	-
C03	TP53	10790	c.455C>T	p.P152L	-	-	-	-	-
C04	TP53	6815	c.461G>T	p.G154V	-	-	-	-	-
C05	TP53	10670	c.469G>T	p.V157F	-	-	-	-	-
C06	TP53	10690	c.473G>A	p.R158H	-	-	+	-	-

C07	TP53	10714	c.473G>T	p.R158L	-	-	-	-	-
C08	TP53	11148	c.476C>T	p.A159V	-	-	-	-	-
C09	TP53	10739	c.481G>A	p.A161T	-	-	-	-	-
C10	TP53	10808	c.488A>G	p.Y163C	-	-	-	-	-
C11	TP53	11084	c.517G>A	p.V173M	-	-	+/-	-	-
C12	TP53	43559	c.517G>T	p.V173L	-	-	-	-	-
D01	TP53	10648	c.524G>A	p.R175H	-	-	-	-	-
D02	TP53	10687	c.527G>A	p.C176Y	-	-	+	-	-
D03	TP53	10645	c.527G>T	p.C176F	-	-	-	-	-
D04	TP53	10768	c.535C>T	p.H179Y	-	+/-	+	-	+/-
D05	TP53	10889	c.536A>G	p.H179R	-	-	-	-	-
D06	TP53	43635	c.536A>T	p.H179L	-	+	+	-	-
D07	TP53	10733	c.574C>T	p.Q192*	-	-	-	-	-
D08	TP53	10742	c.578A>G	p.H193R	-	-	-	-	-
D09	TP53	11066	c.578A>T	p.H193L	-	-	-	-	-
D10	TP53	11089	c.584T>C	p.I195T	-	-	+	-	-

D11	TP53	10705	c.586C>T	p.R196*	-	-	-	-	-
D12	TP53	43947	c.614A>G	p.Y205C	-	-	-	-	+
E01	TP53	10654	c.637C>T	p.R213*	-	-	+/-	-	-
E02	TP53	43687	c.641A>G	p.H214R	-	-	-	-	-
E03	TP53	10667	c.646G>A	p.V216M	-	-	-	-	-
E04	TP53	10758	c.659A>G	p.Y220C	-	-	-	-	-
E05	TP53	10725	c.701A>G	p.Y234C	-	-	-	-	-
E06	TP53	10731	c.707A>G	p.Y236C	-	-	-	-	-
E07	TP53	10834	c.711G>A	p.M237I	-	-	-	-	-
E08	TP53	11059	c.713G>A	p.C238Y	-	-	-	-	-
E09	TP53	10777	c.715A>G	p.N239D	-	-	-	-	-
E10	TP53	10812	c.722C>T	p.S241F	-	+/-	+/-	-	-
E11	TP53	10646	c.725G>A	p.C242Y	-	-	-	-	-
E12	TP53	10810	c.725G>T	p.C242F	-	-	-	-	-
F01	TP53	10941	c.730G>A	p.G244S	-	-	-	-	-
F02	TP53	11524	c.730G>T	p.G244C	-	-	-	-	-



F03	TP53	10883	c.731G>A	p.G244D	-	-	-	-	-
F04	TP53	6932	c.733G>A	p.G245S	-	-	-	-	-
F05	TP53	11081	c.733G>T	p.G245C	-	-	-	-	-
F06	TP53	43606	c.734G>A	p.G245D	-	-	-	-	-
F07	TP53	11196	c.734G>T	p.G245V	-	-	-	-	-
F08	TP53	10656	c.742C>T	p.R248W	-	-	-	-	-
F09	TP53	10662	c.743G>A	p.R248Q	-	-	-	-	-
F10	TP53	6549	c.743G>T	p.R248L	-	-	-	-	-
F11	TP53	10817	c.747G>T	p.R249S	-	-	-	-	-
F12	TP53	10771	c.749C>T	p.P250L	-	-	-	-	-
G01	TP53	10988	c.772G>A	p.E258K	-	-	-	-	-
G02	TP53	10867	c.797G>A	p.G266E	-	-	-	-	-
G03	TP53	10891	c.814G>A	p.V272M	-	-	-	-	-
G04	TP53	10659	c.817C>T	p.R273C	-	-	-	-	+
G05	TP53	10660	c.818G>A	p.R273H	-	+/-	+/-	-	-
G06	TP53	10779	c.818G>T	p.R273L	-	-	-	-	-

G07	TP53	10893	c.824G>A	p.C275Y	-	-	-	-	-
G08	TP53	10701	c.824G>T	p.C275F	-	-	-	-	-
G09	TP53	10939	c.832C>T	p.P278S	-	+/-	+/-	-	-
G10	TP53	10863	c.833C>T	p.P278L	-	+	-	-	-
G11	TP53	43714	c.836G>A	p.G279E	-	-	-	-	-
G12	TP53	10728	c.839G>A	p.R280K	-	-	-	-	-
H01	TP53	10724	c.839G>C	p.R280T	-	-	-	-	-
H02	TP53	10704	c.844C>T	p.R282W	-	+/-	+	-	+/-
H03	TP53	10722	c.853G>A	p.E285K	-	-	-	-	-
H04	TP53	10726	c.856G>A	p.E286K	-	-	+	+/-	-
H05	TP53	10856	c.880G>T	p.E294*	-	-	-	-	-
H06	TP53	10710	c.892G>T	p.E298*	-	-	-	-	-

## Appendix 2 – Real-time PCR results summary

### Real-time PCR experiment 1

Name	Type	Gene	Ct	Replicate Ct	Qubit cDNA (ng/reaction)	qPCR cDNA (ng/reaction)	Average qPCR cDNA (ng/reaction)	Volume of cDNA in qPCR (ul)	Total cDNA conc. (ng/ul)	Total cDNA (ng)	Volume of RNA in qPCR (ul)	RNA conc. (ng/ul)	Total Elution (ul)	Total RNA (ng)
Dilution 1	Standard	RPLP0	17.12	17.14	25.000	24.744	24.483	5.0	4.897	97.933	n/a	n/a	n/a	n/a
Dilution 1	Standard	RPLP0	17.15		25.000	24.223								
Dilution 2	Standard	RPLP0	20.62	20.78	2.500	2.879	2.620	5.0	0.524	10.479				
Dilution 2	Standard	RPLP0	20.95		2.500	2.360								
Dilution 3	Standard	RPLP0	24.54	24.64	0.250	0.260	0.245	5.0	0.049	0.981				
Dilution 3	Standard	RPLP0	24.74		0.250	0.231								
Microbiopsy 1a	Sample	RPLP0	21.92	22.01	n/a	1.298	1.230	5.0	0.246	4.921	4.0	1.230	11.0	13.532
Microbiopsy 1a	Sample	RPLP0	22.10			1.163								
Microbiopsy 1b	Sample	RPLP0	24.88	24.79		0.211	0.224	5.0	0.045	0.897	4.0	0.224	11.0	2.466
Microbiopsy 1b	Sample	RPLP0	24.69			0.238								
Microbiopsy 2a	Sample	RPLP0	24.06	24.12		0.348	0.337	5.0	0.067	1.349	4.0	0.337	11.0	3.709
Microbiopsy 2a	Sample	RPLP0	24.17			0.326								
Microbiopsy 2b	Sample	RPLP0	22.53	22.57		0.892	0.874	5.0	0.175	3.496	4.0	0.874	11.0	9.613
Microbiopsy 2b	Sample	RPLP0	22.60			0.856								
Microbiopsy 5b	Sample	RPLP0	21.06	21.16		2.203	2.073	5.0	0.415	8.290	4.0	2.073	11.0	22.798
Microbiopsy 5b	Sample	RPLP0	21.26			1.942								

## Real-time PCR experiment 2

Name	Type	Gene	Ct	Replicate Ct	Qubit cDNA (ng/reaction)	qPCR cDNA (ng/reaction)	Average qPCR cDNA (ng/reaction)	Volume of cDNA in qPCR (ul)	Total cDNA conc. (ng/ul)	Total cDNA (ng)	Volume of RNA in qPCR (ul)	RNA conc. (ng/ul)	Total Elution (ul)	Total RNA (ng)
Dilution 1	Standard	RPLP0	16.44	16.57	20.000	17.895	16.584	4.0	4.146	82.920				
Dilution 1	Standard	RPLP0	16.70		20.000	15.273								
Dilution 2	Standard	RPLP0	18.64	18.74	4.000	4.826	4.553	4.0	1.138	22.766				
Dilution 2	Standard	RPLP0	18.84		4.000	4.280								
Dilution 3	Standard	RPLP0	21.13	21.35	0.800	1.092	0.968	4.0	0.242	4.840				
Dilution 3	Standard	RPLP0	21.56		0.800	0.844								
Dilution 4	Standard	RPLP0	24.02	24.33	0.160	0.195	0.165	4.0	0.041	0.825				
Dilution 4	Standard	RPLP0	24.63		0.160	0.135								
Dilution 5	Standard	RPLP0	27.24	27.28	0.032	0.029	0.028	4.0	0.007	0.140				
Dilution 5	Standard	RPLP0	27.31		0.032	0.028								
Microbiopsy Normal 1	Sample	RPLP0	24.99	25.04		0.109	0.107	4.0	0.027	0.533	4.0	0.133	11.0	1.465
Microbiopsy Normal 1	Sample	RPLP0	25.08			0.104								
Microbiopsy Normal 2	Sample	RPLP0	24.93	25.18		0.113	0.099	4.0	0.025	0.494	4.0	0.124	11.0	1.359
Microbiopsy Normal 2	Sample	RPLP0	25.42			0.084								
Microbiopsy Naevi 1	Sample	RPLP0	22.04	22.05		0.633	0.632	4.0	0.158	3.159	4.0	0.790	11.0	8.686
Microbiopsy Naevi 1	Sample	RPLP0	22.05			0.630								
Microbiopsy Naevi 2	Sample	RPLP0	21.87	21.97		0.701	0.664	4.0	0.166	3.320	4.0	0.830	11.0	9.129
Microbiopsy Naevi 2	Sample	RPLP0	22.06			0.627								
Microbiopsy Normal 1	Sample	Tyrosinase	Negative	-		-	-		-	-		-	11.0	-
Microbiopsy Normal 1	Sample	Tyrosinase	Negative			-								
Microbiopsy Normal 2	Sample	Tyrosinase	Negative	-		-	-		-	-		-	11.0	-
Microbiopsy Normal 2	Sample	Tyrosinase	Negative			-								
Microbiopsy Naevi 1	Sample	Tyrosinase	24.97	25.34		0.110	0.091	4.0	0.023	0.454	4.0	0.113	11.0	1.248
Microbiopsy Naevi 1	Sample	Tyrosinase	25.71			0.071								
Microbiopsy Naevi 2	Sample	Tyrosinase	25.21	25.60		0.096	0.078	4.0	0.020	0.390	4.0	0.098	11.0	1.073
Microbiopsy Naevi 2	Sample	Tyrosinase	26.00			0.060								

### Appendix 3 – Ethics Approval and Publications

- HREC-09-QPAH-162 approval letter
- HREC-11-QPAH-442 approval letter
- HREC-11-QPAH-363 approval letter
- HREC-11-QPAH-236 approval letter
- HREC-12-QPAH-217 approval letter
- HREC-12-QPAH-082 approval letter
- HREC-12-QPAH-251 approval letter
- HREC-13-QPAH-551 approval letter
- UQ HREC 2008001342 approval letter
- Lin LL, Prow TW, Raphael AP, Harrold III RL, Primiero CA., Ansaldo AB, Soyer HP. 2013. Microbiopsy engineered for minimally invasive and suture-free sub-millimetre skin sampling. *F1000Res*, 2, 120.
- Banan P, Lin LL, Lambie D, Prow TW, Soyer HP. 2013. Effects of ex vivo skin microbiopsy on histopathologic diagnosis in melanocytic skin lesions. *JAMA Dermatol*, 149, 1107-9.
- McClenahan P, Lin LL, Tan JM, Flewell-Smith, Schaidler H, Jagirdar K, Atkinson V, Lambie D, Prow TW, Sturm RA, Soyer HP. 2014. BRAFV600E mutation status of involuting and stable nevi in dabrafenib therapy with or without trametinib. *JAMA Dermatol*, 150, 1079-82.
- Tan JM, Lin LL, Lambie D, Flewell-Smith R, Jagirfdar K, Schaidler H, Sturm RA, Prow TW, Soyer HP. 2015. BRAF Wild-Type Melanoma in Situ Arising In a BRAF V600E Mutant Dysplastic Nevus. *JAMA Dermatol*.

- Soyer HP, Lin LL, Prow TW. A plea for bio-banking of all equivocal melanocytic proliferations. *JAMA Dermatology*. 2013 Sep 1;149(9):1023-4.
- Prow TW, Lin LL, Soyer HP. The opportunity for microbiopsies for skin cancer. *Future Oncology*. 2013 Sep;9(9):1241-3.



Princess Alexandra Hospital  
Health Service District



Queensland  
Government

Queensland Health

Office of the Human Research Ethics Committee

Enquiries to: Ethics Manager  
Phone: (07) 3240 7672  
Fax: (07) 3240 7667  
E-mail: PAH\_Ethics\_Research@health.qld.gov.au  
Date: 26 August 2009

Prof H Peter Soyer  
UQ Dermatology Research Centre  
Level 2 building 7  
Princess Alexandra Hospital  
Woolloongabba 4102

**APPROVAL LETTER – PRINCESS ALEXANDRA HOSPITAL**

Dear Prof Soyer

**Research Protocol: HREC/09/QPAH/162**

<b>Pigmentation genotypes and phenotypic correlations with dermoscopic naevus types and distribution</b>	
<b>NEAF</b>	<b>Version 2.0, dated 18 June 2009</b>
<b>Participant Information and Consent Form – control group</b>	<b>Version 2, dated 1 August 2009</b>
<b>Participant Information and Consent Form – high risk group</b>	<b>Version 2, dated 1 August 2009</b>

At a meeting of the Princess Alexandra Hospital Human Research Ethics Committee (PAH HREC) held on 7 July 2009, the Committee reviewed the above research Protocol. The Princess Alexandra Hospital Human Research Ethics Committee is duly constituted, operates in accordance and complies with the current National Health and Medical Research Council's *National Statement on Ethical Conduct in Human Research 2007*.

On the recommendation of the Human Research Ethics Committee approval is granted for your project to proceed. This approval is subject to researcher(s) compliance throughout the duration of the research with certain requirements as outlined in the *National Statement on Ethical Conduct in Human Research 2007* and *Australian Research Code for the Responsible Conduct of Research*.

The following links have been provided for your convenience:  
<http://www.nhmrc.gov.au/publications/synopses/files/e72.pdf>  
<http://www.nhmrc.gov.au/publications/synopses/files/r39.pdf>

Some requirements are briefly outlined below. Please ensure that you communicate with the PAH HREC on the following:

- **Protocol Changes:** Substantial changes made to the protocol require HREC approval.
- **Problems and SAEs:** The HREC must be informed of any problems that arise during the course of the study which may have ethical implications. Serious adverse events must be notified to the HREC as soon as possible.

**Office**  
Princess Alexandra Hospital  
Health Service District

**Postal**  
Ipswich Road  
Woolloongabba Q 4102

**Phone**  
61 7 3240 7672

**Fax**  
61 7 3240 7667

Enquiries to: Metro South  
Human Research Ethics Committee  
Phone: 07 3443 8049  
Fax: 07 3443 8003  
HREC Ref: HREC/11/QPAH/442  
E-mail: [PAH\\_Ethics\\_Research@health.qld.gov.au](mailto:PAH_Ethics_Research@health.qld.gov.au)  
Amendment AM06

Dr Tarl Prow  
Dermatology Research Centre  
UQ, School of Medicine  
Level 2, Building 33,  
Princess Alexandra Hospital  
Woolloongabba, QLD 4102

Dear Dr Prow,

**HREC Reference number: HREC/11/QPAH/442**  
**Protocol title: Fissure Healing and Drug Delivery via Topical Microneedle Application**

The Office of the Metro South Human Research Ethics Committee noted and approved the following:-

Document	Version	Date
Notification of Amendment/Cover letter in respect to an extension of study approval until September 2015		30 September 2014

The Metro South Hospital and Health Service HREC is constituted and operates in accordance with the National Health and Medical Research Council's "National Statement on Ethical Conduct in Human Research (2007)", NHMRC and Universities Australia Australian Code for the Responsible Conduct of Research (2007) and the "CPMP/ICH Note for Guidance on Good Clinical Practice".

This will be ratified by the HREC at its 4 November 2014 meeting.

**Please provide a copy of this approval letter to the Research Governance Office.**

It should be noted that all requirements of the original approval still apply. Please continue to provide at least annual progress reports until the study has been completed.

If you have any queries please do not hesitate to contact the Human Research Ethics Committee office on +617 3443 8049.

Yours sincerely,



A/Prof Scott Campbell  
**Deputy Chair**  
**Metro South Hospital and Health Service**  
**Human Research Ethics Committee (EC00167)**  
**Centres for Health Research**  
**Princess Alexandra Hospital**  
**Woolloongabba QLD 4102**

8/10/14

C.c. Ms C Primero





# Metro South Human Research Ethics Committee

Enquiries to: Centres For Health Research  
Research Governance  
Phone: (07) 3176 7722  
Fax: (07) 3176 7667  
Our Ref: HREC/11/QPAH/363  
E-mail: PAH-Research@health.qld.gov.au

Professor Peter Soyer  
UQ Dermatology Research Centre  
Princess Alexandra Hospital  
Level 2 Building 7  
Ipswich Road  
Woolloongabba QLD 4102

## SSA AUTHORISATION – PRINCESS ALEXANDRA HOSPITAL METRO SOUTH HEALTH SERVICE DISTRICT

Dear Professor Peter Soyer,

**HREC reference number: HREC/11/QPAH363**

**SSA reference number: SSA/11/QPAH/562**

**Project title:** Immunohistochemistry & Other Molecular analysis of phenotypically characterized equivocal melanocytic proliferations.

Thank you for submitting an application for authorisation of this project. I am pleased to inform you that authorisation has been granted for this study to take place at the.

The following conditions apply to this research proposal. These are additional to those conditions imposed by the Human Research Ethics Committee that granted ethical approval.

1. Problems and SAEs: The Research Governance Office must be informed of any problems that arise during the course of the study which may have ethical implications. Where serious adverse events (SAEs) are encountered, the events must be notified as soon as possible.  
[http://www.health.qld.gov.au/pahospital/research/adverse\\_events.asp](http://www.health.qld.gov.au/pahospital/research/adverse_events.asp)
2. Proposed amendments to the research protocol or conduct of the research which may affect the ethical acceptability of the project are to be submitted to the HREC for review. A copy of the HREC approval/rejection letter must be submitted to the RGO;
3. Proposed amendments to the research protocol or conduct of the research which only affects the ongoing site acceptability of the project, are to be submitted to the research governance officer;
4. Proposed amendments to the research protocol or conduct of the research which may affect both the going ethical acceptability of the project and the site acceptability of the project are to be submitted firstly to the HREC for review and then to the research governance officer after a HREC decision is made.

---

If this research involves the recruitment of patients from the Metro South Health Service District (MSHSD), it is my responsibility to remind you of your ongoing duty of care for all people recruited into projects or clinical trials whilst public patients. All conditions and requirements regarding confidentiality of public information and patient privacy apply. You are required to comply at all times with any application requirements of Australian and Queensland Laws including the Health Services Act, the Privacy Act, Public Health Act (2005) and other relevant legislation, ethics obligations and guidelines which may be applicable to the MSHSD from time to time including, without limitation, any requirement in respect of the maintenance, preservation or destruction of patient records.

When the study involves patient contact, it is your responsibility as the principal investigator to notify the relevant consultant and request their approval.

We wish you every success in undertaking this research.

Yours sincerely,



Dr David Theile Snr  
**DISTRICT CHIEF EXECUTIVE OFFICER  
METRO SOUTH**

11 / 1 / 12

---

**Office**  
Centres for Health Research  
Princess Alexandra Hospital  
Metro South Health Service District

**Postal**  
Ipswich Road  
Woolloongabba Q 4102

**Phone**  
61 7 3176 7722

**Fax**  
61 7 3176 7667

1651  
Metro South  
Human Research Ethics Committee

Date: 10/10/2011

Enquiries to: Melissa Hagan  
Phone: (07) 3176 7722  
Fax: (07) 3176 7667  
Our Ref: HREC/11/QPAH/503  
E-mail: PAH-Research@health.qld.gov.au

Professor Peter Soyer  
Dermatology Research Centre  
The University of Queensland, School of Medicine  
Princess Alexandra Hospital  
Ipswich Road  
Woolloongabba Qld 4102

**SSA Authorisation – PRINCESS ALEXANDRA HOSPITAL  
METRO SOUTH HEALTH SERVICE DISTRICT**

Dear Professor Soyer,

**HREC reference number:** HREC/11/QPAH/236

**SSA reference number:** SSA/11/QPAH/503

**Project title:** AK Surveillance Feasibility Study

Thank you for submitting an application for authorisation of this project. I am pleased to inform you that authorisation has been granted for this study to take place at the following site(s):

Princess Alexandra Hospital

The following conditions apply to this research proposal. These are additional to those conditions imposed by the Human Research Ethics Committee that granted ethical approval.

1. Problems and SAEs: The Research Governance Office must be informed of any problems that arise during the course of the study which may have ethical implications. Where serious adverse events (SAEs) are encountered, the events must be notified as soon as possible.  
[http://www.health.qld.gov.au/pahospital/research/adverse\\_events.asp](http://www.health.qld.gov.au/pahospital/research/adverse_events.asp)
2. Proposed amendments to the research protocol or conduct of the research which may affect the ethical acceptability of the project are to be submitted to the HREC for review. A copy of the HREC approval/rejection letter must be submitted to the RGO;
3. Proposed amendments to the research protocol or conduct of the research which only affects the ongoing site acceptability of the project, are to be submitted to the research governance officer;
4. Proposed amendments to the research protocol or conduct of the research which may affect both the going ethical acceptability of the project and the site acceptability of the project are to be submitted firstly to the HREC for review and then to the research governance officer after a HREC decision is made.

---

If this research involves the recruitment of patients from the Metro South Health Service District (MSHSD), it is my responsibility to remind you of your ongoing duty of care for all people recruited into projects or clinical trials whilst public patients. All conditions and requirements regarding confidentiality of public information and patient privacy apply. You are required to comply at all times with any application requirements of Australian and Queensland Laws including the Health Services Act, the Privacy Act, Public Health Act (2005) and other relevant legislation, ethics obligations and guidelines which may be applicable to the MSHSD from time to time including, without limitation, any requirement in respect of the maintenance, preservation or destruction of patient records.

When the study involves patient contact, it is your responsibility as the principal investigator to notify the relevant consultant and request their approval.

We wish you every success in undertaking this research.

Yours sincerely,



Dr David Theile Snr  
**DISTRICT CHIEF EXECUTIVE OFFICER  
METRO SOUTH**

9, 12, 11

---

<b>Office</b>	<b>Postal</b>	<b>Phone</b>	<b>Fax</b>
Centres for Health Research Princess Alexandra Hospital Metro South Health Service District	Ipswich Road Woolloongabba Q 4102	61 7 3176 7722	61 7 3176 7667

Enquiries to: Centres For Health Research  
Research Governance  
Phone: (07) 3176 7722  
Fax: (07) 3176 7667  
Our Ref: HREC/12/QPAH/217 - SSA/12/QPAH/226  
E-mail: PAH-Research@health.qld.gov.au

Dr. Tarl Prow  
Dermatology Research Centre  
Princess Alexandra Hospital  
199 Ipswich Road  
Woolloongabba QLD 4102

**HREC APPROVAL AND SSA AUTHORISATION  
PRINCESS ALEXANDRA HOSPITAL - METRO SOUTH HEALTH SERVICE DISTRICT**

Dear Dr Prow,

**HREC Reference number: HREC/12/QPAH/217**  
**SSA reference number: SSA/12/QPAH/226**  
**Project title: Request for discarded skin for research**

I am pleased to advise that the above protocol has been recommended for approval by the Low and Negligible Risk Sub Committee of the Metro South Health Service District Human Research Ethics Committee. The Committee is duly constituted, operates in accordance and complies with the current National Health and Medical Research Council's *National Statement on Ethical Conduct in Human Research 2007*.

On the recommendation of the Human Research Ethics Committee approval is granted for your project to proceed.

Document Approved	Version	Date
Participant Information & Consent Form, Clean	2	15/6/12
Participant Information & Consent Form, Tracked	2	15/6/12

**The duration of approval is 3 years from the date of this letter.**

This approval is subject to researcher(s) compliance throughout the duration of the research with certain requirements as outlined in the *National Statement on Ethical Conduct in Human Research 2007* and *Australian Code for the Responsible Conduct of Research*.

The following links have been provided for your convenience:  
<http://www.nhmrc.gov.au/publications/synopses/e72syn.htm>  
<http://www.nhmrc.gov.au/publications/synopses/r39syn.htm>

---

Some requirements are briefly outlined below. Please ensure that you communicate with the HREC on the following:

- **Protocol Changes:** Substantial changes made to the protocol require HREC approval <http://www.health.qld.gov.au/pahospital/research/amendments.asp>
- **Problems and SAEs:** The HREC must be informed of any problems that arise during the course of the study which may have ethical implications. Serious adverse events must be notified to the HREC as soon as possible [http://www.health.qld.gov.au/pahospital/research/adverse\\_events.asp](http://www.health.qld.gov.au/pahospital/research/adverse_events.asp)
- **Lapsed Approval:** If the study has not commenced within twelve months approval will lapse requiring resubmission of the study to the HREC.
- **Annual Reviews:** All studies are required by the NHMRC to be reviewed annually. To assist with reporting obligations an Annual Report template is available on the MSHSD HREC website. This form is required to be completed and returned to the HREC within the 12 month reviewing period <http://www.health.qld.gov.au/pahospital/research/monitoring.asp>

If this research involves the recruitment of patients from the Metro South Health Service District (MSHSD), it is my responsibility to remind you of your ongoing duty of care for all people recruited into projects or clinical trials whilst public patients. All conditions and requirements regarding confidentiality of public information and patient privacy apply. You are required to comply at all times with any application requirements of Australian and Queensland Laws including the Health Services Act, the Privacy Act, Public Health Act (2005) and other relevant legislation, ethics obligations and guidelines which may be applicable to the MSHSD from time to time including, without limitation, any requirement in respect of the maintenance, preservation or destruction of patient records.


When the study involves patient contact, it is your responsibility as the principal investigator to notify the relevant consultant and request their approval.

Should you have any problems, please liaise directly with the Chair of the HREC early in the program.

A copy of this letter should be presented when required as official confirmation of the approval of the Metro South Health Service District Human Research Ethics Committee.

We wish you every success in undertaking this research.

Yours sincerely,

  
Dr David E. Theille Snr  
**DISTRICT CHIEF EXECUTIVE OFFICER  
METRO SOUTH**

Dr Richard Ashby  
Chief Executive  
MSHHS

18/9/14

# Metro South Human Research Ethics Committee

22 March 2012

Enquiries to: Metro South Health Service District  
Human Research Ethics Committee  
Phone: 07 3176 7672  
Fax: 07 3176 7667  
HREC Ref: HREC/12/QPAH/082  
E-mail: [PAH\\_Ethics\\_Research@health.qld.gov.au](mailto:PAH_Ethics_Research@health.qld.gov.au)

Dr Tarl Prow  
Dermatology Research Centre  
The University School of Medicine  
Level 2, Building 33  
Princess Alexandra Hospital  
199 Ipswich Road  
Woolloongabba QLD 4102

Dear Dr Prow

**HREC Reference number:** HREC/12/QPAH/082

**Protocol title:** Topical Application of Minimally Invasive, Novel Microbiopsy Device

Thank you for submitting the above research protocol to the Metro South Health Human Research Ethics Committee for ethical and scientific review. This protocol was first considered by the Human Research Ethics Committee (HREC) at the meeting held on 6<sup>th</sup> March 2012.

I am pleased to advise that the HREC has granted approval of this research protocol.

*You are reminded that this letter constitutes ethical approval only. You must not commence this research protocol at a site until separate authorisation from the District CEO or Delegate of that site has been obtained.*

*A copy of this approval must be submitted to the District Research Governance Office(r)/Delegate of the relevant institution with a completed Site Specific Assessment (SSA) Form for authorisation from the CEO or Delegate to conduct this research at the Princess Alexandra Hospital.*

The documents reviewed and approved include:

Document	Version	Date
Application		
CTN Form:	1	14 February 2012
Protocol: Microbiopsy Device Protocol	1	31 January 2012
Patient Information Sheet/Consent Form:	1	31 January 2012
Questionnaire: Participant Comfort Assessment Form	1	31 January 2012
Response to Request for Further Information		14 March 2012

Please note the following conditions of approval:

1. The Coordinating Principal Investigator will immediately report anything which might warrant review of ethical approval of the protocol in the specified format, including unforeseen events that might affect continued ethical acceptability of the protocol. Serious Adverse Events must be notified to the HREC as soon as possible. In addition the Investigator must provide a summary of the adverse events, in the specified format, including a comment as to suspected causality and whether changes are required to the Patient Information and Consent Form. In the case of Serious Adverse Events occurring at the local site, a full report is required from the Coordinating Principal Investigator, including duration of treatment and outcome of the event.

2. Amendments to the research protocol which may affect the ongoing ethical acceptability of a protocol must be submitted to the HREC for review. Major amendments should be reflected in a revised online NEAF (accompanied by all relevant updated documentation and a cover letter from the principal investigator, providing a brief description of the changes, the rationale for the changes, and their implications for the ongoing conduct of the study). Hard copies of the revised NEAF, the cover letter and all relevant updated documents, with *tracked changes*, must also be submitted to the HREC office as per standard HREC SOP. (Further advice on submitting amendments is available at [http://www.health.qld.gov.au/ohmr/documents/researcher\\_userguide.pdf](http://www.health.qld.gov.au/ohmr/documents/researcher_userguide.pdf) <http://www.health.qld.gov.au/pahospital/research/amendments.asp>)
3. Amendments to the research protocol which only affect the ongoing site acceptability of the protocol are not required to be submitted to the HREC for review. These amendment requests should be submitted directly to the Research Governance Office/r.
4. Proposed amendments to the research protocol which may affect both the ethical acceptability and site suitability of the protocol must be submitted firstly to the HREC for review and, once HREC approval has been granted, then submitted to the Research Governance Office/r.
5. Amendments which do not affect either the ethical acceptability or site acceptability of the protocol (e.g. typographical errors) should be submitted electronically (track changes) and in hard copy (final clean copy) to the Research Ethics Manager. These should include a cover letter from the Coordinating Principal Investigator or Study Co-ordinator providing a brief description of the changes and the rationale for the changes, and accompanied by all relevant updated documents with tracked changes.
6. The HREC will be notified, giving reasons, if the protocol is discontinued at a site before the expected date of completion.
7. The Coordinating Principal Investigator will provide an annual report to the HREC and at completion of the study in the specified format.

This HREC approval is valid for 3 years from the date of this letter.

8. If you require an extension for your study, please submit a request for an extension in writing outlining the reasons. Note: One of the criteria for granting an extension is the compliance with the approval's conditions including submission of progress reports.
9. Any research study that prospectively assigns human participants or groups of humans to one or more health-related interventions to evaluate the effects on health outcomes (WHO / ICMJE 2008 definition) should be registered, including early phase and late phase clinical trials (phases I-III) in patients or healthy volunteers (WHO Recommendation / ICMJE policy). If in doubt, registration is recommended. All studies must be registered prior to the study's inception, i.e. prospectively. <http://www.anzctr.org.au/>

Should you have any queries about the HREC's consideration of your protocol please contact the Ethics Secretariat on 07 3176 7672.

Please note that the Metro South HREC is constituted and operates in accordance with the National Health and Medical Research Council's (NHMRC) *National Statement on Ethical Conduct in Human Research (2007)*, *NHMRC and Universities Australia Australian Code for the Responsible Conduct of Research (2007)* and the *CPMP/ICH Note for Guidance on Good Clinical Practice*. Attached is the HREC Composition with speciality and affiliation with the Hospital (Attachment I).

The HREC Terms of Reference, Standard Operating Procedures, membership and standard forms are available from the following websites:

<http://www.health.qld.gov.au/pahospital/research/ethics.asp>  
[http://www.health.qld.gov.au/ohmr/html/regu/regu\\_home.asp](http://www.health.qld.gov.au/ohmr/html/regu/regu_home.asp)

Office	Postal	Phone	Fax
Centres for Health Research Princess Alexandra Hospital Metro South Health Service District	Ipswich Road Woolloongabba Q 4102	61 7 3176 7672	61 7 3176 7667



---

Once authorisation to conduct the research has been granted, please complete the Commencement Form (Attached) and return to the Metro South Human Research Ethics Committee.

The Metro South HREC wishes you every success in your research.

Yours sincerely,



Associate Professor Maher Gandhi  
**Chair**  
**Metro South Health Service District**  
**Human Research Ethics Committee (EC00167)**  
**Centres for Health Research**  
**Princess Alexandra Hospital**

---

<b>Office</b>	<b>Postal</b>	<b>Phone</b>	<b>Fax</b>
Centres for Health Research Princess Alexandra Hospital Metro South Health Service District	Ipswich Road Woolloongabba Q 4102	61 7 3176 7672	61 7 3176 7667

---

Enquiries to: Centres For Health Research  
Research Governance  
Phone: (07) 3176 7722  
Fax: (07) 3176 7667  
Our Ref: HREC/12/QPAH/251 – SSA/12/QPAH/279  
E-mail: PAH-Research@health.qld.gov.au

Miss Lydia Hang  
Dermatology Research Centre  
Princess Alexandra Hospital  
199 Ipswich Road  
Woolloongabba Qld 4102

## SSA AUTHORISATION – PRINCESS ALEXANDRA HOSPITAL METRO SOUTH HOSPITAL AND HEALTH SERVICE

Dear Ms Hang,

**HREC Reference number:** HREC/12/QPAH/251

**SSA reference number:** SSA/12/QPAH/279

**Project title:** Zinc-Oxide Nanoparticle infiltration into barrier-compromised human skin and its removal

Thank you for submitting an application for authorisation of this project. I am pleased to inform you that authorisation has been granted for this study to take place at the Princess Alexandra Hospital.

On the recommendation of the Human Research Ethics Committee approval is granted for your project to proceed.

Documents Approved	Version	Date
Participant Information & Consent Form	2	15/6/12

The following conditions apply to this research proposal. These are additional to those conditions imposed by the Human Research Ethics Committee that granted ethical approval.

1. Problems and SAEs: The Research Governance Office must be informed of any problems that arise during the course of the study which may have ethical implications. Where serious adverse events (SAEs) are encountered, the events must be notified as soon as possible.  
[http://www.health.qld.gov.au/pahospital/research/adverse\\_events.asp](http://www.health.qld.gov.au/pahospital/research/adverse_events.asp)
2. Proposed amendments to the research protocol or conduct of the research which may affect the ethical acceptability of the project are to be submitted to the HREC for review. A copy of the HREC approval/rejection letter must be submitted to the RGO;
3. Proposed amendments to the research protocol or conduct of the research which only affects the ongoing site acceptability of the project, are to be submitted to the research governance officer;

**Office**  
Centres for Health Research  
Princess Alexandra Hospital  
Metro South Hospital and Health  
Service

**Postal**  
Ipswich Road  
Woolloongabba Q 4102

**Phone**  
61 7 3176 7672

**Fax**  
61 7 3176 7667

4. Proposed amendments to the research protocol or conduct of the research which may affect both the going ethical acceptability of the project and the site acceptability of the project are to be submitted firstly to the HREC for review and then to the research governance officer after a HREC decision is made.

If this research involves the recruitment of patients from the Metro South Health Service District (MSHSD), it is my responsibility to remind you of your ongoing duty of care for all people recruited into projects or clinical trials whilst public patients. All conditions and requirements regarding confidentiality of public information and patient privacy apply. You are required to comply at all times with any application requirements of Australian and Queensland Laws including the Health Services Act, the Privacy Act, Public Health Act (2005) and other relevant legislation, ethics obligations and guidelines which may be applicable to the MSHSD from time to time including, without limitation, any requirement in respect of the maintenance, preservation or destruction of patient records.

When the study involves patient contact, it is your responsibility as the principal investigator to notify the relevant consultant and request their approval.

We wish you every success in undertaking this research.

Yours sincerely,



Dr Richard Ashby  
**HEALTH SERVICE CHIEF EXECUTIVE  
METRO SOUTH HEALTH**

10, 8, 12

---

Office	Postal	Phone	Fax
Centres for Health Research Princess Alexandra Hospital Metro South Health Service District	Ipswich Road Woolloongabba Q 4102	61 7 3176 7722	61 7 3176 7667

Enquiries to: Centres For Health Research  
Research Governance  
Phone: (07) 3443 8050  
Fax: (07) 3443 8003  
Our Ref: HREC/13/QPAH/551  
SSA/13/QPAH/572  
E-mail: [PAH-Research@health.qld.gov.au](mailto:PAH-Research@health.qld.gov.au)

Dr Tarl Prow  
Dermatology Research Centre  
The University of Queensland School of Medicine  
Level 5, Translational Research Institute  
37 Kent St  
Woolloongabba 4102

## SSA AUTHORISATION, PRINCESS ALEXANDRA HOSPITAL METRO SOUTH HOSPITAL AND HEALTH SERVICE

**HREC Reference number:** HREC/13/QPAH/551

**SSA reference number:** SSA/13/QPAH/572

**Project title:** Microbiopsy for characterisation of normal and diseased skin

Dear Dr Prow,

Thank you for submitting an application for authorisation of this project. I am pleased to inform you that authorisation has been granted for this study to take place at the Princess Alexandra Hospital.

On the recommendation of the Human Research Ethics Committee approval is granted for your project to proceed.

The following conditions apply to this research proposal. These are additional to those conditions imposed by the Human Research Ethics Committee that granted ethical approval.

1. Problems and SAEs: The Research Governance Office must be informed of any problems that arise during the course of the study which may have ethical implications. Where serious adverse events (SAEs) are encountered, the events must be notified as soon as possible.  
[http://www.health.qld.gov.au/pahospital/research/adverse\\_events.asp](http://www.health.qld.gov.au/pahospital/research/adverse_events.asp)
2. Proposed amendments to the research protocol or conduct of the research which may affect the ethical acceptability of the project are to be submitted to the HREC for review. A copy of the HREC approval/rejection letter must be submitted to the RGO;
3. Proposed amendments to the research protocol or conduct of the research which only affects the ongoing site acceptability of the project, are to be submitted to the research governance office;
4. Proposed amendments to the research protocol or conduct of the research which may affect both the going ethical acceptability of the project and the site acceptability of the project are to be submitted firstly to the HREC for review and then to the research governance office after a HREC decision is made.

---

**Office**  
Centres for Health Research  
Princess Alexandra Hospital  
Metro South Hospital and Health  
Service

**Postal**  
37 Kent Street  
Woolloongabba Qld 4102

**Phone**  
61 7 3443 8050

**Fax**  
61 7 3443 8003

If this research involves the recruitment of patients from the Metro South Hospital and Health Service (MSHHS), it is my responsibility to remind you of your ongoing duty of care for all people recruited into projects or clinical trials whilst public patients. All conditions and requirements regarding confidentiality of public information and patient privacy apply. You are required to comply at all times with any application requirements of Australian and Queensland Laws including the Health Services Act, the Privacy Act, Public Health Act (2005) and other relevant legislation, ethics obligations and guidelines which may be applicable to the MSHHS from time to time including, without limitation, any requirement in respect of the maintenance, preservation or destruction of patient records.

When the study involves patient contact, it is your responsibility as the principal investigator to notify the relevant consultant and request their approval.

We wish you every success in undertaking this research.

Yours sincerely,



Professor Ken Ho  
**Chair, Centres for Health Research**  
**METRO SOUTH HEALTH**

12, 12, 13

cc Mrs Clare Primiero, Research Assistant, Dermatology Research Centre

---

<b>Office</b>	<b>Postal</b>	<b>Phone</b>	<b>Fax</b>
Centres for Health Research	37, Kent Street	61 7 3443 8050	61 7 3443 8003
Princess Alexandra Hospital	Woolloongabba Qld 4102		
Metro South Hospital and Health Service			



---

**THE UNIVERSITY OF QUEENSLAND**  
**Institutional Approval Form For Experiments On Humans**  
**Including Behavioural Research**

---

**Chief Investigator:** Prof Michael S. Roberts

**Project Title:** Targeted Drug Delivery By Topical Application -  
02/06/2011 - AMENDMENT

**Supervisor:** None

**Co-Investigator(s):** Dr Jeff Grice, Dr Washington Sanchez, Ms Ya Ting  
(Michelle) Wu, Prof Mark Kendall, Dr Chris Flaim, Dr  
Tarl Prow

**Department(s):** Therapeutics Research Unit, School of Medicine -  
Southern Clinical Division

**Project Number:** 2008001342

**Granting Agency/Degree:** NHMRC

**Duration:** 31st December 2020

---

**Comments:**

---

**Name of responsible Committee:-**  
**Medical Research Ethics Committee**

This project complies with the provisions contained in the *National Statement on Ethical Conduct in Human Research* and complies with the regulations governing experimentation on humans.

---

**Name of Ethics Committee representative:-**  
**Professor Bill Vicenzino**  
**Chairperson**  
**Medical Research Ethics Committee**

Date: \_\_\_\_\_

8 JUN 2011

Signature: \_\_\_\_\_



METHOD ARTICLE

**UPDATED**

# Microbiopsy engineered for minimally invasive and suture-free sub-millimetre skin sampling [v2; ref status: indexed, <http://f1000r.es/1h7>]

Lynlee L Lin, Tarl W Prow, Anthony P Raphael, Robert L Harrold III, Clare A Primiero, Alexander B Ansaldo, H Peter Soyer

Dermatology Research Centre, The University of Queensland, School of Medicine, Translational Research Institute, Brisbane, QLD 4012, Australia

**v2** First published: 02 May 2013, 2:120 (doi: [10.12688/f1000research.2-120.v1](https://doi.org/10.12688/f1000research.2-120.v1))  
 Latest published: 31 Jul 2013, 2:120 (doi: [10.12688/f1000research.2-120.v2](https://doi.org/10.12688/f1000research.2-120.v2))

**Abstract**

We describe the development of a sub-millimetre skin punch biopsy device for minimally invasive and suture-free skin sampling for molecular diagnosis and research. Conventional skin punch biopsies range from 2-4 mm in diameter. Local anaesthesia is required and sutures are usually used to close the wound. Our microbiopsy is 0.50 mm wide and 0.20 mm thick. The microbiopsy device is fabricated from three stacked medical grade stainless steel plates tapered to a point and contains a chamber within the centre plate to collect the skin sample. We observed that the application of this device resulted in a  $0.21 \pm 0.04$  mm wide puncture site in volunteer skin using reflectance confocal microscopy. Histological sections from microbiopsied skin revealed  $0.22 \pm 0.12$  mm wide and  $0.26 \pm 0.09$  mm deep puncture sites. Longitudinal observation in microbiopsied volunteers showed that the wound closed within 1 day and was not visible after 7 days. Reflectance confocal microscope images from these same sites showed the formation of a tiny crust that resolved by 3 weeks and was completely undetectable by the naked eye. The design parameters of the device were optimised for molecular analysis using sampled DNA mass as the primary end point in volunteer studies. Finally, total RNA was characterized. The optimised device extracted  $5.9 \pm 3.4$  ng DNA and  $9.0 \pm 10.1$  ng RNA. We foresee that minimally invasive molecular sampling will play an increasingly significant role in diagnostic dermatology and skin research.

**Open Peer Review**

Referee Status:

	Invited Referees		
	1	2	3
<b>version 2</b> published 31 Jul 2013	 report		
<b>version 1</b> published 02 May 2013	 report	 report	 report

- 1 **Jack Arbiser**, Emory University USA
- 2 **Marco Ardigo**, San Gallicano Dermatological Institute Italy
- 3 **Neil Rajan**, Newcastle University UK

**Discuss this article**

Comments (1)

**Corresponding author:** Tarl W Prow ([t.prow@uq.edu.au](mailto:t.prow@uq.edu.au))

**How to cite this article:** Lin LL, Prow TW, Raphael AP *et al.* **Microbiopsy engineered for minimally invasive and suture-free sub-millimetre skin sampling [v2; ref status: indexed, <http://f1000r.es/1h7>]** *F1000Research* 2013, **2**:120 (doi: [10.12688/f1000research.2-120.v2](https://doi.org/10.12688/f1000research.2-120.v2))

**Copyright:** © 2013 Lin LL *et al.* This is an open access article distributed under the terms of the [Creative Commons Attribution Licence](#), which permits unrestricted use, distribution, and reproduction in any medium, provided the original work is properly cited. Data associated with the article are available under the terms of the [Creative Commons Zero "No rights reserved" data waiver](#) (CC0 1.0 Public domain dedication).

**Grant information:** This project was supported by Epiderm (Boronia Park, NSW 2111, Australia) and NHMRC Practitioner Fellowship (APP1020148) (HPS).

**Competing interests:** No competing interests were disclosed.

**First published:** 02 May 2013, **2**:120 (doi: [10.12688/f1000research.2-120.v1](https://doi.org/10.12688/f1000research.2-120.v1))

**First indexed:** 19 Jun 2013, **2**:120 (doi: [10.12688/f1000research.2-120.v1](https://doi.org/10.12688/f1000research.2-120.v1))



**UPDATED Changes from Version 1**

We have replaced the word “painless” to “minimally invasive” throughout the manuscript. We have removed the statement regarding leg complications. We have included additional data on the quality of DNA comparing conventional shave biopsy sample and the micro biopsy sample that was taken from the same lesion and the method to obtain this data has been provided under the ‘Materials and Methods’. We have emphasized in the ‘Discussion’ that unlike the conventional biopsy, the micro biopsy sample cannot be used for histological assessment. We have also addressed in the ‘Discussion’ the importance for using high quality RNA samples in whole transcriptome approaches and future directions for this novel device.

See referee reports

**Introduction**

Skin biopsy is one of the most essential techniques in dermatology for accurate diagnosis of neoplastic or inflammatory skin diseases through histopathological assessment. This technique is performed under local anaesthetic by trained medical personnel, normally a dermatologist, to remove a skin sample 2–4 mm in diameter (Figure 1) that is then preferably sent to a dermatopathologist for histopathological diagnosis. Pathological examination using skin biopsies often complements and/or confirms diagnosis of common neoplastic or inflammatory skin diseases<sup>1</sup>. This technique is usually performed using a punch biopsy tool or a scalpel. The wound is then either sutured or left to heal.

An excisional biopsy, a common alternative in neoplastic skin conditions, is performed when the entire tumour is needed for histopathological examination, or when melanoma is suspected. This depends on the size and location of the lesion and can be performed using a larger 4–6 mm diameter punch biopsy, a deep shave biopsy, or with a fusiform excision<sup>2</sup>. These biopsy techniques coupled with histopathology are able to provide accurate diagnosis of the disease occurrence and progression, however the downsides of these techniques are that they require local anaesthesia and sutures in addition to the time required to carry out the procedure. Furthermore, samples are generally fixed with formalin that hinders molecular analysis. Molecular fingerprinting of skin disease has the potential to dramatically improve diagnostic sensitivity and open the door for personalised medicine<sup>3–5</sup>. To date, there have been no reports on biomarker profiling of lesional samples in a prospective study due to the lack of suitable technologies to perform multiple sampling over time. This is due to the iatrogenic issue of cutting out the lesion through biopsy precluding further study of that lesion.

This problem exists in many medical disciplines and has led to the evolution of experimental diagnostic devices towards miniaturised versions of their predecessors. This miniaturisation trend is enabled by several factors including improved micro-manufacturing tolerances, decreasing costs and increasing availability. One of the earliest micro-devices developed to obtain biopsy samples was patented by Krulevitch *et al.*<sup>6</sup>. They patented micro biopsy/precision cutting devices fabricated by conventional machining, silicon micromachining, precision machining and injection moulding. Over the years, there have been many similar patents that report a variety of such

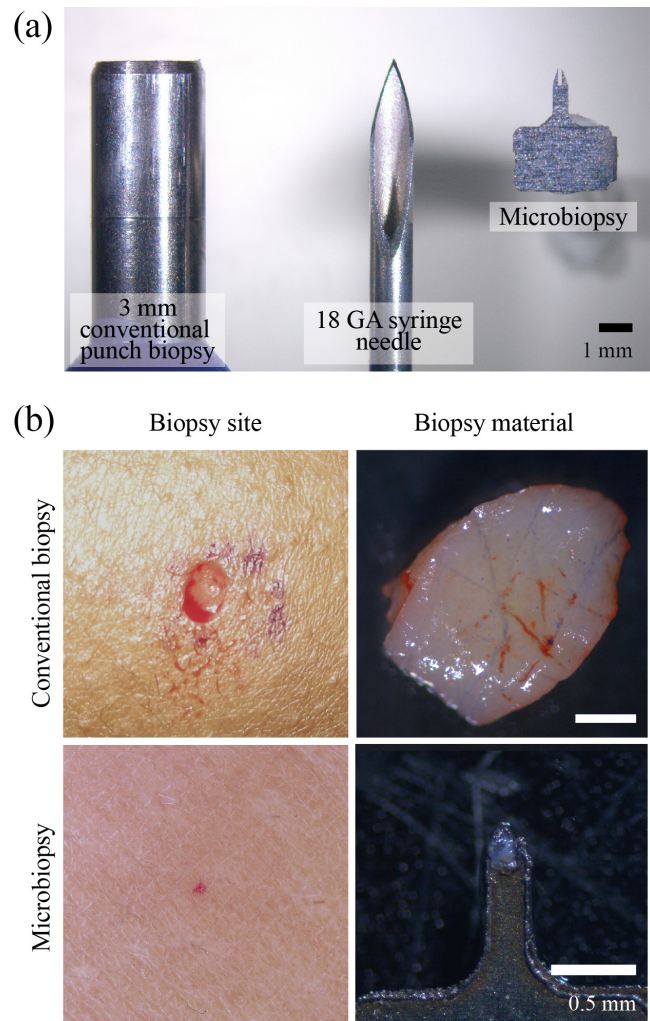


**Figure 1. Size comparison of needle, biopsy devices and biopsy comparisons.** A conventional biopsy punch is shown on the left, an 18 gauge syringe needle in the centre and the inner chamber of our micro biopsy device on the right Panel (a) our micro biopsy device chamber is 0.15 mm in width with an outer width of 0.25 mm. The top row of Panel (b) contains a conventional 3 mm biopsy site and tissue, whereas the bottom panels show micro biopsied skin and tissue.

micro biopsy devices. The unifying theme is that these patents all describe micro-biopsy devices for breast or intestinal tissue sampling<sup>7–10</sup> and importantly none were engineered for skin or skin lesions.

Our group has developed a new micro biopsy platform technology that enables the collection of tiny pieces of skin using a micro-medical device that is minimally invasive and does not require local anaesthesia (IP Australia Appl. Num. 2012901490, filed on 16/04/2012). There are situations when conventional biopsies are not appropriate. Skin disease may present with multiple lesions and/or in a cosmetically sensitive area. The micro biopsy device has the potential to fill a void in dermatology where conventional biopsies are not feasible or could do more harm than good. We have

observed that microbiopsy sampling does not interfere with downstream histopathological diagnosis<sup>11</sup>. The data presented herein describe the fabrication, optimisation and early steps toward the validation of a novel microbiopsy device for use *in vivo*.

## Materials and methods

### Microbiopsy device fabrication

The microbiopsy devices used in our studies were fabricated by laser cutting plates of stainless steel. The in-house fabrication of microbiopsy devices involves laser cutting of two-dimensional designs on 0.05 mm thick medical grade stainless steel (304, Mastercut Technologies, Australia) at 95% power, 30% frequency and speed of 0.9 using a 20 W laser marking system (LaserPro S290, GCC, Taiwan). All of the 2D microbiopsy components were assembled into 3D devices, and sterilized using a glass bead sterilizer (Steri Inotech 350, Sigma-Aldrich, USA) at 250°C for 30 seconds or submerged in 70% ethanol for 1 min and air-dried prior to use. The microbiopsy device was then fitted into a spring-loaded applicator.

### Microbiopsy device imaging

A bench top scanning electron microscope (SEM) (JCM-6000 Neoscope, JEOL, USA) was used to acquire high-resolution images of the microbiopsy device. The roughness amplitude of the microbiopsy chamber was obtained by measuring the average distances of the edge to a regression-fitted straight line using MatLab (Mathworks, Australia).

### Microbiopsy and conventional biopsy sample collection

Microbiopsy samples were either obtained *in vivo* from healthy volunteers (HREC/12/QPAH/082, Metro South Human Research Ethics Committee, Centres for Health Research, Princess Alexandra Hospital) or *ex vivo* from excised actinic keratosis (AK) lesions. The skin of a healthy volunteer was swabbed with alcohol and the microbiopsy applied. Conventional biopsies e.g. punch (Figure 1b) or shave biopsies, were performed with informed consent from patients (HREC/08/QPAH/207 for healthy skin or HREC/11/QPAH/477 for AK lesions) prior to being microbiopsied. Samples were collected in sterile RNase and DNase free 1.5 ml microcentrifuge tubes containing either RNALater<sup>®</sup> (Life Technologies, USA) or pH 7.0 phosphate buffered saline (PBS) on ice within 20 minutes after tissue removal from patients. All samples placed in RNALater<sup>®</sup> were kept overnight at 4°C and then stored at -80°C.

### Measurement of pain score

Volunteer pain scores were evaluated with Metro South Human Research Ethics Committee, Princess Alexandra Hospital approval (HREC/12/QPAH/082). Each of the 20 volunteers (Table 1) was presented with an assessment form to grade his/her expected pain score based on a numerical rating 10-point Likert scale, 0 as having no pain and 10 as pain as bad as they can imagine before the start of the experiment. Each microbiopsy application was performed one minute apart and the pain score recorded immediately after application. Five minutes after the final microbiopsy application, the volunteers were asked to rate the level of pain for each microbiopsy site.

### Reflectance confocal microscopy

Microbiopsy sites were visualized with a reflectance confocal microscope (RCM, Vivascope 1500<sup>®</sup> Multilaser, Lucid, Inc., USA) in volunteers or in excised skin (HREC/12/QPAH/217).

**Table 1. Volunteer summary.** Volunteers for microbiopsy classified by age, ethnic group, gender and Fitzpatrick skin type.

Ethnic group	Fitzpatrick skin type <sup>22</sup>	Gender	Age (as of study year)	Number of participants
Caucasian	II–III	M	23–44	8
Caucasian	I–II	F	22–39	6
Asian	IV	M	27–33	4
Asian	III	F	27	2

RCM was also used to perform *in vivo* examination of the skin after microbiopsy. RCM images were collected through the microscope head, integrated with a water immersion objective, at a near-infrared wavelength of 785 nm. Blocks consisting of 7 × 7 mm mosaics of stitched RCM images and 2 μm to 200 μm vertical z-stacks were acquired at the microbiopsy sampling site. Dermatoscopic images were collected with a Canon Power Shot G10 digital camera (Canon, Japan) and a dermatoscope attachment (Dermlite<sup>®</sup>, 3Gen, USA).

### Microbiopsy site visualisation histology

Microbiopsied tissue was embedded (Optimal cutting temperature compound, Sakura Finetek, USA) and cryosectioned (CM1850, Leica Microsystems Pty Ltd, Australia). The 10 μm thick sections were fixed with 100% cold methanol for 10 minutes, air dried and stained with haematoxylin and eosin (Varistain Gemini ES, Thermo Fisher Scientific Inc., USA) to visualize the microbiopsy sites.

### Nuclear labelling and confocal microscopy

The microbiopsy extracted tissue was incubated with DRAQ5 (BioStatus Limited, UK) at 10 μM in PBS for 30 minutes at room temperature. Confocal microscopy images were taken with a Zeiss 510 META confocal microscope (Carl Zeiss Microscopy GmbH, Germany). A 3D projection was then created from the z-stacks (2 μm steps) of confocal images using Imaris (Bitplane Scientific Software, Switzerland). ImageJ (NIH, USA) was used to estimate the nuclei in microbiopsy samples.

### DNA isolation

DNA was extracted from the microbiopsy samples using QIAamp DNA Micro purification kits (QIAGEN GmbH, Germany) using a protocol modified to accommodate the unique microbiopsy sample. The microbiopsy was removed from the applicator housing after application. The presence of a tissue sample was quickly confirmed by opening the microbiopsy device and visualizing with a stereo microscope (Carl Zeiss Microscopy GmbH, Germany). The opened device was then immersed in 180 μl lysis buffer (Buffer ATL, QIAGEN GmbH, Germany) in the presence of proteinase K (20 μl) in a 1.5 ml tube. Fifteen seconds of pulse-vortexing was applied to ensure that the sample was well-mixed. The sample was then placed in a thermomixer (Eppendorf, Australia) at 56°C with shaking at 800 rpm overnight. The tube containing the device was briefly centrifuged for 10 seconds to remove the solution adhering to the cap of the tube before transferring the lysate into a new tube. The tube containing the device was centrifuged again at 6000 g for 30 seconds to remove any lysate adhering to the device. The lysates were combined and the remaining procedure followed the manufacturer supplied instructions.

### RNA isolation

The modified sample lysing processing described in DNA isolation above was also used with the Arcturus® PicoPure® RNA Isolation Kit (Life Technologies, USA) to obtain total RNA from microbiopsy samples. RNA isolation of lesional samples was performed using RNeasy Mini Kit (QIAGEN GmbH, Germany) according to the RNeasy Mini Handbook (version 2010).

### DNA and RNA quantification

A quantitative fluorometer-based assay (Qubit® 2.0, Life Technologies, USA) was used to determine the concentration of DNA and RNA with the protocol provided by the manufacturer.

### DNA and RNA quality control

Agilent DNA 12000 DNA kit (Agilent Technologies, USA) was used to determine the integrity and quality of DNA after whole genomic amplification of isolated DNA from microbiopsy and matched conventional shave biopsy samples. Agilent RNA 6000 Nano and Pico kits (Agilent Technologies, USA) were used to determine the RNA integrity number (RIN) of lesional and microbiopsy samples after RNA isolation. The supplied protocol was followed.

### Whole genomic amplification

Identical amounts of total DNA (1.85 ng) for both lesional and microbiopsy samples were subjected to whole genomic amplification. The amplification procedure was carried according to manufacturer's instructions (REPLI-g Single Cell Kit, QIAGEN, Australia).

### Whole transcriptome amplification

Identical amounts of total RNA (14 ng) for both lesional and microbiopsy samples were subjected to whole transcriptome amplification. The procedure was carried out using the supplied instructions (QuantiTect Whole Transcriptome Kit, QIAGEN, Australia). The cDNA obtained from the amplification process was used as a template in a polymerase chain reaction (PCR) reaction using human beta actin primers (forward: ATC TGG CAC ACC TTC TAC AAT GA; reverse: CGT CAT ACT CCT GCT TGC TGA TCC AC) (Integrated DNA Technologies, NSW, Australia). There was an initial denaturation for 2 minutes at 98°C, followed by 30 cycles of 98°C for 30s (denaturation), 67°C for 30s (annealing), and 72°C for 1 minute (extension). The cDNA and PCR products were run on a 1% agarose gel (Bio-rad Laboratories, Inc., Australia) and visualized with RedSafe (ChemBio, UK). HyperLadder™ 1 kb (HyperLadder I) (Bioline, UK) was used to determine the mass of cDNA and human beta actin amplicons.

### Statistical analysis

Statistical analysis was performed using PRISM 6 for Windows (GraphPad Software, Inc., USA). Channel width, velocity and roughness amplitude data were presented as mean  $\pm$  SD. Pain score for channel width and velocity were presented as minimum to maximum box-and-whiskers plot. One-way ANOVA combined with a Tukey's multiple comparison post-test was performed to determine the statistical significance.

## Results

Our microbiopsy device has a chamber volumetric size of 0.003 mm<sup>3</sup> that is more than 6000 times smaller than a conventional

3 mm punch biopsy and more than 5 times smaller than an 18 GA syringe needle (Figure 1a). Figure 1b demonstrates the size differences between a conventional 3 mm punch biopsy (top panels) and our microbiopsy (bottom panels).

### Channel width optimisation

We conducted a volunteer study in 20 healthy individuals to determine the optimal channel width and application velocity for this device. Extracted DNA mass was chosen to be the primary indicator for sample-to-sample comparisons. Interestingly, we observed tissue collection ( $4.5 \pm 1.5$  ng DNA) around the rough edges of a microbiopsy device without a chamber (Figure 2a–b, channel width of 0 mm). After applying the microbiopsy, the device was opened up and visualized under a dissecting microscope. Successful collection was achieved when tissue was evident within or around the device and unsuccessful if no tissue was present. Tissue was collected from all volunteers (n=20) when a 0.15 mm channel width microbiopsy device was used. Only 13 successful collections were achieved from 20 applications when a 0.20 mm channel width microbiopsy device was used. This indicated that the collection rate decreased from 100% to 65% when channel width was increased by 0.05 mm. The device without a channel (0 mm channel width) captured tissue around the edges of the tapered plates in all replicates (n=20). This experiment showed that a channel width of 0.15 mm obtained the highest average amount of DNA ( $5.9 \pm 3.4$  ng), which was significantly higher than 0.25 and 0.30 mm channel widths ( $p < 0.0001$ ). There was no significant difference in the total DNA extracted between 0–0.20 mm channel widths (Figure 2a).

### Application velocity optimisation

Microbiopsy application velocity was evaluated by using defined applicator springs to achieve velocities between 0–20.2 m/s (Figure 2d). Only negligible amounts of DNA were recovered when the device was applied at less than 9.2 m/s. However, there was a 7.5-fold increase ( $0.8 \pm 0.8$  to  $6.0 \pm 3.0$  ng) in DNA recovered when the application velocity was increased from 9.2 m/s to 16.6 m/s ( $p < 0.0001$ ). An additional increase to 20.2 m/s increase in application velocity did not result in significant increases in DNA collection.

### Pain scale assessment

There was no change in the level of pain reported when microbiopsies with varying channel widths were applied (Figure 2c). The level of pain significantly increased and variation increased when microbiopsies were applied at increasing velocities (Figure 2e). All of the volunteers had a pain score of 0 at 5 minutes after the final microbiopsy application (data not shown). The volunteers scored pain between 0 to 10 with an average score of  $1.5 \pm 1.1$ , when the 0.15 mm channel width microbiopsy was applied at 20.2 m/s.

### Edge roughness optimisation

We observed DNA collection without a centre chamber (Figure 2a,  $4.5 \pm 1.4$  ng from channel width 0 mm) and hypothesized that surface roughness could be key to successful sample collection. We compared microbiopsy devices with varying roughness amplitudes ( $R_A$ ) and observed an increasing trend in total DNA extracted with increasing  $R_A$  (Figure 3a) (n=20 for  $5.36 R_A$  and n=5 for 0.92 and 1.32). The SEM images of the inner chamber edge

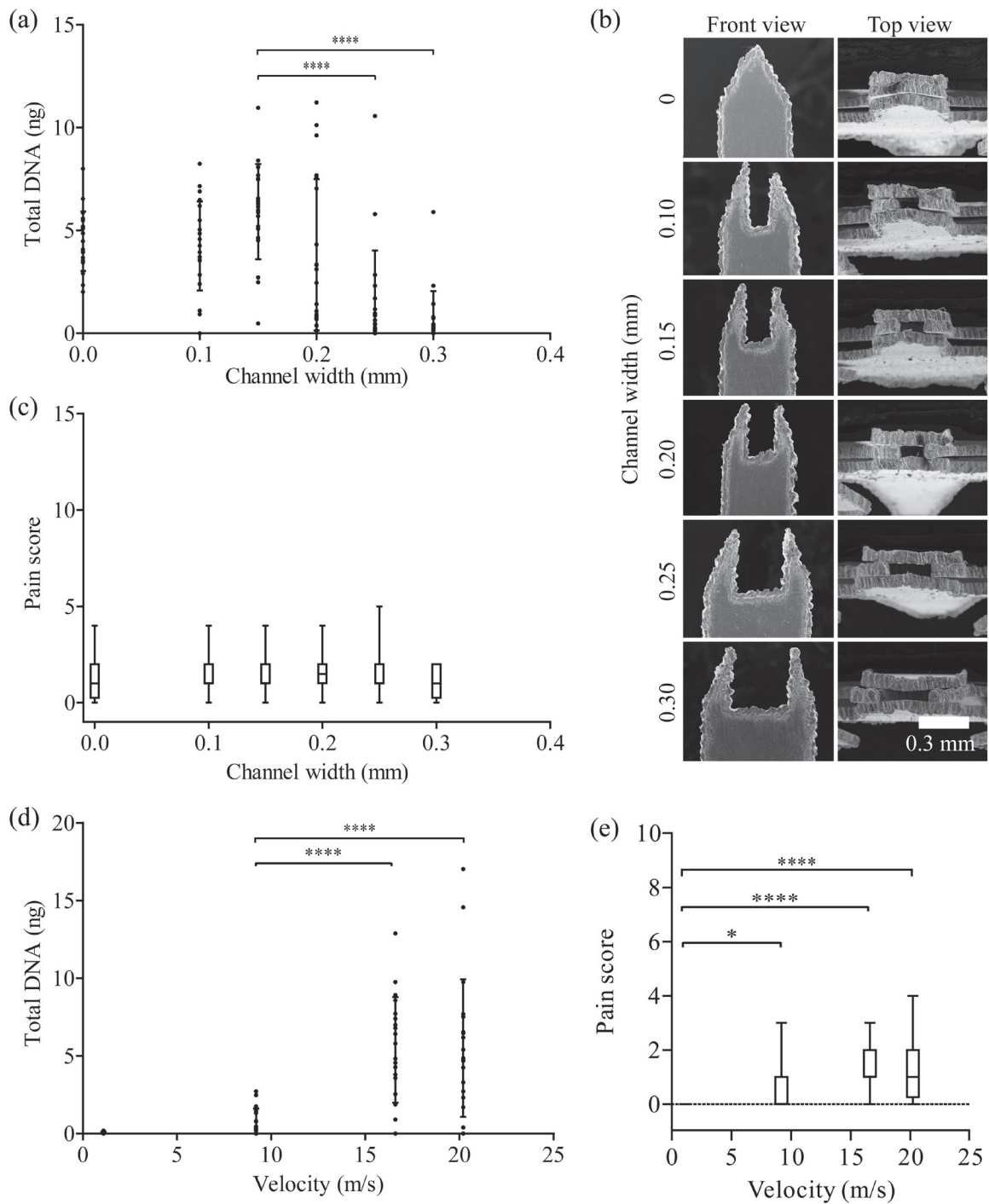


**Figure 2. Microbiopsy channel width and velocity optimisation.** Channel width and velocity were varied to optimise the microbiopsy device configuration. Total DNA was used as a surrogate for sample size. Panel (a) shows the DNA extracted from device with varying channel width and that the maximum amount of DNA was collected with 0.15 mm channel width. Panel (b) displays high resolution scanning electron microscopic images showing different channel widths of the microbiopsy device. Panel (c) shows the level of pain volunteers reported when different channel width microbiopsies were used. Panel (d) shows the varying velocity applied and that the maximum amount of DNA was collected when the device was applied at 16.6 m/s. Panel (e) shows the level of pain volunteers reported when application velocity was varied.

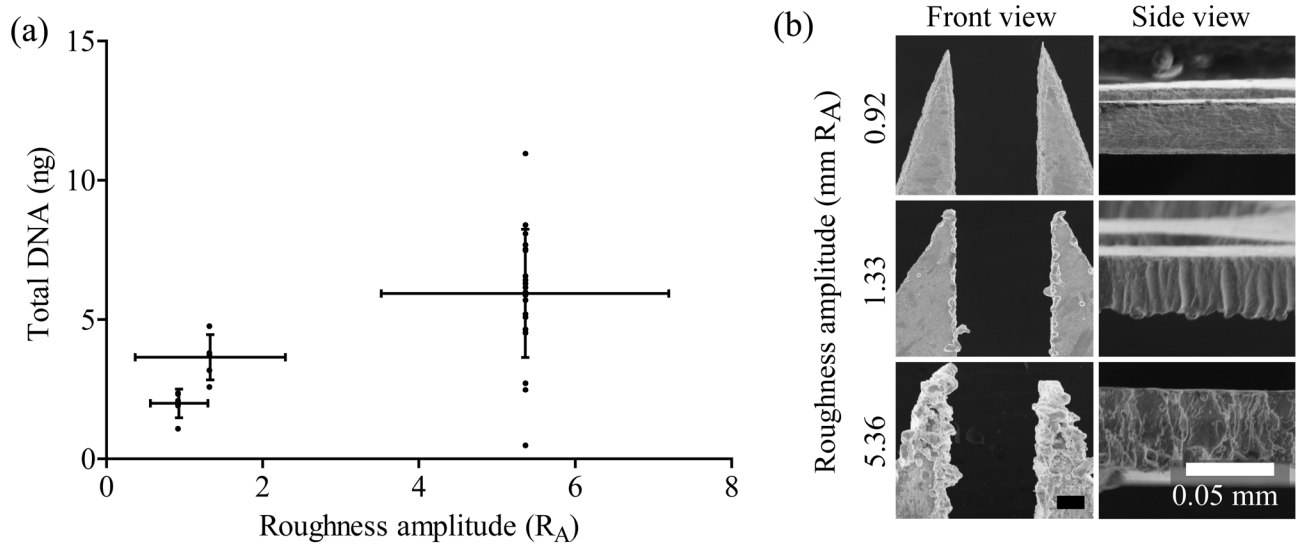


**Figure 3. Microbiopsy roughness amplitude optimisation.** Panel (a) shows that microbiopsy devices with higher roughness amplitude channels are capable of collecting more DNA. Panel (b) contains high resolution scanning electron microscopic images showing different channel widths and roughness of the microbiopsy device.

were used to measure the  $R_A$ . These measurements ranged from relatively smooth ( $R_A$  0.92) to rough ( $R_A$  5.36) (Figure 3b, side view).

#### Microbiopsy site imaging

RCM was used to visualise the microbiopsy application site. RCM images revealed a microbiopsy site similar to the size of a small hair follicle in the dermal papillary post microbiopsy application (Figure 4a and 4b). The inset shows that microbiopsy application resulted in a puncture site that was approximately  $0.10 \times 0.50$  mm in dimension (Figure 4b). Microbiopsy samples were stained with DRAQ5 (BioStatus Limited, UK) to highlight the nuclei. Confocal images were used to generate a 3D model of the microbiopsy sample. The usual skin strata were apparent in this model. We estimated that there were 1634 nuclei in Figure 4c. We observed  $0.22 \pm 0.12$  mm wide and  $0.26 \pm 0.09$  mm deep puncture sites in excised abdominal skin from 10 histological sections (Figure 4d).

#### Microbiopsy sample molecular characterisation

One of our goals was to compare AK lesions to microbiopsy samples since many of these lesions can be present in patients but only a few progress<sup>12</sup> to squamous cell carcinoma and the molecular mechanism behind this transition is a focus of intense research. Microbiopsy samples were taken from freshly excised AKs. The RNA from these matched samples had comparable quality with an average RIN difference of  $-0.85 \pm 0.85$  for  $n=4$ . Representative Bioanalyzer (Agilent Technologies, USA) results for the conventional biopsy (RIN 6.50) and microbiopsy (RIN 5.10) are shown in Figure 5, left panel. The results showed that there are similarities and differences in the RNA bands, which may be due to the large amount of tissue sampled with conventional biopsy and the relatively small number of cells sampled with the microbiopsy.

The small sample size is an inherent limitation of the microbiopsy device. To mitigate this, a pilot experiment was conducted where the microbiopsy sample was subjected to whole transcriptome amplification for RNA analysis. We included a skin sample with the same amount of starting material (14 ng) as an amplification control in the experiment. We observed a 2000-fold increase in cDNA from both samples based on total RNA and cDNA measurements. The cDNAs were of comparable quality and quantity (Figure 5, Transcriptome Amplification to cDNA). Subsequently, we used PCR to amplify human beta-actin mRNA. We observed 2 identical bands at 800 bp with comparable PCR product quality both lanes (Figure 5, Actin PCR).

#### Wound healing kinetics

Immediately after microbiopsy application we observed local erythema that resolved within 24 hours. The tiny excision site from the microbiopsy healed quickly and was invisible to the naked eye after 24 hours (Figure 6). We used dermoscopy and RCM to monitor the wound healing process at regular intervals (Figure 6, center and right columns).

#### Influence of channel width and velocity of microbiopsy on DNA, extraction, RNA extraction and pain scores in volunteers

1 Data File

<http://dx.doi.org/10.6084/m9.figshare.687063>

#### Discussion and conclusion

Whereas conventional biopsies allow accurate diagnosis of tissue sampled through histopathological assessment, there is a need for an

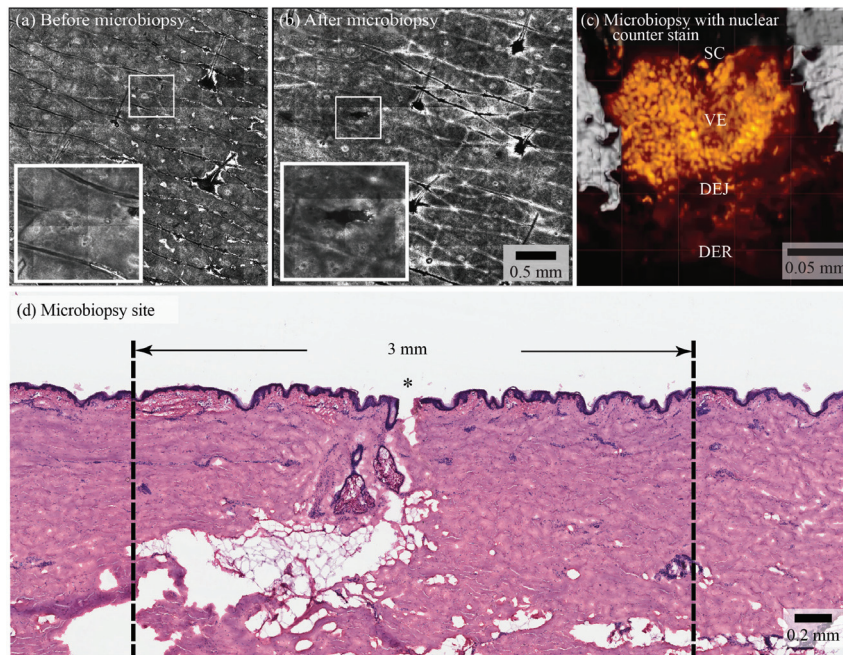


**Figure 4. Site of micro biopsy and micro biopsy content.** Panels (a) and (b) are reflectance confocal microscopy mosaics of a micro biopsy site, see the hair follicles featured in the centre and on the right hand side of the images for size comparison (bar indicates 0.5 mm in a and b). Panel (c) shows a 63x magnification, 3D rendering of the micro biopsy tissue with a nuclear counter stain (orange) derived from a confocal microscopy z-stack of the sample within the micro biopsy device. The stratum corneum (SC), viable epidermis (VE), dermal-epidermal junction (DEJ) and superficial dermis (DER) are labeled. This micro biopsy contained an estimated 1634 nuclei. Haematoxylin and eosin stained section of human skin after micro biopsy application shows a 0.10 mm wide and 0.25 mm deep puncture Panel (d). \* indicates the site of micro biopsy application.

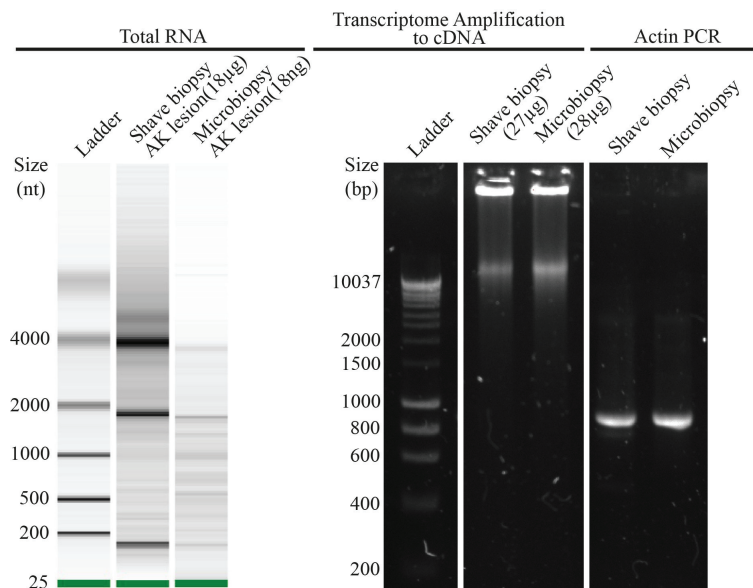


**Figure 5. Molecular characterization of conventional shave biopsies and micro biopsies.** The left panel shows the Bioanalyzer readout from amplified DNA from a conventional actinic keratosis (AK) shave biopsy next to the micro biopsy DNA sample obtained from the same AK lesion. The middle panel shows the Bioanalyzer readout from RNA isolated from a conventional AK shave biopsy and a micro biopsy that was obtained from the same AK lesion. The right panel compares the RNA quality of a shave biopsy and normal skin micro biopsy that were subjected to total transcriptome amplification to generate cDNA. The cDNA was then used as a template for a PCR reaction containing actin specific primers with an expected product at 800 bp.

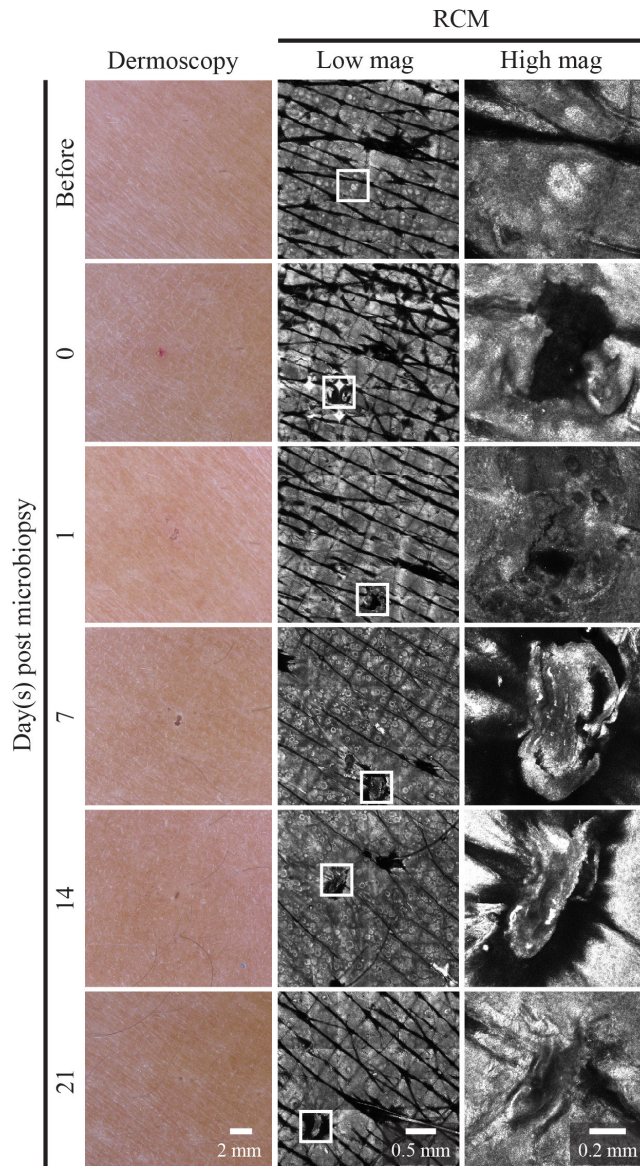


**Figure 6. Wound healing kinetics of micro biopsy site.** The left column shows dermoscopic images of the micro biopsy site over time. The middle and right column are mosaics and at 30x magnification reflectance confocal microscopy (RCM) images, respectively, of the micro biopsy site.

alternative technology, such as the micro biopsy, to screen multiple lesions through molecular diagnosis. In this proof of concept study, we have shown that an arrangement of stacked plates to form a 3D micro biopsy device is capable of providing molecular samples from normal and diseased skin. DNA extraction from human skin is critical for stratifying lesions in terms of mutational status. This type of characterization is becoming more and more relevant as targeted signalling inhibitors are being added to the therapeutic

arsenal. Recent developments in molecular inhibitors for skin cancer, e.g. Vemurafenib<sup>13</sup> and Trametinib<sup>14,15</sup>, are driving a new need for molecular diagnostic information that cannot be gathered through morphologic analysis. Molecular biomarkers have been used to detect cancer, but are now being developed to determine which molecular therapeutic will be the most effective. Melanoma clinical biology research has resulted in genomic data identifying oncogenes that can be targeted by protein kinase inhibitors e.g. *BRAF* and *MEK*<sup>16</sup>. Diagnostic assays to detect *BRAF* and *NRAS* mutations are now being used to stratify skin cancer lesions<sup>17</sup>. The micro biopsy device has the potential to help screen multiple lesions for specific mutations, and to be important in discovery based research.

Yancovitz *et al.* describe intra- and inter-tumour heterogeneity of melanoma in the context of *BRAF*<sup>V600E</sup> mutations<sup>18</sup>. Hematoxylin and eosin stained sections of primary and metastatic lesions were subjected to laser capture microdissection to isolate the lesions of interest. They captured 30–300 cells for each lesion of interest. This is less than 5 times that captured with the micro biopsy device. The authors used the same DNA extraction kit as we did to isolate lesional DNA for analysis. These samples were then used to detect *BRAF*<sup>V600E</sup> tumour heterogeneity. Based on our analysis, we estimate that Yancovitz *et al.* isolated <1 ng of DNA in this study and were able to amplify *BRAF* exon 15 using conventional PCR followed by mutation analysis. We found that we can reproducibly isolate 5 ng of DNA from the superficial skin and in another publication show the use of the micro biopsy device in dysplastic nevi<sup>11</sup>. This work sets the stage for future micro biopsy studies focused on *BRAF* mutational analysis in nevi *in situ*. The addition of RNA analysis to mutational studies would give additional insights into gene expression profiles of these lesions.

Berglund *et al.* (2007) reported that their optimised methodology yielded an average  $1.4 \pm 0.4$   $\mu$ g of consistently high quality RNA (8.4–8.9 RIN) from 3 mm skin punch biopsies<sup>19</sup>. Another group reported that they had isolated an average of 1.5  $\mu$ g of RNA with an average RIN value of 8.1 from half of a 4 mm punch biopsy skin sample (n=97)<sup>20</sup>. The average total RNA yielded from the micro biopsy device is  $9.0 \pm 10.1$  ng (n=5). Even though we isolated far less RNA with the micro biopsy device, our proof of concept study supports the hypothesis that this limitation can be addressed using commercial amplification kits and PCR (Figure 5) for investigating the molecular basis of skin disease. Through the course of these experiments we observed RNA integrity values that ranged between 1.2 and 7.6 with the micro biopsy. We also observed that these values correlated with matched conventional shave biopsies. In some cases the values were quite low (e.g. RIN 5.1 in Figure 5) and would not be considered for whole transcriptome approaches. Sampling for RNA analysis can be difficult and optimizing this application for the micro biopsy is one of our priorities as we move forward with this technology.

Discovering non-melanoma skin cancer biomarkers and potential therapeutic targets is an emerging area of research. For

example, Dang *et al.* (2006) focused on the genetic changes that occur in AK to squamous cell carcinoma (SCC) for prospective development of new diagnostic tools and therapeutic approaches. They reported that 7 out of 14 genes in 10 AK, 10 SCC and 20 normal skin samples related to cell adhesion, communication, metabolism and respiration were significantly dysregulated in AK and SCC ( $p < 0.05$ )<sup>21</sup>. The microbiopsy device has the potential to help facilitate longitudinal studies within a single lesion.

Application of the relatively small microbiopsy device does not require local anaesthesia or sutures and therefore no set up for a minor clinical procedure is necessary. Observations from our volunteer study suggest that collecting multiple microbiopsies within a short period is feasible. We envision that microbiopsy devices will become a routine clinical and research device in dermatology allowing the dermatologist to obtain targeted lesion data for molecular stratification.

### Consent

Written informed consent for publication of their clinical images was obtained from the patients (HREC/11/QPAH/477 and/or HREC/12/QPAH/082, Metro South Human Research Ethics Committee, Centres for Health Research, Princess Alexandra Hospital).

### Author contributions

LLL, HPS and TWP contributed to the experimental design and preparation of the manuscript. LLL, APR, CAP, RLH and ABA carried out the research. APR contributed to the design of experiments. All authors were involved in the revision of the draft manuscript and have agreed to the final content.

### Competing interests

No competing interests were disclosed.

### Grant information

This project was supported by Epiderm (Boronia Park, NSW 2111, Australia) and NHMRC Practitioner Fellowship (APP1020148) (HPS).

*The funders had no role in study design, data collection and analysis, decision to publish, or preparation of the manuscript.*

### Acknowledgements

We thank Drs. Sudipta Sinnya and Jean-Marie Tan for patient recruitment and clinical assistance. We thank Dr. Roy Hall for providing the human actin primers and Dr. Yin Xiang Setoh for assisting in the PCR experiment. We thank Dr. Rick Sturm for his valuable input on the molecular characterization of this device.

### References

- Sina B, Kao GF, Deng AC, *et al.*: **Skin biopsy for inflammatory and common neoplastic skin diseases: optimum time, best location and preferred techniques. A critical review.** *J Cutan Pathol.* 2009; **36**(5): 505–510.  
[PubMed Abstract](#) | [Publisher Full Text](#)
- Pickett H: **Shave and punch biopsy for skin lesions.** *Am Fam Physician.* 2011; **84**(9): 995–1002.  
[PubMed Abstract](#)
- Ugurel S, Utikal J, Becker JC: **Tumor biomarkers in melanoma.** *Cancer Control.* 2009; **16**(3): 219–224.  
[PubMed Abstract](#)
- Shivers S, Jakub J, Pendas S, *et al.*: **Molecular staging for patients with malignant melanoma.** *Expert Rev Anticancer Ther.* 2007; **7**(11): 1665–1674.  
[PubMed Abstract](#) | [Publisher Full Text](#)
- Greiner R: **Skin cancer: new markers for better prevention.** *Pathobiology.* 2009; **76**(2): 64–81.  
[PubMed Abstract](#) | [Publisher Full Text](#)
- Krulevitch PA, Lee AP, Northrup MA, *et al.*: **Microbiopsy/Precision cutting devices.** In. Edited by Patent US. United States: The Regents of the University of California; 1999.  
[Reference Source](#)
- Byun S, Lim JM, Paik SJ, *et al.*: **Barbed micro-spikes for micro-scale biopsy.** *J Micromech Microeng.* 2005; **15**(6): 1279–1284.  
[Publisher Full Text](#)
- Cho D, Park SK, Lee AR, *et al.*: **Catheter capable of being equipped with micro biopsy tool.** In. Edited by Patent US; 2011.  
[Reference Source](#)
- Cosnier ML, Martin F, Bouamrani A, *et al.*: **A minimally invasive microdevice for molecular sampling and analysis.** *IEEE Trans Biomed Eng.* 2009; **56**(12): 2898–2904.  
[PubMed Abstract](#) | [Publisher Full Text](#)
- Pflueger DR: **Micro-invasive breast biopsy device.** In. Edited by Patent US; 2004.  
[Reference Source](#)
- Banan P, Lin LL, Lambie D, *et al.*: **Effects of Ex Vivo Skin Microbiopsy on histopathological diagnosis in melanocytic skin lesions.** *JAMA Dermatol.* 2013; **149**(9): 1107–9.  
[PubMed Abstract](#) | [Publisher Full Text](#)
- Fuchs A, Marmur E: **The kinetics of skin cancer: progression of actinic keratosis to squamous cell carcinoma.** *Dermatol Surg.* 2007; **33**(9): 1099–1101.  
[PubMed Abstract](#) | [Publisher Full Text](#)
- Chapman PB, Hauschild A, Robert C, *et al.*: **Improved survival with vemurafenib in melanoma with BRAF V600E mutation.** *N Engl J Med.* 2011; **364**(26): 2507–2516.  
[PubMed Abstract](#) | [Publisher Full Text](#) | [Free Full Text](#)
- Flaherty KT, Infante JR, Daud A, *et al.*: **Combined BRAF and MEK inhibition in melanoma with BRAF V600 mutations.** *N Engl J Med.* 2012; **367**(18): 1694–1703.  
[PubMed Abstract](#) | [Publisher Full Text](#) | [Free Full Text](#)
- Flaherty KT, Robert C, Hersey P, *et al.*: **Improved survival with MEK inhibition in BRAF-mutated melanoma.** *N Engl J Med.* 2012; **367**(2): 107–114.  
[PubMed Abstract](#) | [Publisher Full Text](#)
- Romano E, Schwartz GK, Chapman PB, *et al.*: **Treatment implications of the emerging molecular classification system for melanoma.** *Lancet Oncol.* 2011; **12**(9): 913–922.  
[PubMed Abstract](#) | [Publisher Full Text](#)
- Jin SA, Chun SM, Choi YD, *et al.*: **BRAF mutations and KIT aberrations and their clinicopathological correlation in 202 Korean melanomas.** *J Invest Dermatol.* 2013; **133**(2): 579–582.  
[PubMed Abstract](#) | [Publisher Full Text](#)
- Yancovitz M, Litterman A, Yoon J, *et al.*: **Intra- and inter-tumor heterogeneity of BRAF(V600E) mutations in primary and metastatic melanoma.** *PLoS One.* 2012; **7**(1): e29336.  
[PubMed Abstract](#) | [Publisher Full Text](#) | [Free Full Text](#)
- Berglund SR, Schwiert CW, Jones AA, *et al.*: **Optimized methodology for sequential extraction of RNA and protein from small human skin biopsies.** *J Invest Dermatol.* 2007; **127**(2): 349–353.  
[PubMed Abstract](#) | [Publisher Full Text](#)
- Bruning O, Rodenburg W, Radonic T, *et al.*: **RNA isolation for transcriptomics of human and mouse small skin biopsies.** *BMC Res Notes.* 2011; **4**: 438.  
[PubMed Abstract](#) | [Publisher Full Text](#) | [Free Full Text](#)
- Dang C, Gottschling M, Manning K, *et al.*: **Identification of dysregulated genes in cutaneous squamous cell carcinoma.** *Oncol Rep.* 2006; **16**(3): 513–519.  
[PubMed Abstract](#)
- Fitzpatrick TB: **The validity and practicality of sun-reactive skin types I through VI.** *Arch Dermatol.* 1988; **124**(6): 869–871.  
[PubMed Abstract](#) | [Publisher Full Text](#)



# Letters

## RESEARCH LETTER

### Effects of Ex Vivo Skin Microbiopsy on Histopathologic Diagnosis in Melanocytic Skin Lesions

Currently, histopathologic analysis represents the practical reference standard for the diagnosis of melanocytic skin lesions. However, there are limitations particularly related to the morphologic nature of the histopathologic interpretation and the influence of the clinical information on the final diagnosis.<sup>1</sup> To provide lesional tissue from melanocytic proliferations for molecular analysis without jeopardizing the conventional histopathologic diagnosis, we invented a miniaturized biopsy device with a total width of 0.35 mm, containing a sample chamber 0.15 mm wide. This device penetrates approximately 250  $\mu\text{m}$  in healthy skin (ie, superficial dermis) to collect approximately 1600 cells.<sup>2</sup> This microbiopsy device can be used without local anesthetic, and there is no need for a suture. Our hypothesis is that the minimal skin damage caused by the microbiopsy does not interfere with the subsequent histopathologic diagnosis.

**Methods** | Five patients scheduled for suspicious pigmented lesion removal at the dermatology department of the Princess Alexandra Hospital, a public tertiary hospital in Brisbane, Australia, were recruited.



Editorial

Consent was obtained from all participants with approval from The University of Queensland/Princess Alexandra Hospital Human Research Ethics Committees. Clinical images of the lesions were taken before surgery and immediately after excision. Each excised lesion was bisected, and 5 microbiopsy specimens were applied ex vivo to one of the halved lesions. The microbiopsy site locations were documented, and the specimens were labeled accordingly. All specimens were sectioned in the hospital's pathology laboratory according to routine protocol.

**Results** | All sections were examined by a dermatopathologist (D.L.) for the histopathologic diagnosis, with special emphasis on the microbiopsy defect. The mean (SD) size of the microbiopsy defect was 113 (50)  $\mu\text{m}$  wide and 146 (37)  $\mu\text{m}$  deep ( $n = 4$ ). These defects are comparable, albeit not identical, to processing artifacts in nonmicrobiopsied specimens ranging from 20 to 2100  $\mu\text{m}$  wide and 70 to 600  $\mu\text{m}$  deep. Histopathologic diagnoses in both halves, while examined separately, were exactly the same in all lesions. Diagnoses included compound nevus, junctional lentiginous nevus, compound dysplastic nevus, junctional dysplastic nevus, and solar lentigo.

From the 5 lesions included in the study, 2 are displayed herein clinically and histopathologically. Patient 1 was an 88-year-old man with a history of metastatic melanoma, who had

a deep shave excision of a new nevus identified on his left flank. One of the microbiopsy defects identified within the melanocytic region was  $132 \times 74 \mu\text{m}$  in size (Figure 1). The diagnosis was a compound dysplastic nevus. Patient 2 was a 56-year-old woman with history of nonmelanoma skin cancer, who presented with a changing nevus on her left scapula. One of the microbiopsy defects found outside the lesional region was  $145 \times 201 \mu\text{m}$  and reached the superficial dermis (Figure 2). Diagnosis of this lesion was junctional lentiginous nevus.

**Discussion** | Over the years, many microdevices have been developed to obtain tissue samples,<sup>3-5</sup> but interestingly enough none of these microdevices are specifically engineered for skin lesions. Because of the new exciting developments of targeted molecular therapies in patients with melanoma,<sup>6</sup> there is a need for a minimally invasive biopsy device enabling small tissue collection with minimal adverse effects to perform downstream molecular diagnosis of melanocytic skin lesions.

The size of microbiopsy defects measured in this study was comparable to other artifacts more or less commonly seen in routine sectioned specimens. The potential diagnostic difficulties for the dermatopathologist encountered with the histopathologic assessment of a microbiopsied melanocytic skin lesion can easily be overcome by ordering multiple levels. All 5 melanocytic lesions included in this study were not difficult to assess, and therefore the diagnostic process was not hampered by the microbiopsy-induced artifacts; however, on the basis of the size of the microbiopsy artifacts, we foresee that the diagnostic process, even in equivocal cases, will not be influenced. The data from this study support the hypothesis that minimal skin damage caused by the microbiopsy does not affect the histopathologic diagnosis.

**Parastoo Banan, MD**

**Lynlee L. Lin, BSc**

**Duncan Lambie, BDSc, MBBS, FRCPA**

**Tarl Prow, BS, MSc, PhD**

**H. Peter Soyer, MD, FACD**

**Author Affiliations:** Dermatology Research Centre, The University of Queensland, School of Medicine, Translational Research Institute, Princess Alexandra Hospital, Brisbane, Queensland, Australia (Banan, Lin, Prow, Soyer); Department of Anatomical Pathology, Princess Alexandra Hospital, Brisbane, Queensland, Australia (Lambie).

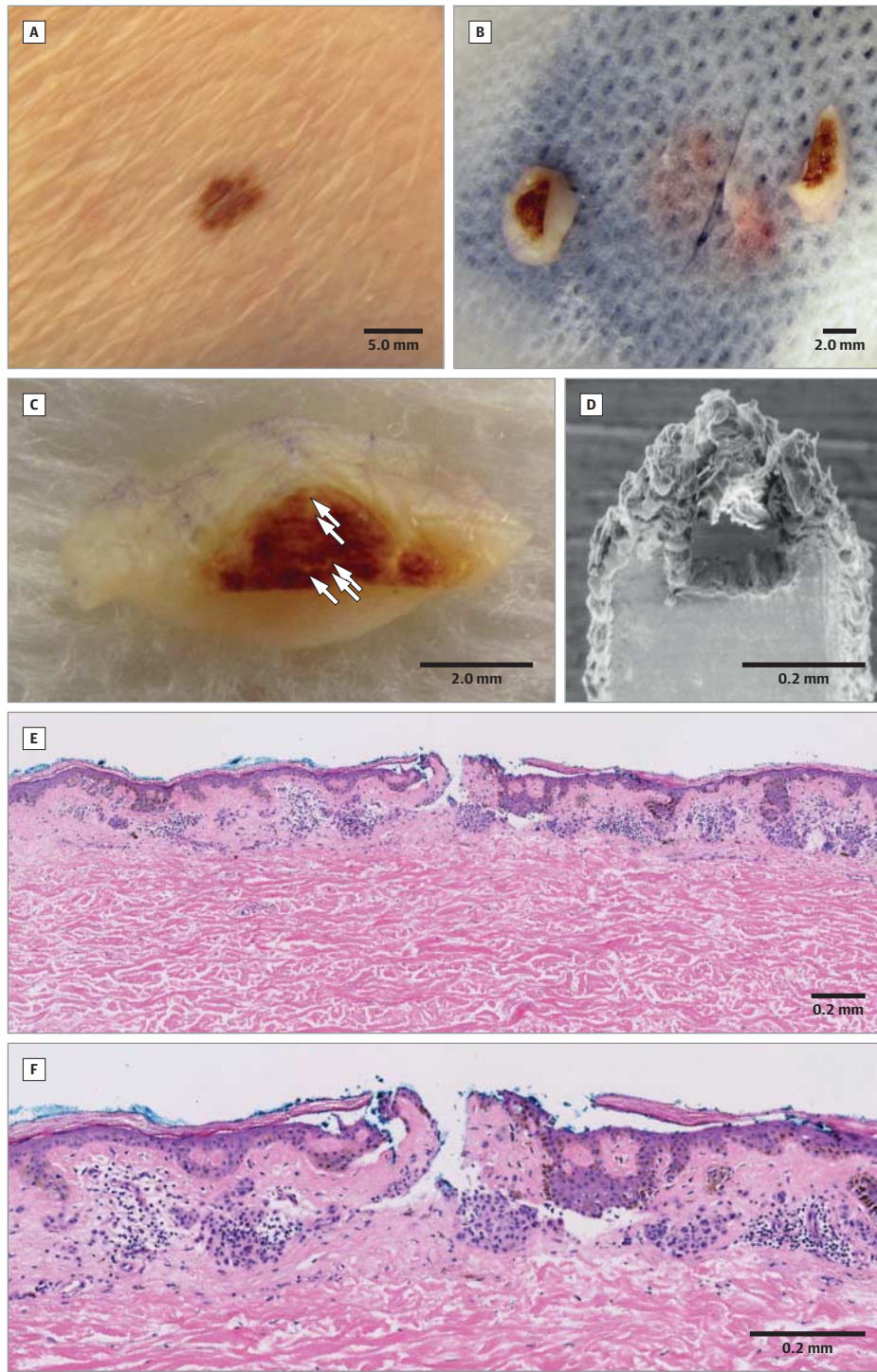
**Corresponding Author:** H. Peter Soyer, MD, FACD, Dermatology Research Centre, The University of Queensland, School of Medicine, Translational Research Institute (TRI), 37 Kent St, Woolloongabba, QLD 4102, Australia (p.soyer@uq.edu.au).

**Accepted for Publication:** May 7, 2013.

**Published Online:** July 17, 2013.  
doi:10.1001/jamadermatol.2013.5020.

**Author Contributions:** All authors had full access to all of the data in the study and take responsibility for the integrity of the data and the accuracy of the data analysis.

Figure 1. Patient 1



A, Patient 1 clinical photograph; B, excised lesions; and C, microbiopsy sites (white arrows). D, The microbiopsy device with a sample; E, the site of microbiopsy at low magnification; and F, the site at high magnification.

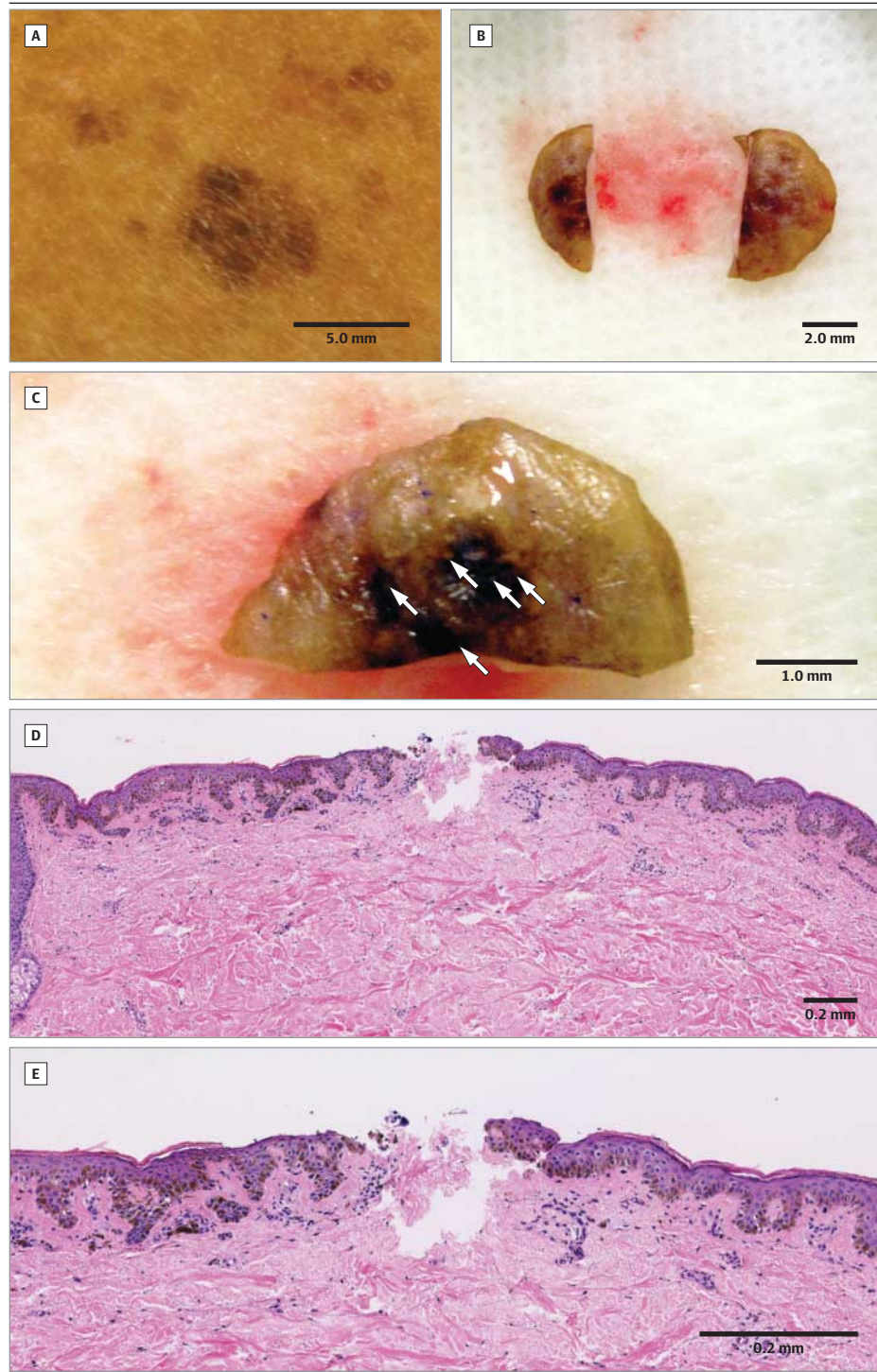
*Study concept and design:* Lambie, Prow, Soyer.  
*Acquisition of data:* Banan, Lin, Lambie.  
*Analysis and interpretation of data:* All authors.  
*Drafting of the manuscript:* Banan, Lin, Prow.  
*Critical revision of the manuscript for important intellectual content:* All authors.  
*Statistical analysis:* Banan.  
*Obtained funding:* Soyer.  
*Administrative, technical, and material support:* Banan, Lin, Lambie, Prow.  
*Study supervision:* Lambie, Prow, Soyer.

**Conflict of Interest Disclosures:** None reported.

**Funding/Support:** This study was supported in part by Epiderm. Dr Soyer has a National Health and Medical Research Council Practitioner Fellowship.

1. Ferrara G, Argenyi Z, Argenziano G, et al. The influence of clinical information in the histopathologic diagnosis of melanocytic skin neoplasms. *PLoS One*. 2009;4(4):e5375.
2. Lin LL, Prow TW, Raphael AP, et al. Microbiopsy engineered for minimally invasive and suture-free sub-millimetre skin sampling. *F1000Research*. 2013;2:

Figure 2. Patient 2



A, Patient 2 clinical photograph; B, excised lesions; and C, microbiopsy sites (white arrows). D, The microbiopsy site at low magnification; and E, the site at high magnification.

120. doi:10.12688/f1000research.2-120.v1. <http://f1000research.com/articles/2-120/v1#reflist>. Accessed May 2, 2013.

3. Cosnier ML, Martin F, Bouamrani A, Berger F, Caillat P. A minimally invasive microdevice for molecular sampling and analysis. *IEEE Trans Biomed Eng*. 2009;56(12):2898-2904.

4. Pflueger DR, inventor; Stryker Puerto Rico Limited, assignee. Micro-invasive breast biopsy device. US patent 6,673,023 B2. January 6, 2004. <http://www.google.com/patents/US6673023>. Accessed January 16, 2013.

5. Cho D, Park SK, Lee AR, et al, inventors; Seoul National University Industry Foundation, assignee. Catheter capable of being equipped with micro biopsy tool. US patent 7,927,289 B2. April 19, 2011. <http://www.google.com/patents/US7927289>. Accessed January 16, 2013.

6. Khattak M, Fisher R, Turajlic S, Larkin J. Targeted therapy and immunotherapy in advanced melanoma: an evolving paradigm. *Ther Adv Med Oncol*. 2013;5(2):105-118.

## Case Report/Case Series

# *BRAF*<sup>V600E</sup> Mutation Status of Involuting and Stable Nevi in Dabrafenib Therapy With or Without Trametinib

Phil McClenahan, BSc; Lynlee L. Lin, BSc; Jean-Marie Tan, MB, BCh, BAO (hons); Ross Flewell-Smith, BCom, BEng; Helmut Schaidler, MD; Kasturee Jagirdar, MSc; Victoria Atkinson, MBBS, FRACP; Duncan Lambie, BSc, MBBS, FRCPA; Tarl W. Prow, BS, MSc, PhD; Richard A. Sturm, PhD; H. Peter Soyer, MD, FACD

**IMPORTANCE** Recent advances in targeting *BRAF*<sup>V600E</sup> mutations, which occur in roughly 50% of melanomas and 70% of benign nevi, have improved response rates and survival in patients with melanoma. With increased survival, the importance of other comorbidities increases and requires consideration in long-term management. This case report discusses dynamic dermoscopic nevus changes that occur during dabrafenib therapy and offers some conclusions regarding *BRAF* mutations and the changes.

**OBSERVATIONS** A man in his 30s had been monitored with whole-body dermoscopy at roughly 7-month intervals as part of a nevus surveillance study. Fourteen months after his initial visit, metastases were found, and the patient entered a clinical trial of dabrafenib with or without trametinib therapy. Continued dermoscopic monitoring for the next 12 months revealed that approximately 50% of the existing acquired melanocytic nevi involuted, while the remaining nevi did not change. Biopsy findings from 1 unchanged and 1 involuted nevus showed *BRAF* wild type in the unchanged nevus, *BRAF*<sup>V600E</sup> mutation in the involuting nevus, and no malignant histopathologic characteristics in either one.

**CONCLUSIONS AND RELEVANCE** Our observations indicate that a previously suggested hypothesis regarding involuting nevi in *BRAF* inhibitor therapy is correct: Nevi that involute while a patient is undergoing *BRAF* V600E inhibitor therapy possess the *BRAF* V600E mutation, while others that grow or remain unchanged are wild type. However larger-scale trials are required to gather conclusive data and create a more complete clinical picture.

*JAMA Dermatol.* doi:10.1001/jamadermatol.2014.436  
Published online April 2, 2014.

**Author Affiliations:** Dermatology Research Centre, The University of Queensland, School of Medicine, Translational Research Institute, Brisbane, Queensland, Australia (McClenahan, Lin, Tan, Flewell-Smith, Schaidler, Jagirdar, Prow, Sturm, Soyer); The University of Queensland, Institute for Molecular Biosciences, Brisbane, Queensland, Australia (Jagirdar, Sturm); Medical Oncology, Princess Alexandra Hospital, Woolloongabba, Queensland, Australia (Atkinson); The University of Queensland, Translational Research Institute, Brisbane, Queensland, Australia (Lambie); IQ Pathology, Brisbane, Queensland, Australia (Lambie).

**Corresponding Author:** H. Peter Soyer, MD, FACD, Level 5, Translational Research Institute (TRI), 37 Kent St, Woolloongabba QLD 4102, Australia (p.soyer@uq.edu.au).

**M**elanocytes, like many other human cells, express the *BRAF* gene. However, mutation of *BRAF* in melanocytes occurs at high frequency in melanocytic proliferations such as nevi (70%-82%) and melanomas (50%-60%).<sup>1,2</sup> Mutation of *BRAF* results in a defect of the mitogen-activated protein kinase (MAPK) pathway causing oncogenic proliferation and avoidance of apoptosis.<sup>3</sup> Most frequently, *BRAF* mutations occur at the V600E position (74%-90%), and the next most common mutation occurs at V600K (16%-29%)<sup>4</sup>; together, these sites account for 95% of all *BRAF* mutations.

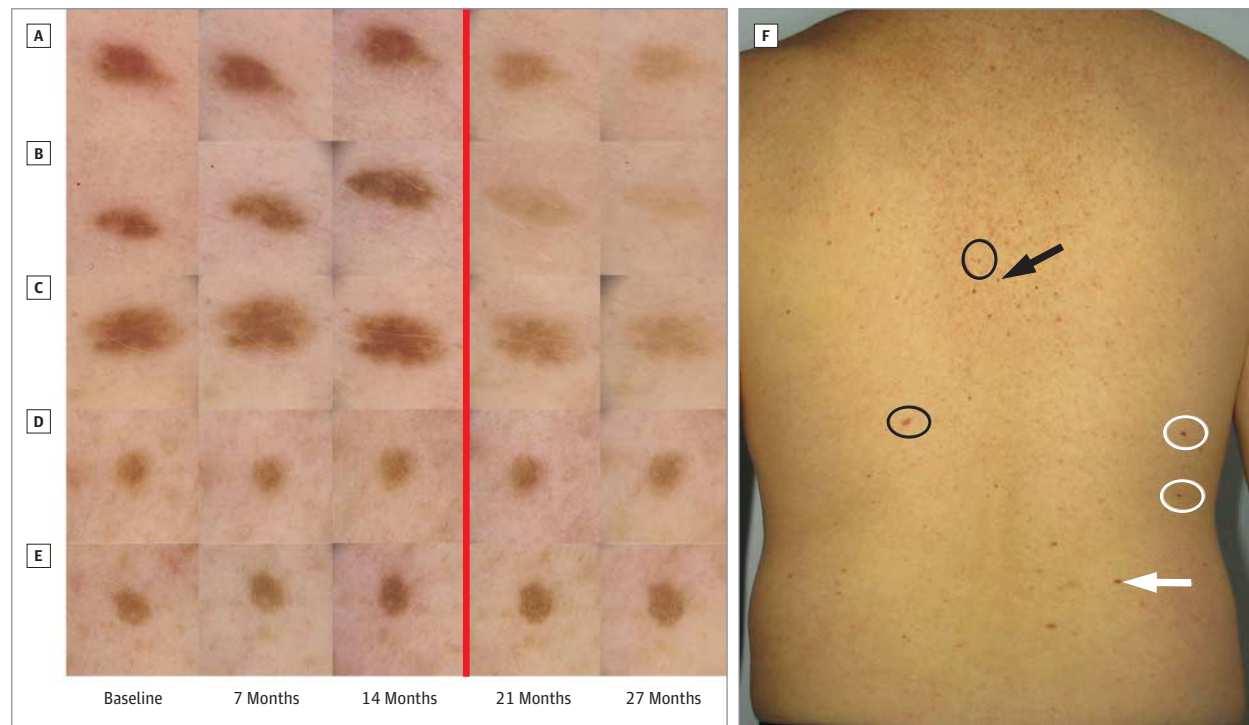
Initial breakthrough treatments were made with vemurafenib, a selective inhibitor of *BRAF*<sup>V600E</sup>-mutated kinase. The inhibition of *BRAF*<sup>V600E</sup> initially induces tumor growth arrest and partial or complete tumor regression in metastatic melanoma.<sup>5</sup> Given the frequency of *BRAF*<sup>V600E</sup> mutations in benign nevi,<sup>2</sup> it is also not surprising that changes have been observed in existing melanocytic nevi and that new nevi appear during *BRAF*<sup>V600E</sup> inhibitor therapy.<sup>6,7</sup> Recently, a study of 42 patients treated with vemurafenib for a mean duration of 6.7 months described a high level of dermoscopic change in pre-existing lesions such as color changes, appearance and disap-

pearance of globules, dermoscopic island pigmentation, and increases in size of nevi.<sup>8</sup> New primary melanomas have also been reported during the early stages of vemurafenib treatment, arising from new erupting melanocytic proliferations or rapidly changing existing nevi.<sup>9</sup> Zimmer et al,<sup>9</sup> Dalle et al,<sup>7</sup> and Perier-Muzet et al<sup>8</sup> report that these new primary melanomas arising during vemurafenib therapy are *BRAF* wild type.

Herein we describe an example of nevus volatility and propose the molecular involvement in a patient undergoing *BRAF*<sup>V600E</sup> inhibition therapy and who participated in a nevus surveillance study. All patients in the surveillance study provided written consent, and the study followed the Declaration of Helsinki protocols and was approved by the Princess Alexandra Hospital human research ethics committee.

## Report of a Case

While participating in a nevus surveillance study, 1 of the patients, a man in his 30s who had been diagnosed 5 years earlier as having a superficial melanoma (Clark level 3, Breslow

Figure 1. Surveillance of Involuting Nevus During BRAF<sup>V600E</sup> Inhibitor Therapy and Clinical Image of Back

A-C, Three nevi have undergone involution 7 months after initiation of BRAF<sup>V600E</sup> inhibitor therapy. D and E, The other 2 nevi remain unchanged. Excisional shave biopsies and numerous ex vivo microbiopsies were performed on nevi C and E. Images to the left of the vertical red line were obtained before the patient commenced participation in the BRAF inhibitor trial; images to the

right of the line were obtained after he entered the trial. F, Clinical image of the back shows nevi locations: white arrow indicates biopsied involuting nevus; white circles indicate involuting nevi; black arrow indicates biopsied unchanged nevus; black circles indicate unchanged nevi.

index 0.64 mm), developed metastases in the pancreas, liver, and mesenteric lymph nodes. Two months later, he was enrolled in a clinical trial of dabrafenib with or without trametinib therapy. Dabrafenib is a BRAF inhibitor similar to vemurafenib, and it was being tested with trametinib, a MEK (MAPK kinase) inhibitor that targets the same MAPK pathway. The trial was blinded and still ongoing at the time of the present report, and so it is unknown whether this patient's treatment regimen included trametinib.

The patient presented with Fitzpatrick skin type III, dark brown hair, and green eyes. He underwent imaging with a FotoFinder system (FotoFinder Systems GmbH) of all nevi larger than 2 mm on the back and larger than 5 mm on the rest of the body. No significant changes were observed dermoscopically throughout. Ten nevi larger than 5 mm were identified on the body, while 25 nevi larger than 2 mm were identified on the back, for a total of 31 nevi included in our analysis. There were 2 globular, 15 reticular, and 14 nonspecific/homogeneous nevi.

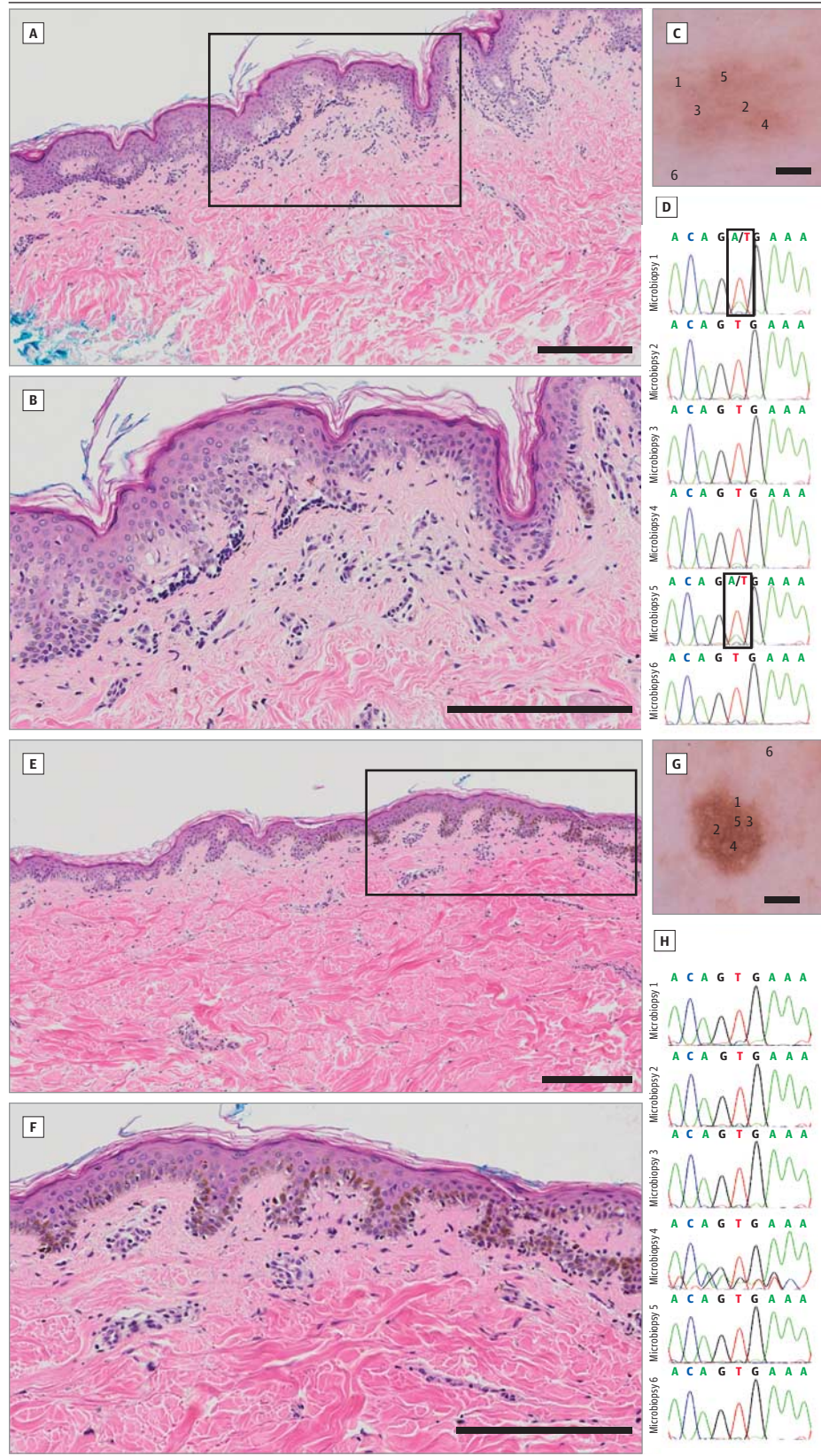
Full-body and dermoscopic imaging was conducted 5 times over the next 27 months at roughly 7-month intervals, and no significant dermoscopic changes were identified by assessment of imaged nevi at the 7- or 14-month visits. However, at the 21-month visit, 6 months after he commenced participation in the BRAF inhibitor trial, assessment revealed significant dermoscopic changes 16 nevi (51% of total) (Figure 1). The

nevi changes predominantly involved involution and a decrease in pigmentation and size. In addition, in concurrence with other reports,<sup>6</sup> flattening of raised nevi was also observed. By dermoscopic pattern, 4 reticular, 10 homogeneous, and 2 globular nevi showed signs of involution. Therefore, 71% of the unspecific and 26% of the reticular nevi showed signs of involution, while both raised globular nevi decreased in pigmentation and flattened.

By the time of final imaging at 27 months' surveillance (12 months into the BRAF inhibitor trial), the nevi had generally not further changed, but 5 nevi had continued to involute: 3 reticular and 2 homogeneous nevi. Again, no increase in pigmentation was observed in any lesions, and no new nevi were observed. The patient had an otherwise excellent systemic response to the targeted therapy and an excellent partial response to the point of almost a complete response, with the exception of a small unchanged node near the pancreas that was seen on computed tomographic imaging.

There are a number of external and endogenous factors influencing changes and appearance of nevi over time. These include UV radiation exposure, hormonal changes associated with pregnancy,<sup>10</sup> and targeted melanoma therapies such as selective BRAF<sup>V600E</sup> inhibitors.<sup>6</sup> As unchanged and changed nevi were at times adjacent at the same body site, UV exposure was not considered to be a major influencing factor, and

Figure 2. Histopathologic Images and Molecular Sequencing Charts for *BRAF*<sup>V600E</sup> Status of 1 Involving Nevus and 1 Noninvolving Nevus



A-D, Workup of an involving nevus. E-H, Workup of a noninvolving nevus. C and G, Dermoscopic images show microbiopsy sites 1 through 5 (scale bar = 1 mm); site 6 in each panel is a control biopsy site adjacent to the nevus. D and H, Molecular analysis charts for microbiopsy sites shown in panels C and G, respectively. A and E, Histopathologic images of the nevi, neither of which shows any histopathological criteria for melanoma (scale bars = 200  $\mu$ m; boxes enclose areas shown at higher magnification in panels B and F). The involved nevus in panel A is a benign, predominantly junctional nevus with few discrete nests of nonpigmented nevus cells at the dermal-epidermal junction; subtle lymphatic infiltration around suprapapillary vascular plexus; and no obvious signs of fibrosis or regression; sequencing (D) reveals that the nevus is heterogeneous for *BRAF*<sup>V600E</sup> mutation at sites 1 and 5. The noninvolved nevus in panel E is a benign lentiginous melanocytic nevus with elongated pigmented rete ridges and slightly increased numbers of melanocytes at the dermal-epidermal junction; small junctional nests of melanocytes are also present; and sequencing (H) reveals no presence of *BRAF*<sup>V600E</sup> mutation. B and F, Greater magnifications of the boxed areas of panels A and E, respectively (scale bars = 200  $\mu$ m).

pregnancy cannot be considered in our male patient. Therefore to sample molecular markers, specifically *BRAF* mutation status of changed and unchanged nevi, we used a newly described microbiopsy device.<sup>11-13</sup>

Diagnostic shave excisions were performed on 1 involuted nevus and 1 unchanged nevus (Figure 1). The histopathologic diagnosis for the involuted lesion was a predominantly junctional compound nevus without significant inflammation or fibrosis, and the unchanged lesion was characterized as a junctional nevus with a lentiginous melanocytic pattern. Microbiopsy specimens were taken from 6 locations on both of the excised nevi (Figure 2). DNA samples extracted from microbiopsy specimens were subjected to polymerase chain reaction amplification using selected forward and reverse primers to flank the *BRAF* exon 15 and *NRAS* exon 2 mutation hotspots.<sup>14</sup> Molecular sequencing of the samples for *BRAF* and *NRAS* mutations were performed after extraction of amplified products from the DNA gel. Sequencing revealed heterogeneous *BRAF*<sup>V600E</sup> mutation in the involuting nevus and *BRAF* wild type in the unchanged nevus, while both lesions were *NRAS* wild type.

## Discussion

The involution of nevi in *BRAF*<sup>V600E</sup> inhibitor therapy has been reported, but herein we report findings that support the hypothesis<sup>6</sup> that these nevi are *BRAF*<sup>V600E</sup> positive. This is related to decreased MAPK activity due to *BRAF* inhibition. In contrast to reports in vemurafenib-treated patients of increased size and pigmentation in some nevi and the appearance of new *BRAF* wild-type melanoma through paradoxical *BRAF* activation,<sup>15</sup> we observed no increase in pigmentation of nevi or suspect changes in our patient. Because we could not know whether our dabrafenib-treated patient was also receiving trametinib, conclusions regarding the combination regimen cannot be drawn. However, our long-term monitoring prior to and during therapy combined with confirmation of involuting nevi possessing *BRAF*<sup>V600E</sup> mutation adds another component to the dermoscopic changes in long-term therapy with *BRAF*<sup>V600E</sup> inhibitors. Larger-scale and longer-term trials will give a broader and more accurate description of specific medication effects required for dermatologic follow-up.

### ARTICLE INFORMATION

**Accepted for Publication:** February 26, 2014.

**Published Online:** April 2, 2014.  
doi:10.1001/jamadermatol.2014.436.

**Author Contributions:** Mr McClenahan had full access to all of the data in the study and takes responsibility for the integrity of the data and the accuracy of the data analysis.

**Study concept and design:** McClenahan, Flewell-Smith, Soyer.

**Acquisition of data:** McClenahan, Lin, Tan, Jagirdar, Atkinson, Lambie, Prow, Sturm, Soyer.

**Analysis and interpretation of data:** McClenahan, Lin, Schaidler, Jagirdar, Prow, Sturm, Soyer.

**Drafting of the manuscript:** McClenahan, Lin, Flewell-Smith, Schaidler, Prow, Soyer.

**Critical revision of the manuscript for important intellectual content:** McClenahan, Tan, Jagirdar, Atkinson, Lambie, Sturm, Soyer.

**Statistical analysis:** McClenahan, Sturm, Soyer.

**Obtained funding:** Soyer.

**Administrative, technical, or material support:** Lin, Tan, Flewell-Smith, Jagirdar, Lambie, Prow, Sturm, Soyer.

**Study supervision:** Schaidler, Sturm, Soyer.

**Conflict of Interest Disclosures:** None reported.

**Funding/Support:** This study was supported in part by research grant APPI004999 from the National Health and Medical Research Council, Canberra, Australian Capital Territory, Australia.

**Role of the Sponsor:** The National Health and Medical Research Council had no role in the design and conduct of the study; collection, management, analysis, and interpretation of the data;

preparation, review, or approval of the manuscript; and decision to submit the manuscript for publication.

### REFERENCES

- Davies H, Bignell GR, Cox C, et al. Mutations of the *BRAF* gene in human cancer. *Nature*. 2002;417(6892):949-954.
- Pollock PM, Harper UL, Hansen KS, et al. High frequency of *BRAF* mutations in nevi. *Nat Genet*. 2003;33(1):19-20.
- Wan PT, Garnett MJ, Roe SM, et al; Cancer Genome Project. Mechanism of activation of the RAF-ERK signaling pathway by oncogenic mutations of B-RAF. *Cell*. 2004;116(6):855-867.
- Thomas NE. *BRAF* somatic mutations in malignant melanoma and melanocytic naevi. *Melanoma Res*. 2006;16(2):97-103.
- Flaherty KT, Puzanov I, Kim KB, et al. Inhibition of mutated, activated *BRAF* in metastatic melanoma. *N Engl J Med*. 2010;363(9):809-819.
- Haenssle HA, Kraus SL, Brehmer F, et al. Dynamic changes in nevi of a patient with melanoma treated with vemurafenib: importance of sequential dermoscopy. *Arch Dermatol*. 2012;148(10):1183-1185.
- Dalle S, Poulalhon N, Thomas L. Vemurafenib in melanoma with *BRAF* V600E mutation. *N Engl J Med*. 2011;365(15):1448-1450.
- Perier-Muzet M, Thomas L, Poulalhon N, et al. Melanoma patients under vemurafenib: prospective follow-up of melanocytic lesions by digital dermoscopy [published online November 7, 2013]. *J Invest Dermatol*. doi:10.1038/jid.2013.462.
- Zimmer L, Hillen U, Livingstone E, et al. Atypical melanocytic proliferations and new primary melanomas in patients with advanced melanoma undergoing selective *BRAF* inhibition. *J Clin Oncol*. 2012;30(19):2375-2383.
- Hofmann-Wellenhof R, Wolf P, Smolle J, Reimann-Weber A, Soyer HP, Kerl H. Influence of UVB therapy on dermoscopic features of acquired melanocytic nevi. *J Am Acad Dermatol*. 1997;37(4):559-563.
- Soyer HP, Lin LL, Prow TW. A plea for biobanking of all equivocal melanocytic proliferations. *JAMA Dermatol*. 2013;149(9):1023-1024.
- Banan P, Lin LL, Lambie D, Prow T, Soyer HP. Effects of ex vivo skin microbiopsy on histopathologic diagnosis in melanocytic skin lesions. *JAMA Dermatol*. 2013;149(9):1107-1109.
- Lin LL, Prow TW, Raphael AP, et al. Microbiopsy engineered for minimally invasive and suture-free sub-millimetre skin sampling. *F1000 Res*. 2013;2:120. doi:10.12688/f1000research.2-120.v2. http://f1000research.com/articles/2-120/v2. Accessed February 26, 2013.
- Tschandl P, Berghoff AS, Preusser M, et al. *NRAS* and *BRAF* mutations in melanoma-associated nevi and uninvolved nevi. *PLoS One*. 2013;8(7):e69639.
- Hatzivassiliou G, Song K, Yen I, et al. *RAF* inhibitors prime wild-type *RAF* to activate the *MAPK* pathway and enhance growth. *Nature*. 2010;464(7287):431-435.

## Case Report/Case Series

# *BRAF* Wild-Type Melanoma In Situ Arising In a *BRAF* V600E Mutant Dysplastic Nevus


Jean-Marie Tan, MB, BCh, BAO (Hons); Lynlee L. Lin, BSc; Duncan Lambie, BSc, MBBS, FRCPA; Ross Flewell-Smith, BCom, BEng; Kasturee Jagirdar, MSc; Helmut Schaidler, MD; Richard A. Sturm, PhD; Tarl W. Prow, BS, MSc, PhD; H. Peter Soyer, MD, FACD

**IMPORTANCE** The *BRAF* V600E mutation accounts for the majority of *BRAF* mutations found in cutaneous melanoma and is also commonly found in nevi. We used dermoscopy-targeted sampling and a microbiopsy device coupled with DNA sequence analysis to highlight *BRAF* V600E heterogeneity within a multicomponent melanocytic proliferation. This sampling technique demonstrates the prospect of in vivo application in a clinical setting.

**OBSERVATIONS** A man in his 50s with Fitzpatrick skin type II presented with an irregularly pigmented melanocytic lesion on his back that met melanoma-specific dermoscopic criteria, and diagnostic shave excision of the lesion was performed. Histopathologic analysis revealed a melanoma in situ arising in a dysplastic nevus. Dermoscopy-targeted microbiopsy specimens were taken across the lesion, and genotyping was carried out on extracted DNA samples for *BRAF* and *NRAS* mutations. The melanoma in situ showed only *BRAF* wild-type results, while the dysplastic nevus showed both *BRAF* wild-type and *BRAF* V600E mutations. Sequencing in all DNA samples revealed *NRAS* wild-type genotype.

**CONCLUSIONS AND RELEVANCE** Dermoscopy-targeted sampling and genotyping of a melanoma in situ arising in a dysplastic nevus revealed a phenotype-genotype paradox that confounds the exclusive significance of *BRAF* and *NRAS* mutations in melanoma pathogenesis. Further studies are required to investigate the importance of other candidate genes linked to melanomagenesis.

*JAMA Dermatol.* doi:10.1001/jamadermatol.2014.3775  
Published online January 21, 2015.

 Supplemental content at  
jamadermatology.com

**Author Affiliations:** Dermatology Research Centre, The University of Queensland, School of Medicine, Translational Research Institute, Brisbane, Australia (Tan, Lin, Flewell-Smith, Jagirdar, Schaidler, Sturm, Prow, Soyer); School of Medicine, The University of Queensland, Brisbane, Australia (Lambie); IQ Pathology, Brisbane, Queensland, Australia (Lambie).

**Corresponding Author:** H. Peter Soyer, MD, FACD, Dermatology Research Centre, University of Queensland School of Medicine, Level 5, Translational Research Institute, 37 Kent St, Woolloongabba, Brisbane, QLD 4102, Australia (p.soyer@uq.edu.au).

Initiation of malignant melanocytic proliferation through activation of the mitogen-activated protein kinase (MAPK) pathway most commonly involves the mutation of mutually exclusive *BRAF* or *NRAS*.<sup>1</sup> Constitutive activation of the MAPK pathway drives subsequent expression of a variety of oncogenes resulting in a transformed phenotype secondary to cell growth promotion.<sup>2</sup> *BRAF* mutational frequency in melanoma is commonly a substitution of valine by glutamic acid at codon 600 (V600E),<sup>3</sup> accounting for 74% to 90% of *BRAF* mutations in this malignant neoplasm.<sup>4</sup> The *BRAF* V600E mutation has also been detected in 73% to 82% of melanocytic nevi, implicating this gene mutation in the initiation of melanocytic neoplasia.<sup>1,2</sup>

The role of the *BRAF* mutation in the current genetic basis of melanoma development and progression is based on the Clark model for melanoma progression,<sup>5</sup> corresponding to the proposed morphologic changes from a benign nevus to a dysplastic nevus to a melanoma.<sup>6</sup> Thus, an alternative divergent molecular pathway genetic model has been proposed for *BRAF* or *NRAS* wild-type melanomas, developing possibly by activation of cell-cycle regulatory genes serving independent on-

cogenic function.<sup>2</sup> We herein describe the phenotypic characteristics and highlight the molecular complexity of a melanoma in situ arising within a dysplastic nevus via dermoscopy-targeted sampling and genotyping using a miniaturized biopsy device.

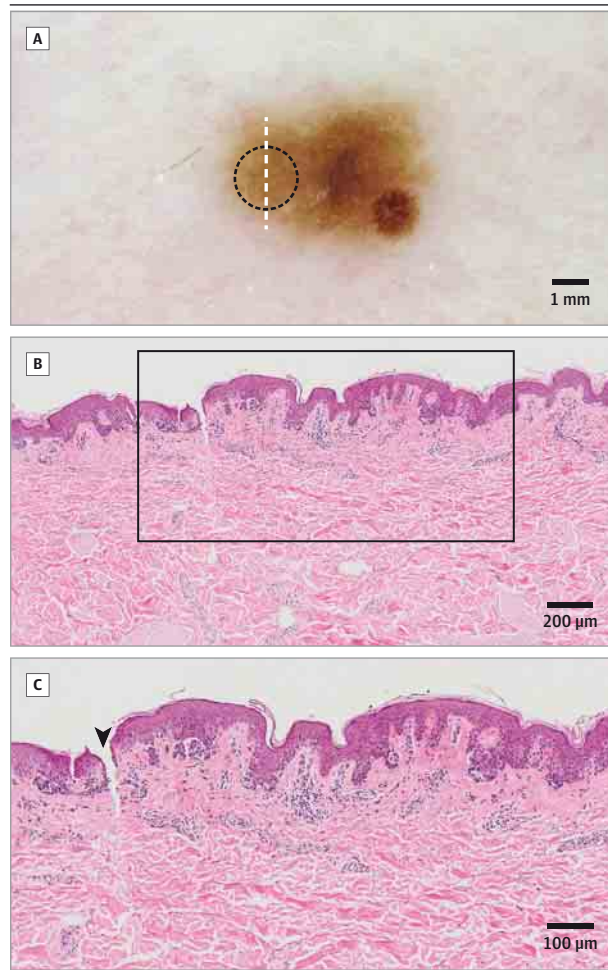
## Report of a Case

This study was approved by the Princess Alexandra Hospital human research ethics committee. The patient provided written informed consent in accordance with the Declaration of Helsinki.

A man in his 50s with Fitzpatrick skin type II and a family history of melanoma presented with a 5 × 3-mm irregularly pigmented melanocytic lesion on his left lower back detected on routine skin examination. The patient underwent imaging with the FotoFinder system (FotoFinder Systems Inc) of all nevi larger than 5 mm and also those between 2 and 5 mm on the back as part of a study on nevus morphology.<sup>7</sup> The total nevi count was 42, with 36 nevi on the back and 6 nevi on the rest



**Figure 1. Dermoscopy and Hematoxylin-Eosin–Stained Histopathology Images Corresponding to the Left Side of the Subject Lesion**

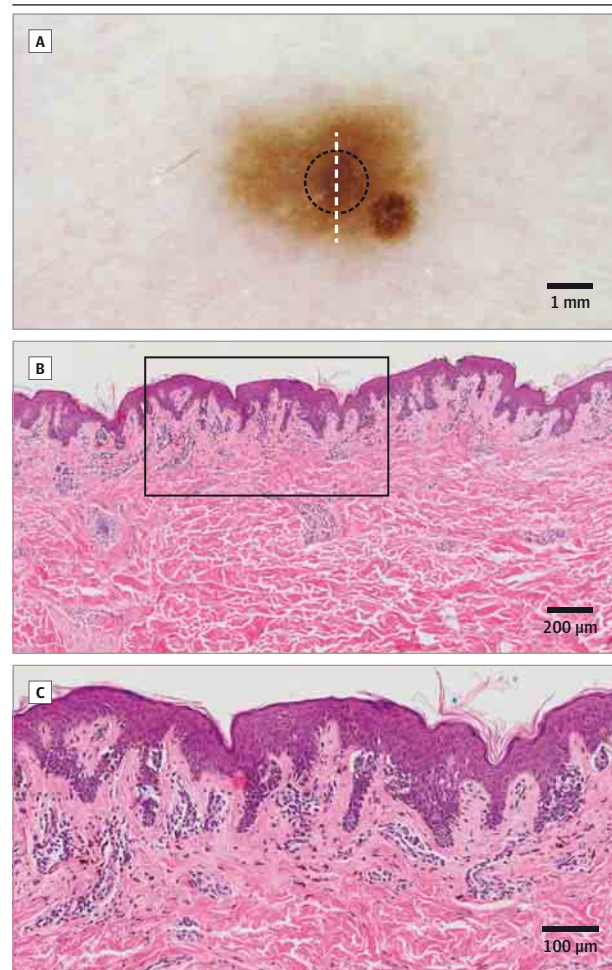


A, Circled area of the dermoscopy image reveals a normal reticular pattern without any dermoscopic criteria suggestive for melanoma; dermoscopy-targeted microbiodesert samples were taken from this circled area; vertical line corresponds to the site of the specimen shown in panel B. B, Photomicrograph of the histologic specimen reveals a rather conventional dysplastic nevus; boxed area corresponds to the magnified area shown in panel C. C, Higher magnification of the boxed section displays elongated pigmented rete ridges, discrete nests of melanocytes, and few single melanocytes, mostly along the dermoepidermal junction; a microbiodesert defect can be seen in this frame (arrowhead).

of the body; 35 of 36 of the nevi on the back measured between 2 and 5 mm. The patient's germline *MC1R* genotype was wild-type.

Dermoscopy unveiled a pigmented macule with multi-component pattern (Figure 1A, Figure 2A, and Figure 3A)—a normal reticular pattern on the left side of the lesion, some confluent blue areas at the center of the lesion, and a well-circumscribed area measuring 1 × 1 mm and characterized by an atypical pigment network and a few irregular streaks on the right side of the lesion at the 4-o'clock corner. The lesion met the 3-point checklist criteria for a melanoma with the presence of 2 features in that it had asymmetry and an atypical pigment network. It also showed melanoma-specific local crite-

**Figure 2. Dermoscopy and Hematoxylin-Eosin–Stained Histopathology Images Corresponding to the Center of the Subject Lesion**



A, Circled area of the dermoscopy image reveals a slightly more pigmented typical pigment network and subtle blue areas; dermoscopy-targeted microbiodesert samples were taken from this circled area; vertical line corresponds to the site of the specimen shown in panel B. B, Photomicrograph of the histologic specimen reveals a dysplastic nevus without any remarkable histopathologic findings; boxed area corresponds to the magnified area shown in panel C. C, Higher magnification of the boxed section exhibits a slightly increased number of melanophages in the papillary dermis, most probably reflecting the subtle bluish pigmentation at the center of the lesion.

ria (atypical pigment network and irregular streaks), and so a diagnostic shave excision of the lesion was performed.

The excised lesion was evaluated by 2 independent board-certified dermatopathologists (D.L. and H.P.S.). Histopathologic findings of the left side of the lesion were consistent with a dysplastic nevus characterized by elongated pigmented rete ridges, discrete nests of melanocytes, and few single melanocytes mostly along the dermoepidermal junction corresponding with the typical pigment network seen on dermoscopy (Figure 1). Similar morphologic findings were present at the center of the lesion with evidence of ample melanophages in the papillary dermis accounting for the subtle blue areas noted on dermoscopy (Figure 2). Histopathologic analysis of the right side of the lesion revealed features suggestive of an early melanoma in situ characterized by an increased number of atypi-

cal melanocytes at all levels of the epidermis corresponding to the well-circumscribed area at the 4-o'clock corner arising in an otherwise conventional predominantly junctional dysplastic nevus (Figure 3).

We used a new miniaturized biopsy device to sample lesional tissue for molecular analysis.<sup>8</sup> This sampling technique has been shown not to cause significant disruption to the lesion architecture and thus would not compromise the histopathologic assessment.<sup>9,10</sup> First, a transparent plate with a pinhole was coupled with a dermoscope to visualize the desired area for sampling. The dermoscope was removed once the area was identified through the pinhole, leaving the plate in contact with the lesion and rendering the area for sampling accessible to the biopsy device microneedle. The micro-biopsy device applicator was then aligned with the pinhole allowing for targeted sampling of the tissue. Three dermoscopy-guided micro-biopsy specimens were taken from each of the described dermoscopic areas in the excised lesion using this technique (Figure 4A).

Samples of DNA were extracted from the micro-biopsy tissue specimens using the QIAamp DNA Micro Kit followed by whole genomic amplification carried out with REPLI-g Single Cell Kit according to manufacturer's protocols (QIAGEN). The quality and integrity of amplified DNA was validated using the Bioanalyzer DNA 12000 kit (Agilent Technologies Inc). Gene-specific forward and reverse primers flanking BRAF exon 15 and NRAS exon 2 mutation hotspots were used for polymerase chain reaction.<sup>10,11</sup> Sanger sequencing was then carried out on the DNA amplified products for BRAF and NRAS mutation detection, with BRAF V600E mutation detection confirmed using a MALDI-TOF mass spectrometry assay (eFigure in the Supplement).

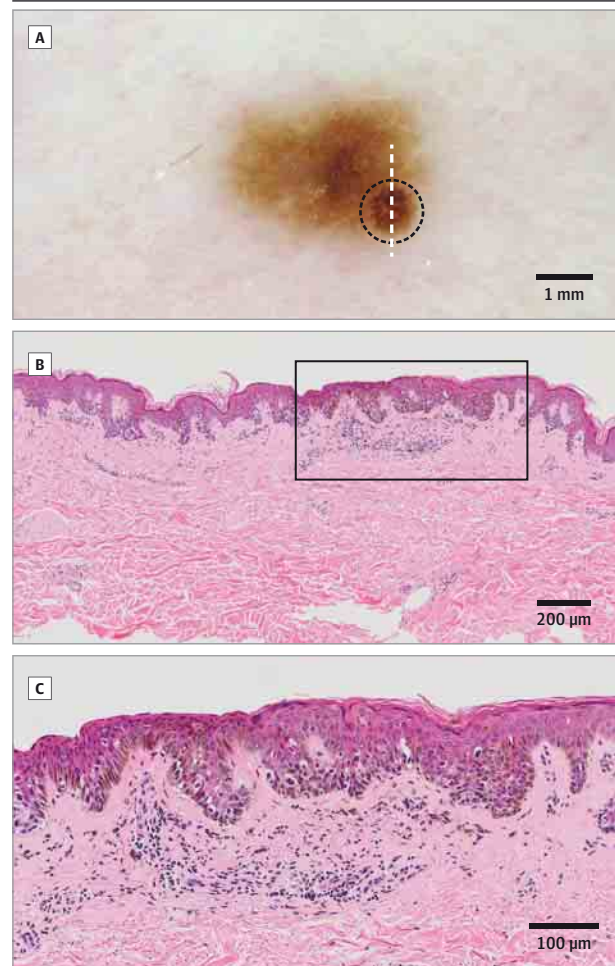
The micro-biopsy-extracted DNA samples from the left side and center of the lesion revealed BRAF V600E heterogeneity, while no BRAF V600E mutation was found in any of the samples taken from the melanoma in situ (Figure 4B). Of note, molecular sequencing of all micro-biopsy specimens across the lesion revealed no NRAS mutation at codon 61. Thus, somatic genomic profiling and molecular landscaping of this lesion revealed the paradoxical finding of a melanoma in situ with BRAF wild-type DNA arising in a dysplastic nevus heterogeneous for the BRAF V600E mutation.

## Discussion

We describe herein the use of a miniaturized biopsy device to evaluate a melanoma in situ with a BRAF wild-type DNA sequence developing within a heterogeneous BRAF V600E mutant dysplastic nevus. A dermoscope was used as a targeting tool to improve the sampling of distinct dermoscopic areas from within this multicomponent lesion. We observed that all samples from the melanoma in situ were concordantly BRAF wild-type, whereas the BRAF V600E mutation was detected in the other 2 dermoscopic areas within the same melanocytic lesion.

Mutation of the BRAF gene in melanoma arising within nevi was recently studied using DNA extraction of 1 or mul-

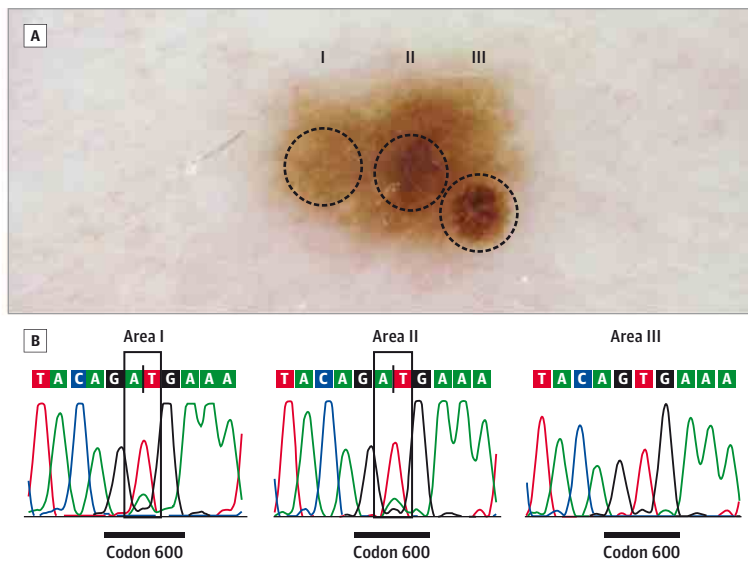
Figure 3. Dermoscopy and Hematoxylin-Eosin-Stained Histopathology Images Corresponding to the Right Side of the Subject Lesion



A, Circled area of the dermoscopy image displays a 1 × 1-mm well-circumscribed area with an atypical broadened pigment network and irregular streaks at the 4-o'clock corner; dermoscopy-targeted micro-biopsy samples were taken from this circled area; vertical line corresponds to the site of the specimen shown in panel B. B, Photomicrograph of the histologic specimen reveals features suggestive of an early evolving melanoma in situ arising within a dysplastic nevus. C, Higher magnification of the boxed section shows architectural disarray with predominantly single atypical melanocytes at all levels of the epidermis.

tle laser-capture-microdissected, formalin-fixed, paraffin-embedded, 5-µm-thick histologic sections that were hematoxylin-eosin stained and then subjected to Sanger sequencing and immunohistochemical analysis.<sup>11</sup> This study observed 5 cases (about 11%) of BRAF wild-type superficial spreading melanoma adjacent to a BRAF V600E mutated nevus, which was not statistically significant. Additionally, the investigators found melanoma-associated nevi to be either strictly dermal or compound type, leading Tschandl et al<sup>11</sup> to conclude that their phenotypic and genotypic findings did not mirror the traditional model of stepwise tumor progression. In comparison, we were able to demonstrate this phenomenon in a thinner melanoma using dermoscopy-targeted sampling with a micro-biopsy device coupled with DNA sequence analysis, accentuating the potential role of this minimally invasive tech-

Figure 4. Three Sampled Sectors of the Subject Lesion and Their Corresponding BRAF V600E Mutation Status



A, Dermoscopy image specifying the locations where microbiopsy samples were taken from each dermoscopic area (circles) of the subject lesion with the aid of a dermoscope; area I corresponds to Figure 1; area II, to Figure 2; and area III, to Figure 3. B, Representative chromatograms corresponding to areas I, II, and III of the lesion, as shown in panel A; BRAF V600E mutation was detected in areas I and II (highlighted as A/T in the boxed areas); conversely, no mutation was detected in area III.

nique in providing insight into intralesional heterogeneity in melanocytic lesions in vivo.<sup>12</sup> Moreover, the phenotypic characteristics of our melanocytic lesion fits with the Clark clinicopathologic model in that the melanoma developed within a dysplastic nevus,<sup>6</sup> though this is undermined by the paradox in our lesion's genetic signature.

Although histopathologic criteria have traditionally been the practical reference standard in melanoma diagnosis and staging, recent discovery of tumors harboring different oncogenic mutations has implicated the existence of molecular subgroups of melanoma.<sup>2</sup> The evaluation of early cutaneous melanomas in particular would benefit from a shift toward an integrated phenotype-genotype melanoma classification system, instead of using morphologic criteria alone, because this enables future development of melanoma-specific biomarkers to aid in melanoma detection independent of disease stage. Other candidate genes linked to melanomagenesis such as *CKIT*, *GNAQ*, *GNA11*, *RAC1*, *TERT*, *PTEN*, and *NF1*<sup>13</sup> remain to be studied in the lesion described herein.

Similarly, *BRAF* and *NRAS* gene mutations have been used as genetic markers in studies attempting to integrate genetic and morphologic features to improve melanoma classification.<sup>14,15</sup> However, the high concordance rate (80.4%) of *BRAF* mutation between melanoma and its associated nevus counterpart dem-

onstrated by Tschandl et al<sup>11</sup> as well as the occurrence of *BRAF* wild-type melanoma arising in a *BRAF* V600E mutated nevus suggest that other molecular signatures are involved in melanoma development. One may argue that our findings might result from the microneedle deviating from the exact desired location despite an attempt to improve sampling accuracy using a dermoscope, as well as the remote possibility that the microneedle did not sample melanocytes and so consequently yielded the wild-type sequence. Nonetheless, conventional methods such as laser-capture microdissection also present a probability of not sampling *BRAF*-mutant melanocytes.

## Conclusions

Our observation supports other reports on the limitations of current melanoma biomarkers in deconstructing the molecular events responsible for tumorigenesis. Further large-scale studies are required to investigate the significance of other candidate genes linked to melanomagenesis. Translation of a minimally invasive in vivo microbiopsy device in sampling for melanoma-specific biomarkers may have a prospective role in the next phase of melanoma diagnosis, risk stratification, and personalized therapeutics.

### ARTICLE INFORMATION

**Accepted for Publication:** September 14, 2014.

**Published Online:** January 21, 2015.  
doi:10.1001/jamadermatol.2014.3775.

**Author Contributions:** Drs Tan and Soyer had full access to all of the data in the study and take responsibility for the integrity of the data and the accuracy of the data analysis.

**Study concept and design:** Tan, Lambie, Sturm, Prow, Soyer.

**Acquisition, analysis, or interpretation of data:** Tan, Lin, Lambie, Flewell-Smith, Jagirdar, Schaidler,

Sturm, Soyer.

**Drafting of the manuscript:** Tan, Flewell-Smith.

**Critical revision of the manuscript for important intellectual content:** Lin, Lambie, Jagirdar, Schaidler, Sturm, Prow, Soyer.

**Obtained funding:** Sturm, Soyer.

**Administrative, technical, or material support:** Tan, Lin, Lambie, Flewell-Smith, Jagirdar, Sturm, Prow.

**Study supervision:** Schaidler, Sturm, Soyer.

**Conflict of Interest Disclosures:** None reported.

**Funding/Support:** This project was supported in part by research grant APPI062935 from the

National Health Medical Research Council (NHMRC), Canberra, Australian Capital Territory, Australia.

**Role of the Sponsor:** The NHMRC had no role in the design and conduct of the study; collection, management, analysis, and interpretation of the data; preparation, review, or approval of the manuscript; and decision to submit the manuscript for publication.

**Additional Information:** Dr Tan and Ms Lin contributed equally to this work.

## REFERENCES

1. Pollock PM, Harper UL, Hansen KS, et al. High frequency of *BRAF* mutations in nevi. *Nat Genet*. 2003;33(1):19-20.
2. DeLuca AM, Srinivas A, Alani RM. BRAF kinase in melanoma development and progression. *Expert Rev Mol Med*. 2008;10:e6.
3. Davies H, Bignell GR, Cox C, et al. Mutations of the *BRAF* gene in human cancer. *Nature*. 2002;417(6892):949-954.
4. Thomas NE. *BRAF* somatic mutations in malignant melanoma and melanocytic naevi. *Melanoma Res*. 2006;16(2):97-103.
5. Bennett DC. Human melanocyte senescence and melanoma susceptibility genes. *Oncogene*. 2003;22(20):3063-3069.
6. Damsky WE, Theodosakis N, Bosenberg M. Melanoma metastasis: new concepts and evolving paradigms. *Oncogene*. 2014;33(19):2413-2422.
7. Sturm RA, Fox C, McClenahan P, et al. Phenotypic characterization of nevus and tumor patterns in *MITF* E318K mutation carrier melanoma patients. *J Invest Dermatol*. 2014;134(1):141-149.
8. Lin LL, Prow TW, Raphael AP, et al. Microbiopsy engineered for minimally invasive and suture-free sub-millimetre skin sampling. *F1000Res*. 2013;2:120.
9. Banan P, Lin LL, Lambie D, Prow T, Soyer HP. Effects of ex vivo skin microbiopsy on histopathologic diagnosis in melanocytic skin lesions. *JAMA Dermatol*. 2013;149(9):1107-1109.
10. McClenahan P, Lin LL, Tan JM, et al. BRAFV600E mutation status of involuting and stable nevi in dabrafenib therapy with or without trametinib. *JAMA Dermatol*. 2014;150(10):1079-1082.
11. Tschandi P, Berghoff AS, Preusser M, et al. NRAS and *BRAF* mutations in melanoma-associated nevi and uninvolved nevi. *PLoS One*. 2013;8(7):e69639.
12. Prow TW, Lin LL, Soyer HP. The opportunity for microbiopsies for skin cancer. *Future Oncol*. 2013;9(9):1241-1243.
13. Xia J, Jia P, Hutchinson KE, et al. A meta-analysis of somatic mutations from next generation sequencing of 241 melanomas: a road map for the study of genes with potential clinical relevance. *Mol Cancer Ther*. 2014;13(7):1918-1928.
14. Viros A, Fridlyand J, Bauer J, et al. Improving melanoma classification by integrating genetic and morphologic features. *PLoS Med*. 2008;5(6):e120.
15. Pozzobon FC, Puig-Butillé JA, González-Alvarez T, et al. Dermoscopic criteria associated with BRAF and NRAS mutation status in primary cutaneous melanoma [published online April 21, 2014]. *Br J Dermatol*. 2014.

# A Plea for Biobanking of All Equivocal Melanocytic Proliferations

H. Peter Soyer, MD, FACD; Lynlee L. Lin, BSc; Tarl W. Prow, PhD

**In 2005, in an editorial** in the *Archives of Dermatology* (now *JAMA Dermatology*), we made a plea for a combined diagnostic approach to histopathologic and dermoscopic evaluation.<sup>1</sup> We concluded our editorial with the following statement<sup>1</sup> (p211):

*Histopathology, as every other purely morphologic method, is limited by methodologic drawbacks and sometimes by practitioners' personal limitations. Today we are on the edge of a new biology in histopathology, and one can foresee that our beloved classic morphology will soon be replaced by new technologies. In the meantime, a combined morphologic approach linking dermoscopy and histopathology might be helpful for pathologists to come to more reliable diagnostic conclusions for patients and their physicians.*

And it is encouraging to see that indeed there is an increased awareness by colleagues dealing with problematic and borderline melanocytic proliferations that has led to a more refined clinicodermoscopic and pathologic approach in the interpretation of these lesions.

In the present editorial, we take the opportunity to make another plea, namely, a plea for biobanking of all equivocal melanocytic proliferations. This plea is based on our interpretation of the pioneering study by Malvehy and colleagues<sup>2</sup> in this



Related articles pages 1060 and 1107

issue of *JAMA Dermatology*. This original morphologic study combining expertise in dermoscopy and dermatopathology will doubtless lead to a redefinition of the way traditional gross pathologic procedures are carried out for equivocal pigmented skin lesions. We commend the authors of this seminal, albeit contested, work, and we agree with them that highly specialized providers of skin pathologic analysis will embrace more advanced sampling technologies that use dermoscopy guidance in the future, thus reflecting the paradigmatic shift from conventional surgical pathologic analysis to molecular pathologic analysis, in order to remain competitive and, most importantly, do the most good for our patients.

## Why Biobanking?

The new credo of personalized medicine has already reached dermatology, and more and more of our patients with melanoma are no longer asking about their prognosis or about an estimated survival time but whether their melanoma is a *BRAF* melanoma. Whereas this specific query can be answered rather easily by performing, for example, the cobas 4800 *BRAF* V600 Mutation Test (Roche) on formalin-fixed paraffin-embedded samples, there is a growing need for frozen

tissue samples for those molecular and genetic tests that might be available by the time today's primary melanoma metastasizes in 5 or 10 years' time. There is no doubt that biobanking is one of the central tools for clinical and translational medicine.<sup>3</sup> The challenge is, of course, to organize the biobank sampling with minimal disruption to the busy daily practice of dealing with patients with melanomas and clinically suspicious pigmented skin lesions. Malvehy and colleagues<sup>2</sup> correctly note that their sophisticated protocol for biobank sampling has been developed for "experienced research centers." Of interest is a recent publication by Caenazzo and colleagues<sup>4</sup> on the ethical issues of balancing the rights of the individual and the interest of society in biobanking research on oncological residual material. Biobank research cannot be conducted without considering arguments for obtaining the donors' consent. The authors described the type of consent that "would be appropriate in this context, considering the ethical principles of donation, solidarity, protection of the donors' rights and the requirements of scientific progress."<sup>4</sup> The authors concluded that an important ethical aspect in regard to the role of biobanking is the need to encourage sample donation.

## Dermoscopy, Dermatopathology, and Targeted Sampling

The "ex vivo dermoscopic-oriented sampling of melanoma" protocol has been designed in close collaboration by a group of dermatologists and dermatopathologists, all of them with great expertise in dermoscopy, with the specific aim of not jeopardizing the conventional histopathologic diagnosis. The protocol includes conservation of the thickest part of the lesion for measuring the Breslow index. The authors nicely showed that by creating a "dermoscopic melanoma map" they were able to successfully sample the nonthickest part of the lesion and also avoided sampling areas that contain dermoscopic melanoma-specific features whose absence could interfere with the dermatopathologist's ability to render a conclusive diagnosis. Unfortunately, their targeted sampling protocol excludes small melanomas, dermoscopically equivocal lesions, and other melanocytic lesions for which they suspect that the histopathologic evaluation may prove difficult. The authors fear that insufficient material will be provided for the pathological assessment and that this may lead to clinical and medicolegal consequences.<sup>5</sup> Also, the issue of shave biopsies or saucerizations was not mentioned at all. Only completely excised lesions can be included. All these exclusion criteria are, in our estimation, serious limitations for the purpose of "biosampling" even in

a highly specialized melanoma center because as many suspicious melanocytic skin proliferations as possible should be biosampled. However, one can imagine that, inspired by this original and authentic work by Malvey and colleagues,<sup>2</sup> several dermatology and/or pathology teams worldwide will come up with their own solutions and protocols for molecular sampling of suspicious melanocytic proliferations.

### Microbiopsies for Molecular Sampling

Recently, we have developed a submillimeter skin punch biopsy device for minimally invasive and suture-free skin sampling that extracts approximately 1500 keratinocytes and 5 to 10 ng DNA and RNA for molecular diagnosis in dermatology and dermato-oncology (L. L. Lin, BSc; T. W. Prow, PhD; A. P. Raphael, PhD; R. L. Harrold III, MD; C. A. Primiero, BSc; A. B. Ansaldo, BE; H. P. Soyer, MD, FACD; unpublished data; May 2013). Our microbiopsy device is 0.50 mm wide and 0.15 mm thick and results in a  $0.21 \pm 0.04$ -mm-wide puncture site in voluteer skin as measured using reflectance confocal microscopy. In a research letter in this issue of *JAMA Dermatology*, we have demonstrated the minimal impact that the choice of microbiopsy site has on the histopathologic diagnosis of a given melanocytic proliferation.<sup>6</sup> The size of microbiopsy defects measured in this study was comparable to those of other artifacts more or less commonly seen in routine sectioned specimens, and the inherent diagnostic difficulties for the dermatopathologist encountered with the histopathologic assessment of a microbiopsied melanocytic skin lesion can easily be overcome by ordering of multiple levels.

### Synopsis and Utopia

Microbiopsy devices have already been developed for breast and intestinal tissue on the basis of the step change advances in micromanufacturing and in molecular and genetic testing. The ingenious outcomes are meaningful analyses that can be obtained nowadays even from a few cells. We foresee that microbiopsies will become a feasible molecular sampling option for biobanking of equivocal melanocytic proliferations, and because of the simplicity of the sampling procedure, a multitude of melanocytic lesions can be biobanked easily in due course. In addition, the use of these samples can be maximized with nucleic acid amplification followed by whole genome and transcriptome sequencing that will be made open source, thereby creating a sort of virtual biobank in the cloud in the spirit of the ubiquitous big data concept. If only 1 or a few expert laboratories in collaboration with a few melanoma centers does this, our patients will benefit through open source data analysis linking the microbiome, virome, genome, transcriptome, and the noncoding RNA world with the clinical and dermoscopic phenotypes. Such an approach will probably change our understanding of the enigmatic and so often fateful nature of melanocytic proliferations to the better. One possible outcome may be a molecular profile assigned to a specific dermoscopic morphology, ie, a molecular imaging profile, that could give us insight into the molecular pathologic characteristics of a lesion using just dermoscopy imaging. Biobanking of melanomas and equivocal melanocytic proliferations will lose its research status soon and become a standard of care in dermato-oncology as an integral part of personalized medicine.

#### ARTICLE INFORMATION

**Author Affiliations:** Dermatology Research Centre, The University of Queensland, School of Medicine, Translational Research Institute, Brisbane, Queensland, Australia (Soyer, Lin, Prow); Department of Dermatology, Princess Alexandra Hospital, Brisbane, Queensland, Australia (Soyer).

**Corresponding Author:** H. Peter Soyer, MD, FACD, Dermatology Research Centre, The University of Queensland, School of Medicine I, Level 5, Translational Research Institute (TRI), 37 Kent Street, Brisbane QLD 4102, Australia (p.soyer@uq.edu.au).

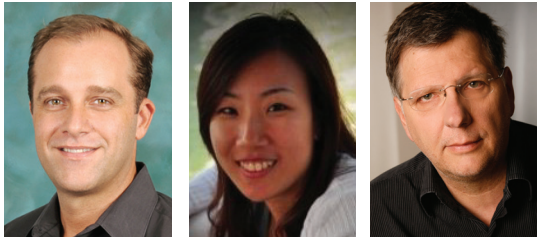
**Published Online:** July 17, 2013.  
doi:10.1001/jamadermatol.2013.4478.

**Conflict of Interest Disclosures:** None reported.

#### REFERENCES

1. Soyer HP, Massone C, Ferrara G, Argenziano G. Limitations of histopathologic analysis in the recognition of melanoma: a plea for a combined diagnostic approach of histopathologic and dermoscopic evaluation. *Arch Dermatol*. 2005;141(2):209-211.
2. Malvey J, Aguilera P, Carrera C, et al. Ex vivo dermoscopy for biobank-oriented sampling of melanoma [published online July 17, 2013]. *JAMA Dermatol*. doi:10.1001/jamadermatol.2013.4724.
3. Marko-Varga G. BioBanking as the central tool for translational medicine CTM issue 2013. *Clin Transl Med*. 2013;2(1):4.
4. Caenazzo L, Tozzo P, Pegoraro R. Biobanking research on oncological residual material: a framework between the rights of the individual and the interest of society. *BMC Med Ethics*. 2013;14:17.
5. Troxel DB. Medicolegal aspects of error in pathology. *Arch Pathol Lab Med*. 2006;130(5):617-619.
6. Banan P, Lin LL, Lambie D, Prow T, Soyer HP. Effects of ex vivo skin microbiopsy on histopathologic diagnosis in melanocytic skin lesions [published online July 17, 2013]. *JAMA Dermatol*. doi:10.1001/jamadermatol.2013.5020.

# The opportunity for microbiopsies for skin cancer



Tarl W Prow<sup>\*1</sup>, Lynlee L Lin<sup>1</sup> & H Peter Soyer<sup>1</sup>

<sup>1</sup>Dermatology Research Centre, The University of Queensland, School of Medicine, Translational Research Institute, Princess Alexandra Hospital, Brisbane, QLD, Australia

\*Author for correspondence: Tel.: +61 7 3343 8019 ■ Fax: +61 7 3443 7779 ■ [t.prow@uq.edu.au](mailto:t.prow@uq.edu.au)

“...the clinical promise of microbiopsy is early detection, risk assessment and to aid therapeutic selection.”

High-throughput sequencing and bioinformatics are laying bare the molecular mechanisms of disease [1,2]. This rapidly expanding foundation of knowledge is supporting the evolution of targeted molecular medicine in oncology. Although targeted molecular medicine is at a relatively early stage, the future of oncology will likely have a strong personalized treatment component [3–5]. We have recently developed the first submillimeter skin microbiopsy device to be used in patients and foresee this technology enabling personalized dermato-oncology [6,7].

Personalized oncology is a recent diagnostic and treatment-based clinical approach that addresses the issues of intra- and inter-tumor heterogeneity within the scope of personalized medicine [3–5]. If we look at recent reports on inter- and intra-tumor heterogeneity of squamous cell carcinoma/melanoma it is conceivable that targeted drug development will make individualized care commonplace, but this can only happen by first identifying the molecular signatures and targets within lesions [8,9]. Mutations can cause changes in cell signaling and molecular interactions that result in transformation. The resulting uncontrolled proliferation results in an unstable genome that can give rise to the evolution of unique transformed cell clones within a given lesion, also known as intratumor heterogeneity. This is well known in melanoma, but there is also evidence that supports the hypothesis that this can occur in non-melanoma skin cancer [10]. Similar circumstances can lead to intertumor heterogeneity, such as two melanomas with different mutations in the same person. This facet of cancer biology has direct consequences for tumor diagnostic markers and the clinical therapeutic outcome. The concept of personalized dermato-oncology is predicated on the capacity to identify and treat based on the presence of a validated biomarker [5].

One example of this principle in dermato-oncology can be found in melanomas with the *BRAF*V600E mutation, reviewed in [4] and [11]. Not all melanomas have this mutation, but if one does, then vemurafenib, a US FDA-approved specific signaling pathway inhibitor, can be used to target the metastases of the particular melanoma harboring the *BRAF*V600E mutation [12]. Today's clinical reality is that the primary melanoma lesion is excised before the *BRAF* status is known and that information is used to treat the metastatic tumors. In the future, a microbiopsy could be taken from every naevi, clinically more or less suspicious, and a prognostic biomarker can be assessed to determine the likelihood of transformation and the precursor or even the primary lesion treated before metastasis occurs.

As a rule, skin cancer is currently identified by morphological assessment. This can be as simple as looking at a lesion with the trained eye of a dermatologist or using dermoscopy, a noninvasive diagnostic technique that enables an experienced clinician to perform direct microscopic examination of the surface and architecture of a given skin lesion or histopathologic examination following excision of the lesion [13]. The latter represents the current diagnostic gold standard. In both scenarios, the dermatologist or dermatopathologist require there to be cancer already present and cannot visually identify the crucial molecular signatures that can be used to determine whether one or the other highly specific signaling inhibitors will be beneficial. This is one case that supports the use of a tiny molecular sampling device coupled with validated biomarkers for melanoma.

Nonmelanoma skin cancer is far more prevalent, especially in organ transplant patients [14], and more costly compared with melanoma, albeit with a much lower incidence of mortality. Sun-damaged and/or transplant patients

## Keywords

- cancer drug target
- diagnostic ■ microneedle
- skin cancer

can present with many precancerous actinic keratoses, some of which will progress into an overt squamous cell carcinoma. Selecting a few of the many lesions that are most suspicious for biopsy and histopathology can be a daunting task. There are also significant cosmetic challenges that cannot be ignored because actinic keratoses are present on sun-exposed areas, such as the face. In this arena, a tiny biopsy device could yield molecular signature data capable of being used to assess the presence of transformed cells or the potential for neoplastic transformation. However, this improvement in patient care is dependent on validated biomarkers and the development/approval of new targeted therapies.

---

“With a microbiopsy-based approach to collect just a few cells from a lesion repeatedly over time, without destroying that lesion, a new dimension of biological replication is now possible.”

---

Thus, the clinical promise of microbiopsy is early detection, risk assessment and to aid therapeutic selection. Recently, we developed a microbiopsy device for rapid, minimally invasive and suture-free sampling and we foresee several research applications in dermatology far beyond dermatology-oncology. The challenge is to define informative molecular signatures, similar in principle to the morphological signatures elaborated in conventional histopathology nearly a century ago, in order for this approach to effectively diagnose melanoma/skin cancer with a higher diagnostic accuracy [15]. We envision that the future adoption of the microbiopsy will be guided by the use of the device in the clinical research arena. We are using the term ‘biomarker’ as a relatively broad descriptor for one or more molecular signatures from only the primary lesion that can be used to identify whether a disease is present, predict clinical outcome or predict the response to targeted molecular therapies – that is, diagnostic, prognostic or therapeutic biomarkers. This field is more mature in other areas of oncology, but is relatively young in dermatology-oncology, with the main driver being improved survival in melanoma. However, the significant cost and common drug resistance over time are important sources of controversy [16].

The microbiopsy approach is currently used in other oncology specialties, such as breast cancer [17], but not for skin cancer, where conventional biopsies range from 2 to 4 mm. This size range is

key for enabling histopathological diagnosis. The outstanding question is of the value of molecular profiling in the treatment cycle. Oncogene mutations are clues that can help predict the disease course. The immune system function is inexorably tied to the suppression of skin cancer and the usefulness of immunotherapy [14]. Therefore, this area of research could become essential for predicting risk, stratifying skin cancer and therapeutic effectiveness. The combination of oncogene mutations, expression profiles and immune-profiling may give a comprehensive overview of what processes are likely to occur and predict the likelihood of successful small molecule therapy. This could, in theory, all be carried out with a single microbiopsy given the rapid advances in nanomedicine and bioengineering.

Mutational analysis can be performed on DNA or RNA, both have the capacity to be amplified with high fidelity [18]. Immune status can be assessed with very small protein samples with cytometric bead arrays or indirectly characterized by examining RNA expression profiles. One example is the positive correlation of CXCL8 with melanoma progression [19]. There are many research publications with putative biomarker lists for both melanoma and nonmelanoma skin cancers. The significant challenge is to standardize profiles in a similar way to histopathological analysis of lesion morphology.

---

“We foresee microbiopsy-enabled elaboration of molecular profiling for early skin cancer diagnosis/prognosis and the identification of therapeutic targets as the future of dermatology-oncology research.”

---

Research is moving at a hurried pace towards the goal of molecular diagnosis. Conceptually, one of the stumbling blocks is that the transformation from a functional skin cell to an anarchic cancer cell is a continuum. The use of a microbiopsy approach will open new doors for research in the field of molecular skin pathology. Paradoxically, we seem to know genetic markers for rare diseases, but not common ones. Therefore, studies on common skin cancers could reveal critical information for diagnostics, prognostics and targeted therapeutics. With a microbiopsy-based approach to collect just a few cells from a lesion repeatedly over time, without destroying that lesion, a new dimension of biological replication is now possible. Collecting cells from many lesions in an animal model or a given patient



is also possible. These new avenues of research enable scientists to look even more closely at the molecular mechanisms of disease as it unfolds. However, smaller samples require sensitive assays and selective targeting. The application of our device captures approximately 1600 keratinocytes, from which 5 ng of RNA or DNA can be isolated. This is more than the picograms of genetic material isolated from single cells, but less than the micrograms of genetic material we isolate from convention biopsies.

It is also important to note that environmental factors, such as sunlight exposure and microbiome, can play significant roles in cancer. Sun-damaged skin is the fertile soil for the formation of actinic keratoses. The transformation of this precursor lesion into a squamous cell carcinoma could be tied to bacteria/viruses living on the skin. The skin produces antimicrobial peptides that have been shown to have altered expression levels in squamous cell carcinomas compared with actinic keratoses or normal skin [20]. The biodiversity of the skin microbiome could also be investigated with a microbiopsy-based approach.

### Conclusion

We have developed a skin microbiopsy device for quick, simple, minimally invasive and suture-free sampling for neoplastic and inflammatory skin diseases. We foresee microbiopsy-enabled elaboration of molecular profiling for early skin cancer diagnosis/prognosis and the identification of therapeutic targets as the future of dermatology research. The long-term benefits of using microbiopsies in the laboratory and clinic are projected to be earlier detection of neoplastic skin diseases, more accurate prognosis estimates and targeted skin cancer therapy without all the nuisances related to conventional skin biopsies.

### Financial & competing interests disclosure

*The authors have no relevant affiliations or financial involvement with any organization or entity with a financial interest in or financial conflict with the subject matter or materials discussed in the manuscript. This includes employment, consultancies, honoraria, stock ownership or options, expert testimony, grants or patents received or pending, or royalties.*

*No writing assistance was utilized in the production of this manuscript.*

### References

- Haqq C, Nosrati M, Sudilovsky D *et al.* The gene expression signatures of melanoma progression. *Proc. Natl Acad. Sci. USA* 102(17), 6092–6097 (2005).
- Kemp CJ, Grandori C. Functional genomics to identify unforeseen cancer drug targets. *Future Oncol.* 9(4), 473–476 (2013).
- Blay JY, Lacombe D, Meunier F, Stupp R. Personalised medicine in oncology: questions for the next 20 years. *Lancet Oncol.* 13(5), 448–449 (2012).
- Bradish JR, Montironi R, Lopez-Beltran A, Post KM, Maclennan GT, Cheng L. Towards personalized therapy for patients with malignant melanoma: molecular insights into the biology of BRAF mutations. *Future Oncol.* 9(2), 245–253 (2013).
- Cho W, Ziogas DE, Katsios C, Roukos DH. Emerging personalized oncology: sequencing and systems strategies. *Future Oncol.* 8(6), 637–641 (2012).
- Banan P, Lin LL, Lambie D, Prow TW, Soyer HP. *Ex-vivo* skin microbiopsy effects on histopathological diagnosis in melanocytic skin lesions. *JAMA Dermatol.* (2013) (In Press).
- Lin LL, Prow TW, Raphael AP, Primiero CA, Soyer HP. Microbiopsy engineered for pain- and suture-free, sub-millimetre skin sampling. *F1000 Research* (2013) (In Press).
- Yancovitz M, Litterman A, Yoon J *et al.* Intra- and inter-tumor heterogeneity of BRAF<sup>V600E</sup> mutations in primary and metastatic melanoma. *PLoS ONE* 7(1), e29336 (2012).
- Wilmott JS, Tembe V, Howle JR *et al.* Intratumoral molecular heterogeneity in a BRAF-mutant, BRAF inhibitor-resistant melanoma: a case illustrating the challenges for personalized medicine. *Mol. Cancer Ther.* 11(12), 2704–2708 (2012).
- Cohen N, Kravchenko-Balasha N, Klein S, Levitzki A. Heterogeneity of gene expression in murine squamous cell carcinoma development—the same tumor by different means. *PLoS ONE* 8(3), e57748 (2013).
- Ji Z, Flaherty KT, Tsao H. Targeting the RAS pathway in melanoma. *Trends Mol. Med.* 18(1), 27–35 (2012).
- Ascierto PA, Kirkwood JM, Grob JJ *et al.* The role of BRAF V600 mutation in melanoma. *J. Transl. Med.* 10, 85 (2012).
- Argenziano G, Soyer HP. Dermoscopy of pigmented skin lesions – a valuable tool for early diagnosis of melanoma. *Lancet Oncol.* 2(7), 443–449 (2001).
- Bangash HK, Colegio OR. Management of non-melanoma skin cancer in immunocompromised solid organ transplant recipients. *Curr. Treat. Options Oncol.* 13(3), 354–376 (2012).
- Moore DA, Pringle JH, Saldanha GS. Prognostic tissue markers in melanoma. *Histopathology* 60(5), 679–689 (2012).
- Pollack A. Doctors denounce cancer drug prices of \$100,000 a year. *New York Times*, 25th April (2013).
- Krainick-Strobel U, Huber B, Majer I *et al.* Complete extirpation of benign breast lesions with an ultrasound-guided vacuum biopsy system. *Ultrasound Obstet. Gynecol.* 29(3), 342–346 (2007).
- Patel LR, Nykter M, Chen K, Zhang W. Cancer genome sequencing: understanding malignancy as a disease of the genome, its conformation, and its evolution. *Cancer Lett.* doi:10.1016/j.canlet.2012.10.018 (2012) (Epub ahead of print).
- Singh S, Singh AP, Sharma B, Owen LB, Singh RK. CXCL8 and its cognate receptors in melanoma progression and metastasis. *Future Oncol.* 6(1), 111–116 (2010).
- Scola N, Gambichler T, Saklaoui H *et al.* The expression of antimicrobial peptides is significantly altered in cutaneous squamous cell carcinoma and precursor lesions. *Br. J. Dermatol.* 167(3), 591–597 (2012).